# MOLECULAR DESIGN AND SYNTHESIS OF DYES

# FOR DYE-SENSITIZED SOLAR CELLS (DSSCs)

**ELENA LONGHI**
**Matr. R08300**

**Advisor: Prof. Emanuela LICANDRO**

**Co-advisor: Prof. Stefano MAIORANA**
**Dr. Clara BALDOLI**

**Coordinator: Prof. Dominique ROBERTO**

*"...I was sitting writing on my textbook, but the work did not progress; my thoughts were elsewhere. I turned my chair to the fire and dozed. Again the atoms were gamboling before my eyes. This time the smaller groups kept modestly in the background. My mental eye, rendered more acute by the repeated visions of the kind, could now distinguish larger structures of manifold conformation; long rows sometimes more closely fitted together all twining and twisting in snake-like motion. But look! What was that? One of the snakes had seized hold of its own tail, and the form whirled mockingly before my eyes. As if by a flash of lightning I awoke; and this time also I spent the rest of the night in working out the consequences of the hypothesis."*

*-August Kekulé-*

*1980*

# ABSTRACT

**Background**

Solar energy plays a critical role in meeting the global energy challenge and represents one of the most promising energy sources for the future of the planet. Solar or photovoltaic cells are currently a hot topic on the market, these are devices that convert the energy of sunlight directly into electricity trough the photovoltaic effect. Strong and competitive research is currently devoted to lower the material costs of solar cells, and to increase their energy conversion efficiency.

Up to now, commercially available photovoltaic technologies are based on inorganic materials, mainly crystalline silicon (first generation) and other semiconductors, such as gallium arsenide, indium phosphide and cadmium telluride (second generation In addition to high costs, also in terms of energy consuming, in fabrication processes, several of those materials are toxic and have low natural abundance. Therefore, in the last two decades the research focused on the development of a third generation of solar cells based on hybrid or organic materials, that offers a number of advantages, such as: high molar extinction coefficients, versatility of the chemical design for modulating the electronic properties, easy processability as well as low manufacturing costs. Although the efficiencies of organic-based photovoltaic cells ($\sim$ 8%) are still at the moment a long way behind those obtained with purely inorganic based photovoltaic technologies ( $\sim$20%), the power conversion efficiency of organic solar cells have been significantly improved and there are expectations for more important results.

Among the third generation of solar cells, the Dye-Sensitized Solar Cells (DSSC), also called Grätzel cells, have emerged as very promising candidates for low-cost alternative to conventional semiconductor photovoltaic devices.[1] A DSSC cell scheme is shown in Figure 1. The cell components are: a mesoporous film of $TiO_2$ (anode), a dye-sensitizer, an electrolyte, an electrochemical mediator and a cathode. The photovoltaic process in this cells can be resumed as follows: the dye-sensitizer (S), linked to semiconducting $TiO_2$ surface (usually through a carboxylic group), absorbs a photon passing to the excited

---

1 O'Reagan, B.; Graetzel, M. *Nature* **1991**, *353*, 737.

state S*, which transfers an electron to the conduction band of $TiO_2$. The oxidized $S^+$ thus obtained, is reduced by a *redox* mediator, generally $I^-$ from the couple $I^-/I_3^-$ dissolved in the electrolyte. The electron injected in $TiO_2$ through the external circuit arrives to the cathode, where the reduction of $I_3^-$ regenerates the iodide, closing the circuit. (Figure 1).
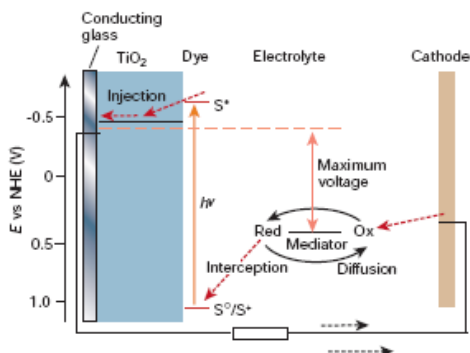


**Figure 1**

The DSSC technology separates two requirements as: i) the charge generation, done at the semiconductor-dye interface and ii) the charge transport, done by the semiconductor and the electrolyte. Consequently, carrier transport properties can be improved by optimizing the semiconductor and electrolyte composition, while the spectral properties and thus charge generation can be improved by modifying the dye structure, that can be tailored in many ways by organic chemistry contribution.

Many kinds of dyes have been studied for DSSCs application and in principle they could be divided in two classes (Figure 2):

1.  metal complexes (**N719**, Zn-porphyrine e.g **YD2-o-C8**)[2, 3, 4]

2.  metal-free system Donor-Spacer-Acceptor (**TA-St-CA**) [5]

2 M. Graetzel, *J. Photochem. Photobiol. A* **2004**, *164*, 3.

3 M. K. Nazeeruddin, A. Kay, I. Rodicio, R. Humphry-Baker, E. Mueller, P. Liska, N. Vlachopoulos, M. Graetzel, *J. Am. Chem. Soc.* **1993**, *115*, 6382.

[4] Aswani Yella,1 Hsuan-Wei Lee,2 Hoi Nok Tsao,1 Chenyi Yi,1 Aravind Kumar Chandiran,1 Md.Khaja Nazeeruddin,1 Eric Wei-Guang Diau,3* Chen-Yu Yeh,2* Shaik M Zakeeruddin,1* Michael Grätzel1* *Science* **2011**, *334*, 629.

5 S. Hwang, J. H. Lee, C. Park, H. Lee, C. Kim, C. Park, M.-H. Lee, W. Lee, J. Park, K. Kim, N.-G. Park, C. Kim, *Chem. Commun*. **2007**, 4887.
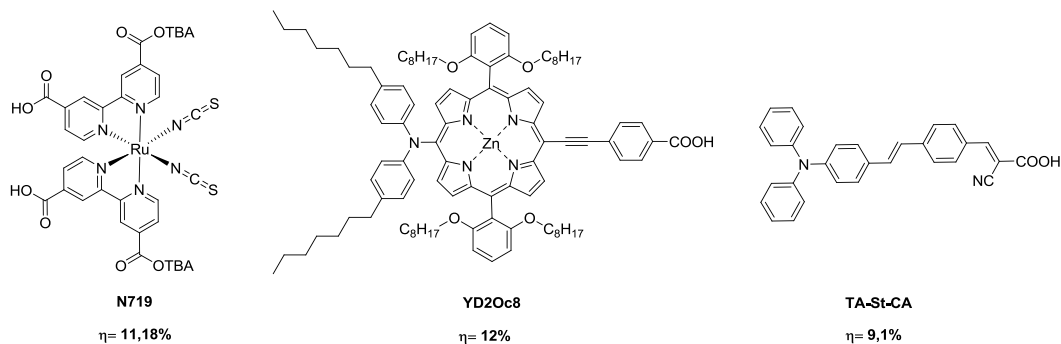
**Figure 2**

Up to now the best efficiencies (~11%) have been reached using ruthenium complexes, thanks to their large absorption range from visible to near infrared (NIR), and their capability to easily inject electrons in the conducting band of the semiconductor.[6] The metal based chromophores still have several disadvantages such as not very high molar extinction coefficient and the presence of the expensive metal, such as ruthenium, which involves complicated synthesis and hard purification steps. On the contrary, metal-free dyes are simple and cheap to prepare and it is possible to easily modulate their photo- and electrochemical properties varying the functionalization, but very high efficiencies have not been achieved yet.[7] The obtainment of new and more efficient dyes is therefore object of competitive international researches. Within this context, the present Ph.D. research project has focused on the synthesis of new metal-complexes and metal-free organic dyes characterized by a Donor-Spacer-Acceptor (D-π-A) structure, (Figure 3) in which the novelty is represented by the presence of benzo-condensed thiophene units as π bridge spacer.



**Figure 3**

6 A. Hagfeldt, M. Graetzel, *Chem. Rev.* **1995**, *95*, 49.

7 H. Tian, F. Meng in Organic Photovoltaics: Mechanisms, Materials, and Devices (Eds.: S.-S. Sun, N. S. Sariciftci), CRC, London, **2005**, p. 313.

**Aim of the work**

In such chromophores the π spacer plays a fundamental role, as it is responsible for the electronic communication between acceptor and donor moiety and for the extension of the conjugation that lead to wider and red-shifted absorption spectra. To date a number of new π-conjugated aromatic and heteroaromatic systems have been investigated[8] and among these, thiophene or thienothiophene π-bridges have been reported to give remarkable efficiency.[9] Benzodithiophenes systems **BDT** and **BDT₁** (Figure 4) attracted our attention because their rigid, π-conjugated, condensed-polycyclic structure[10,11] leads to unique electronic properties such as conductivity, high field effect mobility and tunable stacking in the solid state; rigid structures hamper the roto- vibrational modes responsible for the deactivation of the excited states in functional materials.
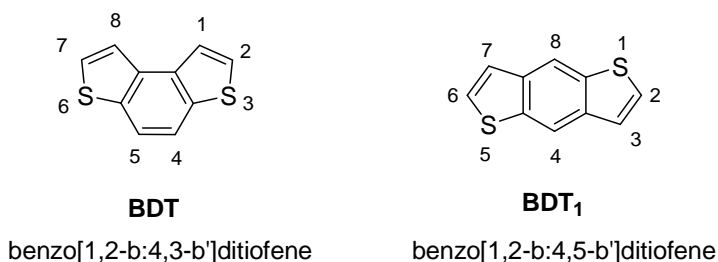


**BDT**
benzo[1,2-b:4,3-b']ditiofene

**BDT₁**
benzo[1,2-b:4,5-b']ditiofene

**Figure 4**

In this Ph. D. work we investigated synthesis of suitably functionalized **BDT** and **BDT₁** derivatives as well as their use for the construction of two classes of dyes: 1) Zn-porphyrin based dyes (in collaboration with the research group of Prof. Pizzotti and Prof. Ugo) and 2) metal-free dyes and, Zn-porphyrin based dyes

In addition the design of the new dyes have been oriented by preliminary theoretical calculations, done in collaboration with Dr. Filippo De Angelis of CNR-ISTM in Perugia,

---

[8] M. Amaresh, K. Markus, R. Fischer and P. Bäuerle *Angew. Chem*. **2009**, *48*, 2474.

[9] H. Choi, I. Raabe, D. Kim, F. Teocoli, C. Kim, K. Song, J-H Yum, J. Ko, Md. K. Nazeeruddin and M. Grätzel, *Chem. Eur. J.* **2010**, *16*, 1193.

[10] B. Wex, B. R. Kaafarani, E. O. Danilov and D. C. Neckers *J. Phys. Chem. A*, **2006**, *110*, 13754.

[11] K. Takimiya, Y. Konda, H. Ebata, N. Niihara and T. Otsubo *J. Org. Chem*. **2005**, *70*, 10569.

that allowed to gain insight into the molecular, ground and excited state electronic structure of the new chromophores.

### 1. Synthesis of new benzodithiophene containing Zn-porphyrins

Metal porphyrins, characterised by very strong absorption bands around 450 nm (Soret band) and 600-700 nm (Q band) are potentially interesting as dyes for DSSC. For example, some push-pull type porphyrins bearing a carboxylic acid moiety as an anchoring group, have disclosed a remarkably high power conversion efficiency (6-7%),[12] therefore in the recent years some research efforts have been devoted to the design, synthesis and application of new porphyrin-based chromophores for DSSC.[13, 14, 15]

The unique feature of these sensitizers is that the porphyrin chromophore itself constitutes the π-bridge of the D-π-A structure and with the aim of increasing the conjugation of the system, some new Zn porphyrins, containing the **BDT$_1$** unit (Figure 5), have been designed in our group.

These porphyrin molecules are differently functionalized in 5,15 and 10,20 *meso* positions. In positions 5 and 15, aromatic rings bearing bulky groups are needed to avoid aggregation on the semiconductor surface, that drastically
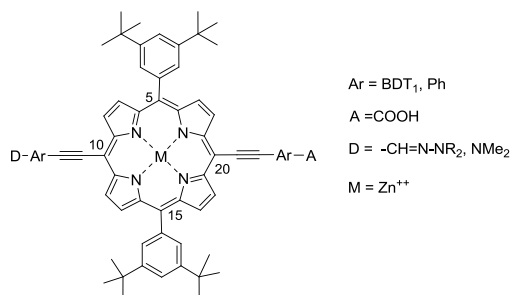


Ar = BDT$_1$, Ph
A =COOH
D = -CH=N-NR$_2$, NMe$_2$
M = Zn$^{++}$

**Figure 5**

reduce the dye light-harvesting by a filtering effect. In 10,20 *meso* positions the structure presents two π-delocalized aromatic systems with opposite (electron-withdrawing or electron-donating) properties, in order to realize a push-pull system in which is possible to modulate the position and the intensity of the Q band and to favor

---

[12] H. Imahori, T. Umeyama, S. Ito, *Accounts Of Chemical Research*, 2009, **42**, 11, 1809.

[13] Hagfeldt, A.; Boschloo, G.; Sun, L.; Kloo, L.; Pettersson, H. *Chem. Rev.* **2010**, *110*, 6595.

[14] Campbell, W. M.; Jolley, K. W.; Wagner, P.; Wagner, K.; Walsh, P. J.; Gordon, K. C.; Schmidt-Mende, L.; Nazeeruddin, M. K.; Wang, Q.; Grätzel, M.; Officer, D.L. *J.Phys. Chem. C Letters* **2007**, *111*, 11760.

[15] A. Hagfeldt, G. Boschloo, L. Sun, L. Kloo, and H. Pettersson *Chem. Rev.* **2010,** *110,* 6595.

the electron flow. The most promising structures were selected on the basis of preliminary theoretical calculations done by Dr. De Angelis and synthesized in collaboration with Prof. Ugo and Prof. Pizzotti's research group. The novel Zn-porphyrin system **1** (Figure 6) was first synthesized, whose structure is characterized by the presence of $BDT_1$ system in the acceptor part of the molecule. The suitable 2,6 di-functionalized BDT1 derivative was prepared and then linked to the porphyrin core.
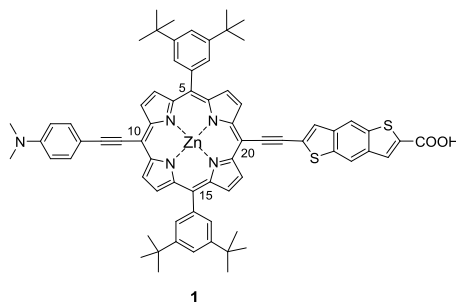


**Figure 6**

The resulting new Zn-porphyrin **1** was completely characterized from the analytical and photophysical point of view and used in preliminary tests as dye in Grätzel solar cells, giving an efficiency of 0.6%. Slightly optimization of the cell structure and in the composition of the electrolyte led to an increased efficiency of 2,54%. This result, although unsatisfactory, served as a starting point for the set-up of a number of synthetic protocols and for designing more targeted substitution and variation in the molecule structure. This part of the work is currently under progress.

## 2. Synthesis of benzodithiophene containing metal-free dye

As already mentioned, the general structure of a metal-free dye, reported in Figure 3, presents a donor and an acceptor unit linked by a π-conjugate system. The most efficient structures reported in the literature contain triarylamines as donor unit, because of the prominent electron-donating ability and hole-transport of such molecules. Within this topic we designed novel metal-free triarylamine-containing organic dyes endowed with the innovative spacers $BDT_1$ and its isomer **BDT**. Also in this case the design of the new compounds was oriented by preliminary TD-DFT calculations

made by Dr. De Angelis, on two parent BDT$_1$-containing structures **15** and **16,** which differ from each other by the presence of a triple or a double bond. (Figure 7)

With the aim to investigate the structure-performance relationship of the dyes in the cell, we designed a small library of structures, changing the BDT-bridge (**17**), the acceptor group (**18**) or the donor (**19**, **20**) with respect of the model compound **16**. (Figure **7**). This allowed us to investigate the potentiality of **BDT** and **BDT$_1$** in the dyes in combination with double or triple bond in order to elongate the conjugation, and to obtain band gap reduction and enlarge the absorption spectra. In particular, the presence of the triple bond should ensures more planarity and therefore conjugation and avoids energy losses due to photoisomerization.[16] The series of synthesized dyes are reported in figure 7.
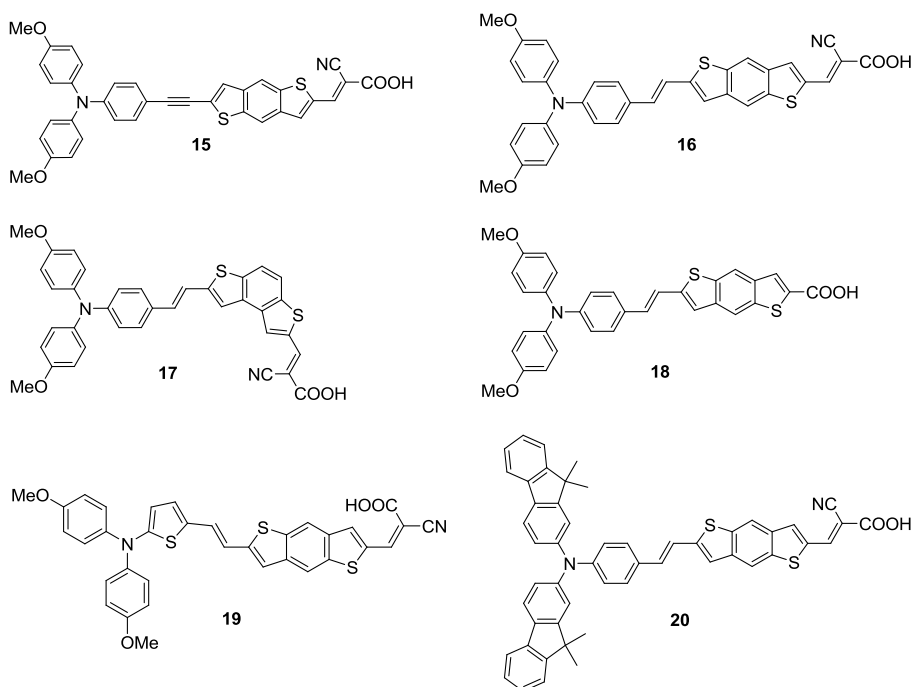


**Figure 7**

---

[16] A. Mishra, M. K. R. Fischer, and P. Bauerle, *Angew. Chem. Int*. Ed. **2009**, *48*, 2474.

Almost all the dyes synthesized have also been characterized from a photophysical as well as electrochemical point of view, with the aim of identifying, among them, the most interesting and promising compounds for application in solar cells and try to clarify the relationship between the chemical structure and photovoltaic performances.

Preliminary test in DSCs have been carried out for some of the dyes and among these dye **16** has emerged as the most promising one leading to an efficiency in liquid state cell of 5.11% and confirming the potential of **BDT$_1$** π-spacer for application in DSSCs.

The cell efficiency found for **16**, which is however still under optimization, allows us to say that this dye ranks among the promising dyes to date reported in literature. In addition, it must be pointed out that dye **16** seems to possess most of the essential chromophore characteristics required for obtaining high-performance DSSCs.

The systematic study developed during the present Ph.D. thesis will be very useful for future improvement of the synthesized structures and their photovoltaic performances in DSSCs.

Table of contents

# INTRODUCTION



*"Come into the light of things*

*let nature be your teacher"*

WILLIAM WORDSWORTH

## 1.1   WORLD ENERGY CONSUMPTION AND NEEDS OF

## RENEWABLE ENERGY

One of the most challenging issue in the recent years concern the energetic provisioning.

From the beginning of the last century, the energy demand has quickly grown up mainly due to an increasing global population and leading to the depletion of fossil fuels that arethe key energy sources of today at an alarming rate. The 2009 has been dominated by a global recession with a consequent reduction in consumption fell by 1.1%, of the total world consumption of primary energy amounted to 11200 Million tones oil equivalent (Mtoe).[1] In 2010 consumption growth reached 5.6%, the highest rate since 1973. It increased strongly for all forms of energy and in all regions so that total consumption of energy easily surpassed the pre-recession peak reached in 2008, with 12002,4 Mtoe. (Figure 1.1)



**World consumption**
Million tonnes oil equivalent

Coal
Renewables
Hydroelectricity
Nuclear energy
Natural gas
Oil

World primary energy consumption grew by 5.6% in 2010, the strongest growth since 1973. Growth was above average for oil, natural gas, coal, nuclear, hydroelectricity, as well as for renewables in power generation. Oil remains the dominant fuel (33.6% of the global total) but has lost share for 11 consecutive years. The share of coal in total energy consumption continues to rise, and the share of natural gas was the highest on record.

**Figura 1.1**

Moreover forecasts show up that the world primary energy demand will increas between 2008 and 2035, by 36%, to over 16,700 Mtoe. As almost everybody knows fossil fuel have a finite lifetime and also has negative effects on the environment.[2] With this trend and without decisive action, energy-related emissions of $CO_2$ will more than double by 2050 with unsustainable consequence economically, environmentally and socially.

Therefore there is a pressing need to accelerate the discover of advanced clean energy technologies (renewable energy) in order to address the global challenges of energy security, climate change and sustainable development.

Renewable energy includes energy derived from natural processes, that do not involve the consumption of exhaustible resources, such as fossil fuels and uranium; the main constituents are hydropower, wind and wave power, solar and geothermal energy, combustible renewable and renewable waste.

Despite high growth rates, this "clean" energy still represent only a small fraction of today's global energy consumption. Geothermal, wind and solar electricity generation combined is estimated to account for approximately 1.7% of global electricity generation.

Among them, solar photovoltaic has a very promising future.

## 1.2 SOLAR ENERGY AND PHOTOVOLTAIC

The sun is the one source that on its own could supply the world's projected energy demand and in a sustainable fashion.[3] To put it in perspective, the amount of solar energy reaching the earth in one day could power the planet for an entire year. [4] (Figure 1.2). Morover unlike other sources of energy, photovoltaic has a negligible environmental footprint, can be deployed almost anywhere and utilizes existing technologies and manufacturing processes, making it cheap and efficient to implement. Remaining is the challenge of harvesting and storing this energy in a cost-effective way.
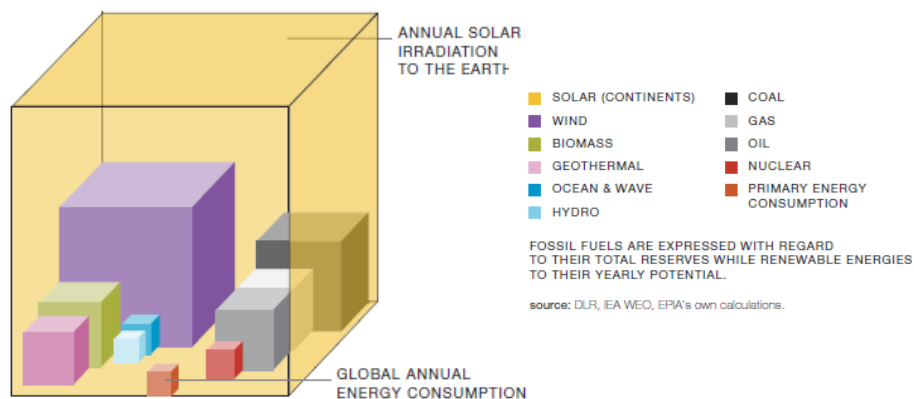
**Figura 1.2**

## 1.2.1 SOLAR HISTORY AND BASICS

A solar cell is a device that permit the direct conversion of solar light in electricity throw the photoelectric effect.

One of the first scientist to give a definition of the photovoltaic phenomena was Leon B. Linford, in "*Recent developments in the study of the external Photoelectric Effect*" (1933)[5] as: "Any processes whereby an electron absorbs an incident quantum of radiation, thereby receiving sufficient energy to free itself from its constraints may be said to be a photoelectric effect….the electrons thus set free may move in a suitable electric circuit and produce a current which would not flow in the absence of radiation".

The photovoltaic effect consists therefore of removal and confinement of elementary electric charges in distinct regions of a material when it is irradiated by electromagnetic waves in order to generate a potential difference available outside.

Photovoltaic cells are generally composed of a light absorber, either an inorganic semiconductors, an organic molecular structures, or a combination of both, that will only absorb solar photons above a certain minimum photon energy. This minimum threshold energy is the "energy gap" or "band gap" ($E_g$); photons with energies below the band gap pass through the absorber, while photons with energies above the band gap are absorbed.

## 1.2.1.1    INORGANIC CELLS

In an inorganic cell are generally present several layers of semi-conducting material (Figure 1.3), one type has mobile free negative electrons (called n-type semiconductor),

the other type has mobile free positive holes (called p-type semiconductor) and the pn-junction (the connection formed between the previous two). The operation is quite simple: light falling on the cell creates an electric field across the layers, causing electricity to flow. In particular, light reception occurs in the pn-junction. Each photon by exciting electrons from the junction valence band generates an electron-hole pair that separate and move to opposite sides of the cell structure (electrons are driven to the negative layer while "holes"



**Figure 1.3**

are left as positive). This mechanism leads to different potentials in the anode and cathode, inducing an electron flow, and in doing so generates an electrical current.
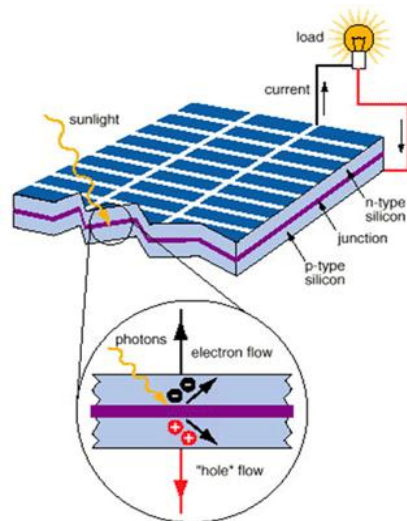
## 1.2.1.2    ORGANIC CELLS

Organic solar cells have the same working principle of inorganic cells, it consist in two layers of organic materials that differ in electron donating and accepting properties that are close together. Charges are created by photoinduced electron transfer between the

two components. This photoinduced electron transfer between donor and acceptor boosts the photogeneration of free charge carriers compared to the individual, pure materials, in which the formation of bound electron-hole pairs, or excitons is



**Figure 1.4**

generally favored. As before, the energy of the photons must first exceed a certain threshold to be absorbed, that is the energy gap between LUMO (Lowest Unoccupied
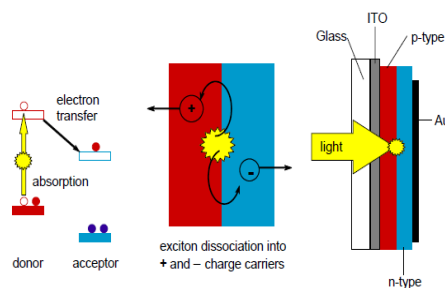
Molecular orbital)and HOMO (Highest Occupied Molecular Orbital). In particular, the illumination of the donor layer(in red) result in the photoexcited state in which an electron is promoted from the HOMO to the LUMO of the donor.Subsequently, the excited electron is transferred to the LUMO of the acceptor (in blue), resulting in an extra electron on the acceptor (A•-) and leaving a hole at the donor (D•+). The photogenerated charges are then transported and collected at opposite electrodes.

## 1.2.1.3    HYBRIDE ORGANIC-INORGANIC CELLS

In Hybrid organic-inorganic cells (Dye Sensitized Solar Cells, DSSCs) the light absorber layer is constituted of an organic dye (also called sensitizer) adsorbed at the surface of an inorganic wideband-gap semiconductor. The working principle is different in respect to the other kind of cells: after absorption of light by the dye, an electron is transferred to the inorganic semiconductor. The dye is then reduced by a redox electrolyte, which in turn, is reduced at the metal counter electrode, while the electron is transported to the electrode.
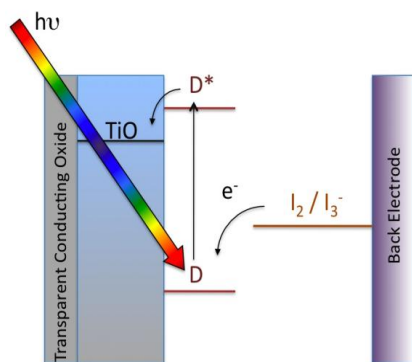


**Figure 1.5**

This technology, object of this thesis, will be extensively treated in the next chapters.

Between this last technology and the previous two the main difference is that: in inorganic and totally organic cell the light absorption and charge separation are directly coupled and both occur within the semiconductor; in dye sensitized solar cells these two processes are separated. Light adsorption is achieved by the dye, while charge separation occurs when the acquired light energy of the now excited dye is passed to the semiconductor in the form of an electron.

## 1.2.2 SOLAR SPECTRUM

Each second, the sun releases an enormous amount of radiant energy into the solar system. The temperature at the centre of the sun is high enough to facilitate nuclear reactions, which are assumed to be the source of the sun's energy. It emits light with a

range of wavelengths from the ultraviolet (200 - 400 nm) and visible (violet, 390 nm -
red ,740 nm) to the infrared (700 nm to 1mm).[6] (Dotted line Figure 1.6) It peaks in the
visible, resembling the spectrum of a blackbody at a temperature of 5760 K. It is,
however, influenced by atmospheric absorption and the position of the sun.

As the Sun's rays pass through the atmosphere certain wavelengths are absorbed and a
proportion of the total energy is scattered. Thus the solar spectrum at the Earth's
surface has some wavelengths missing (Solid line Figure 1.6)[7] and the overall intensity is
reduced. In particular, ultraviolet light is filtered out by ozone, and water and $CO_2$
absorb mainly in the infrared making dips in the solar spectrum at 900, 1100, 1400, and
1900 nm ($H_2O$) and at 1800 and 2600 nm ($CO_2$), respectively.
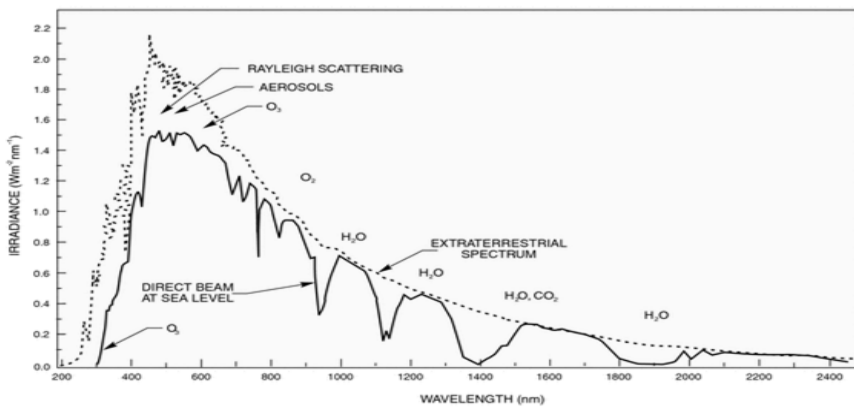


**Figure 1.6**

The amount of energy reflected, scattered and absorbed depends on the amount of
atmosphere that the incident radiation travels through as well as the levels of dust
particles and water vapour present in the atmosphere. The latter is difficult to judge but
the distance travelled through the atmosphere by incident radiation depends on the
angle of the Sun. This distance is the shortest when the sun is at the zenith, i.e. directly
overhead. The ratio of an actual path length of the sunlight to this minimal distance is
known as the optical air mass. When the sun is at its zenith the optical air mass is unity
and the radiation is described as air mass one (AM1) radiation. When the sun is at an
angle $\vartheta$ to the zenith, the air mass is given by the equation:

$$Air\ mass\ = (\cos\vartheta)^{-1} \qquad\qquad eq\ 1.1$$

AM0 radiation is the extraterrestrial spectrum of solar radiation outside the Earth's atmosphere, which power density is the solar constant. Opposed to the situation outside the Earth's atmosphere, terrestrial solar radiation varies both in intensity and spectral distribution depending on the position on the Earth and the position of the sun in the sky. In order to allow comparison between the performances of solar cells tested at different locations, a terrestrial solar radiation standard has to be defined and measurements referred to this standard. The standard solar spectrum used for efficiency measurements of solar cells is AM 1.5 G (global), that corresponds to an angle of 48.2 degrees between the Sun's position and the zenith. (Figure 1.7)

This spectrum is normalized so that the integrated irradiance (the amount of radiant energy received from the sun per unit area per unit time) is 1000 W m$^{-2}$. The standard solar spectrum used for efficient AM1.5 G (global)radiation serves at present as the standard spectral distribution.



**Figure 1.7**

The irradiance varies depending on the position of the Sun, orientation of the Earth, and sky conditions. We can also distinguish sunlight in direct or diffuse light. The direct component can be concentrated, which increases the solar cell efficiency by increasing cell voltage outputs. Diffuse light arises by scattering of the sunlight in the atmosphere. This fraction is around 15% on average but larger at higher latitudes and in regions with a significant amount of cloud cover. Materials with rough surfaces such as DSCs are relatively better suited for diffuse light than perfectly flat surfaces and are less sensitive to movements of the sun.
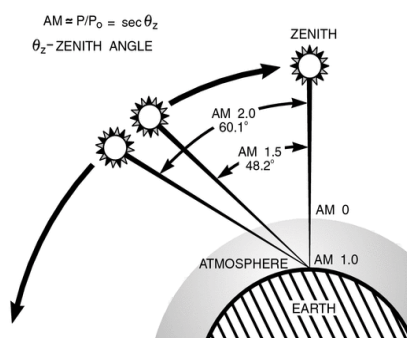
## 1.2.3 PHOTOVOLTAIC CELL PERFORMANCE

The performance of a cell is evaluated by means of several parameters such as "external quantum efficiency", which in the DSC community is normally called the incident photon to current conversion efficiency (IPCE), the relationship ($J/V$), open circuit voltage ($V_{OC}$), the shortcircuit current ($J_{SC}$), fill factor (FF), and the light-to-electrical power conversion efficiency of a solar cell ($\eta$).

The parameter $\eta$, for a solar cell is given by the photocurrent density measured at short-circuit ($J_{SC}$), the open-circuit photovoltage ($V_{OC}$), the fill factor of the cell (FF), and the intensity of the incident light ($P_{in}$) according with the formula:

$$\eta = (J_{SC} \times V_{OC} \times FF) / P_{in} \qquad \text{Eq 1.2}$$

The fill factor can assume values between 0 and less than 1 and describes how well the area under the $JV$ curve "fills in" the maximum possible rectangle defined by $J_{SC} \times V_{OC}$. (Figure 1.8). It is defined by the ratio of the maximum power ($P_{max}$) of the solar cell per unit area divided by the $V_{OC}$ and $J_{SC}$ following the formula:

$$FF = P_{max} / (J_{SC} \times V_{OC}) \qquad \text{Eq 1.3}$$

The maximum power is obtained as the product of the photocurrent $J_p$ and at the voltage $V_p$ where the power output of the cell is maximal as shown in Figure 1.8.
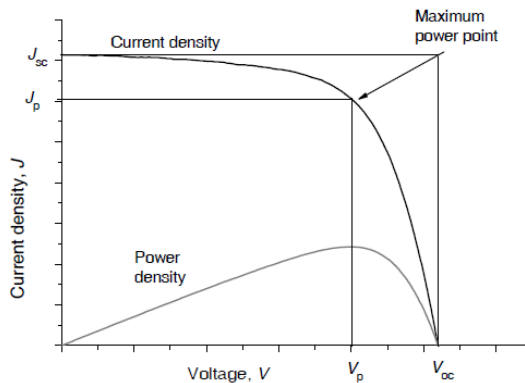


**Figure 1.8**

This current-voltage (*JV*) curves represent the most important and most direct characterization method for DSCs and for solar cells in general. The open circuit voltage ($V_{OC}$), short circuit current ($J_{SC}$) and the shape of the JV curve determine the efficiency η of DSCs under any given light condition.

In particular $J_{SC}$ is the photocurrent per unit area under short-circuit condition, it is related to the optical properties of the dye, as well as to different dynamic processes in the cell, while $V_{OC}$ is the maximum voltage available from a solar cell at zero current. It is the difference between the *quasi*-Fermi level of the semiconductor and the redox potential of the electrolyte. The Fermi Level is defined as the highest occupied molecular orbital in the valence band at 0 K, in semiconductors its position of the is in the band gap, close to the valence band.

IPCE is defined as the number of collected electrons under short circuit conditions per number of incident photons at a given excitation wavelength λ and gives the ability of a cell to generate current as a function of the wavelength of the incident monochromatic light. IPCE is calculated by measuring the short-circuit photocurrent as a function of the monochromatic photon flux.

$$IPCE\ (\%) = (1240\ (eV\ nm)\ x\ J_{sc}\ (mA\ cm^{-2})\ )/\ (\lambda\ (nm)\ P_{in}\ (mW\ cm^{-2})) \qquad \text{Eq. 1.4}$$

In a DSC cell EQE/IPCE is determined by the sensitizer light harvesting efficiency at λ (LHE), the quantum yield for electron injection from S* to the semiconductor oxide ($\Phi_{inj}$), and the charge collection efficiency ($\Phi_{coll}$), the product of the latter two parameters giving the absorbed photon-to-current efficiency (APCE) or internal quantum efficiency.

$$IPCE\ (\lambda) = LHE\ \Phi_{inj}\ \Phi_{coll} \qquad \text{Eq. 1.5}$$

The integral of IPCE with the AM 1.5 G spectrum gives the photocurrent, which should match that measured under the solar simulator. Therefore higher IPCE and broader spectra correspond to higher $J_{sc}$.

The efficiency of the solar cell depends also by its temperature and, even more important, on the quality of the illumination, i.e. the total light intensity and the spectral distribution of the intensity. For this reason, a standard measurement condition has been developed to facilitate comparable testing of the solar cells between different laboratories. In the standard condition used for testing of terrestrial solar cells, the light intensity is 1000 W/m$^2$ the spectral distribution of the light source is of AM1.5 global standard solar spectrum (Figure 1.6), and temperature of the cell is 25°C. The power output of the solar cell at these conditions is the nominal power of the cell, or module, and is reported in *peak* watts, W$_p$. In practice, special solar simulator light sources are used for the standard measurements.

## 1.2.4 SOLAR TECHNOLOGY

The main solar active technologies are three: photovoltaic (PV) cells, concentrating solar power (CSP) systems and solar thermal collectors for heating and cooling (SHC).

PV systems directly convert solar energy into electricity, CSP use concentrated solar radiation as a high temperature energy source to produce electrical power and drive chemical reactions while SHC uses the thermal energy directly from the sun to heat or cool domestic water or building spaces.

PV technologies are classified as first, second or third generation. First generation technology is the basic crystalline silicon (c-Si). Second generation includes Thin Film technologies, while third generation includes concentrator photovoltaics, organics, and other technologies that have not been commercialized yet at large scale.

### 1.2.4.1 CRYSTALLINE SILICON TECHNOLOGY

Crystalline silicon is the most common and mature technology representing about 80% of the market today. Cells, called mono crystalline (mc-Si), multi or polycrystalline (pc-Si) depending on the fabrication route, can turn between 14 and 22% of the sunlight that reaches them into electricity and efficiency ranges between 12 and 19%.

Despite these efficiencies are the highest never reached, this technology has several disadvantages such as important consumption of the raw materials and high-temperature fabrication processes that are very energy intensive and expensive.

## 1.2.4.2    THIN FILMS

Thin Film modules are constructed by depositing extremely thin layers of photosensitive material onto a low-cost backing such as glass, stainless steel or plastic. Once the deposited material is attached to the backing, it is laser-cut into multiple thin cells. Thin Film modules are normally enclosed between two layers of glass and are frameless. If the photosensitive material has been deposited on a thin plastic film, the module is flexible. This creates opportunities to integrate solar power generation into the fabric of a building or end-consumer applications.

The main advantages of thin films are therefore their relatively low consumption of raw materials, high automation and production efficiency, ease of building integration and improved appearance, good performance at high ambient temperature, and reduced sensitivity to overheating. The current drawbacks are lower efficiency and the industry's limited experience with lifetime performances. Increased R&D is needed to bring thin film technologies to market and to create the necessary experience in industrial manufacturing and long term reliability.

Four types of Thin Film modules are commercially available: amorphous silicon, Multi-junction thin silicon film, Cadmium telluride, indium-gallium-(di)selenide/(di)sulphide (IGS) and copper-indium-(di)selenide/(di)sulphide (CIGS).

**Amorphous silicon (a-si)**

Amorphous silicon can absorb more sunlight than c-Si structures therefore the semiconductor layer is only about 1 µm thick. However it leads to lower efficiencies in the range of 4 to 8% but has other advantages such as a lower temperature coefficient for power loss. With this technology the absorption material can be deposited onto very large substrates (up to 5.7 m² on glass), reducing manufacturing costs that are therefore only slightly lower than that of c-Si mainly because of expensive manufacturing equipment.

## Multi-junction thin silicon film (a-Si/µc-Si)

This consists of an a-Si cell with additional layers of a-Si and micro-crystalline silicon (µc-Si) applied onto the substrate. The µc-Si layer absorbs more light from the red and near infrared part of the light spectrum. This increases efficiency by up to 10%. The thickness of the µc- Si layer is in the order of 3 µm, making the cells thicker but also more stable.

## Cadmium telluride (CdTe)

CdTe Thin Films cost less to manufacture and have a module efficiency of up to 11%. This makes it the most economical Thin Film technology currently available.

The two main raw materials are cadmium and tellurium. Cadmium is a by-product of zinc mining, while tellurium is a by-product of copper processing. Tellurium is produced in far lower quantities than cadmium and its availability in the long-term may depend on whether the copper industry can optimise extraction, refining and recycling yields. The drawbacks include the toxicity and low abundance of the materials, temperature-dependent efficiencies, and only an average light tolerance.

## Copper, indium, gallium, (di)selenide/ (di)sulphide (CIGS) and copper, indium, (di)selenide/(di)sulphide (CIS)

CIGS and CIS offer the highest efficiencies of all Thin Film technologies. Efficiencies of 20% have been achieved in the laboratory, close to the levels achieved with c-Si cells. The manufacturing process is more complex and less standardized than for other types of cells and this tends to increase manufacturing costs. Current module efficiencies are in the range of 7 to 12%.

There are no long-term availability issues for selenium and gallium, Indium is available in limited quantities but there are no signs of an incoming shortage. While there is a lot of indium in tin and tungsten ores, extracting it could drive the prices higher. A number of industries compete for the indium resources it is  therefore highly likely that indium prices will remain high in the coming years.

## 1.2.4.3     THIRD GENERATION PHOTOVOLTAIC

After more than 20 years of research and development, third generation solar devices are beginning to emerge in the marketplace. Many of the new technologies are very promising. One exciting development is organic PV cells. These include both fully organic PV (OPV) solar cells and the hybrid dye-sensitised solar cells (DSSC).

Current OPV cell efficiencies are about 6% for very small areas and below 4% for larger areas, while for DSSCs efficiencies achieved at the laboratory across a very small area are in the range of 8 to 12%. Some low-power application already commercially available still have efficiency below 4%. The next section will give more details on this type of photovoltaics.

For both technologies several are the advantages such as the possibilities of design molecule and materials with the characteristics needed (facile chemical tailoring to alter their properties, such as the band gap), the low cost of starting material and the possibility of using standard manufacturing process and printing technologies for the preparation of the cells. The manufacturing costs is in addition constantly decreasing and is expected to reach 0.50€/W by 2020. Still the major challenges for this sector are the low device efficiency and their instability in the long-term.

In Table 1.1 are review the efficiency and main characteristic ranges of photovoltaics technologies.[8]

| Type | Material | Structure/process | Measured conversion efficiency (%)[3] | Cost competitiveness | Advantages | Disadvantages (Necessary improvements) |
|---|---|---|---|---|---|---|
| Si-based | Single-crystal Si | n-type Si layer doped on single-crystal p-type Si layer | 25.0 | × | High efficiency, high reliability | Not suited for mass production; High cost, variable raw material price, little room for improvement in conversion efficiency |
| | Polycrystalline Si | n-type Si layer doped on polycrystalline p-type Si layer | 20.4 | △ | Lower cost than single-crystal Si; High efficiency, high reliability | Lower efficiency than single-crystal Si; Variable raw material price |
| | Amorphous Si | p-layer, i layer, and n layer deposited by CVD process | 9.5 | △ | Relatively small use of Si material; Lower cost than single-crystal Si | Lower efficiency than single-crystal Si; Light degradation |
| Compound-based | GaAs | Metal-organic CVD | 26.1 | × | High efficiency; Endure radiations in space | Low deposition rate; Using toxic As; High cost |
| | CdTe | p-type CdTe polycrystalline layer on n-type CdS layer | 16.7 | △ | A variety of production methods; Optimum band gap for generation; Lower cost than single-crystal Si | Using highly toxic Cd; Dependent on the amount of Te resources |
| | CIS/CIGS | Vapor deposition of CIS/CIGS layers | 19.4 | △ | High optical absorbance | Dependent on In resources |
| Dye-sensitized | Dye, semiconductor, electrolyte | Place dye-absorbed TiO2 electrode in electrolyte | 10.4 | ○ | Capable of production by simple process in open air; Colorable, transparent; Maintain generation characteristics under room light etc. | Ultraviolet degradation |
| Organic thin film based | Fullerene, polymer | Apply mixture of p-type polymer and n-type fullerene etc. | 5.2 | ○ | Little thickness; Capable of manufacturing by inexpensive application process | Ultraviolet degradation; Low efficiency |

Prepared by the STFC

**Table 1.1**

## 1.2.5 MARKET TRENDS

Today, PV provides only 0.1% of total global electricity generation but, due to effective supporting policies and recent dramatic cost reductions, it is expanding very rapidly and it has significant potential for long-term growth over the next decades (5% of global electricity consumption in 2030).[9] Since 2000 global PV capacity has been increasing at an average annual growth rate of more than 40%. The cumulative installed[1] PV power capacity has grown in 2010 from 0.1 GW in 1992 to 40 GW world-wide, producing some 50 terawatt-hours (TWh) of electrical power every year. Figure 1.9.
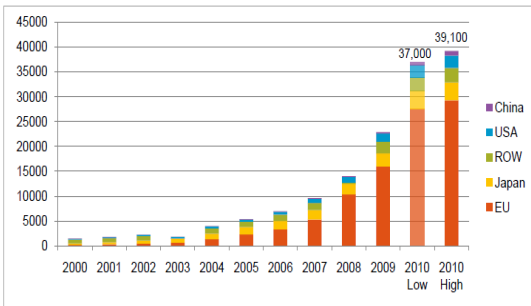
**FIGURE 1.9**

In terms of global cumulative installed capacity, the EU leads the way with almost 30 GW installed as of 2010. This represents about 75% of the world's total cumulative PV capacity (up from 70% in 2009). Japan (3.6 GW) and USA (2.5 GW) are some way behind, while China has already entered the Top 10 of the world's PV markets and should reach its first GW in 2011. Forecast made by EPIA (European Photovoltaic Industry Association) shows that installed PV capacity in the world could reach 131 GW in 2015, more than the double of today.[9] Figure 1.10

|  | 2010 | 2011 | 2012 | 2013 | 2014 | 2015 |
|---|---|---|---|---|---|---|
| China | 893 | 1,643 | 3,143 | 5,143 | 7,643 | 10,643 |
| APEC | 1,191 | 1,605 | 2,347 | 3,274 | 4,577 | 6,089 |
| Rest of the world | 1,844 | 2,644 | 4,144 | 6,144 | 8,144 | 10,144 |
| North America | 2,727 | 4,477 | 7,827 | 12,227 | 17,677 | 24,177 |
| Japan | 3,622 | 4,672 | 5,922 | 7,422 | 9,172 | 11,172 |
| EU | 29,252 | 37,817 | 44,812 | 52,222 | 60,072 | 68,992 |
| Total | 39,531 | 52,930 | 68,175 | 86,415 | 107,300 | 131,255 |
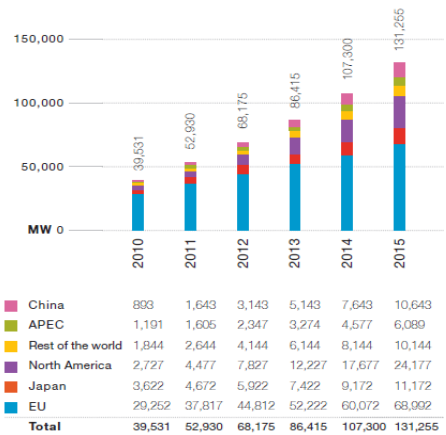
**FIGURE 1.10**

---

[1]The cumulative installed capacity refers to installations that can make a real contribution to meeting the energy demand

## 1.2.6 PRICES

Over the past 30 years the PV industry has achieved impressive price decreases. The price of PV modules has reduced by 22% each time the cumulative installed capacity (in MW) has doubled. (Figure 1.11 ) The decrease in manufacturing costs and retail prices of PV modules and systems (including electronics and safety devices, cabling, mounting structures, and installation) have come as the industry has gained from economies of scale and experience. This has been brought about by extensive innovation, research, development and ongoing political

kWh (depending on the region and the amplitude of the system estimated between) almost the same cost of the electricity generated in existing



price-experience factor of 22%

(US$/Wp) 2010

MW

— c-Si LOW
-- c-Si HIGH
— c-Si TREND
— TF
— TF TREND

source: Navigant Consulting, EPIA.

**FIGURE 1.11**

gas and coal-fired power plants. However the use of finite resources for power generation (such as oil, gas, coal and uranium), in addition to growing economic and environmental costs will lead to increased price for energy generated from fossil and nuclear fuels creating a real driver for the full competitiveness of PV.
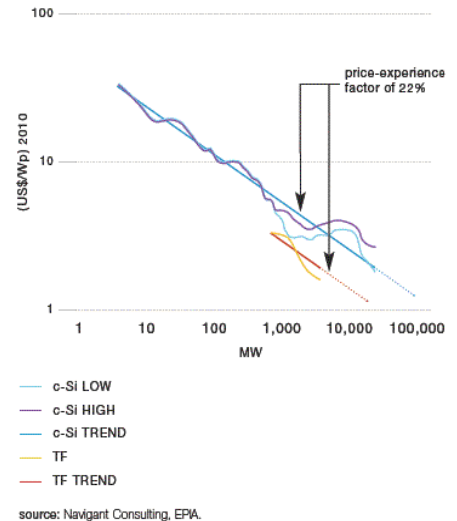
Making a comparison between the prices of the different technologies present on the market, the crystalline Silicon technology has the lowest price thanks mainly to his maturity followed by thin film technologies in which the reduction depend basically from the lower amount of material used. On the contrary, for the moment the new organic technologies costs are still the highest due to the initial level of the development. Moreover organic based photovoltaic seems to be the most promising technology in line with the primary goal to introduce more environmentally friendly materials, to replace scarce resources (silver, indium, tellurium, lead, cadmium) and reduce material usage and energy requirements.

# REFERENCES

[1] BP Statistical Review of World Energy June **2010**.

[2] A. M. J. Omer, Renewable Sustainable Energy **2009**, 1, 053101.

[3] United States, Department of Energy, Energy Information Administration, http://www.eia.doe.gov/.

[4] Solar generation 6: Solar photovoltaic electricity empowering the world **2011**.

[5] L. B. Linford, *Rev. Mod. Phys.*, **1933**, *5*, 34.

[6] A. Hagfeldt,G. Boschloo, L. Sun, L. Kloo, H. Pettersson, *Chemical Reviews*, **2010**, *110*(11), 6595.

[7]http://www.newport.com/Introduction-to-Solar-radiation/411919/1033/content.aspx.

[8] J. Kawakita, *Science and technology trends- Quarterly Review,* April **2010**, *35*, 70.

[9] EPIA, Global Market for photovoltaic until 2015

# DYE-SENSITIZED SOLAR CELLS (DSSCS)



*Nature has put itself the problem of how to catch in flight light streaming to the Earth and to store the most elusive of all powers in rigid form. The plants take in one form of power, light; and produce another power, chemical difference.*
ROBERT MAYER

## 2.1   FROM THE BEGINNING TO NOWADAYS

Scientists have been infatuated with photoelectric molecules since more than 100 years ago. Sensitization of wide band gap semiconductors using dyes has a long history, dating back to early days of photography of the 19$^{th}$ century:[1] after Vogel's discovery[2] in 1883 that silver halide emulsions could be sensitized by adding a dye extended the photosensitivity to longer wavelengths, Moser observed that the photoelectric effect on silver plates was enhanced in the presence of erythrosine dye.[3]

It is an interesting convergence of photography and photo-electrochemistry, both of which rely on photo-induced charge separation at a liquid–solid interface.

However the foundation of modern photoelectrochemistry, marking its change from a mere support of photography to a thriving research direction on its own, is due to the work of Brattain and Garret[4] and subsequently Gerischer[5] who undertook the first detailed electrochemical and photoelectrochemical studies of the semiconductor–electrolyte interface. Most of these early studies were aimed to understand electron–transfer processes involving valence and conduction bands of a semiconductor immersed in a redox electrolyte.

In subsequent years the idea that the dye could function most efficiently if chemisorbed on the surface of the semiconductor[6, 7], emerged in the use of dispersed particles to provide a sufficient interface[8], and subsequently photo-electrodes were employed.[9]

The first dye-sensitized solar cell present to the world, was developed in 1976 by Professor Tsubomura et al. at Osaka University, using porous zinc oxide as the dye support. The energy conversion efficiency was 2.5%.[7] The next year a US patent entitled *Dye-sensitized Schottky barrier solar cells* was submitted by Terje A. Skotheim including almost all the major characteristics of today's DSSC. In 1980 Ruthenium based dyes had been identified by the Dare-Edwards group in England[10] and this represented a starting point for DSSCs. The use of dye-sensitization in photovoltaics remained however rather unsuccessful until a breakthrough: the publication of an article by Professor Grätzel et al. at EPFL, Switzerland, in 1991[11]. In this paper he reported an improved conversion

efficiency of 7.12% using Titanium dioxide as semiconductor and a *tris*(2,2'-bipyridyl-4,4'-carboxylate) ruthenium(II) as dye.

That evolution has continued progressively until the first half of 2009, when the maximum cell conversion efficiency of 11.2% was reported by Sharp Corporation and the maximum module efficiency of 8.4% by Sony Corporation. In August 2010 the same company announced a prototype DSC module with a power conversion efficiency of 9.9%.

Since 1991 the interest in this technology increase rapidly and tremendously as confirmed by a simple and limited literature search on the growth of the number of research papers (Figure 2.1a) and patents (Figure 2.1b) over the last years, using the keywords "dye-sensitized" and "solar".
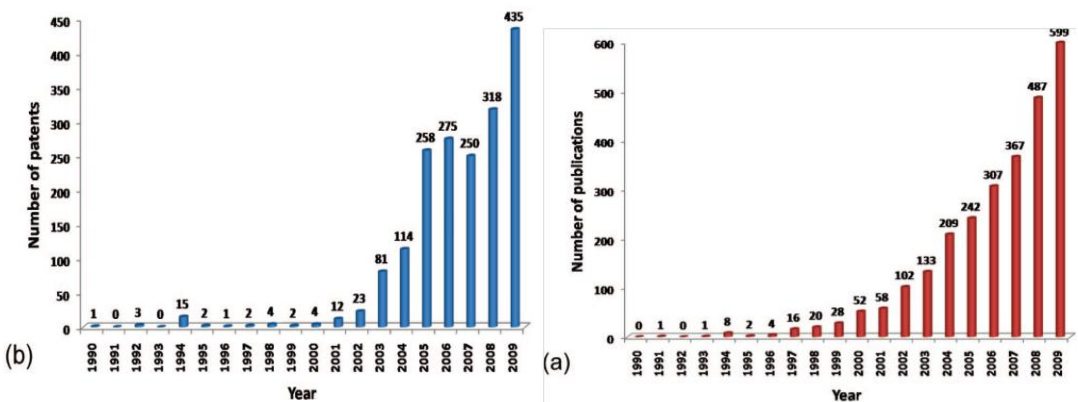


**Figure 2.1**

This surprising development is due to the great potentiality of this technology and its advantages:[12]

1. The solar cells and panels can be produced in a simple way in open air, no vacuum process is required for manufacturing. This means a significant cost reduction of 1/5 to 1/10 as compared to silicon solar cells.

2. The use of dye and its wide selection allow colored cells and transparent cells.

3. Using aggregates of fine particles of photoelectric conversion materials, the solar cells can be formed as flexible thin films.

4. Charge generation characteristics insusceptible to the incident angle and intensity of the sunlight it can be maintained even in a weak light condition, such as under faint light in the morning and evening and when indoors.

5. Plastic substrates can be used to reduce the weight of solar cells and panels.

6. Short energy payback time.

With these advantages, dye-sensitized solar cells can be installed in locations where appearance is important and other solar cells are hardly applicable, such as the glass panes and inner and outer walls of a building, the sunroof and outer panels of an automobile, and the enclosure of a cellular phone. This allows the creation of new markets with expanded demand. Figure 2.2 shows a prototype models for dye-sensitized solar cell panels.

**Figure 2.2**

Such panels can be installed on the colored arched roof of a garage, taking advantage of the excellent design and drainage performance. The panels can be variously freely decorated for room walls, windows, and interior use.

## 2.2 OPERATING PRINCIPLE

The dye sensitized solar cell (DSSC) is a photoelectrochemical device that is inspired to the photosynthesis process, where a dye is used to catch the light then transformed in an other form of energy. The device is comprised of two faced electrodes, a photoanode and a counter electrode, with an electrolyte in between. Figure 2.3 Both electrodes are usually made from a sheet of common float glass coated on one side with a thin transparent conductive layer of fluorine-doped tin dioxide (FTO) or indium-doped tin oxide (ITO). The cathode is a conductive glass covered with a few clusters of metallic platinum which has a catalytic effect in the reduction process of the electronic mediator acceptor member.
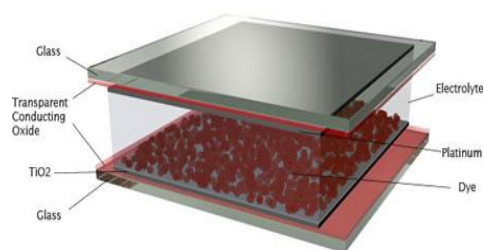
**Figura 2.3**

In the photoanode, the transparent conductive electrode is covered with a thin film of a mesoporous semiconductor oxide, normally $TiO_2$ (anatase) although alternative wide band gap oxides such as $ZnO$,[13] and $Nb_2O_5$[14] have also been investigated.

Attached to the surface of the nanocrystalline film is a monolayer of the charge transfer dye (S). Photo-excitation of the sensitizer in his excited state (S*) results in the injection of an electron into the conduction band of the oxide. The original state of the dye (S) is subsequently restored by electron donation from the electrolyte, usually an organic solvent containing redox system, such as the iodide/triiodide ($I^-/I_3^-$) couple. The regeneration of the sensitizer by iodide intercepts the recapture of the conduction band electron by the oxidized dye. The iodide is regenerated in turn by the reduction of triiodide at the counterelectrode and the circuit being completed via electron migration through the external load. A schematic presentation of the operating principles of the DSSC is given in Figure 2.4

Fundamental requirement for the well-working of the process are that the excited state of the sensitizer must be higher in energy in respect of the bottom of the semiconductor's conduction band while the dye's oxidized state must be lower in energy of the potential of the redox system.



| | | |
|---|---|---|
| $S° + h\nu$ | $S*$ | photoexcitation |
| $S* + TiO_2$ | $S^+ + (e^-, TiO_2)$ | electron injection |
| $2S^+ + I^-$ | $2S + I_3^-$ | sensitizer regeneration |
| $I_3^- + 2e^-$ | $3 I^-$ | electron donor regeneration |
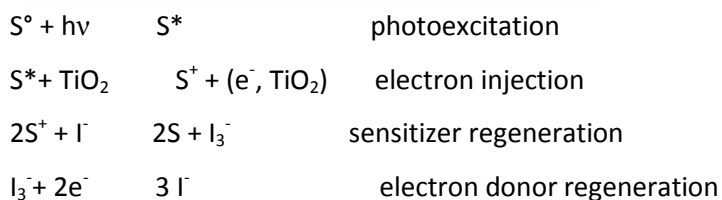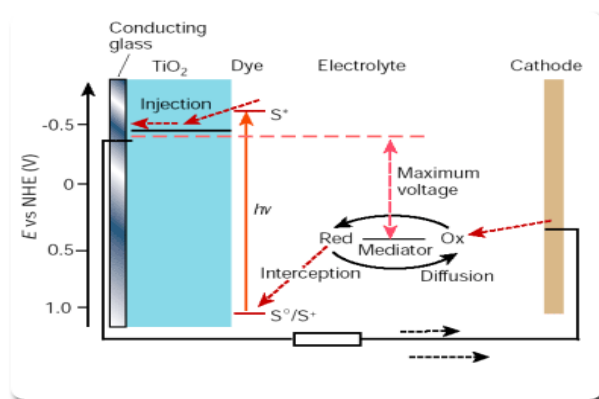
**Figure 2.4**

The entire cycle consists in the quantum conversion of photons to electrons as a result, no net chemistry occurs, but electrical work has been produced.

These reactions enter in competition with a series of unwanted reactions that might occur within the system. Photoinjected electrons should escape from any recombination process in order to have a unit charge collection efficiency at the photoelectrode back contact. The two major waste processes in a DSC are due to back electron transfer, at the semiconductor-electrolyte interface, between electrons in the conduction band and the oxidized dye molecules, and reduction of $I_3^-$ at the semiconductor nanoparticles surface:

$$S^+ + (e^-, TiO_2) \longrightarrow S \qquad \text{back electron transfer}$$
$$I_3^- + 2(e^-, TiO_2) \longrightarrow 3\,I^- \qquad \text{electron capture from mediator}$$

**Figure 2.5**

As a consequence, the timescales of these reactions and the competition between different channels are the key point for efficient current collection. Figure 2.6 is a photochemical view of the function of a DSSC, illustrating the sequence of electron transfer and charge-transport processes which result in photovoltaic device function and their kinetics. In addition to the forward electron transfer and transport processes (blue arrows), this figure also illustrates several competing loss pathways, shown as black arrows. These loss pathways include decay of the dye excited state to ground, and charge recombination of injected electrons with dye cations and with the redox couple. Each charge-transfer step results in an increased spatial separation of electrons reducing the free energy stored in this state. This functionality exhibits a close parallel to function of photosynthetic reaction centres. As in natural photosynthesis, kinetic competitions between the various forward and loss pathways are critical to determine the quantum efficiencies of charge separation and collection, and are therefore key factors determining energy conversion efficiency. For this reason the various processes in the cell have been widely studied in the last decade.
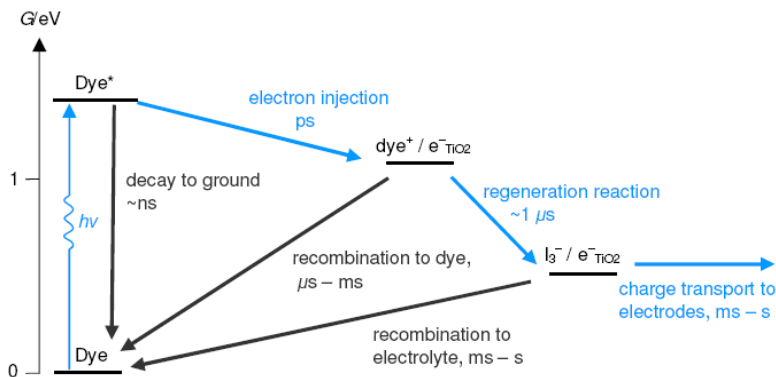
**Figure 2.6**

The vertical scale correspond to the free energy G stored in the charge separated steps. Note the free energy of injected electrons is determined by the Fermi level of the TiO$_2$; the figure is drawn assuming a TiO$_2$ Fermi level 0.6 V above the chemical potential of the redox electrolyte (corresponding to a cell voltage of ~0.6 V, close to the maximum power point of typical DSSCs)

Principles of functioning and main components of dye sensitized solar cells, as the electron transfer processes, the properties of the semiconductor materials, the sensitization of the semiconductor and the kinetic requirements of the electron transfer mediators, will be described in the next paragraphs of this chapter.

# 2.3   CELL COMPONENTS

## 2.3.1 CONDUCTING SUBSTRATE

DSSCs are typically fabricated on transparent conducting oxide (TCO) glass substrates, enabling light irradiance through this substrate under photovoltaic operation. Suitable TCO must have high electrical conductivity to efficiently collect all the generated photocurrent. Among a high variety of TCOs, the conductive coating typically used is fluorine-doped SnO$_2$ (FTO), preferred over its indium-doped analogue (ITO) for reasons of lower cost and enhanced stability.

These conducting glass electrodes are known not to be really efficient in the reduction of $I_3^-$, therefore a catalyst is needed in the counter electrode to overcome the high activation energy of the two-electron transfer. Since the electrolyte is corrosive, the counter electrode requires high corrosion resistance as well as high reaction rate when reducing iodine in the electrolyte to an iodide ion. Considering the balance between these factors, platinum is clearly the most widely used material, acting as a catalyst in the redox reaction at the counter electrode and thus avoiding this process becoming rate limiting in the light energy harvesting system.

This material, however, has some disadvantages: apart from its high price, there is a non-confirmed possibility of corrosion by the iodide solution, which leads to the formation of $PtI_4$.[15] Carbon electrodes[16] and conductive polymers have been therefore examined as an alternative to expensive Pt, whereas such materials are not so efficient in terms of the reduction rate.

## 2.3.2 SEMICONDUCTOR

The main used semiconductor for this application is the titanium dioxide, that presents many advantages for sensitized photochemistry and photo-electrochemistry: it is a low cost, chemically inert, widely available, non-toxic and biocompatible material, as demonstrated by its use in health care products as well as domestic applications, such as paint pigmentation. [17]

It is present in nature in several form: rutile ,the most common, brookite and anatase, which is the thermodynamically stable crystalline form at high pressure.

Anatase has been widely used because because its high band gap energy (3.2 eV, and absorbs only below 388 nm) making it invisible to most of the solar spectrum, reducing the recombination rate of photo-injected electrons.

At first, most sensitization studies involved electrochemical measurements of sensitized wide-bandgap semiconductor planar electrodes. (Figure 2.7a) These allowed to measure efficient electron injection and demonstrated that dye sensitization was a strategy for populating the conduction band of semiconductors with electrons under visible light. However, the development of efficient devices for current collection was impossible,

due to the low light harvesting capability of single layers of the absorber on the surface and therefore low current densities.[18] A breakthrough was constituted by the replacement of the planar electrode by a mesoporous nanocrystalline semiconductor film (Figure2.7b), possessing a high surface area[19] that allows a bind of the sensitizer three orders of magnitude larger than the geometric area of a 10 $\mu m$ thick sample.
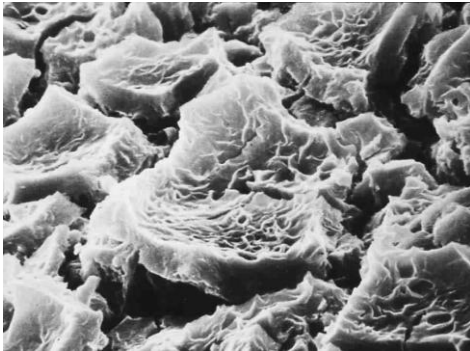


**a**

Scanning electron microscope picture of the fractal TiO$_2$ film used in the first DSC embodiment (1988)
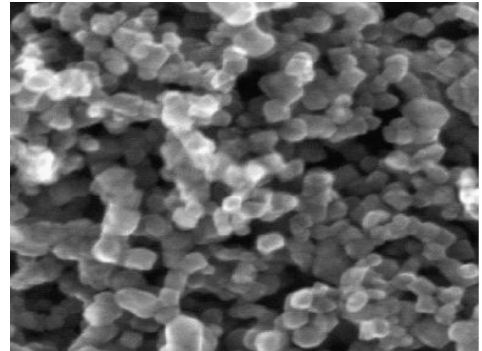


**b**

Scanning electron microscope picture of a nanocrystalline TiO2 (anatase) film used in DSC[20].

**Figure 2.7**

This permitted a drastic increase of the performances of DSSCs, reaching currently a power conversion yield of 12 %.[3]

Indeed, nanocrystalline morphology of TiO$_2$ indeed is a fundamental requirement in determining the solar conversion efficiency. The use of a porous nanostructured film of very high surface roughness directly affects the light harvesting efficiency. When light penetrates the photosensitized semiconductor "sponge" it crosses hundreds of adsorbed dye monolayers. Thereby photons whose energy is close to the absorption maximum of the dye are almost completely absorbed.[3] Thus the mesoporous morphology of the film, consisting of nanocrystalline oxide particles with a diameter of 10-20 nm[21] sintered together to allow electronic conduction plays a crucial role in the harvesting of sunlight. Depending on film thickness, their real surface area can easily be made 100-1000 times larger than the apparent one.

It's known in the literature[22] that this mesoporous films doesn't promote charge carrier loss by recombination, but because the injected electron has to be transported across a

large number of colloidal particles and grain boundaries, there is an increased probability of recombination with increased film thickness. Thus, there's an optimal thickness that permit to obtain maximum photocurrent.

It has also been observed that recombination occurs close to the glass coated with a TCO layer and not throughout the entire titania matrix. For this reason, present researchers use a compact[23] or nanocrystalline[24] TiO$_2$ "blocking layer". The use of a light-scattering layer is also quite common; it consists of larger star-shaped titania particles that work as a photo-trapping system[12,25] to provide a cell conversion efficiency of above 10% (Sumitomo Osaka Cement Co., Ltd.).[26]

An improvement of the conversion efficiency over a wide range of wavelengths by TiCl$_4$ surface treatment (Grätzel et al.) has also been reported.[27]

In these years a lot of efforts have been also made to improve the conductivity of TiO$_2$ through morphological control, such as the formation of nanotubes, as well as to coat the surface of TiO$_2$ with a different type of oxide, such as niobium oxide (Nb$_2$O$_5$), thereby suppressing electron leakage from the titanium oxide to the electrolyte solution. Research papers have been published for oxide semiconductor materials other than titanium oxide to the electrolyte solution. Research papers have been published for oxide semiconductor materials other than titanium oxide and also composite materials with other oxide semiconductors for the sake of improved charge separation efficiency have been presented. Such works, however, have not been successful in providing characteristics superior to those of simple titanium oxide and therefore the research in this aspect of this DSSCs is still open.

Regarding the deposition techniques generally used to deposit the semiconductor onto the glass substrate, screen-printing and doctorblading are the favorite . Typical film thicknesses are 5-20 µm, with TiO$_2$ mass of about 1-4 mg cm$^{-2}$, film porosity 50-65%, average pore size 15 nm and particle diameters of 15-20 nm.[28]

## 2.3.3 LIQUID STATE ELECTROLYTE

The electrolyte is an important  part of the cells: it is the hole-transport material responsible for inner charge carrier between electrodes. It regenerates the dye at the

photoelectrode with the charge collected at the counter electrode. For stable operation of the solar cell and maximal power output, the oxidized dye must be reduced back to the ground state as rapidly as possible by a suitable electron donor.

## 2.3.3.1    SOLVENT FOR LIQUID ELECTROLYTE

A suitable solvent for a high efficiency liquid electrolyte should have this characteristic:

1.  be liquid with low volatility at the operating temperatures, to avoid freezing or expansion of the electrolyte, which would damage the cells;
2.  be few viscosity to permit the rapid diffusion of charge carriers;
3.  be a good solvent for the redox couple and the various additives;
4.  not cause the desorption of the sensitizing dye or dissolution of the semiconducting materials of the electrodes;
5.  be chemically stable over long periods of time;
6.  be compatible with a suitable sealing material to avoid losses by evaporation or leakage;
7.  be of low cost and low toxicity.

The use of higher viscosity solvents, more suitable for practical device applications (for reasons of device stability), can result in significantly lower ionic diffusion constants and therefore an iodide/triiodide concentration gradients causing significant free energy (series resistance) losses, and also potentially accelerating interfacial charge recombination.

Acetonitrile is the most common solvent used in DSSCs fabrication. It is particularly employ to maximize the cell efficiency, but presents problems of spillage out of the cell, through possible holes or cracks in the sealant due to its high volatility, drops in the conversion efficiency at high temperatures or with long-term use and, in addition, is highly toxic and carcinogenic chemical therefore cannot be used in the commercial DSSCs.

Among the numbers of solvents employed for the redox couple some examples are: methoxypropionitrile,[29] butyronitrile   and/or methoxyacetonitrile[30]. In particular, methoxypropionitrile seems arise as a potential candidate for the commercial DSSCs. In

fact contrarily to acetonitrile and propionitrile it is nontoxic and has a boiling point of 160°C.

Use of other solvents or mixed solvents (i.e. $CH_2Cl_2$, DMF, $H_2O$ and mixtures with $CH_3CN$) resulted in reduced lifetimes of the sensitized $TiO_2$ working electrode. The study of pure and mixed electrolytes based on propylene carbonate, *γ*-butyrolactone, *N*-methylpyrrolidone, and pyridine showed similar results, where stronger donating solvents enhance photovoltage but decrease photocurrent.[31]

Because many organometallic sensitizing dyes are sensitive toward hydrolysis, water and reactive protic solvents are normally not optimal choices.

## 2.3.3.2    REDOX MEDIATOR

Ideal characteristics of redox couple have been listed by Wolfbauer et al. in 2001[32]:

1. Redox potential. In order to be able to reduce the oxidized dye back into its initial oxidation state, the redox couple reversible potential has to be negative respect of the dye reversible potential. The more negative the potential for the redox mediator, the larger the thermodynamic driving force for the dye regeneration.[29] However, as illustrated in Figure 2.3, the more negative the potential or the higher the energy for this process, the smaller the open-circuit potential and hence the effciency of the solar cell. ($V_{OC}$ corresponds to the difference between the Fermi level of the electron in the $TiO_2$ and the redox potential of the electrolyte). Thus, the reversible potential for a redox shuttle must be more negative of the reversible potential for the dye but as positive as possible to avoid unnecessary loss of usable energy.

2. High solubility. Concentration ranges commonly used for redox shuttles are 0.1-0.5M to ensure sufficient supply of the redox mediator and to minimize diffusion-limited situations which would result in an undesirable extended lifetime of the oxidized form of the dye and consequently in an increased probability of dye decomposition.

3. High diffusion coefficient. It is essential because mass transport of the redox couple in a solar cell (through solution and $TiO_2$ network) occurs solely by diffusion.

4. Absence of significant spectral characteristics in the visible region. Absorbance of visible light by the redox system results in less light being available for the light-to-electricity conversion and thus low energy conversion. Since it is present in a relatively large concentration, even small extinction coefficients can adversely affect the solution absorbance characteristics.

5. High stability of both the reduced and oxidized forms of the couple. For efficient redox "shuttling" in solar cells, both the oxidized and reduced forms need to be present in solution and both forms must have high stability.

6. Highly reversible couple. It must be electrochemically and chemically reversible to guarantee fast electron transfer and to avoid unwanted side reactions.[17]

7. Chemically inert system. The components of the redox system must be chemically inert toward any adverse side reaction that may occur with any part of the solar cell, e.g. no chemical reactivity with $TiO_2$, no surface activity, etc.

## Iodine Based Mediator

So far the highest conversion efficiency ever has been achieved by an electrolyte solution of acetonitrile in which iodine ions and iodine are dissolved. This redox cuple is really hard to replace; it simply performs better than all alternatives tested.

The good performance of this redox mediator is based on the kinectics of the processes: first, the photo-oxidized dye injects an electron into the conduction band of the semiconductor much faster than electron recombination with $I_3^-$. Second, the oxidized dye preferably reacts with $I^-$ than recombines with the injected electron. Finally, the two electron process of $I^-$ regeneration from $I_3^-$ occurs quickly enough at the catalyst-coated counter electrode to be productive.

However some issues have to be taken into consideration when employing this redox couple as electrolyte: first the choice of the opportune cation of the iodine salt (photocurrent output increase linearly with decreasing of cation radius), second its

concentration. Obviously, at low concentrations conductivity will be insufficient and rapid reduction will not be ensured. On the other hand, when employed in high concentrations, apart from possible corrosion problems, iodide can substantially suppress cell efficiency up to 50% by increasing the recombination of $I_3^-$ and injected electrons, and increasing the rate of light absorption by the redox couple

Nevertheless the corrosive and photochemical properties of iodine are strong driving forces in the search for alternative redox couples.

## Alternative Redox Couple

For replacing the non ideal $I^-/I_3^-$ redox couple, two main directions can be identified, one toward molecular species of similar types and another aiming at transition-metal based systems. In minor part also organic donors have been investigated.

The step away from halogens to pseudohalogens is not so large, so the use of the corresponding $(SeCN)_2/SeCN^-$, $(SCN)_2/SCN^-$,[33] $Br_3^-/Br^-$,[34] have also been investigated[30] showing to be very promising from an electrochemical and noncorrosion aspect, for instance, generating similar photovoltages as the standard $I^-/I_3^-$ couple. Unfortunately, none of them proved being as efficient as iodide mainly because of chemical instability is a disqualifying property for practical use.[35,36] Some cobalt complexes have also been tested [37,38] for instance, cobalt(II)/(III)-bis[2,6-bis(1'-butylbenzimidazol-2'-yl)pyridine] $(Co(dbbip)_2^{2+}/^{3+})$.[38]

Compared to iodide, their advantage is that they are non-volatile, non-corrosive and have the benefit of being easy for molecular modifications. However, with present technology the current exchange rate at the counter electrode is much smaller and leads to voltage losses.[35, 39]

Phenothiazine[40] donors are able to efficiently regenerate oxidized sensitizers. However, the recombination of the injected electrons with the oxidized phenothiazine is too fast to allow for an efficient transport of the holes to the cathode of a DSSC.

Stable organic radicals originating from 2,2,6,6-tetramethyl-1-piperidinyloxy (TEMPO) have shown promising performance as a replacement to the standard iodine-based

redox system with efficiencies above 5%, despite suffering from drawbacks caused by higher recombination rates (common for all one-electron systems).[41]

## 2.3.3.3 ADDITIVES

Additives play a central role in the enhancement of photoelectrochemical performance of DSCs. Most additives are understood at a fairly phenomenological level, and their effects are often attributed to modification of redox couple potential, band shifts of the semiconducting electrode material, effects of surface blocking, or surface dye organization.

Most additives that have been reported contain an electrondonating nitrogen heterocycle, such as 4-*tert*-butylpyridine (TBP), in combination with LiI-based electrolytes.[42] TBP shifts the titania band edge toward higher energies.[43] Although TBP and Li+ ions have opposite effects on the conduction band and trap states, and thus on the kinetics of electron injection and recombination, it is a very common combination of additives in solar cell electrolytes, demonstrating a remarkable increase in $V_{oc}$. The reason for the good overall performance of this combination is not fully understood. A large number of pyridines and other N-heterocycles have been investigated as additives in DSC, generally giving similar results as TBP.

Tetrabutylammoniumhydroxide (TBAOH), is instead commonly used to avoid filtering effect of  triiodide (that absorbs light below 500 nm). In particular, TBAOH converts the light absorbing $I_3^-$ complexes into colorless $IO^-$ ions, which are reduced to $I^-$ + $OH^-$ at the counter-electrode.[44]

Another important purpose of this additives is to suppressed the dark currents coming from the reduction of the redox mediator by the collector electrode with the oxide layer. Chenodeoxycholic acid, methylbenzimidazole and TBAOH can therefore also be used  to avoid the mediator get to the  uncovered oxide surfaces. [45,46]

Studies in organic solvents have demonstrated shifts of the conduction band of mesoporous $TiO_2$ films of up to 1 V depending on the concentration of potential-determining ions (primarily small cations such as protons or lithium cations) in the electrolyte.[47] For this reason, the concentration of such potential-determining ions in

the electrolyte plays a key role in determining the energetics of the dye-sensitised interface, and thereby device performance. Additives added to the electrolyte to determine such energetic include Li$^+$, guanadinium ions, N-methylbenzimidazol and t-butyl pyridine. Further influence on these interfacial energetics can be achieved by variation of the extent of protonation of the sensitiser dye.

Additionally, these additives also enhance the cell's long-term stability.[48]

## 2.3.3.4    IONIC LIQUIDS

While promising result has been reached in the development of stable, nonvolatile electrolyte formulations, the conversion yields obtained with these systems are presently in the 7–10% range, below the 11.1% reached with volatile solvents. The research is therefore focusing on solvent-free electrolytes such as ionic liquids. They are ideally a particularly attractive choice for the first commercial modules, thanks to their good chemical and thermal stability, negligible vapor pressure, non-flammability, high ionic conductivity,  wide electrochemical window and excellent compatibility with the environment. They appear to solve problems such as dye desorption, solvent evaporation and sealing degradation, however, until now their performance has been consistently lower.

Between them, Molten salts based on imidazolium iodides have revealed very attractive[49,50] Despite their high viscosity, linear photocurrent response up to full solar light intensities has been observed.

## 2.3.3.5    GEL AND POLYMER ELECTROLYTES

Electrolytes based on both organic solvents and ionic liquids can be gelated, polymerized, or dispersed with
polymeric materials. Both types of liquids have been used as starting materials, and the inclusion of gelating or polymeric agents transforms the electrolyte into a quasi-solid electrolyte.[51] In this type of electrolyte a redox mediator is included (almost exclusively the iodide/triiodide couple) and charge transport occurs mainly by diffusion of molecules.

Typically, these quasi-solid electrolytes show conversion efficiencies that are slightly lower than that of the host liquid redox electrolyte. This effect can most likely be attributed to limitations in the mobility of the redox couple components within the quasi-solid electrolyte.

## 2.3.4 SOLID STATE ELECTROLYTE

Solid-state DSSCs seems to viable alternative to the use of liquid electrolytes and the problems related to them.

Aiming at a fully solid electrolyte (hole transporting material, HTM), there have been researches on the use of inorganic compounds such as CuI and CuSCN, conductive polymers such as



Catodo
HTM
TiO$_2$ mesoporoso + dye
TiO$_2$ compatto
FTO
Vetro

**Figure 2.8**

polypyrrole, low-molecular materials such as triphenyldiamine and amorphous organic compounds such as spiro-OMeTAD (2,2′,7,7′-tetrakis(N,N-di-p-methoxyphenylamine)-9,9′-spirobifluorene).
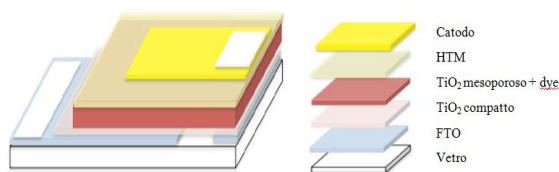
### 2.3.4.1   ORGANIC HOLE CONDUCTORS

In organic hole conductors, positive charge moves by a hopping mechanism between neighboring molecules or moieties, as opposed to redox electrolytes where charge transport is due to movement of redox molecules. (Figure 2.9) The hole conductors
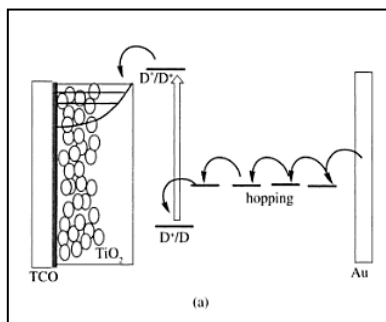


**FIGURE 2.9**

typically also contain additives of salts allowing for some ionic conductivity, which is important for local charge compensation. Organic hole conductors can be divided into two classes, conducting polymers and molecularhole conductors.

One example is solid-state DSCs based on dyes with thienyl groups and P$_3$HT doped with ionic liquids and TBP as hole conductor that showed good performance (efficiency 2.7%), attributed to

the good interaction between dye and polymer and good electrostatic shielding effect due the ions.[52] (Figure 2.10)



**Figure 2.10**

Triarylamine-based compounds are the most popular molecular hole conductors in solid-state DSCs. The most successfully employed organic charge transfer material is spiro-MeOTAD (2,2′,7,7′-tetrakis(N,N-di-p-methoxyphenylamine)-9,9′-spirobifluorene). (Figure 2.11) It was initially pres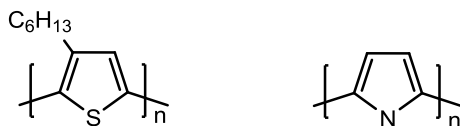ented by Grätzel *et al.* in 1998[53] and presently attains conversion yields above 4%.[54] Although promising, this efficiency is still much lower than those reported for analogous liquid-electrolyte devices. One of the limitations that has been suggested is the low hole mobility of spiro-



**Figure 2.11**

OMeTAD,[55] causing excessive interfacial recombination losses.[56] A number of studies have focused on replacing OMeTAD with alternative high-mobility hole conductors whithout the spiro center, but problems like strong tendency to crystallize (resulting in poor device performance) and reduced thermal stability were found.[57-73]

Also the organic hole conductors are subjected to modifications using similar additives as in liquid electrolytes, such as lithium salts and TBP, in order to increase conversion efficiencies.[74] The observed effects are in part analogous to the ones in liquid electrolytes, although the complexity of the system cannot rule out that also effects from ion conduction play a role. The addition of non-redox-active lithium salts, for instance, increased the hole conductivity considerably, an effect not fully characterized.[75]

A general problem with solid hole conductors is optimizing the interface between the sensitized semiconductor and the electrolyte, the pore filling does not need to be 100%, but for efficient cells, it is necessary that all dye molecules are in contact with both the
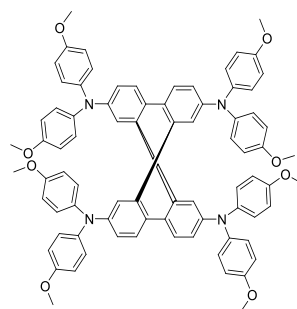
$TiO_2$ and the hole conductor and that there are any (or very few) interruptions in the hole-conducting path must be present. To overcome this problem several approach have been tried, such as reducing the thickness of the semiconducting layer or melt the hole conductor to fill the pores, however the proper solution has not been found yet, leaving this matter open.

## 2.3.5 THE DYE SENSITIZER

The dye-sensitizer is one of the crucial parts in DSCs, it is responsible for the light harvesting and upon absorption of light for the begin of charge separation that generally initiated at the interface between the dye bound to the $TiO_2$ surface and the hole-transporting material. It should fulfil some essential characteristics. Its absorption spectrum should cover the whole visible region and even the part of the near-infrared (NIR), it must carry anchoring groups ($-COOH$, $-H_2PO_3$, $-SO_3H$, etc.) to strongly bind the semiconductor surface. On excitation, it should inject electrons into the solid with a quantum yield of unity. The energy of the excited state level should be well-matched with the conduction band of the semiconductor, higher enough so that an efficient electron transfer process between the excited dye and conduction band (CB) of the semiconductor can take place.

The oxidized state level of the photosensitizer must be more positive than the redox potential of electrolyte, for efficient regeneration. The process of electron injection from the exited state to the conduction band of the semiconductor should be fast enough to outrun competing unwanted relaxation and reaction pathways. It should not create aggregate on the semiconductor surface, should be photostable, and electrochemical and thermal stability are also required, in particular it should be stable enough to sustain about 100 million turnover cycles, corresponding to about twenty years of exposure to natural light.

Based on these requirements, many different photosensitizers including metal complexes, porphyrins and phthalocyanines have been designed and applied to DSCs in the past decades.

The dye that was first used in the Grätzel cell is a ruthenium (Ru) bipyridine complex (Figure 2.12) efficiently absorb visible light in a wavelength range of up to 800 nm. The carboxy group, as explained later on, provides the anchoring of the dye to the surfaces of titanium oxide particles.
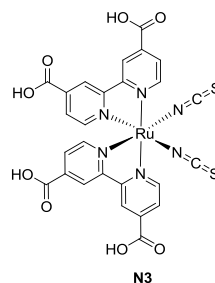


**Figure 2.12**

The main drawbacks of ruthenium are its high costs and its limitate availability; moreover, as the other metal based dyes, it requires complicated synthesis and purification steps. Therefore in this years a new generation of dyes is conquering the scene: metal-free dyes.
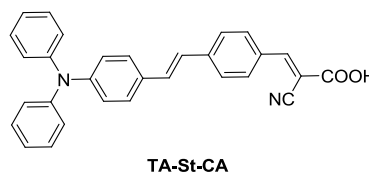


**Figure 2.12**

These are simple and cheap to prepare and their photo- and electrochemical properties can be easily modulate varying the functionalization.

To date, these two classes of compound gave similar cell efficiencies around 10%, but many are the possibility of improvement; thus, the international researches are very active in both these fields.

The synthesis of new dyes both metal-free and metal based is object of this thesis; therefore the argument will be treated more in detail in the next chapters.

## 2.3.5.1    THE ANCHORING GROUP

The adsorption mode of dyes on semiconductor surfaces is very important for the DSC efficiency.[76] To construct workable and efficient DSCs, the dye must be adsorbed on the surface of the semiconductor intimately. Therefore, the covalent attachment by linking groups of interest or via linking agents provides an approved strategy to accomplish a strong inter-linkage between the dye and the semiconductor. It requires that the dye possess an anchoring group, which should react with surface hydroxyl groups of the semiconductor oxide to form chemical bonds.

The standard anchoring group for sensitizers is carboxylic acid (-COOH). Its derivatives, such as ester, acid chloride, acetic anhydride, carboxylate salt, or amide, have also been used. Furthermore, sulfonate ($-SO_3^-$) and silane ($SiX_3$ or $Si(OX)_3$) have also been adopted.[77] Efficient sensitizers with phosphonic acid binding groups were found in some cases to bind about 80 times stronger to $TiO_2$ than other COOH-bearing dyes and do not desorb in presence of water.[78]

Nevertheless, the most of the photosensitizers employ the carboxylic acid as anchoring group due to its relative stability and easy synthesis.

There are different binding modes between the oxide surface and the carboxylic acid (Figure 2.13).[79] In general, the carboxylic acid group can coordinate to the $TiO_2$ surface in



unidentate    bidendate chelating    bidentate bridging
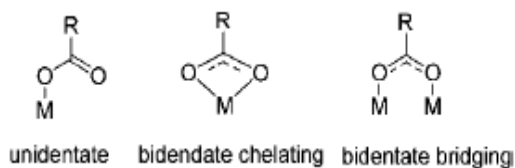
**Figure 2.13**

three ways: [80, 81] unidentate mode, chelating mode, and bridging bidentate mode. The binding modes can be determined by the molecular structure and adsorption environment.[82] The bidentate structure is superior to unidentate ones in the stability of the anchored dye and in the interfacial quantum yields of electron injection, due to the intimate contact with the semiconductor surface.[83]

## 2.4   FUTURE OUTLOOK

After more than 15 years of intense research, the physical chemistry of several of the basic operations in the DSC device still remains far from fully understood. It is, however, still not possible to predict accurately how a small change in the system, such as replacing one component or changing the electrolyte composition, will affect the DSC performance. With time, the chemical complexity of DSCs has become clear, and the main challenge for future research is to understand and master this complexity in particular at the oxide/dye/electrolyte interface.

A challenging, but realizable, goal for the present DSC technology is to achieve efficiencies above 15%. We know where the main losses in the "state of the art" of DSC

devices are, as the potential drop in the regeneration process, the recombination loss between electrons in the $TiO_2$ and the acceptor species in the electrolyte, (Figure 2.6). Decreasing the 0.6 V of the potential drop to about 0.3 V would give efficiencies of 15%. The challenge is to develop dye-electrolyte systems that give efficient regeneration of the oxidized dye at a driving force of 0.2-0.4 V. Such systems must probably be combined with efficient blocking layers of the mesoporous oxide film and TCO substrate. Moreover, new more efficient dye are needed with extended absorption in the visible range.

The aim of this thesis is the development of new high molar coefficient extinction dyes for DSSCs application with improved light harvesting capability and cell efficiency.

# REFERENCES

[1] M. Grätzel, Nature, **2001**, *414*,338.

[2] W. West, *First hundred years of spectral sensitization. Proc. Vogel Cent. Symp. Photogr. Sci. Eng.,* **1974** , *18*, 35.

[3] J. Moser, *Notiz über die Verstärkung photoelectrischer Ströme durch optische Sensibilisierung. Monatsh. Chem.,* **1887**, *8*, 373.

[4] W. H. ,Brattain, C. G. B. Garrett, *Experiments on the interface between germanium and an electrolyte. Bell Syst. Tech. J.,* **1955,** *34*, 129.

[5] H. Gerischer, E*lectrochemical behavior of semiconductors under illumination. J. Electrochem. Soc.,* **1966**, *113*, 1174.

[6] M.P. Dare-Edwards, J.B. Goodenough, A. Hamnet, K.R. Seddon, R.D. Wright, Faraday Disc., Chem. Soc. 70 (1980) 285.

[7] H. Tsubomura, *Nature*, 261 (1976), p. 402

[8] D. Duonghong, N. Serpone, M. Grätzel, Helv. Chim. Acta 67 (1984) 1012

[9] J. DeSilvestro, M. Grätzel, L. Kavan, J. Moser, J. Augustynski, J. Am. Chem. Soc. **1985** 107 2988.

[10] *Faraday Discuss. Chem. Soc.*, **1980**, *70*, 285.

[11] B. O'Regan, M. Grätzel, *Nature (London)*, **1991**, *353*, 737.

[12] J. Kawakita, *Science and technology trends- Quarterly Review,* April **2010**, *35*, 70.

[13] K. Tennakone, G.R.R. Kumara, I.R.M. Kottegoda. , V.S.P. Perera,Chem. Commun. **1999**, *15* .

[14] K. Sayama, H. Suguhara, H. Arakawa, *Chem. Mater.*, 1998, *10*, 3825.

[15] E. Olsen, G. Hagen, S. E. Lindquist, *Sol. Energy Mater. Sol. Cells*, **2000**, *63*, 267.

[16] T. Kitamura, M. Maitani, M. Matsuda, Y. Wada, S. Yanagida, *Chem. Lett.*, **2001**, *30,* 1054.

[17] K. Kalyanasundaram and M. Gratzel, *Coord. Chem. Rev.*, 1998, **177**, 347-414

[18] D. Watson, G. Meyer,. *Annu. Rev. Phys. Chem*., **2005**, *56*, 1196.

[19] B. C. O'Regan, J.E. Moser, M. Anderson, M. Grätzel, *J. Phys. Chem-Us*, **1990**, *94*, 8720.

[20] *M. Grätzel, Journal of Photochemistry and Photobiology C: Photochemistry, **2003**, 4,* 145.

[21] C. J. Barbè, F. Arendse, P. Comte, M. jirousek, F. Lenzmann, V. Shklover, M. Graetzel, *J.Am.Chem.Soc.,* **1997**, *80*, 3157.

[22] R. J. Ellingson, J. B. Asbury, S. Ferrere, H. N. Ghosh, J. R. Sprague, T. Lian, A. J. Nozik, *J. Phys. Chem. B*, **1998**, *102*, 6455.

[23] J. N. Hart, D. Menzies, Y.-B. Cheng, G. P. Simon, L. Spiccia, *C. R. Chim.*, **2006**, *9*, 622.

[24] S. Ito, K. Ishikawa, C.-J. Wen, S. Yoshida, T. Watanabe, *Bull. Chem. Soc. Jpn.*, **2000**, *73*, 2609.

[25] Z.-S. Wang, H. Kawauchi, T. Kashima, H. Arakawa, *Coord. Chem. Rev.*, **2004**, *248*, 1381.

[26] H. Arakawa, *Recent Advances in Research and Development for Dye-Sensitized Solar Cells II*, CMC Publishing, **2007**, *9.*

[27] C. J. Barbe, F. Arendse, P. Comte, M. Jirousek, F. Lenzmann, V. Shklover, M. Grätzel, Journal of the American Ceramic Society, **1977**, *80*, 3167.

[28] M. Grätzel, *Journal of Photochemistry and Photobiology A: Chemistr,* **2004**, *164,* 3.

[29] T. Ma, X. Fang, M. Akiyama, K. Inoue, H. Noma, E. Abe, *J. Electroanal. Chem.*, **2004**, *574*, 77.

[30] Y. Saito, W. Kubo, T. Kitamura, Y. Wada, S. Yanagida, *J. Photochem. Photobiol*. A, **2004**, *164*, 153.

[31] J. H. Wu, Z. Lan, J. M. Lin, M. L. Huang, P. J. Li, *J. Power Sources,* **2007**, *173*, 585.

[32] G. Wolfbauer, A. M. Bond, J. C. Eklund, D. R. MacFarlane, *Solar Energy Materials & Solar Cells* **2001**, *70*, 85.

[33] G. Oskam, B. V. Bergeron, G. J. Meyer, P. C. Searson, *J. Phys. Chem. B*, **2001**, *105*, 6867.

[34] Z.-S. Wang, K. Sayama and H. Sugihara, *J. Phys. Chem. B*, **2005**, *109*, 22449.

[35] B. V. Bergeron, A. Marton, G. Oskam, G. J. Meyer, *J. Phys. Chem.B*, **2005**, *109*, 937.

[36] P. Wang, S. M. Zakeeruddin, J. E. Moser, R. Humphry-Baker, M. Grätzel, *J. Am. Chem. Soc.,* **2004**, *126*, 7164.

[37] H. Nusbaumer, J. E. Moser, S. Zakeeruddin, M. Nazeeruddin, M. Grätzel, *J.Phys. Chem. B,* **2001**, *105*, 10461.

[38] H. Nusbaumer, S. Zakeeruddin, J. E. Moser, M. Grätzel*, Chem-Eur. J.,* **2003**, *9*, 3756.

[39] P. J. Cameron, L. M. Peter, S. M. Zakeeruddin, M. Grätzel, *Coord. Chem. Rev.*, **2004**, *248*, 1447.

[40] R. Argazzi, C. A. Bignozzi, T. A. Heimer, F. N. Castellano, G. J. Meyer, *J. Phys. Chem. B*, **1997**, *101*, 2591.

[41] Z. Zhang, P. Chen, T. N. Murakami, S. M. Zakeeruddin, M. Graätzel, *AdV. Funct. Mater.,* **2008**, *18*, 341.

[42] M. K. Nazeeruddin, A. Kay, I. Rodicio, R. Humphry-Baker, E. Müller, P. Liska, N. Vlachopoulos, M. Grätzel, *J. Am. Chem. Soc.,* **1993**, *115*, 6382.

[43] G. Ramakrishna, D. A. Jose, D. K. Kumar, A. Das, D. K. Palit, H. N. Ghosh, *J. Phys. Chem. B,* **2005**, *109*, 15445.

[44] A. Kay, M. Grätzel, *Sol. Energ. Mat. Sol. C.,* **1996,** *44,* 99.

[45] K. Kalyanasundaram, M. Grätzel*, Coord. Chem. Rev.,* **1998**, *177*, 347.

[46] A. Burke, L. Schmidt-Mende, S. Ito, M. Grätzel, *Chem. Commun.*, **2007**, *3*, 234.

[47] G. Redmond, D. Fitzmaurice, *J. Phys. Chem*. **1993**, *97*, 1426.

[48] E. Figgemeier, A. Hagfeldt, *Int. J. Photoenergy*, **2004**, *6*, 127.

[49] H. Matsumoto, T. Matsuda, T. Tsuda, R. Hagiwara, Y. Ito, Y. Miyazaki, *Chem. Lett.*, **2001**, *30,* 26*.*

[50] P. Wang, S. M. Zakeeruddin, P. Comte, I. Exnar, M. Grätzel, *J. Am. Chem. Soc.*, **2003***, 125*, 1167.

[51] W. Kubo, K. Murakoshi, T. Kitamura, Y. Wada, K. Hanabusa, H. Shirai, S. Yanagida, *Chem. Lett.* **1998**, 1241.

[52] K. J. Jiang, K. Manseki, Y. H. Yu, N. Masaki, K. Suzuki, Y. L. Song, S. Yanagida, *AdV. Funct. Mater*., **2009**, *19*, 2481.

[53] U. Bach, D. Lupo, P. Comte, J. E. Moser, F. Weissortel, J. Salbeck, H. Spreitzer M. Grätzel, *Nature (London)*, **1998**, *395*, 583.

[54] L. Schmidt-Mende, U. Bach, R. Humphry-Baker, T. Horiuchi, H. Miura, S. Ito, S. Uchida M. Grätzel, *Adv. Mater. (Weinheim, Ger.),* **2005**, *17*, 813.

[55] D. Poplavskyy, J. Nelson, *J. Appl. Phys.* **2003**, *93*, 341.

[56] G. Kron, T. Egerter, J. H. Werner, U. Rau, *J. Phys. Chem. B*,**2003**, *107*, 3556.

[57] C. Jäger, R. Bilke, M. Heim, D. Haarer, H. Karickal, M. Thelakkat, *Synth. Met*., **2001**, *121*, 1543.

[61] B. O'Regan, F. Lenzmann, R. Muis, J. Wienke, Chem. Mater. **2002**, *14*, 5023.

[69] K. Peter, H. Wietasch, B. Peng, M. Thelakkat, *Appl. Phys. A*, **2004**, *79*, 65.

[70] Y. Saito, N. Fukuri, R. Senadeera, T. Kitamura, Y. Wada, S. Yanagida, *Electrochem. Commun*., **2004**, *6*, 71.

[71] R. Cervini, Y. B. Cheng, G. Simon, J. Phys. D **2004**, *37*, 13.

[72] K. R. Haridas, J. Ostrauskaite, M. Thelakkat, M. Heim, R. Bilke, D. Haarer, *Synth. Met*., **2001**, *121*, 1573.

[73] S. Spiekermann, G. Smestad, J. Kowalik, L. M. Tolbert, M. Grätzel, *Synth. Met.,* **2001**, *121*, 1603.

[74] J. Kruger, R. Plass, L. Cevey, M. Piccirelli, M. Grätzel, U. Bach, *Appl. Phys. Lett.* **2001**, *79*, 2085.

[75] H. J. Snaith, M. Grätzel, *Appl. Phys. Lett.,* **2006**, *89*, 3.

[76] K. Murakoshi, G.Kano, Y. Wada, S. Yanagida, H. Miyazaki, M. Matsumoto, S. Murasawa,. *J. Electroanal. Chem.,* **1995**, *396*, 27.

[77] S. Ardo, G. J. Meyer, *Chem. Soc. Rev*. **2009**, *38*, 115.

[78] P. Pechy, F. P. Rotzinger, M. K. Nazeeruddin, O. Kohle, S. M. Zakeeruddin, R. Humphry-Baker, M. Grätzel, *J. Chem. Soc. Chem. Commun.,* **1995**, *1*, 65.

[79] E. Galoppini, *Coord. Chem. ReV.,* **2004**, *248*, 1283.

[80] Z. S. Wang, K. Hara, Y. Dan-Oh, C. Kasada, A. Shinpo, S. Suga, H. Arakawa, H.Sugihara, *J. Phys. Chem. B,* **2005**, *109*, 3907.

[81] M. K. Nazeeruddin, R. Humphry-Baker, P. Liska, M. Grätzel, *J.Phys. Chem. B,* **2003**, *107*, 8981

[82] H. N. Tian, X. C. Yang, R. K. Chen, R. Zhang, A. Hagfeldt, L. C. Sunt, *J. Phys. Chem. C.,* **2008**, *112*, 11023.

[83] G. L. Zhang, H. Bala, Y. M. Cheng, D. Shi, X. J. Lv, Q. J. Yu, P. Wang, *Chem. Commun.,* **2009**, 16, 2198.

# METAL-FREE

# ORGANIC DYES
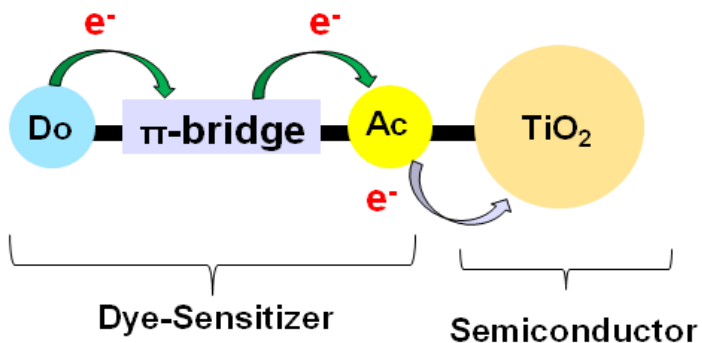
## 3.1 INTRODUCTION

Organic dyes are a really promising alternative to the noble ruthenium complexes sensitizers. Indeed, they exhibit many advantages, such as easy tailoring of the structure and properties, higher molar extinction coefficients and less complicated synthesis and purification step with respect to the metal-based ones. In addition, concerning cost and environment issues, they are superior to metal complexes since they are cheaper and without problem of limited source.

To date, as a consequence of a lot of work appeared in the literature aimed at the optimization of the design of metal-free dyes, organic sensitizers with higher efficiencies are known.

The general structural architecture of these dyes is generally composed of a push-pull system of the type donor-$\pi$ bridge-acceptor (D-$\pi$-A) shown in Figure 3.1.
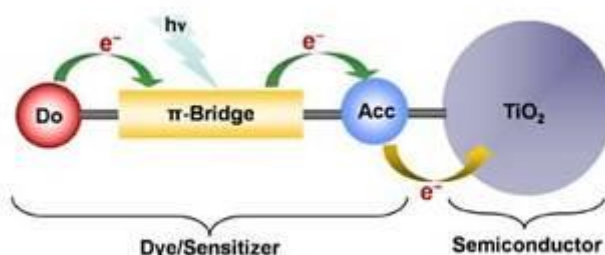


**Figura 3.1**

This construction permits an easy design of new structures with extended absorption spectra, adjusted HOMO and LUMO levels and ensures the necessary intramolecular charge separation. When the dye absorbs the light, intramolecular charge transfer occurs from subunit D to subunit A through the $\pi$-bridge. The excited dye then injects the electron into the conduction band of the semiconductor via the electron acceptor group, A.

Many efforts have been made to change the different parts of organic dyes for optimizing DSC performance. Up to now, hundreds of organic dyes, including coumarin, indoline, tetrahydroquinoline, triarylamine, carbazole, squaraine, perylene,

oligothiophene, and natural dyes have been studied as sensitizers for DSCs and have showed impressive efficiencies.

The careful study of the existing literature is a good way to understand factors involved in performancies of dyes and therefore to rationalize the design of new sensitizers for obtaining improved efficiencies. Some representative organic dyes are shown below.

## 3.2 STATE OF THE ART

### 3.2.1 COUMARIN DYES

Arakawa, Hara, Wang, and coworkers developed a class of organic dyes consisting of a coumarin unit and a cyanoacrylic acid unit linked by vinylene, isophorone, or thienyl.[1,2] The coumarin unit acts as electron donor while the cyanoacrylic acid group is considered as the electron acceptor due to the strong electron-withdrawing ability of cyano and carboxyl groups. Dye **C343** (Figure 3.2), the original coumarin sensitizer, exhibits an effective electron injection process but efficiency lower than that of the Ru complex, due to the narrow light response range in the visible region. Therefore, to enhance and red-shift the absorption spectra, a vinylene spacer was introduced. However, this leads to more complicated synthesis, and problems of possible isomerization. Moreover, enhancement of dye aggregation on $TiO_2$ surface with the increase of the length of vinylene units is observed, resulting in a decrease of electron injection yield owing to the intermolecular charge transfer.

Because of this, thienyl and isophorone units have been inserted in place of the vinylene units, to expand the conjugated system and to enlarge absorption spectra and improve efficiencies. Dye **NKX-2677** (Figure 3.2), bearing two thiophene units,[1] gave 7.4% overall efficiency.[3] The authors observed that, increasing the number of thiophene units, the absorption spectra of dyes were not affected, while effects were observed on photovoltaic properties, due to different aggregation issues on $TiO_2$.

Introducing an additional CN group on the $\pi$-bridge of the dye further extends the absorption region of organic dye in that this enhances the electron-withdrawing ability

of the electron acceptor part. The enhancement appears to be slightly less when the added –CN group is separated from the cyanoacrylic acid group.

In addition, after structure optimization, one of the main problem of this class of dyes is the lower $V_{OC}$ value, due to significant charge recombination resulting from strong intermolecular π–π interaction.
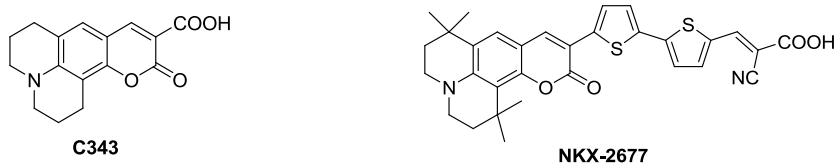


**Figure 3.2**

## 3.2.2 INDOLINE DYES

Horiuchi, Uchida and co-workers first reported this type of organic dyes, which can be prepared with simple synthetic procedures, low costs, and good efficiencies, obtaining, in particular, 6.1% power conversion efficiency for dye **D102**.[4] (Figure 3.3) This dye was employed by Schmidt-Mende et al. for assembling a solid-state DSCs, obtaining an efficiency over 4.0%, superior to that of an N719-based DSC.[5] To further improve the DSC performance, an additional rhodanine framework was introduced to extend the absorption spectrum, giving a series of novel indoline dyes.[6] Among these dyes, **D149** (Figure 3.3) showed the most prominent efficiency, exhibiting an initial 8.0% that, after optimization of the $TiO_2$ electrode thickness, by Grätzel and co-workers became 9.0%.[7]

After structural optimization, Ito and co-workers developed the efficient indoline dye **D205** (Figure 3.3), containing a rhodanine framework substituted with a *n*-octyl chain to suppress the dye π-stacked aggregation on the semiconductor surface, which gave a 9.5% efficiency.[8] This is one of the best efficiencies for organic dye-sensitized solar cells never reported. The *n-octyl* chain effectively suppresses electron recombination between electrons in the conduction band of $TiO_2$ and electrolyte, resulting in higher open-circuit voltage and short-circuit current.

Moreover, Matsui and co-workers modified the indoline dyes by introducing the thiophene system as a $\pi$ bridge, slightly improving the photovoltaic properties.[9]
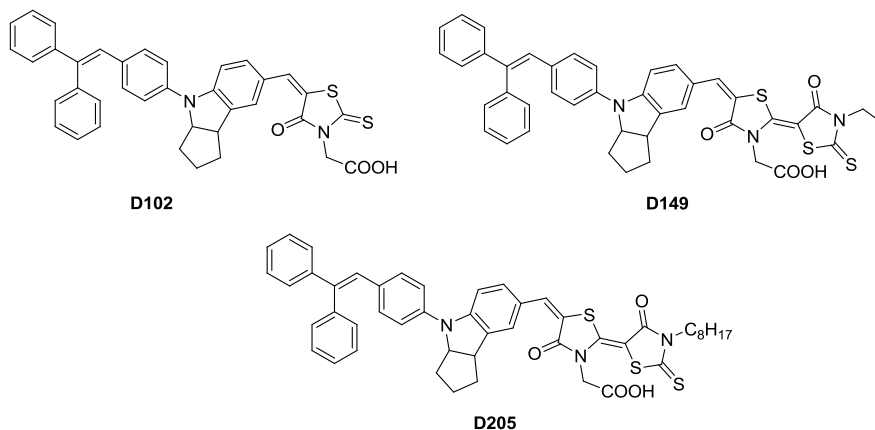


**Figure 3.3**

Ko and co-workers also developed a new series of indolene dyes substituted by bis-dimethylfluorenyl unit,[10,11,12] the best one (**JK51** Figure 3.4) gave a maximum overall efficiency of 8.4%.
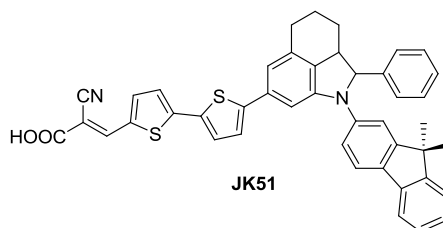


**Figure 3.4**

## 3.2.3 TETRAHYDROQUINOLINE DYES

Tetrahydroquinoline dyes have been developed by Sun, Yang, and co-workers.[13,14,15] that systematically investigated the relationship between dye structure and performance of DSCs. They found that the elimination of the double bond and adoption of suitable electron spacers with rigid molecular structures was useful for getting higher efficiencies of DSCs. The low performance of C=C bond containing dyes, indeed, could be explained as due to the existence of a twisting process, which leads to possible cis-trans photoisomerization.[16] They also studied the influence of incorporating one or more

thiophene units in the dye, finding that increasing the number of spacers could easily increase the recombination reaction of electrons in the TiO$_2$ and in the electrolyte, leading to a lower photovoltage.[14] Among the compounds studied, **C2-2**- (Figure 3.5) showed the higher efficiency of 4.5% in DSC.

Moreover, a new type of organic dye for DSCs, in which the anchoring group was separated from the acceptor group of the dye, was successfully obtained, giving a new class of D-$\pi$-A organic dyes for sensitization in the NIR region.[15] Among these dyes, **HY103** (Figure 3.5) gave a maximum IPCE value of 86% at 660 nm, which was one of the highest reported so far for the D-$\pi$-A organic dyes in the NIR region and an overall 3.7% efficiency.
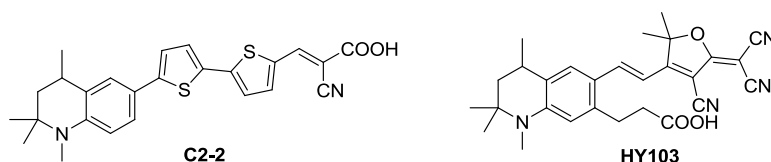


**Figure 3.5**

## 3.2.4 TRIARYLAMINE DYES.

This class of organic sensitizers has been investigated widely due to prominent electron-donating ability and hole-transport properties of the triarylamine unit. To date, a very large number of triarylamine dyes have been developed and most of them have shown good power conversion efficiencies in DSCs.[17,18]

Yanagida and co-workers first introduced the triphenylamine unit as electron donor in organic dyes and obtained overall DSC efficiencies of 3.3% and 5.3% for dye **TA1** and **TA2**, respectively.[19] Figure 3.6



**Figure 3.6**

Later, Sun and co-workers further optimized triphenylamine dyes and reported a series of efficient organic dyes. Dye **L2** (Figure 3.7), which has a very simple structure and can be easily synthesized, showed over 5.1% efficiency.[20,21]

They also observed that the introduction of methoxy groups in the electron donor moiety can extend the absorption region in the visible light and increases the electron lifetime, which is important for the open-circuit potential of DSSCs, as in **D9** (6.9%). (Figure 3.7) When these dyes were fabricated to solid-state DSCs, dye **D9** gave a prominent efficiency of 3.3%.
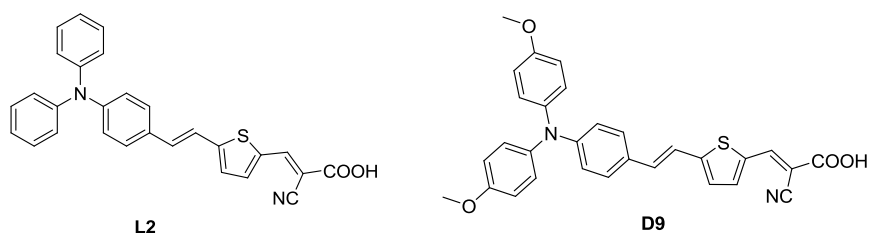


**Figure 3.7**

The addition of one or more thiophene $\pi$-bridge and longer alkyl chains in the electron donor, leads to dye **D21L6** (Figure 3.8) for which efficiency of 7.3% in liquid DSCs and a 4.4% efficiency in solid-state DSCs were achieved. The same dye, used in an ionic liquid electrolyte based DSCs, also exhibited prominent photochemical stability.[22] By adjusting the structures and introducing one or more triphenylamine units or additional methoxy groups in the donor part, or both, the authors also obtained a series of dyes among which **D11** (Figure 3.8) exhibited the highest efficiency of 7.2%.[23] The disubstituted donor moiety of **D11** prevents the recombination of $I_3^-$ ions of the electrolyte with injected electrons in the $TiO_2$ conduction band, thus leading to an increased open-circuit potentials.
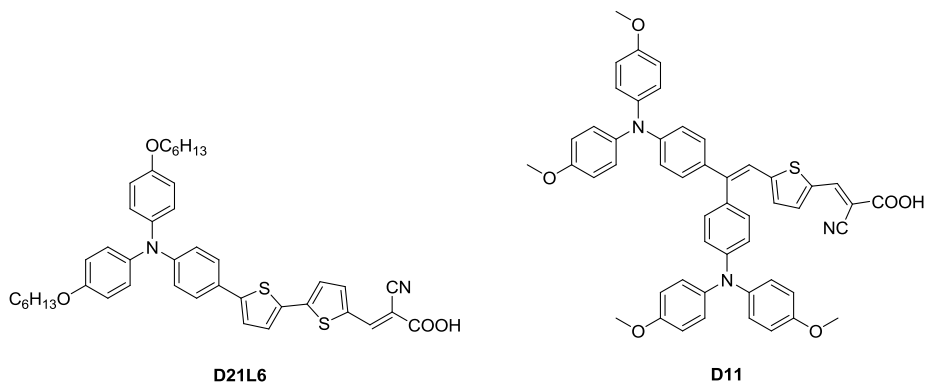
**Figure 3.8**

Yang and coworkers also developed a series of triphenylamine dyes consisting of different substituted phenylene $\pi$-bridges and different electron acceptors. They first introduced the concept of using a triple bond as spacer instead of a double bond. Making a comparison between **TC103** and **L2** (Figure 3.9), the author found that the introduction of the triple bond can red-shift the dye absorption due to the enhancement of $\pi$-spacer. However, the red-shift caused has much less degree than that observed when a double bond was present as in dye **L2**. Introduction of triple bond shows that a larger electron transfer and an hardly changes in the electron lifetimes in TiO$_2$ films but with a decrease in the effective diffusion lengths.[24]The efficiencies achieved with TC103 and D5 are respectively 5% and 6.25%.
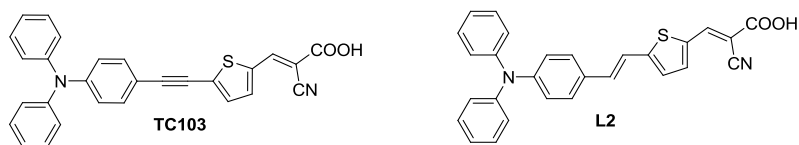


**Figure 3.9**

They also studied in detail the effect of different dye baths and dye structures on DSC performances, discovering that the dye baths for semiconductor sensitization has a crucial effect, due to different dye loading, absorption spectra, and binding modes of the anchored dyes on the TiO$_2$ surface in various solvents.[25]

On the basis of optimized dye bath, dye **TA-St-CA** (Figure 3.10) showed a power conversion efficiency of 5.3%. The introduction of different electron-withdrawing

substituents on the π-spacers phenylene units, or rhodanine-acetic acid as electron acceptor in the molecular structures can give bathochromic shifts of absorption spectra. Significant differences in the redox potential of these dyes also are caused by small structure changes. The same dye was then studied by Kim and co-workers and, after optimization, they found an efficiency of 9.1%[26]
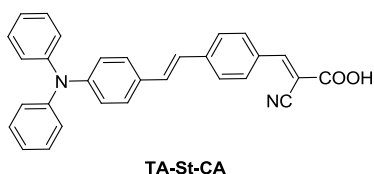


**TA-St-CA**

**Figure 3.10**

Wang and co-workers, using both EDOT and thienothiophene (TT) π-bridges and alkoxy-substituted triphenylamine as electron donors, obtained dye **C217** (Figure 3.11), that showed efficiencies of 9.8% and 8.1% with liquid electrolyte and solvent-free ionic electrolyte respectively. So far, the two efficiency values are the records of DSCs based on organic dyes.[17]



**C217**
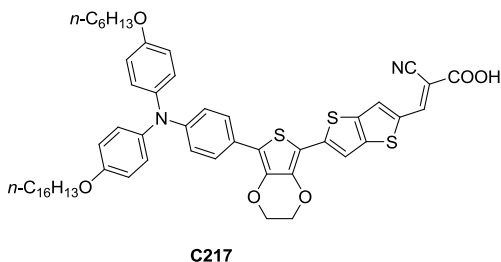
**Figure 3.11**

Lin and co-workers synthesized a series of triarylamine dyes[27] based on benzothiadiazole and benzoselendiazole chromophores. Among these dyes, the comparison between **S1** and **S3** (Figure 3.12) is particularly interesting The former, which is characterized by the presence of a phenylene linked benzothiadiazole, shows an efficiency value of 3.8%, while **S3,** that contains a thiophene unit in the place of the phenyl, only exhibits a 1.15% of efficiency. This feature is in the opposite tendency with respect to the absorption spectra; indeed, **S3** has a bathochromic shift for the charge-transfer band. Probably this is due to a difference degree of planarity of the aromatic segments (phenyl *versus* thiophene) that bridge the donor and acceptor units.

Molecular modeling studies reveal in fact that the phenylene derivative possesses a twisted non-planar geometry, which will decelerate the recombination of charges in the charge separated state.
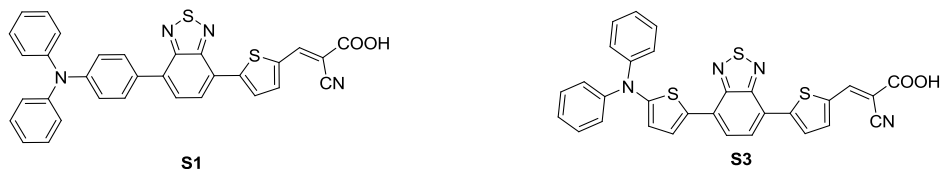


**Figure 3.12**

Starting from **S1**, Lee et al. developed a series of dyes with a π-extended benzothiadiazole associate with different linkers, such as single, double, and triple bonds, to investigate the structure-property relationship between the conversion efficiency and π-bridging system.[28]

In particular, they observed that the presence of a double bond (**HKK-BTZ2**, Figure 3.13) instead of a single bond (**HKK-BTZ1**, Figure 3.13) between the triphenylamine and the thiophene linked benzothiadizole, red-shift the absorption maximum and decreased the ε value. On the contrary, the absorption maximum of **HKK-BTZ3** (Figure 3.13), that contains a triple bond, is blue-shifted relative to both **HKK-BTZ1** and **HKK-BTZ2** sensitizers. This may be attributed to the fact that, in the alkene bridged chromophores, all of the carbon atoms on the branches are $sp^2$ hybridized to give a relatively longer conjugation, while in the case of the alkyne chromophores the carbon atoms are sp and $sp^2$ hybridized. This results in poorer π-orbital overlap and mismatch in energy of the π-orbitals, leading to a blue shift.

This hypsochromic shift leads to a larger band-gap between HOMO and LUMO level. Generally this hands to a rising in the LUMO level and a decrease in the HOMO level. By contrast, in **HKK-BTZ3**, the more electron negativity of sp orbitals with respect to that of $sp^2$ orbitals (**HKK-BTZ2**) leads to the lower of the LUMO level.

Looking at the photovoltaic performance of the three dyes, **HKK-BTZ1** gave the best efficiency of 5.72%, followed by **HKK-BTZ3** (4.55%) **HKK-BTZ2** (3.37%). This result, in contrast with the absorption spectra, could be explained with a better electronic

coupling between the subunit of the triple bond dye, mainly due to an increase planarity of the structure.[29]



HKK-BTZ1

HKK-BTZ2

HKK-BTZ3
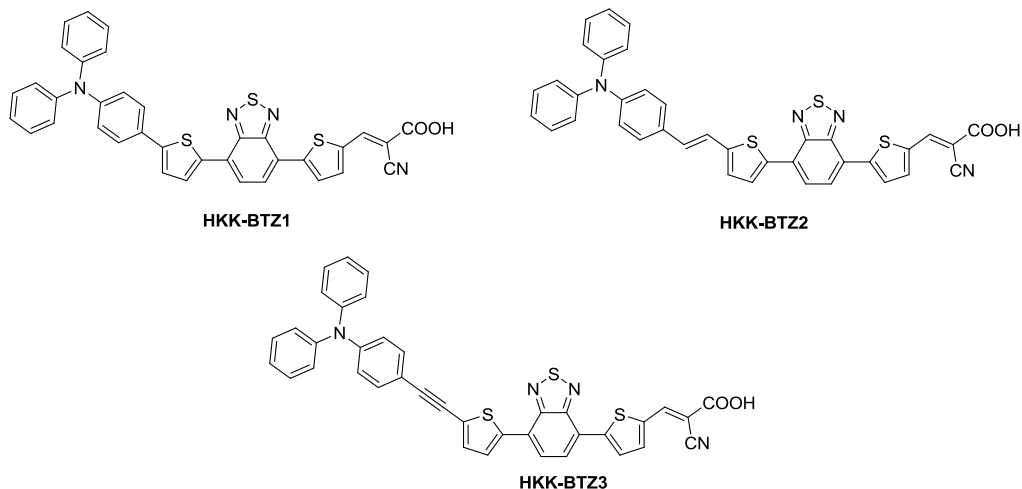
**Figure 3.13**

The introduction of bulky alkoxy groups to triphenylamine (TPA) donor leads in **HKK-BTZ4** (Figure 3.14) to a slight red-shift of the absorption spectrum, essentially due to the TPA-based HOMO destabilization, while the LUMO energy is essentially unaltered. This energy gain in HOMO is explained by strong electron donating effect of the OR substituents.

The alkoxy groups also avoid dye aggregation and lead to a fast dye regeneration, important to avoid the geminate charge recombination between oxidized sensitizers and photoinjected electrons in the nanocrystalline $TiO_2$ film, thus enhancing the efficiency to 7.30%.



HKK-BTZ4

**Figure 3.14**

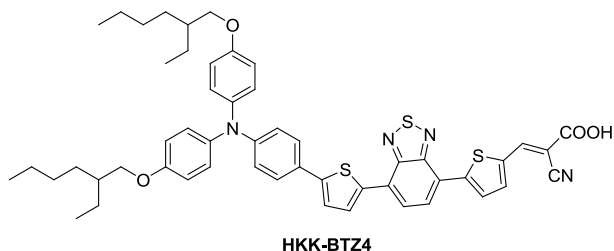Lin and co-worker also reported advanced fluorene-based organic dyes with a narrow absorption region, of which dye **F9** (Figure 3.15) achieved 5.2% efficiency.[30] The efficiency was reduced to about 3.9% with longer bridges (n=2, 3). This finding was attributed to the efficient charge separation. Moreover eplacing the thiophene unit of dye **L2** with furan, Lin and co-workers achieved the efficient organic dye **O1**, which gave 7.4% overall efficiency.[31]
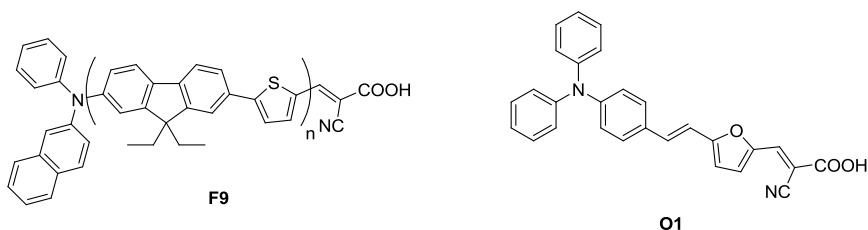


**Figure 3.15**

Great efforts in developing dimethylfluorenylamino-based organic dyes have been made by Ko and co-workers.[32,33] The tailored dimethylfluorenylamino moiety can ensure greater resistance to degradation when exposed to light or high temperature, thanks to its bipolar character that allows the formation of both stable cation and anion radicals. This bulky group is also useful for reducing the aggregation of the dye. Between the number of dyes studied, **JK1** and **JK2**[34] (Figure 3.16) gave efficiencies of 7.2% and 8.0% respectively. This small difference is due to a red-shifted IPCE spectrum of **JK2** compared with that of **JK1** as a result of the presence of an additional thiophene units and therefore of an extended π-conjugation.
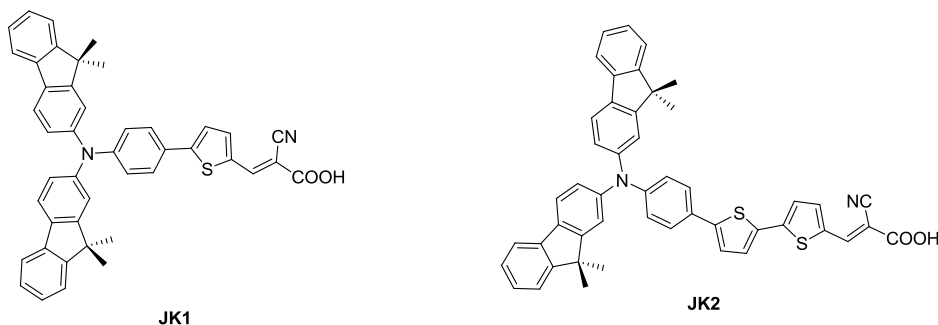


**Figure 3.16**

More structural modifications of fluorenyl-based organic dyes have been performed through changing, $\pi$-bridge, electron acceptor or introducing alkyl chains into the structure. In **JK45** (Figure 3.17), the introduction of long alkyl chains into thiophene $\pi$-bridge enhanced the tolerance toward water in the electrolytes and increased the stability under light, leading to an efficiency of 7.42%. In **JK46** (Figure 3.17), the substitution of a the phenyl spacer with a benzothiophene gave a dye that reached an overall conversion efficiency of 8.6%.[35]



JK45        JK46

**Figure 3.17**

Furthermore, the introduction of long alkyl chains into dimethylfluorenylamino units can lead to an effective spatial separation of the charges, which aids the retardation of charge recombination and gives longer electron lifetime, improving photovoltaic performance and stability of the organic dyes.[36] An example is **JK71** that gave an efficiency of 8.39%.



JK71

**Figure 3.18**

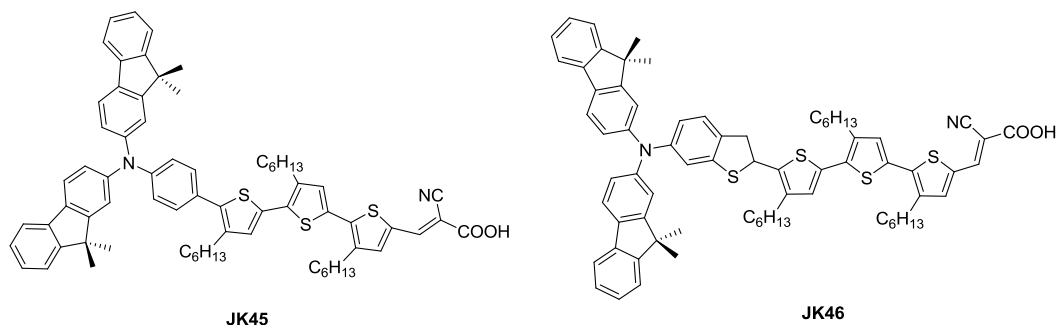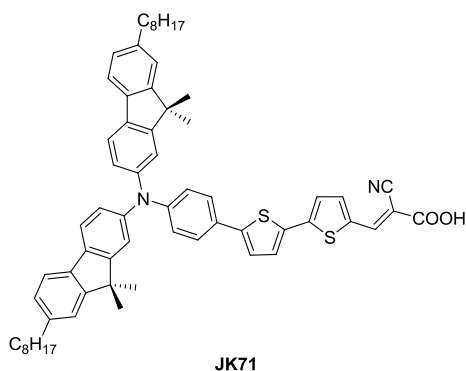Wang and co-workers have made a great progress in developing efficient triarylamine organic dyes.[17, 37, 38,39]

Dye **C203**[40] (Figure 3.19) consists of dimethylfluorenylamino electron donor, dithienothiophene (DTT) $\pi$-bridge, and cyanoacrylic acid acceptor. The DTT has a low free energy of solvation in the high polarity electrolyte, therefore has been insert in the structure in order to avoid the dye desorption during the long-term device operation. The dye exhibits a broad absorption band and high molar extinction coefficient and gives an efficiency of 8.0%. Using the thienothiophene (TT) to replace the DTT unit, they obtained another efficient organic dye, **C201** (Figure 3.19), which exhibited 7.8% in liquid DSSCs but an impressive 4.8% efficiency in solid-state.[41] Later, they further optimized the dye structure with a 3,4-ethylenedioxythiophene (EDOT) $\pi$-bridge, which could red-shift the photocurrent action spectra of dyes compared with thiophene and bithiophene.[42] Dye **C205** (Figure 3.19) with a bi-EDOT unit gave high efficiency, 8.3%. They attributed the improved efficiency to its good spectral match with the solar irradiation spectrum by introducing the bi-EDOT unit.
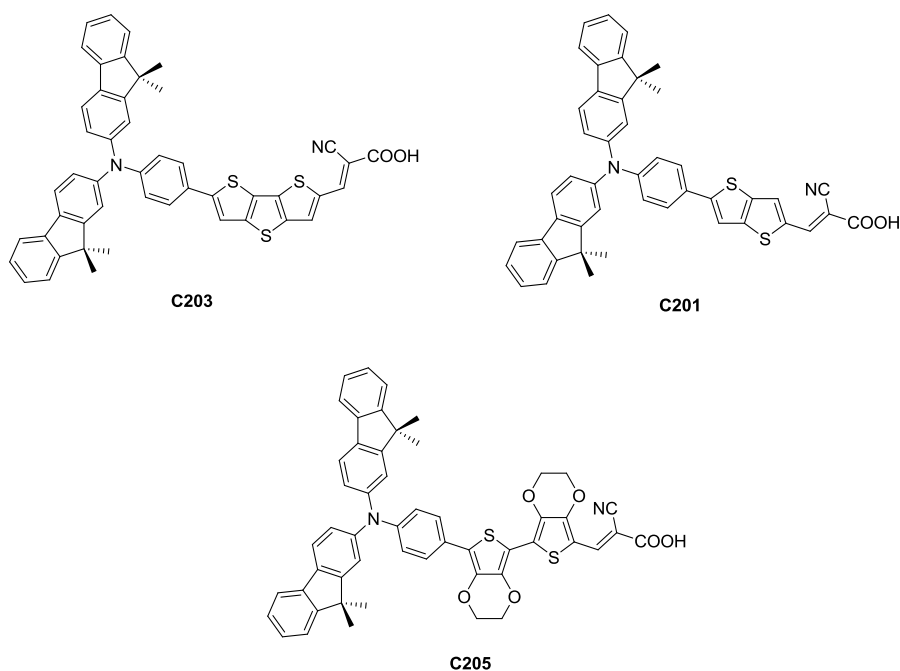


**Figure 3.19**

## 3.2.5 INDOLE

Hara et al.[43] first introduced the thieno[3,2,-*b*]indole as donor group in organic dyes, *n*-hexyl substituted oligothiophene units as a π-conjugated bridge, and cyanoacrylic acid group as an electron acceptor and anchoring group. Thieno[3,2-*b*]indole features an electron-rich thiophene ring, therefore has a strong electron donating ability and a great planarity, leading to an extended π-conjugation of the molecule, a red shift of the absorption spectra and an enhancement molar extinction coefficient and light harvesting ability. In their study they investigate the effect of the chain length on the cell's performance, finding that increasing the number of the thiophene units, a red-shifted absorption, due to an extend π-conjugation, is observed but, at same time, also an increase of HOMO energy level is noticed.

DSSCs based on these dyes have shown high photo-electricity conversion efficiency up to 7.8%. (**MKZ39-41**, Figure 3.20)



n = 1-4
**MKZ39-41**
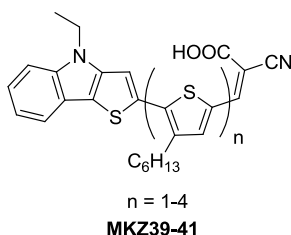
**Figure 3.20**

## 3.2.6 HETEROANTHRACENE DYES

Recently, Sun, Yang, and co-workers developed a novel phenoxazine dye **TH304** consisting of a thienyl π-bridge and a bi-rhodanine electron acceptor, in which the alkyl chains were adopted to increase the solubility and suppress aggregation.[44] Although the **TH304**-based DSCs did not obtain a higher efficiency value than 3.0%, they showed a broad IPCE spectrum over the whole visible range extending into the near-IR region up to 920 nm, which is the broadest IPCE spectrum in the organic dye-based DSCs.
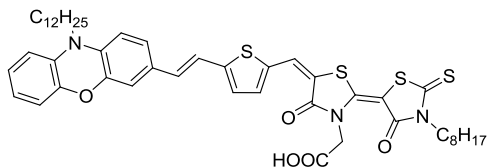
**TH304**
**Figure 3.21**

## 3.3 CONCLUSION

In summary, in these years a lot of research work on metal-free dyes have been done, achieving very good efficiency also higher than that of Ruthenium complexes. By the way, value more than 11% have not been reached yet, therefore still a great interest in this field is present.

As treated above, each part of the push-pull system have been extensively studied and the following consideration have emerged.

As donor system, triarylamines are the most studied, thanks to their great stability, electron mobility, strong donating ability and aggregation resistance due to non-planar molecular configuration .

In the correct geometry, the energy level of the nitrogen nonbonding lone pair is well matched to donate into the $\pi^*$ of the attached aromatic ring.[45] This arrangement destabilizes the HOMO and reduces ionization potential creating a strong electron density donating effect, that further improve with the introduction of various alkoxy substituents.[46] 4-(*N,N*-(di-*p*-anisyl)amin) phenyl moiety as the electron donor is known to show long-lived charge separated states.[47]

Replacement of the phenyl ring that is directly conjugated with the bridge with a heteroaromatic ring, such as a thiophene, can increase the donating strength, reducing aromatic stabilization contributes.[48]

Concerning the spacer, in order to broaden the absorption spectra of the sensitizers in the visible and near-IR region, one strategy is to introduce more conjugate bridges between the donor and acceptor. The π-conjugated linker plays an important role not only in tuning and modifying the optical properties of DSSC devices under the sun light

radiation, but also controlling the intra-molecular electron-transfer and electron-injection from the excited dye to the conduction band of semiconductor.

Starting from the double bond, several are the bridges employed in the dyes, such as triple bond, aromatic and heteroaromatic rings. Among these, thiophene is an appealing linker extensively used in the literature as single unit or condensed in more complex structure thanks to its electron-donor ability. However, a lot of activity in this field is still devoted to the research of a excellent bridge, able to give a broad red-shifted absorption spectra but also a good electronic connection between A and D unit.

Regarding acceptor groups, the most used are carboxylic acid alone or coupled to a rhodanine and cyanoacrilic acid. The latter seems to be the best one thanks to the electron-withdrawing ability of CN, rhodanine acetic acid has a good influence on the absorption spectra but also problems in electron injecton due to the fact that the acidic group is not fully conjugated with the rest of the moiety.

In our research group, we are currently investigating all three this component of the push-pull system, with the aim to understand the influence structure-properties of each-one as treated in the next chapter.

# REFERENCES

[1] K.Hara, Z.Wang, S. T.Sato, A.Furube, R.Katoh, H.Sugihara, Y.Dan-Oh, C. Kasada, A. Shinpo, S. Suga, *J. Phys. Chem. B,* **2005**, *109*, 15476.

[2] J. M. Rehm, G. L.McLendon, Y. Nagasawa, K. Yoshihara, J. Moser, M. Grätzel, *J. Phys. Chem.,* **1996**, *100*, 9577.

[3] K. Hara, M. Kurashige, Y. Dan-oh,; C. Kasada,; A. Shinpo, S. Suga, K. Sayama,; H. Arakawa, *New J. Chem.* **2003**, *27*, 783.

[4] T. Horiuchi, H. Miura, S. Uchida, *Chem. Commun.,* **2003**, *24*, 3036.

[5] L. Schmidt-Mende, U.Bach, R. Humphry-Baker, T. Horiuchi, H. Miura, S. Ito, S. Uchida, M. Grätzel, *AdV. Mater.,* **2005**, *17*, 813.

[6] T. Horiuchi, H. Miura, K. Sumioka, S. Uchida, *J. Am. Chem. Soc.,* **2004**, *126*, 12218.

[7] S. Ito, S. M. Zakeeruddin, R. Humphry-Baker, P. Liska, R. Charvet, P. Comte, M. K. Nazeeruddin, P. Pechy, M. Takata, H. Miura, S. Uchida, M. Grätzel, *AdV. Mater.,* **2006**, *18*, 1202.

[8] S. Ito, H. Miura, S. Uchida, M. Takata, K. Sumioka, P. Liska, P. Comte, P. Pechy, M. Grätzel, *Chem. Commun.* **2008**, 5194.

[9] T. Dentani, Y. Kubota, K. Funabiki, J. Jin, T. Yoshida, H. Minoura, H. Miura, M. Matsui, *New J. Chem.,* **2009**, *33*, 93.

[10] D. Kim, M. S. Kang, K. Song, S. O. Kang, J. Ko, *Tetrahedron,* **2008**, *64*, 10417.

[11] D. Kuang, S. Uchida, R. Humphry-Baker, S. M. Zakeeruddin, M. Grätzel, *Angew. Chem. Int. Ed.,* **2008**, *47*, 1923.

[12] D. Kim, K. Song, M. S. Kang, J. W. Lee, S. O. Kang, J. Ko, *J. Photochem. Photobiol. A,* **2009**, *201*, 102.

[13] R. Chen, X. Yang, H. Tian, L. Sun, *J. Photochem. Photobiol. A,* **2007**, *189*, 295.

[14] R. Chen, X. Yang, H. Tian, X. Wang, A. Hagfeldt, L. Sun, *Chem. Mater.,* **2007**, *19*, 4007.

[15] Y. Hao, X. Yang, J. Cong, H. Tian, A. Hagfeldt, L. Sun, *Chem.Commun.,* **2009**, *27*, 4031.

[16] R. Chen, G. Zhao, X. Yang, X.Jiang, J. Liu, H. Tian, Y. Gao, X. Liu, K. Han, M. Sun, L. Sun, *J. Mol. Struct.,* **2008**, *876*, 102.

[17] G. L. Zhang, H. Bala, Y. M. Cheng, D. Shi, X. J. Lv, Q. J. Yu, P. Wang, *Chem. Commun.,* **2009**, *16*, 2198.

[18] W.-H. Liu,I-C. Wu, C.-H. Lai, C.-H. Lai,P.-T. Chou,Y.-T. Li,C.-L. Chen,Y.-Y. Hsub, Y. Chi, *Chem. Commun.,* **2008**, *41*, 5152.

[19] T. Kitamura, M. Ikeda, K. Shigaki, T. Inoue, N. A. Anderson, X. Ai, T. Q. Lian, S. Yanagida, *Chem. Mater.* **2004**, *16*, 1806.

[20] D. P. Hagberg, T. Edvinsson,; T. Marinado, G. Boschloo, A. Hagfeldt, L. C. Sun, *Chem. Commun.,* **2006**, *21*, 2245.

[21] D. P. Hagberg, T. Marinado, K. M. Karlsson, K. Nonomura, P. Qin, G. Boschloo, T. Brinck, A. Hagfeldt, L. Sun, *J Org. Chem*, **2007**, *72(25),* 9550.

[22] J. H. Yum, D. P. Hagberg, S. J. Moon, K. M. Karlsson, T. Marinado, L. C. Sun, A. Hagfeldt, M. K. Nazeeruddin, M. Grätzel, *Angew. Chem. Int. Ed.,* **2009**, *48*, 1576.

[23] D. P.,Hagberg, J. H. Yum, H. Lee,; F. De Angelis, T. Marinado, K. M. Karlsson, R. Humphry-Baker, L. C. Sun, A.Hagfeldt, M. Grätzel, M. K. Nazeeruddin, *J. Am. Chem. Soc.,* **2008**, *130*, 6259.

[24] C. Teng, X. Yang, C. Yang, H. Tian, S. Li, X. Wang, A. Hagfeldt, L. Sun, *J. Phys. Chem. C,* **2010**, *114,* 11305.

[25] H. N. Tian, X. C. Yang, R. K. Chen, R. Zhang,; A. Hagfeldt,; L. C. Sunt, *J. Phys. Chem. C,* **2008**, *112*, 11023.

[26] S. Hwang,J. H. Lee, C. Park, H. Lee, C. Kim, C. Park,M.-H. Lee, W. Lee, J. Park, K. Kim, N.-G. Park C. Kim, *Chem. Commun*., **2007**, *46*, 4887–4889.

[27] M. Velusamy, K. R. J. Thomas, , J. T. Lin, Y. C Hsu, K. C. Ho, *Org. Lett.* **2005**, *7*, 1899.

[28] D. H. Lee, M. J. Lee, H. M. Song, B. J. Song, K. D. Seo, M. Pastore,C. Anselmi, S. Fantacci, F. De Angelis, M. K. Nazeeruddin, M. Grätzel, H. K. Kim, *Dyes and Pigments,* **2011 ,** *91,* 192.

[29] N. S. Baek, J.-H. Yum, X. Zhang, H. K. Kim, M. K. Nazeeruddin, M. Grätzel, *Energy Environ. Sci.*, **2009**, *2*, 1082.

[30] K. R. J. Thomas, J. T. Lin, Y. C. Hsu, K. C. Ho, *Chem. Commun.,***2005**, *32,* 4098.

[31] J. T. Lin, P.-C. Chen, Y.-S. Yen, Y.-C. Hsu, H.-H. Chou, M.-C. P. Yeh, Org. Lett.*,* **2009**, *11*, 97.

[32] S. Kim, H. Choi, D. Kim, K. Song, S. O. Kang, J. Ko, *Tetrahedron,* **2007**, *63*, 9206.

[33] S. Kim, H. Choi, C. Baik, K. Song, S. O. Kang, J. Ko, *Tetrahedron,* **2007**, *63*, 11436.

[34] S. Kim, J. K. Lee, S. O. Kang, J. Ko, J. H. Yum, S. Fantacci, F. De Angelis, D. Di Censo, M. K. Nazeeruddin, M. Grätzel, *J. Am.Chem. Soc.,* **2006**, *128*, 16701.

[35] H. Choi, C. Baik, S. O. Kang, J. Ko, M. S. Kang, M. K. Nazeeruddin, M.Grätzel, *Angew. Chem. Int. Ed.,* **2008**, *47*, 327.

[36] S. Kim, D. Kim, H. Choi, M. S. Kang, K. Song, S. O. Kang, J. Ko, *Chem. Commun.,* **2008**, 4951.

[37] M. F. Xu, R. Z. Li, N. Pootrakulchote, D. Shi, J. Guo, Z. H. Yi, S. M. Zakeeruddin, M. Grätzel, P. Wang, *J. Phys. Chem. C,* **2008**,*112*, 1977.

[38]M. Xu, S. Wenger, H. Bala, D. Shi, R. Li, Y. Zhou, S. M. Zakeeruddin, M. Grätzel, P. Wang, *J. Phys. Chem. C,* **2009,** *113,* 2966.

[39] G. L. Zhang, Y. Bai, R. Z. Li, D. Shi, S. Wenger, S. M. Zakeeruddin, M. Grätzel, P. Wang, *Energy En*V*iron. Sci.,* **2009**, *2*, 92.

[40] H. Qin, S. Wenger,M. Xu, F. Gao, X. Jing, P. Wang, S. M. Zakeeruddin, M. Grätzel, *J. Am. Chem. Soc.* **2008**, *130*, 9202–9203

[41] Wang, M. K.; Xu, M. F.; Shi, D.; Li, R. Z.; Gao, F. F.; Zhang, G. L.;Yi, Z. H.; Humphry-Baker, R.; Wang, P.; Zakeeruddin, S. M.;Gra¨tzel, M. *Ad*V*. Mater.* **2008**, *20*, 4460.

[42] Xu, M. F.; Wenger, S.; Bala, H.; Shi, D.; Li, R. Z.; Zhou, Y. Z.;Zakeeruddin, S. M.; Gra¨tzel, M.; Wang, P. *J. Phys. Chem. C,* **2009**, *113*, 2966.

[43] X.-H. Zhang, Y. Cui, R. Katoh, N. Koumura, K. Hara, *J. Phys. Chem. C,* **2010,** *114,* 18283.

[44] H. N. Tian, X. C. Yang, R. K. Chen, A. Hagfeldt, L. C. Sun, *Energy En*V*iron. Sci.* **2009**, *2*, 674.

[45] Larry R. Dalton,* Philip A. Sullivan, and Denise H. Bale *Chem. Rev.* **2010**, *110,* 25.

[46] Y. Cheng, J. Luo, S. Hau, D. H. Bale, T.-D. Kim, Z. Shi, D. B. Lao, N. M. Tucker, Y. Tian, L. R. Dalton, P. J. Reid, A. K-Y. Jen, *Chemistry of Materials*, **2007**, *19(5)*, 1154.

[47] B. K. Spraul, S. Suresh, T. Sassa, M. A. Herranz, L. Echegoyen, T. Wada, D. Perahiaa D. W. Smith Jr. *Tetrahedron Letters*, **2004**, 45(16), 3253.

[48] J. A. Davies, A. Elangovan, P. A. Sullivan, B. C. Olbricht, D. H. Bale, T. R. Ewy, C. M. Isborn, B. E. Eichinger, B. H. Robinson, P. J. Reid, X. Li, L. R. Dalton, *J. Am. Chem. Soc.,* **2008**, *130*, 10565.

# NOVEL BDTs-BASED

# METAL-FREE DYES
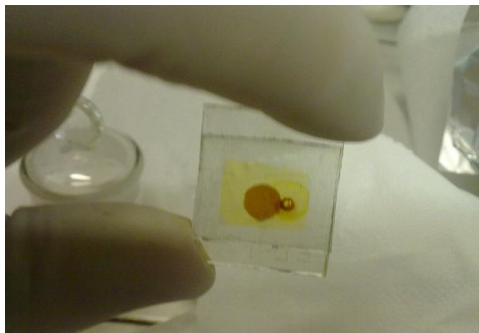
## 4.1 INTRODUCTION

As discussed in the previous chapter, all of the components of the system D-π bridge-A are important and have been extensively studied, looking for new structures to insert in the push-pull system or for the best combination of known units. Up to now, even if efficiencies comparable to those of Ru based dyes have been reached, a lot of work still remain to do, with the aim to get close to inorganic cell efficiency.

In this thesis our contribution in this field, concerning the synthesis of new spacers to be inserted in the push-pull system for DSSCs, is reported.

## 4.2 THE π-BRIDGE

The π-conjugated linker connecting the electron-donor and the acceptor/anchoring group of a dye (see **Chapter 3**, par. 3.1) plays an important role, not only in tuning and modifying the optical properties of DSSC devices under the sun light radiation, but also in controlling the intra-molecular electron-transfer and electron-injection from the excited dye to the conduction band of semiconductor.

Organic sensitizers with extended π-conjugated spacers have been shown to be operative in increasing the molar extinction coefficients as well as in realizing panchromatic light harvesting, giving moderate DSSC efficiency and stability. [1-4] In addition to the length, the intrinsic electronic characteristics of the π-conjugated spacer may also affect the spectral response of the dye. [4] In most organic D–π–A dyes, the π-conjugated spacers linked to the acceptor (cyanoacrylic acid) are typically electron-rich systems, such as thiophene, [5] furan, [6] selenophene, [7] and pyrrole derivatives. [8]

Notably, the introduction of fused ring building blocks, [9,10] in the structure of the dye has proved to be an effective strategy for enhancing the light-harvesting capacity, leading to impressive performances.

Thiophene-containing fused-aromatic compounds, in particular, have recently attracted much attention; they represent an interesting source for electronic materials to be used

in organic devices, such as organic field-effect transistors (OFETs),[11] organic light emitting diodes (OLEDs),[12,13] and photovoltaic cells conductors.[14,15]

This is mainly due to their advantageous characteristics such as facile synthesis, chemical stability, extended π-frameworks, favorable stacking behavior in the solid state, conductivity, high polarizability, tunable spectroscopic and electrochemical properties, high field effect mobility and enhanced solubility compared to hydrocarbon compounds.[16,17] In DSSC dyes, spacers such as cyclopentadithiophene, thieno[3,4-b]-thiophene, dithienosilole, benzothiadiazole have been largely employed with good results. Searching for more efficient high performance dyes, the development of new fused ring building blocks may lead to synthesis of interesting molecules with tailor-made photophysical, electrochemical and chemico-physical properties.

In this context, we focused our research on the design and synthesis of novel π-bridge molecules based on two isomeric heteroaromatic polyconjugate systems: namely benzo[1,2-*b*:4,3-*b'*]dithiophene (**BDT**) and benzo[1,2-*b*:4,5-*b'*]dithiophene (**BDT₁**) (Figure 4.1)

## 4.2.1 BENZO[1,2-b:4,5-b']DITHIOPHENE AND BENZO[1,2-b:4,3:b']DITHIOPHENE

Benzo[1,2-*b*:4,3-*b'*]dithiophene (**BDT**) and benzo[1,2-*b*:4,5-*b'*]dithiophene (**BDT₁**) are ortho-fused heterocyclic systems (Figure 4.1) known in the literature since the seventies that recently gained a lot of interest for applications in optoelectronic and photovoltaic fields.

**BDT** and **BDT₁** attracted our attention because their rigid, π-conjugated, condensed-polycyclic structure[18,19] leads to unique electronic properties such as conductivity, high field effect mobility and tunable stacking in the solid state; rigid structures hamper the roto-vibrational modes responsible for the deactivation of the excited states in functional materials. In this perspective, **BDT** and **BDT₁** are therefore important frameworks in functional organic materials for optoelectronic devices.[20,21,22]
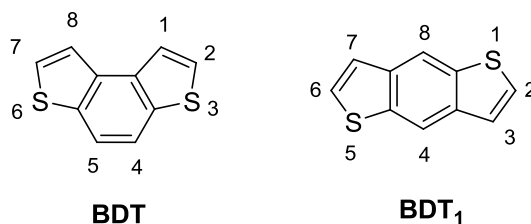
**Figura 4.1**

## 4.2.1.1    PHYSICAL AND ELECTRONIC PROPERTIES

Both the molecules, that are white solids, are characterized by a completely planar structure as demonstrated by the X-ray analysis.[23, 24] (Figure 4.2)



**Figure 4.2**

Their electrochemical properties, studied by means of cyclic voltammetry (CV), are summarized in Table 1. The two molecules show irreversible oxidation and reduction waves (Figure 4.3) with the oxidation potentials, defined by anodic peaks, that shift catodically from 1.448 V for **BDT** to 1.395 V for **BDT$_1$**.
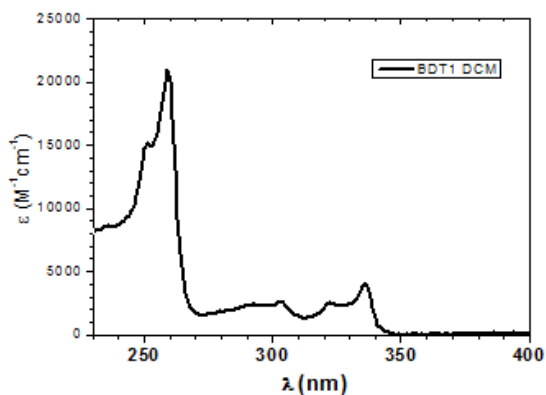


**Figure 4.3**
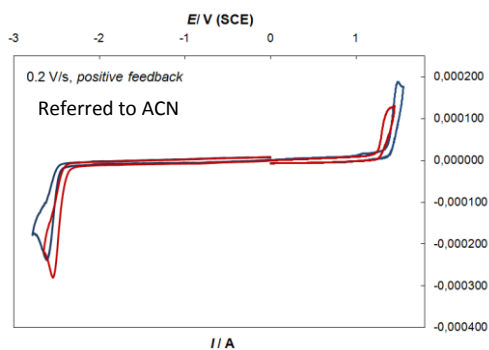
The HOMO levels are estimated to be -5.81 eV for **BDT₁** and -5.90 eV for **BDT**, while the LUMO -1.87 eV and -1.80 eV respectively. The energy gaps result therefore 3.93 eV for **BDT₁** and 4.10 eV **BDT** (the latter in agreement with the data reported in the literature).[51] (Table 4.1)

| | $E_{p,a}$ [V(SCE)] | $\lambda_{max}$ ($CH_2Cl_2$) [nm] | HOMO [eV] | LUMO [eV] | $E_g$ [eV] |
|---|---|---|---|---|---|
| **BDT₁** | 1.395 | 335/344 | -5.81 | -1.87 | 3.93 |
| **BDT** | 1.488 | 318 | -5.90 | -1.80 | 4.10 |

**Table 4.1**

The UV spectra of the two compounds are reported below. **BDT₁** (a) presents three bands, located at around 260, 300, and 330 nm, while the **BDT** (b) spectrum consists of several bands between 240-260 nm e 290-330 nm. (Figure 4.4)



**(a)**
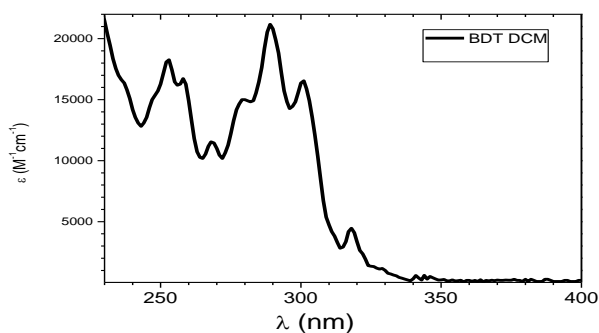


**(b)**

**Figure 4.4**

In Figure 4.5, the fluorescence spectra are shown. The **BDT$_1$** (a) shows an emission at 340 nm characterized also at room temperature by a resolved vibronic structure. This band slightly blu-shifts in solid matrix at low temperature (77K, 2-MeTHF) in which a further increased of the band resolution can be noted. (Figure 4.5) On the contrary, **BDT** (b) presents an emission at about 330 nm, with a quite different vibronic structure that again increases in resolution once measured in 2-MeTHF at 77K.
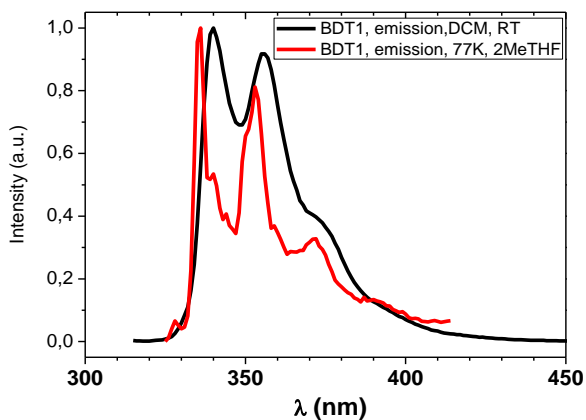


(a)
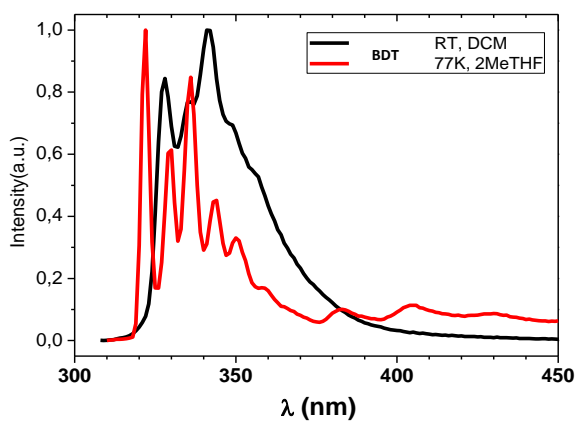


(b)

**Figure 4.5**

## 4.2.1.2 REACTIVITY, USE AND APPLICATIONS

As aforementioned, the two benzodithiophenes gain a great importance for the development of new materials since the opening of the field of organic conductors.

In literature, **BDT** and **BDT₁** are mainly employed as monomers for the synthesis of various polymers. To this aim, they are therefore symmetrically functionalized in the $\alpha$ position of the two thiophene rings (that are 2,6 in **BDT₁** or 2,7 in **BDT**) with groups such as –CHO, -Br, -I or –TMS (Figure 4.6), useful for subsequent condensation or coupling reactions. The introduction of substituents in the central benzene ring is, on the contrary, accomplished during the synthesis of the heteroaromatic scaffold, following different synthetic strategies.[18,25]



CHO; I; Br; TMS; $C_nH_{2n+1}$; $CH(CN)_2$;

$R' = CO_2Et$; $CO_2H$; $CH_3$; $CHCH_3$; $C_{12}H_{25}$; ⤳≡—$C_{10}H_{21}$
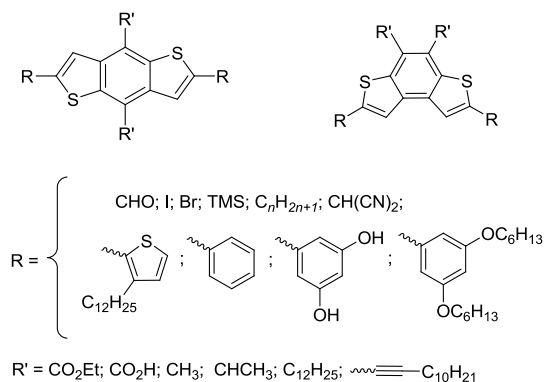
**Figura 4. 6**

Some mono-functionalized **BDT** and **BDT₁** derivatives are also known (Figure 4.7), while only few examples of benzodithiophenes bearing two different groups in 2,6 (**BDT₁**) or 2,7 (**BDT**) positions has been reported. [26,27,28].
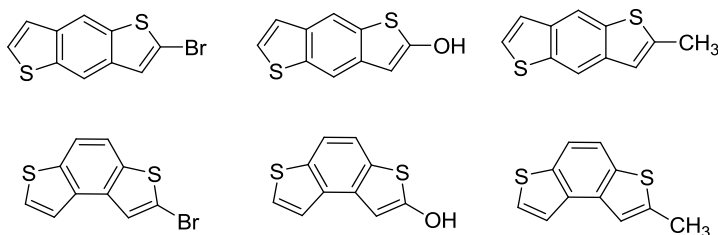


**Figure 4.7**

Recently, copolymers containing benzo[1,2-b:4,3-b']-dithiophene (**BDT**) and benzo[1,2-b:4,5-b']-dithiophene (**BDT$_1$**) as the donor unit have exhibited outstanding photovoltaic properties for applications in polymer bulk heterojunction (BHJ) solar cells.[29,21]

## 4.2.1.3 BDT DERIVATIVES AS Π-SPACERS

The attractiveness of **BDT** isomers as π-conjugated spacer in organic dyes for DSSCs is justified by a number of properties such as thermal stability, large entirely and planar conjugated structure, that favors light harvesting. Moreover their higher oxidation potential relative to other fused thiophene may result in a low HOMO level and therefore in high open-circuit voltage.[30]

For these reasons we decided to develop new organic sensitizers containing benzodithiophene spacers, with the aim of studying their properties in comparison with those of dyes bearing thiophene units, already reported in the literature.

During our investigation, similar molecules have been published by Xue and coworkers.[24] They synthesized a series of **BDT$_1$** -containing chromophores bearing an alkoxy-substituted triphenylamine as electron donor and a hydrophilic cyanoacrylic acid as electron acceptor. (Figure 4.8)
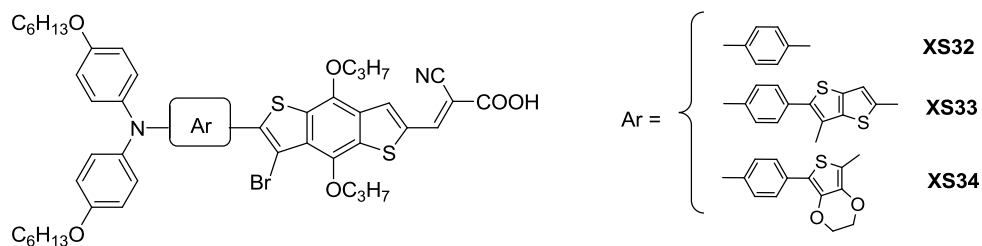


**Figure 4.8**

In particular, apart from **XS32**, they combined **BDT**1 spacer with other electron-rich condensed heteroaromatic systems such as thienothiophene (**XS33**) and EDOT (**XS34**). Interestingly, the simplest chromophore **XS32** gave the best performance with an efficiency of 5.68%, followed by **XS34** (5.05%) and **XS33** (4.17%). From this study, it resulted that this new class of compounds has the appropriate characteristics required

for the successfully application in DSSCs, thus confirming the foresight of our interest toward these spacers.

Concerning **BDT**, to the best of our knowledge , organic dyes based on this unit have not yet been reported in the literature.

## 4.2.1.4    SYNTHESIS

**Benzo [1,2-b:4,5-b']dithiophene (1)**

**BDT$_1$ (1)** is known in the literature[31] since 1970 and several synthetic strategies for its preparation are reported. Among these, the best one seems to be that shown in Scheme 4.1.
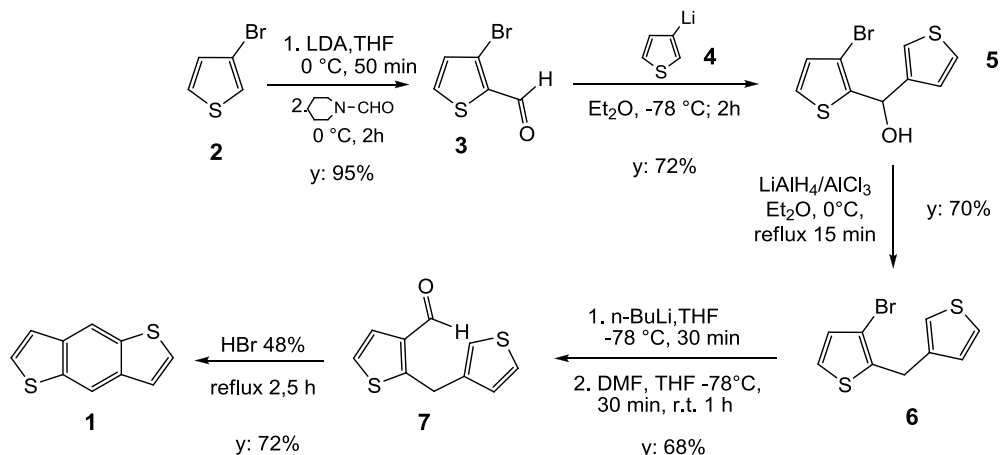


**Scheme 4.1**

The synthetic sequence consists of five steps. Starting from 3-bromothiophene **2**, the first reaction is a formylation with *N*-formyl piperidine to obtain 3-bromothiophene-2-carbaldehyde **3** in 95% yield. This aldehyde is then reacted with the *in situ* generated 3-litiothiofene **4** to give 3-bromo-α-(3-thienyl)-2-thiofenemethanol (**5**) in 70% yield, which in turn, is reduced with LiAlH$_4$/AlCl$_3$ to give 3-bromo-2-(3-thienylmethyl)thiofene (**6**). Product **6** is then formylated in the same conditions of **2**, to give in good yield the aldehyde derivative **7**, which is eventually treated with HBr or PPA to give the target product **BDT$_1$ 1**, with a overall yield of 24% for the five steps.

The drawback of this synthesis is the number of steps, but, on the other hand, yields are quite high and the reaction conditions are rather simple, except for the reduction step. Scaling up this reaction, indeed, in additions to the use of hazardous $LiAlH_4/AlCl_3$ mixture, poor yield of **6** was achieved.

Trying to optimize this reaction, we found that it can be easily performed using as reducing system TMSCl and NaI[32] in $CH_3CN$ at 0 °C for 2 hours. Compound **6** was obtained in 95% yield. (Scheme 4.2)
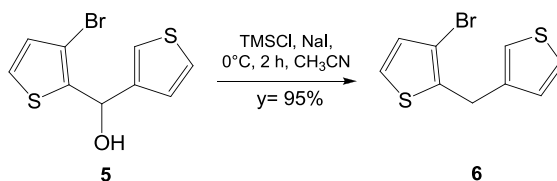


**Scheme 4.2**

Concerning the mechanism of this reduction, to date only one hypothesis has been reported.[33] (Scheme 4.3) The first step could be the generation of the silyl derivative (a) which is subsequently transformed into the iodide derivative (b) *via* the carbocation intermediate. Finally, a radicalic reaction occurs by means of the *in situ* generated hydriodic acid .
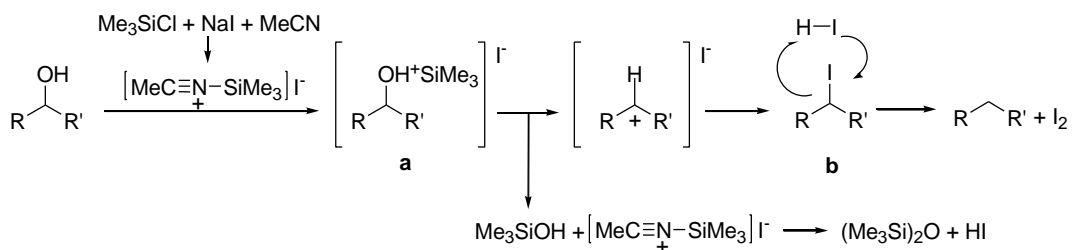


**Scheme 4.3**

A further improvement in the synthesis reported in Scheme 4.1 was obtained in the last step, running the cyclization with PPA in $CH_3COOH$ as solvent, and heating for 30 minutes at 70 °C. (Scheme 4.4) At the end of the reaction, the mixture was poured in ice-water and the product was simply isolated by filtration. The previous condition that

employed HBr (48%) led to the formation of degradation products, on the contrary the use of PPA made the reaction cleaner and simpler. [34]
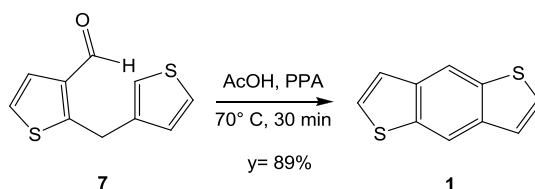


**Scheme 4.4**

The optimization work resulted in a really efficient synthetic procedure for $BDT_1$ that allowed us to increase the overall yield from 24% to 39%, working on 10 gram scale.

**Benzo [1,2-b:3,4-b']ditiofene 8**

The two-steps synthesis of **BDT 8** is shown in Scheme 4.5. [35]
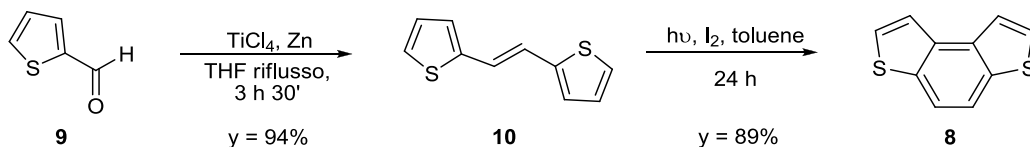


**Scheme 4.5**

Starting from 2-thiophene carboxyaldehyde (**9**) a McMurry coupling with $TiCl_4$, and Zn, gave the 1,2-bis(2-thienyl)ethylene (**10**) in 94% yield.[36] This was then photocyclized by means of a low pressure Hg lamp (500 W), with a catalytic amount of $I_2$ in toluene for 24 h, affording BDT **8** in 89% yield.[36]

## 4.3  AIM OF THE WORK

The aim of the present part of this Ph.D. thesis has been the design and synthesis of new and efficient **BDT** and $BDT_1$ containing organic dyes for DSSCs applications. Within this aim we have also addressed our study to understand the influence of each component of the D-π-A system on the dye properties in order to design the chromophores with a rational approach.

## 4.3.1 DYE DESIGN

After an extensive study of the literature and assisted by preliminary molecular modeling calculations done in collaboration with Dr. Filippo De Angelis, we designed the synthesis of several novel benzodithiophene-based sensitizers. In order to investigate the structure-performance relationship of the dyes in the solar cells, starting from the model compound **11** (Figure 4.9), we designed a small library of homogenous compounds that differ for the π-bridge (**12**-**16,** figure 4.10), the donor group (**17**, **18,** figure 4.11) or the acceptor group (**19**, **20,** figure 4.12). In particular compound **11** presents the classical *N,N*-bis(-methoxyphenyl)aniline (here indicated as MTPA) as donor group, the 2-ethenyl substituted **BDT$_1$** as spacer and the cyanoacrylic acid as acceptor-anchoring group. MTPA has been chosen thanks to its great stability, electron mobility, strong donating ability and aggregation resistance due to non-planar molecular configuration. In addition, the presence of the two *p*-methoxy groups would further enrich the electron-donating system, thus extending the absorption region in the visible light, avoiding charge recombination and increasing the electron lifetime.[37,38]

The double bond is known to give a red-shift as well as to extend the absorption spectrum, as a consequence of the increased conjugation of the system. Moreover, the cyanoacrylic group has been inserted in order to further increase the pull ability of the acceptor unit.
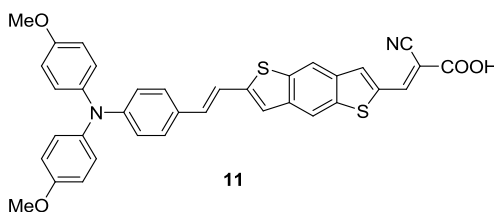


**Figure 4.9**

As we were interested in investigating the potentiality of **BDT** and **BDT$_1$** as spacers, we designed derivatives in which the benzodithiophene scaffolds alone (compounds **12** and **16**) or in combination with double or triple bonds, for extending the conjugation,

(compounds **13**-**15**) are present, with the aim to obtain band gap reduction and enlargement of the absorption spectra. In particular, the presence of a triple bond should ensure more planarity and therefore more conjugation to the molecule, thus avoiding energy losses due to photoisomerization processes.[39]
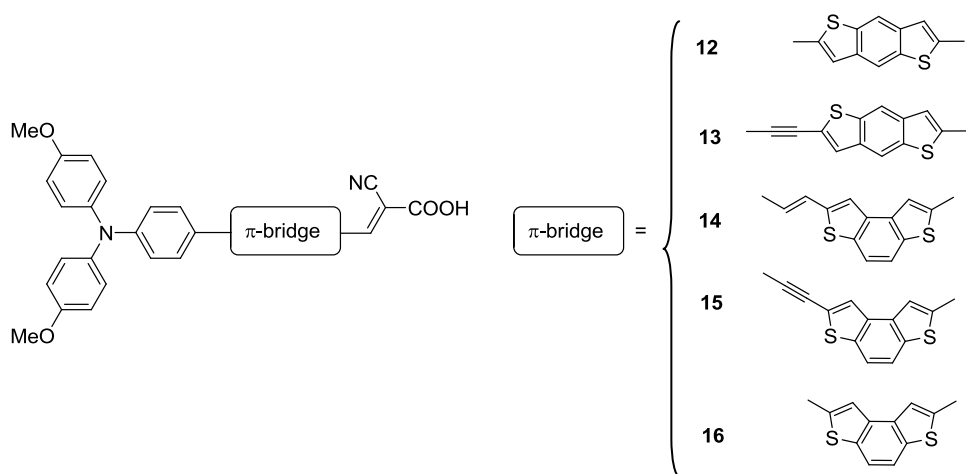


**Figure 4.10**

Studying the influence of the donor group D in these dyes, we decided to substitute the MTPA with the bis-dimethylfluorenyl-aniline (**17**) and the *N,N*-(*p*-dimethoxyphenyl)thiophenamine (**18**). (Figure 4.11) The former triarylamine group has been chosen for its steric hindrance, useful to avoid aggregation on TiO$_2$ surface: in fact, it has a tridimensional structure due to the out of plane orientation of the methyl groups.[40,41]

In derivative **18** with the introduction of a thiophene instead of a benzene ring in the donor moiety, we expected to obtain a more electron-rich unit with improved electron-donating capability and a strongly red-shifted absorption spectra.[42]
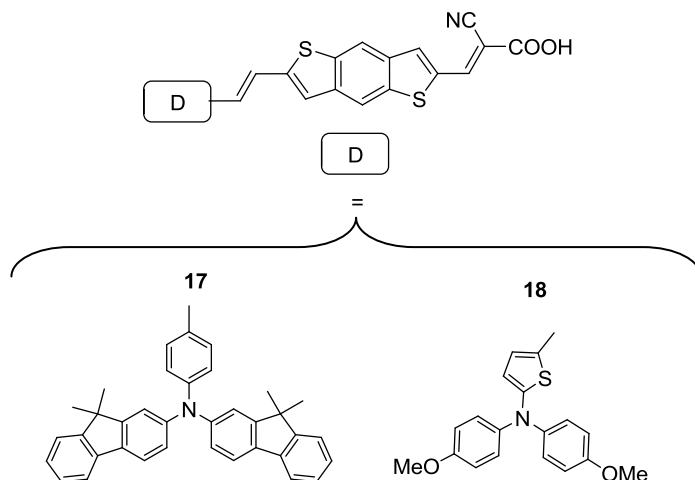
**Figure 4.11**

Finally the presence in dyes **19** and **20** of the less conjugated and electron-withdrawing carboxylic group in place of the cyanoacrylic acid as anchoring group is interesting for evaluating the effective anchoring ability of the dyes to the semiconductor. (Figure 4.12)
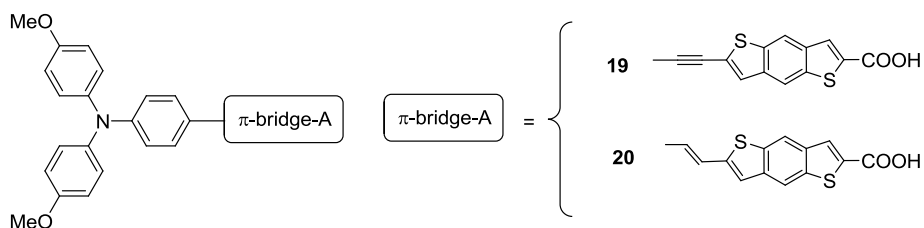


**Figure 4.12**

## 4.3.2 THEORETICAL INVESTIGATIONS

Before dye synthesis, to gain insight into the molecular, ground and excited state electronic structure of these new dyes, theoretical calculations and spectra simulation were performed through Density Functional Theory, DFT, and its extension to the Time-Dependent formulation, TDDFT, as implemented in Gaussian program suite.[43] The ground state geometry for the protonated dyes was optimized in gas-phase within the B3LYP functional with the 6-31G* basis set. At the optimized ground state geometries

were performed TDDFT (MPW1K/6-31G*) excited state calculations in gas phase as well as in acetonitrile, adopting the non-equilibrium Conductor-like Polarization Model, CPCM. This computational set-up has been previously shown to adequately describe the electronic and optical properties of similar push-pull dyes.[44, 45]

Between the above series of sensitizers we started to investigate compounds **11**, **13**, **14** and **18**.The optimized molecular structures of the dyes are reported in Figure 4.13.



| **11** | **14** | **18** |



| **13a** | **13b** | **13c** | **13d** |
| +0,3 Kcal | +0,0 Kcal | +3,6 Kcal | +4,4 Kcal |

**Figure 4.13**

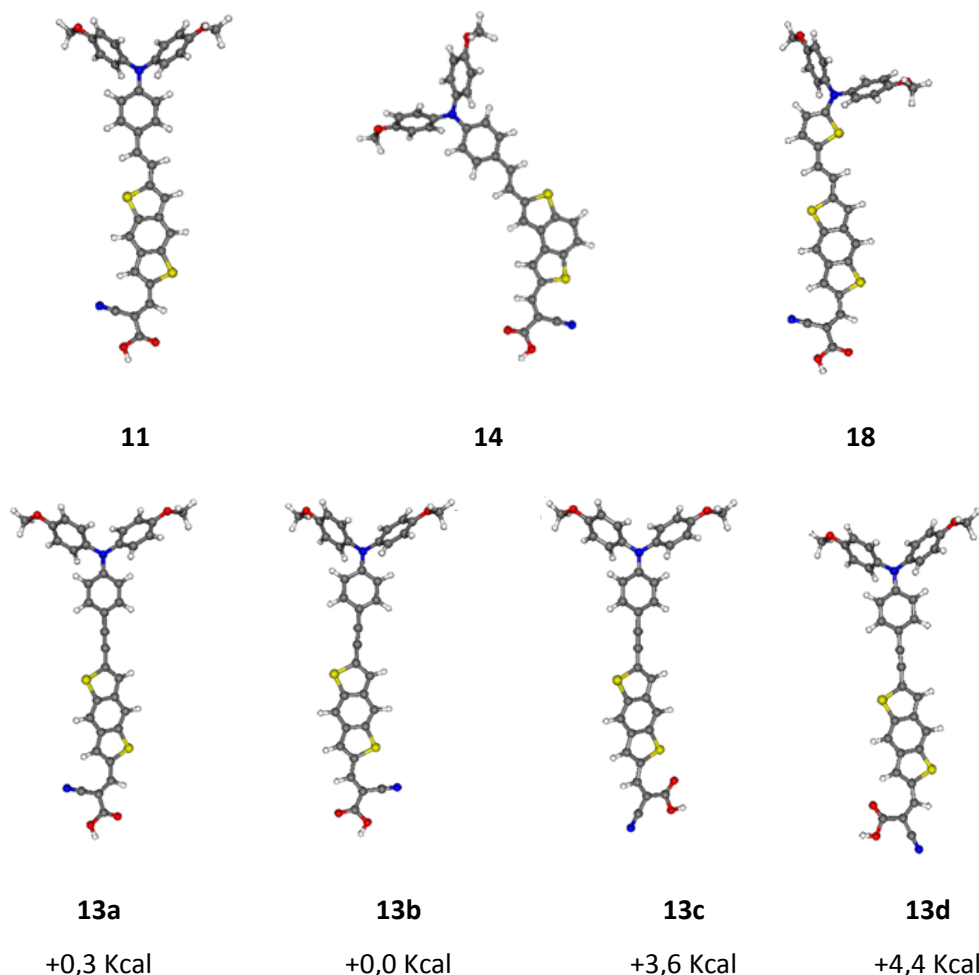As reported in the Figure 4.13, four possible isomers of the dye **13** were simulated. They differ each other by the acceptor group configuration. From the energy values it can be seen as the a-b configurations are more stable with respect to the other two structures

(c-d). For the four configurations we found only slight differences between the energy levels for the LUMO orbitals that are localized in the acceptor part of the molecules, while HOMOs orbitals are not affected by the variation of the acceptor group configuration, therefore for simplicity only value obtained for 13b are shown here below.

All the molecules are characterized by a substantially planar donor-acceptor arrangement, except for the methoxyphenyl substituent on the aniline moiety, which are enforced by the conjugation occurring along the push-pull system. For all of the dyes, the cyanoacrylic acid group is coplanar with respect to its adjacent thiophene unit, indicating the strong conjugation through the thiophene-cyanoacrylic acid groups.

In dye **18**, is present a bending of the donor moiety of the molecule with respect to the dye **11**, due to the substitution of the phenyl with the thiophene unit. This group causes also a slight deviation from the planarity with a dihedral angle between the C-C double bond and the thiophene C atoms of about 175°.

A schematic representation of the HOMO and LUMO energy levels of the molecules, obtained in acetonitrile solution from MPW1K/631-G* calculations, [46, 47] is displayed in Figure 4.14, where the plots of the isodensity surfaces of the considered molecular orbitals are also reported. These dyes are characterized by a push-pull arrangements with a good charge separation. The HOMOs are localized in the amine group and along the C-C triple/double bond, while the LUMOs are mainly delocalized along the **BDT/BDT$_1$** spacer and the cyanoacrylic acceptor group (Figure 4.14), with the largest components being localized on the latter, that is the charge transfer character. The HOMO localization in the outer molecular region ensures exposure of the charge hole, generated after electron injection, to the electrolyte side, ensuring rapid regeneration of the oxidized dye and efficient charge separation. The LUMO distribution close to the anchoring group enhances the orbital overlap with the titanium manifold of unoccupied states, assisting the electron injection step.
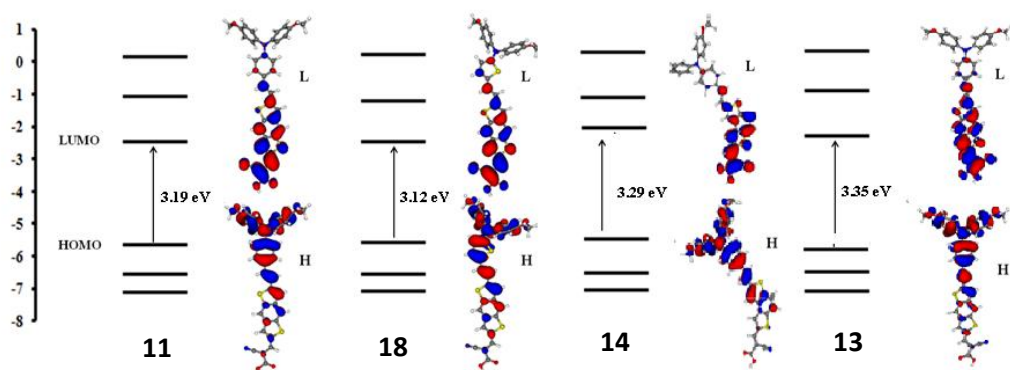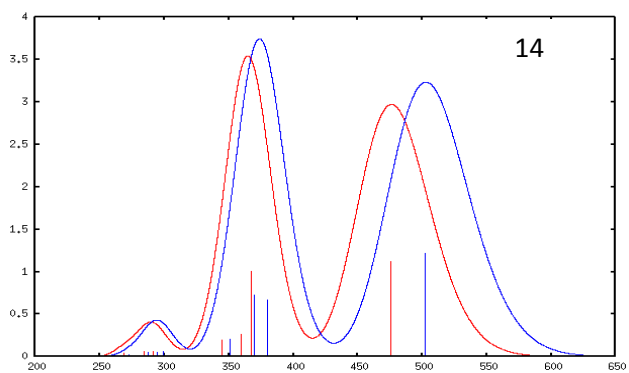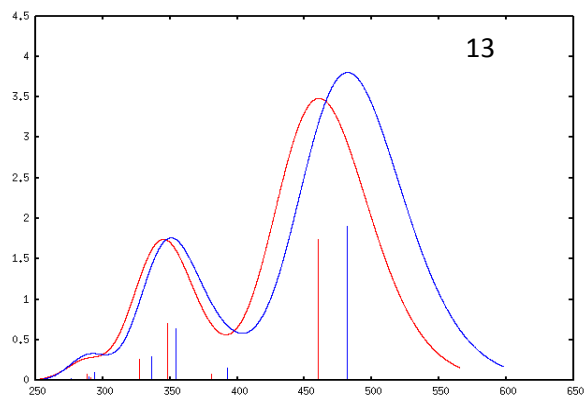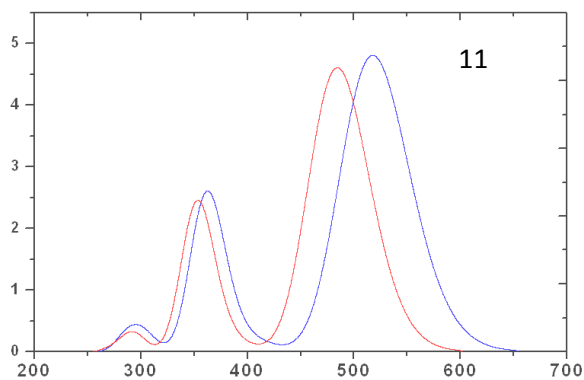
**Figure 4.14**

As depicted in the figure above, the Energy gaps decrease in the order **13** (3.35 eV), **14** (3.29 eV), **11** (3.19 eV), **18** (3.12eV). Observing Table 4.2, in which are reported the molecular orbital energies in vacuo and in solution, is clear that, in comparison to **13** and **14, 11** shows a smaller HOMO-LUMO energy gap due to a slight destabilization of HOMO orbital, **14** that contains **BDT** has the highest LUMO level, while the large Eg of **13** that has a triple bond is due to a great stabilization of the HOMO. The most important result from these calculation is that all the sensitizers designed seem have proper HOMO-LUMO levels for the injection of the electrons in the TiO$_2$ conduction band (-4 eV) and for the regeneration by means of the couple I$^-$/I$_3^-$ (-4.80 eV).

|       | 11 | | 14 | | 18 | | 13b | |
|-------|-------|-----------------------|-------|-----------------------|-------|-----------------------|-------|-----------------------|
|       | **Vacuo** | **Solution** (CH$_3$CN) | **Vacuo** | **Solution** (CH$_3$CN) | **Vacuo** | **Solution** (CH$_3$CN) | **Vacuo** | **Solution** (CH$_3$CN) |
| **L+2** | 0.11  | 0.18  | +0.13 | +0.19 | 0.17  | 0.22  | 0.08  | 0.14  |
| **L+1** | -1.08 | -1.07 | -1.16 | -1.13 | -1.16 | -1.19 | -0.96 | -1.02 |
| **L**   | -2.36 | -2.45 | -2.27 | -2.34 | -2.34 | -2.46 | -2.36 | -2.44 |
| **H**   | -5.69 | -5.64 | -5.68 | -5.63 | -5.59 | -5.57 | -5.80 | -5.79 |
| **H-1** | -6.52 | -6.52 | -6.58 | -6.56 | -6.53 | -6.55 | -6.60 | -6.64 |
| **H-2** | -7.07 | -7.09 | -7.15 | -7.20 | -7.03 | -7.07 | -7.15 | -7.22 |

**Table 4.2**

In Figure 4.15 the simulated absorption spectra of the dyes in vacuo (red line) and in acetonitrile solution (blue line) are reported.
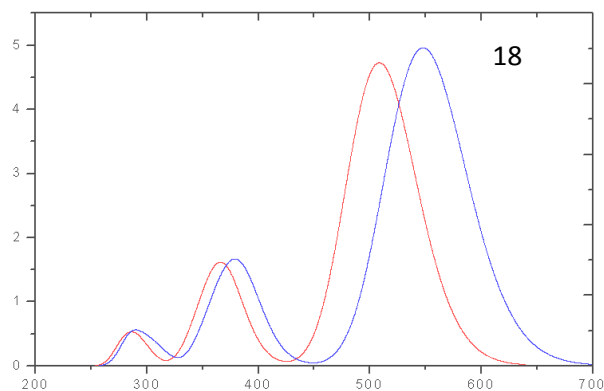
**Figure 4.15**

A comparison of the calculated absorption spectra evidence that **18** should be the more red-shifted dye, followed by **11** and **14**, while **13** is predicted the more blue-shifted one. TDDFT excited state calculations provided for **18**, **11** and **13**, two transitions with large oscillator strengths (f): a HOMO/LUMO transition in the visible region, centered at 450-460 nm (charge transfer transition), and a combined HOMO-1/LUMO and HOMO/LUMO+1 transition in the near UV region, tentatively attributed to a $\pi$-$\pi$* transition of the conjugated D-$\pi$-bridge system. On the contrary **14** has a different spectrum characterized by an intense signal centered at 375 nm (HOMO-1/LUMO and HOMO/LUMO+1 transitions) and a less intense one in the visible region, slightly centered at 502 nm, with a HOMO/LUMO character.

The results of TDDFT excited state calculations on the dyes in vacuo are reported in Table 4.3.

| | State | E (eV) | λ (nm) | *f* | composition (%) | |
|---|---|---|---|---|---|---|
| **11** | **1** | 2.56 | 484 | 1.73 | H → L | 79% |
| | **2** | 3.50 | 354 | 0.81 | H-2 → L | 40% |
| | | | | | H → L+1 | 23% |
| | **3** | 3.62 | 342 | 0.15 | H-2 → L | 19% |
| | | | | | H → L+1 | 58% |
| **13** | **1** | 2.69 | 460 | 1.75 | H → L | 78% |
| | **2** | 3.56 | 348 | 0.70 | H-2 → LH-1 → L | 48% 18% |
| | **3** | 3.79 | 327 | 0.26 | H → L+1 | 72% |
| **14** | **1** | 2.61 | 476 | 1.12 | H → L | 82% |
| | **2** | 3.38 | 367 | 1.01 | H-1 → L | 40% |
| | | | | | H → L | 14% |
| | | | | | H → L+1 | 27% |
| | **3** | 3.44 | 360 | 0.26 | H-1 → L | 36% |
| | | | | | H → L+1 | 46% |
| | **4** | 3.60 | 344 | 0.20 | H-4 → L | 13% |
| | | | | | H-2 → L | 63% |
| **18** | **1** | 2.44 | 508 | 1.78 | H → L | 80% |
| | **2** | 3.36 | 348 | 0.49 | H → L+1 | 75% |
| | **3** | 3.56 | 348 | 0.21 | H-2 → L | 53% |
| | | | | | H-1 → L | 16% |

**Table 4.3**

For all the dyes a single low-lying transition with large oscillator strength (f) has been calculated, followed at higher energy by a series of additional transitions. The low-energy excitations are calculated at 484 and 476 nm, respectively, consistent with the experimental absorption spectrum showing intense absorptions in this energy region. These transitions, of HOMO-LUMO character, are the typical charge transfer excitations of this type of push-pull dyes, leading to charge displacement from the donor to the acceptor dye moiety. In particular it has to be noted as in **14** there is a considerable decrease of the oscillator strength (1.12 instead of ~1.7 as in the others dye) for the charge transfer transition which is observed along with a slight blue-shift of the excitation (484 vs. 476 nm).

## 4.4   SYNTHESIS OF DYES

### 4.4.1  SYNTHESIS OF DYES 11, 13 ,14 AND 18

In this paragraph is reported the synthesis of all of the dyes for which the complete photophysical characterization has already been done as well as the preliminary test in solar cells. The results of this study will be reported and discussed in paragraph 4.5.3.

Looking for the best synthetic approach to the series of different dyes, we observed that all of the compounds containing the double bond could be easily prepared by a Wittig reaction between a formyl-substituted **BDT** subunit **A** and phosphonium salt of **D** subunit. For the triple bond containing molecules, the best way seemed to be a Sonogashira reaction between the ethynyl- or halogen-functionalized **BDT** subunit **D** and the halogen- or ethynyl derivative of subunit **D**. (Scheme 4.6)
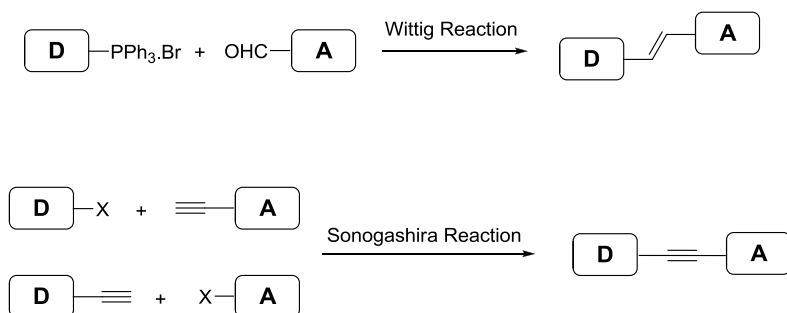


**Scheme 4.6**

The synthesis of first model **BDT$_1$** based dye **11** is depicted in Scheme 4.7.

Starting from the known phosphonium salt **21** [48] (prepared as described later on) a Wittig reaction was performed on one of the two formyl groups of 2,6-benzo[1,2-b:4,5-b']dithiophenedicarboxaldehyde **22**[49] This reaction was run with K$_2$CO$_3$ as base and 18-crown-6 ether in DMF and gave the aldehyde derivative **23**, as *E*-isomer, in 63% yield. The subsequent Knoevenagel condensation with 2-cyanoacetic acid, in AcCN solution and in the presence of piperidine, led to the target dye **11** as dark orange solid (90% yield).[39]
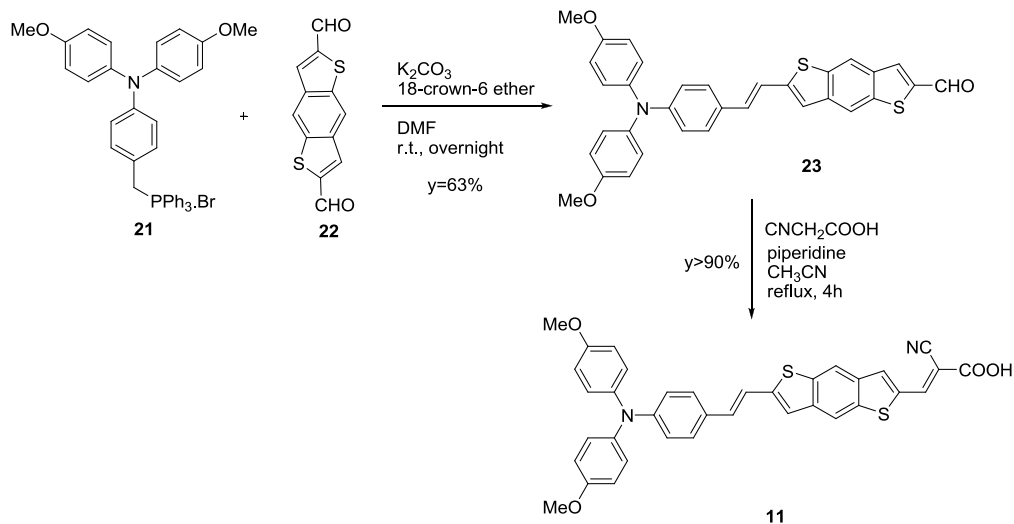
**Scheme 4.7**

The same procedure was used for the synthesis of the corresponding **BDT** containing dye **14** (Scheme 4.8). Wittig reaction of the same phosphonium bromide **21** with of 2,7-benzo[1,2-b:4,3-b']dithiophenedicarboxaldehyde **24** gave the corresponding formyl derivative **25**, which was reacted with cyanoacetic acid. The desired dye **14** was isolated in 55%. (Scheme 4.8)

In all of the Wittig reactions performed we always observed the selective formation of the *E* isomer.
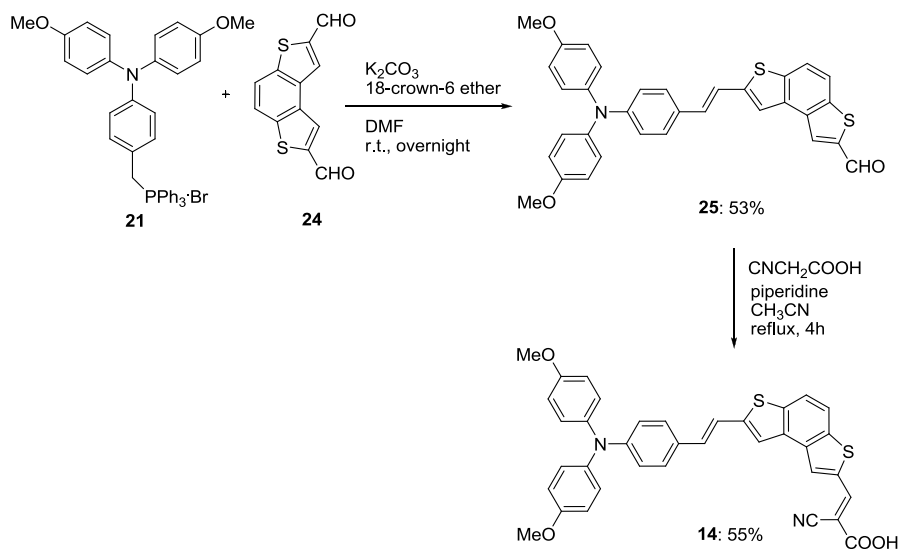


**Scheme 4.8**

The phosphonium salt **21** was prepared trough a known procedure starting from aldehyde **26**[50] which was reduced to benzylic alcohol **27** with NaBH$_4$ (91% yield), and then reacted with PPh$_3$·HBr to give directly salt **21**. (Scheme 4.9).
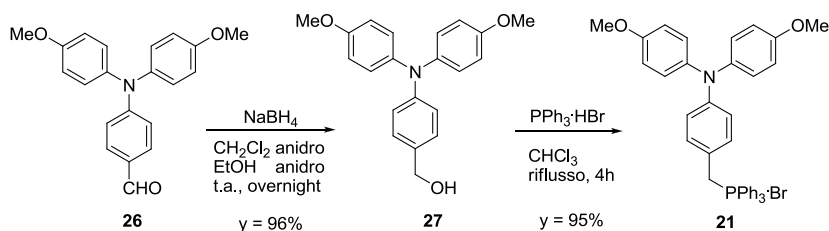


**Scheme 4.9**

The synthesis of 2,6-benzo[1,2-b:4,5-b']dithiophenedicarboxaldehyde (**22**) and 2,7-benzo[1,2-b:4,3-b']dithiophenedicarboxaldehyde (**24**)[5152] used in the previous Wittig reaction, was performed reacting the corresponding **BDT$_1$** (**1**) or **BDT** (**8**) with *n*-BuLi and DMF affording the products **22** and **24** in 91% and 85% yield respectively (Scheme 4.10)
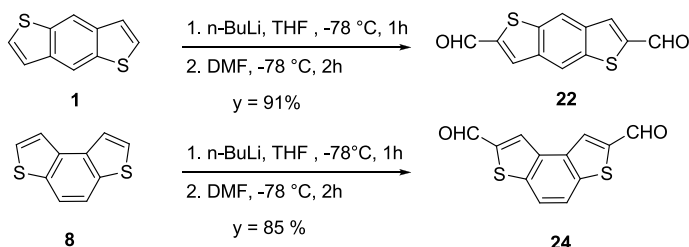


**Scheme 4.10**

As aforementioned, the Wittig strategy was employed also in the synthesis of the thiophene containing dye **18**, reacting the new phosphonium bromide **28** with the dialdehyde **22** to give the monoaldehyde **29** in 28% yield. The reaction with cyanoacetic acid was performed in presence of piperidine at reflux in CH$_3$CN for 4 h and gave the desired product **18** in 89% yield. (Scheme 4.11)
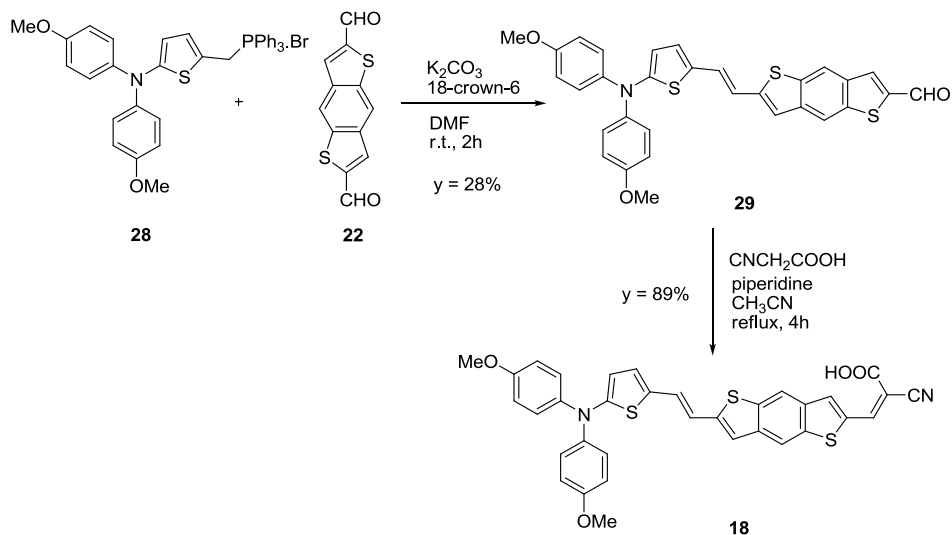
**Scheme 4.11**

As told before the phosphonium salt **28** is a new compound that was prepared from the suitable precursors as described here below. Triarylamine **30** was the starting material that was prepared by means of a Büchwald coupling between *N,N*-bis(4-methoxyphenyl) **31** and 2-bromothiophene **32**, in presence of Pd(dba)$_2$ and (*t*-Bu)$_3$P as catalytic system, at 85 °C under microwave (100-200 W) irradiation, according to a procedure reported in the literature.[53] The compound **30** was isolated in 86% yield. (Scheme 4.12)
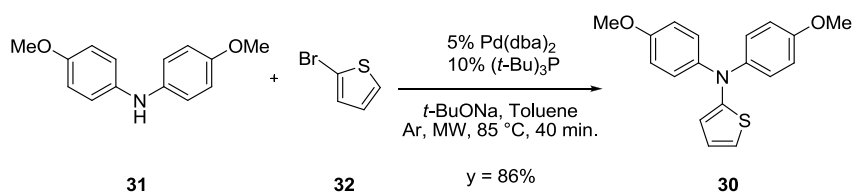


**Scheme 4.12**

The amine **30** was then formylated through a Vilsmeier reaction, using POCl$_3$ in DMF as solvent, heating at 35 °C for 10 minutes and collecting, without further purification, the product **33** in 95% yield.[48] (Scheme 4.13)
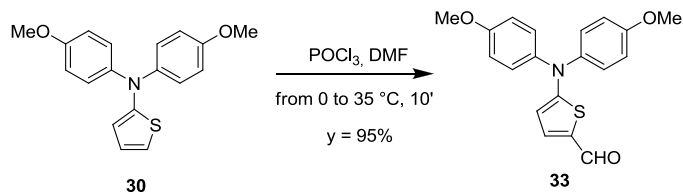
**Scheme 4.13**

Finally, the phosphonium bromide **28** (never reported in the literature) was prepared following the procedure known for a classical triarylamine:[43] the aldehyde **33** was reduced using NaBH$_4$ in a mixture of ethanol-dichloromethane at 20 °C for 1h, to give **34** in 80% yield. The alcohol was then reacted with PPh$_3$·HBr to give the phosphonium salt **28** in 97% yield. (Scheme 4.14)
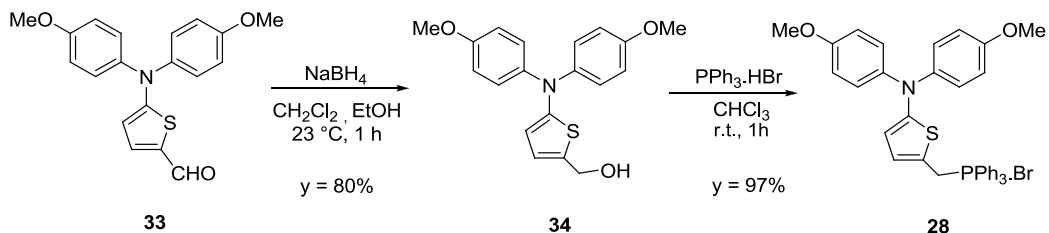


**Schema 4.14**

The synthesis of dye **13**, containing the triple bond, was accomplished following the reaction sequence reported in Scheme 4.15, in which the appropriately 2,6-functionalized benzo[1,2-b:4,5-b']dithiophene derivative **35** was coupled, in a Sonogashira reaction, with the known *N,N*-di(4-methoxyphenyl)-4'-iodophenylamine **36**[54] affording the compound **37** in 56% yield. The reaction was run under microwave irradiation for 40 minutes, in DMF and in presence of PdCl$_2$(PPh$_3$)$_2$ as catalyst, CuI as co-catalyst, diethylamine as base. The subsequent Knovenagel condensation with cyano acetic acid, in the same conditions used for **18**, gave the dye **13** in 95% yield.
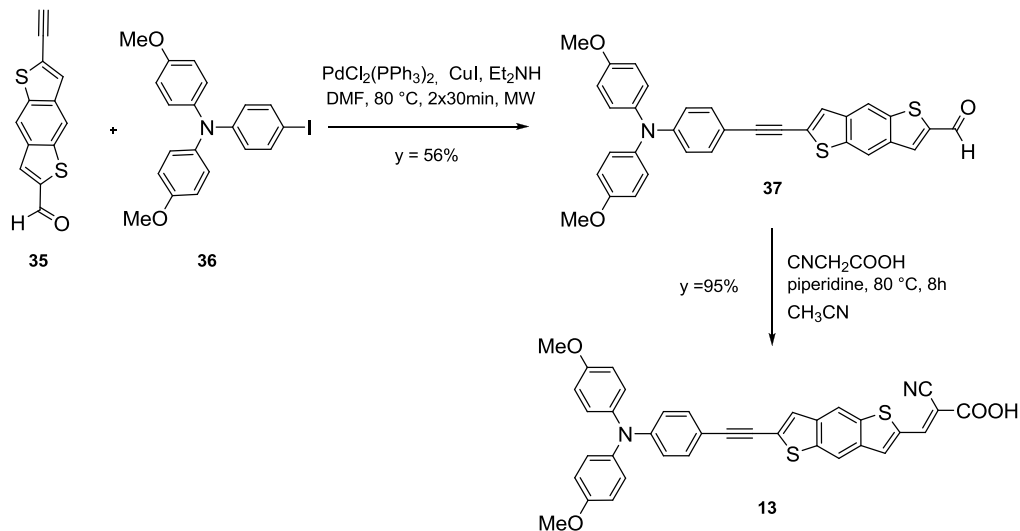
**Scheme 4.15**

The iodo derivative of MTPA **36** was prepared as reported in the literature, adding a preformed solution of [bis(trifluoroacetoxy)iodo] benzene and iodine in dry CHCl$_3$, under nitrogen atmosphere and exclusion of light, to *N,N*-di(4-methoxyphenyl)phenylamine **38** heating at 50 °C for 1. (Scheme 4.16).[55] Product **36** was obtained in 85% yield.
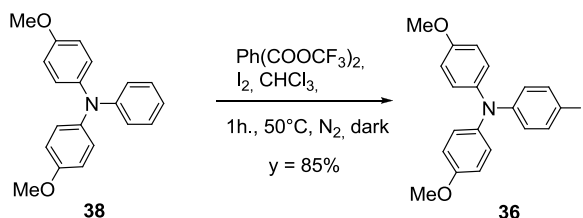


**Scheme 4.16**

We found that this reaction can be carried out in milder condition reacting the amine **38** with *N*-iodo succinimide (NIS) in DMF at room temperature for 1h, leading to the formation of **36** in 95% yield.
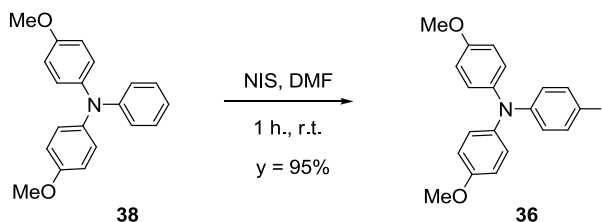


**Scheme 4.17**

The preparation of the benzodithiophene derivative **35**, the key intermediate for preparation of **13**, has been the object of an extensive research work in our laboratories. Not very much is indeed known in the literature on asymmetrical di-functionalized benzodithiophene.

We found as the best procedure the synthesis reported in scheme 4.18. benzodithiophene **1** (prepared as previously described in Scheme 4.1.[52]) was treated *n*-BuLi and *N*-formylpiperidine of to give benzo[1,2-b:4,5-b']dithiophen-2-carboxaldehyde **39** in 83% yield. This aldehyde derivative was then transformed in 6-bromo-benzo[1,2-b:4,5-b']dithiophen-2-carboxaldehyde **40** in 80% yield, using NBS as brominating agent. It is noteworthy that the same reaction conducted with NIS was not effective.
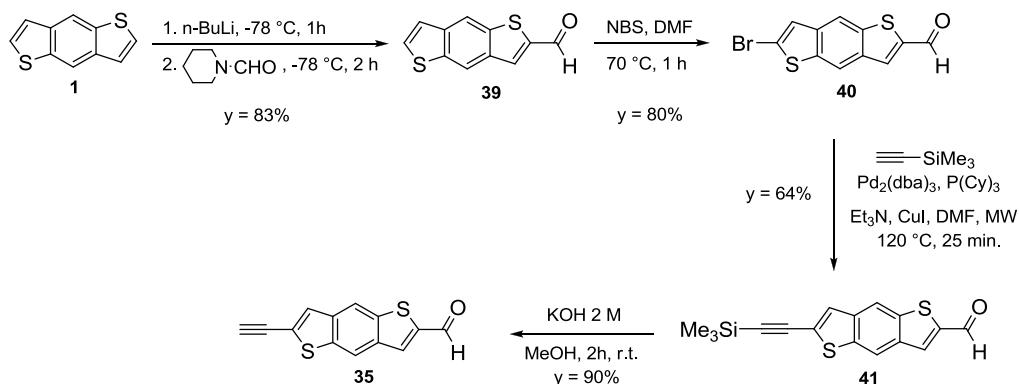


**Scheme 4.18**

The subsequent introduction of the triple bond on compound **40** was run through a Sonogashira coupling with trimethylsilylacetylene, using Pd$_2$(dba)$_3$ as the catalyst. Several attempts to perform this reaction in different conditions had been made, but it was possible to obtain 6-trimethylsilylethynyl-benzo[1,2-b:4,5-b']dithiophen-2-carboxaldehyde **41** (64% yield) only running the reaction under microwave irradiation. The final step was the deprotection of the triple bond in the presence of KOH and MeOH to give the target compound **35** in 90% yield.

An alternative synthetic way to compound **37** starting from **BDT$_1$** derivative **40** and the known triarylamine **42**[56] was also investigated (Scheme 4.19), however, even after microwave irradiation for 2 hours, only the starting material was recovered.
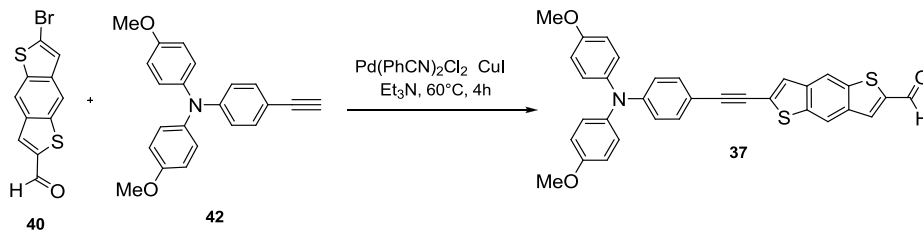
**Scheme 4.19**

The molecular structure of all of the dyes synthesized was confirmed by NMR, and MS characterizations. HPLC analysis was employed to establish the purity of the samples submitted to DSSC fabrication being, in all cases, higher than 98%.

## 4.4.2 DYES 15, 17 AND 20: WORK IN PROGRESS

In this paragraph, the synthesis of dyes **17** and **20,** for which the complete photophysical characterization is not done yet, is reported. Moreover, the synthetic strategy under investigation for dye **15** is also shown.

The dye **17**, bearing the bis-dimethylfluorenyl-aniline, was prepared in 96% yield by the usual Knovenagel reaction, starting from **43** in the conditions depicted in Scheme 4.20. This in turn was synthesized in 53% yield starting from **22** and the ylide precursor **44** in the reaction conditions already reported.
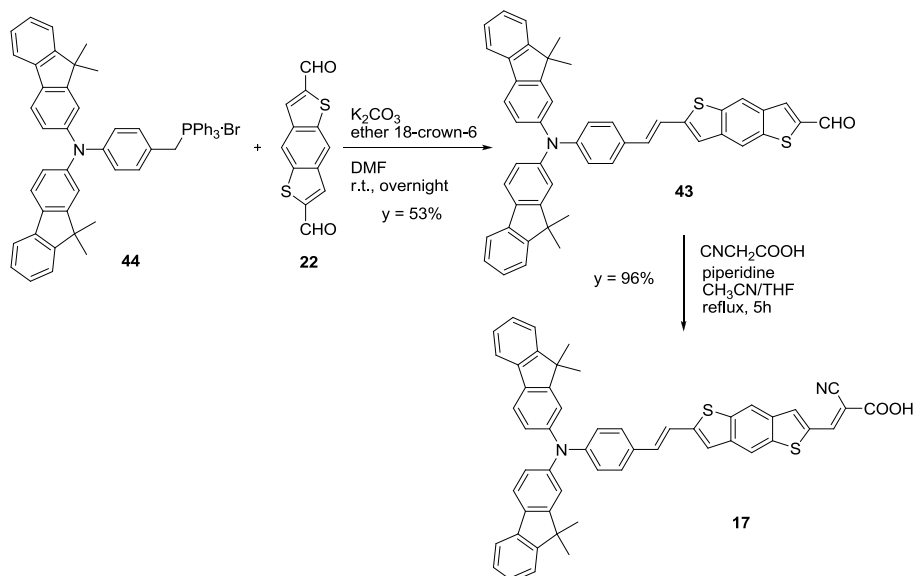


**Scheme 4.20**

The phosphonium bromide **44**, never reported in the literature, was synthesized in our laboratories in a six steps procedure (Scheme 4.21) starting from the 2-iodofluorene **45** that was dimethylated with $CH_3I$ in phase transfer condition using NaOH (50%) and TEBAC to give **46** in 56% yield. 9,9-Dimethyl-2-iodofluorene **46** was then reacted with aniline in an Ullmann coupling using $K_2CO_3$, Cu, ether 18-crown-6 in mesitylene affording compound **47** in 64% yield. Next step was the Vilsmeier formylation that led to aldehyde **48** in 95% yield, that was transformed into the phosphonium salt **44** following the sequences previously reported.
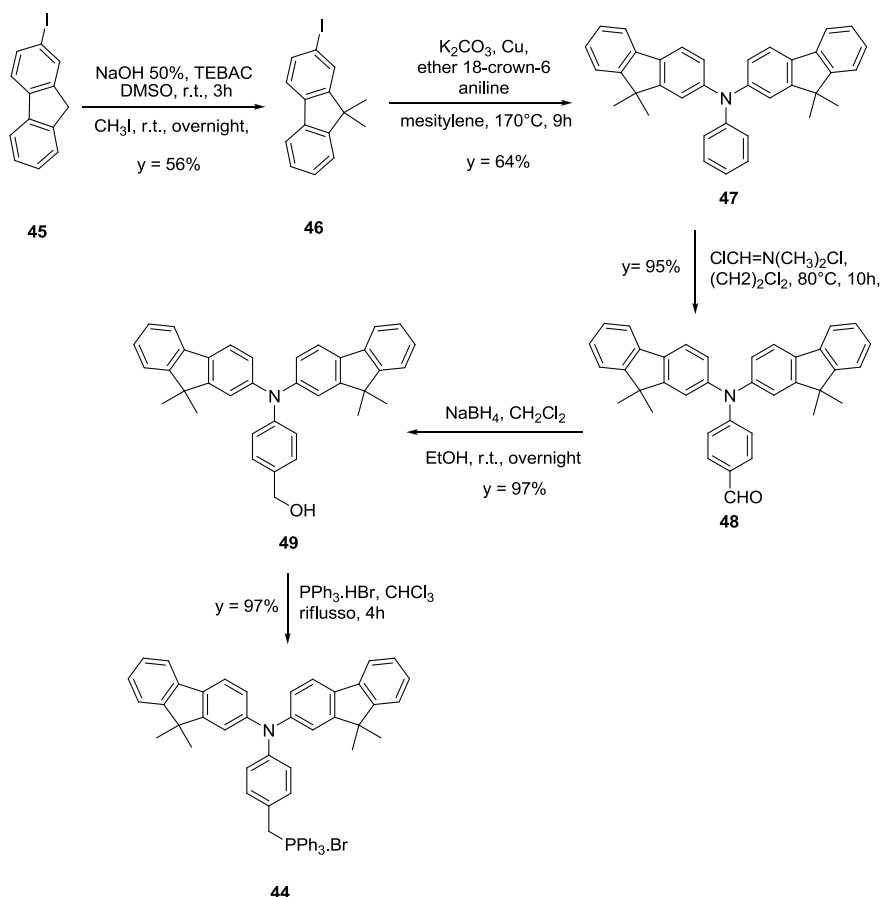


**Scheme 4.21**

Concerning the synthesis of compound **20**, again a Wittig reaction was performed between **21** and the new 2-ethoxy-carbonyl-6-formyl-benzo[1,2-b:4,5-b']dithiophene **50**.

The hydrolysis of the ester group in **51** using KOH at room temperature in a mixture ethanol/ dichloromethane gave the desired product **20** in 95% yield. (Scheme 4.22)
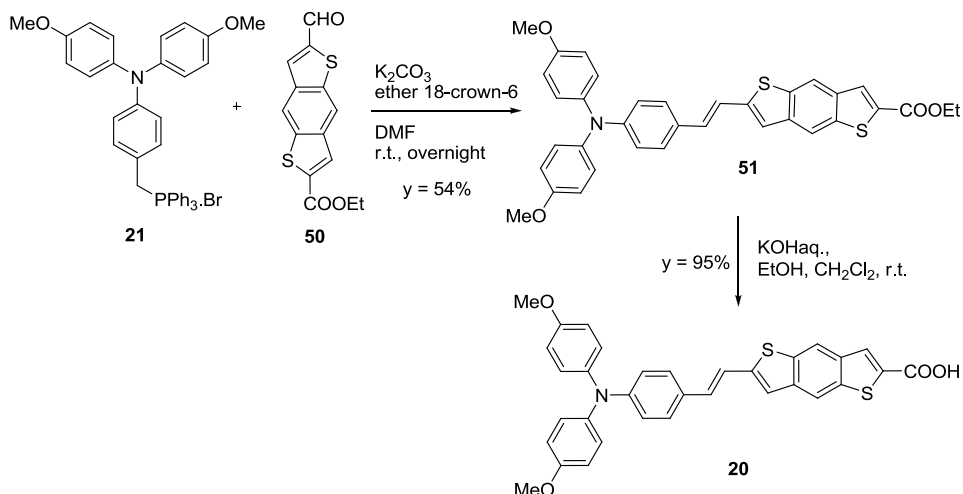


**Scheme 4.22**

The **BDT1** derivative **50** was prepared starting from the 2-formyl-benzodithiophene **39**. The formyl group was protected as ethylendioxy acetal to give derivative **54** in 95% yield. Compound **54** was then treated with *n*-BuLi and ethyl chloroformate and the acetal group was deprotected with HCl at 10% in THF affording **50** in 30% yield. Scheme 4.23
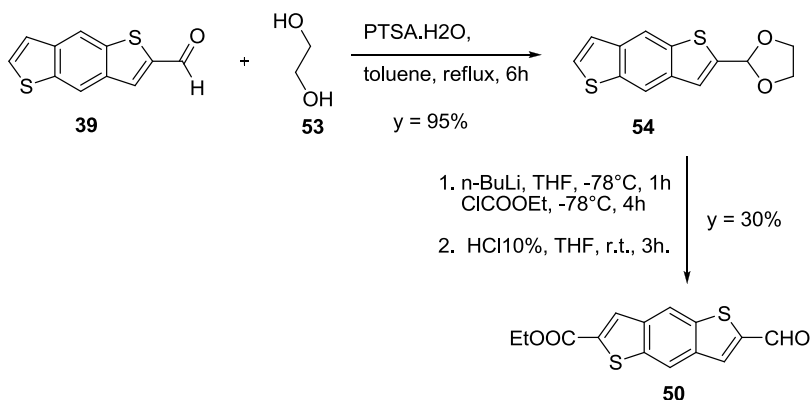


**Scheme 4.23**

To date, the synthesis of triple bond containing **15** is currently under progress. A synthetic route, similar to that described for dye **13** in scheme 4.15, was designed. The

key step being a coupling reaction between the 7-bromo-benzo[1,2-b:4,3-b']dithiophen-2-carboxaldehyde (**55**) and iodo tri-arylamine **36**. (Scheme 4.24)
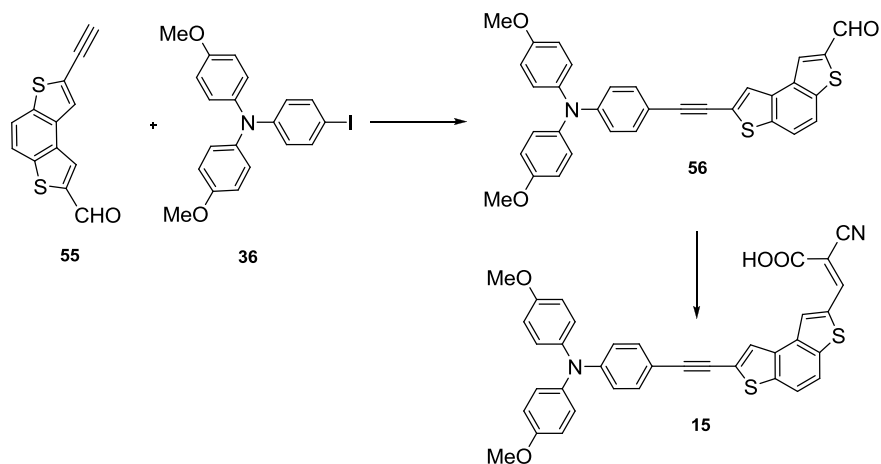


**Scheme 4.24**

In principle starting BDT derivative **55** could be obtained by a synthetic way, shown below, analogous to that of **35** (see scheme 4.18).
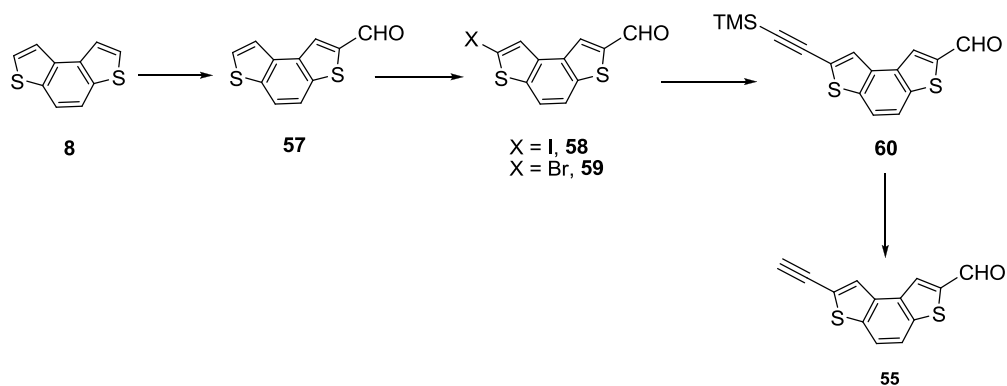


**Schema 4.25**

Indeed we found that the two isomers have a completely different reactivity and electrofilic bromination and iodination of the benzo[1,2-b:4,3-b']dithiophene-2-carboxaldehyde **57**, tried under different conditions did not lead to the desired product. (Scheme 4.26)  A number of different reaction conditions were tried as summarized in Table 4.4, but the expected product was not obtained.

100
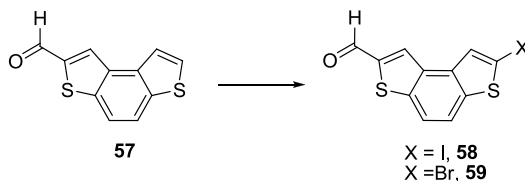
**Scheme 4.26**

| Entry | Reaction Condition | Equivalents | Results |
|-------|-------------------|-------------|---------|
| 1 | NBS, DMF, r.t | 1 | No reaction. |
| 2 | NBS, DMF, 70°C | 1 | Complex mixture containing starting material in predominance product together with desired compound but also starting material, byproducts such as dibromo derivative and others. Difficult the separation for chromatography. |
| 3 | NBS, DMF, 80°C | 1+ 0.1 | Complex mixture of product still mainly containing **BDT** (**8**) with desired product and several byproducts. |
| 4 | NIS, DMF, r.t. | 1 | No reaction. |
| 5 | NIS, DMF, 80°C | 1+ 0.2 | No reaction. |
| 6 | NIS, DMF, 40°C, CF$_3$COOH (cat.) | 1.2 | Complex mixture of product still mainly containing **BDT** (**8**) with desired product and several byproducts. |

**Table 4.4**

In the literature, the bromination reaction on a similar substrate, that is the 4,5-bis(*n*-hexyl-(benzo[1,2-*b*:4,3-*b'*]ditiofene))-2-carboxaldheyde, is reported,[18] performed at room temperature in DMF and with NBS. As shown in Table 4.4, the application of this procedure on product **57** did not give any result (entry 1, Table 4.4 ), but using more harsh conditions there is a lack in selectivity without the complete conversion of the starting material (entry 2 and 3, Table 4.4). The difference in reactivity of 4,5-bis(n-hexyl-(benzo[1,2-*b*:4,3-*b'*]dithiophene))-2-carboxaldehyde is mainly due to the presence of the alkyl chain, that change the electronic properties of the system and remove two possible reaction site, increasing the selectivity. Also, the use of NIS was investigated (Entries 4-5-

6 Table 4.4) without success. As it can be seen only the addition of catalytic amount of trifluoroacetic acid, that bring to the formation of the more electrophilic species $CF_3COO^-$ $I^+$,[57] lead to the obtainment of the compound in a complex mixture with by-products which was not possible to purify.

Due to the failure of the above described strategy the synthetic approach was changed according to the following Scheme 4.27.
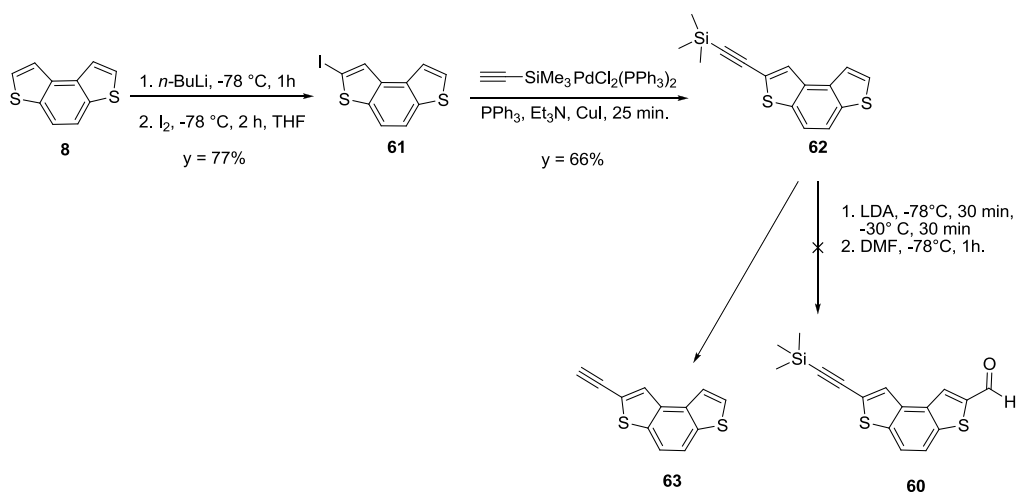


**Scheme 4.27**

The procedure involved the iodination of **BDT 8** followed by a Sonogashira coupling with trimethylsilylacetylene, a formylation in the 6 position and finally the deprotection of triple bond. Scheme 4.27

The first step was carried out in THF with *n*-BuLi and $I_2$ at -78°C affording the product **61** in 77%. Then the Sonogashira reaction in conditions reported above, led to **62** in 66% yield. The formylation reaction, performed with LDA using DMF at -78°C, did not give the expected product **60**, but furnished a mixture of starting compound **62** together with **63.** (Scheme 4.27) Therefore the synthesis was modified as follow. Scheme 4.27
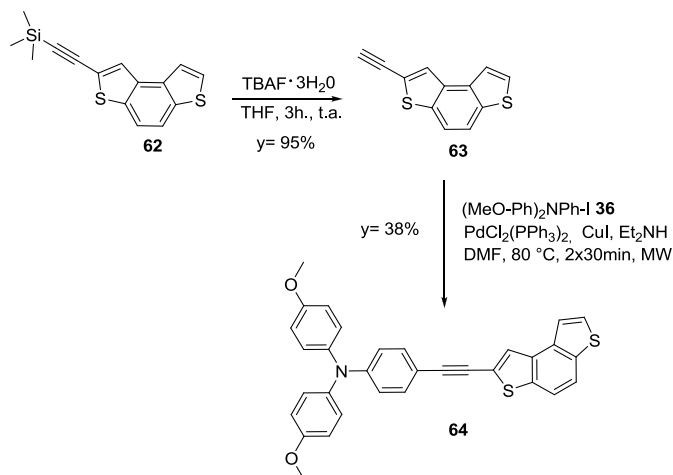
**Scheme 4.28**

Compound **63** was obtained in 95% yield treating **62** with TBAF in THF for 3 hours at room temperature. The coupling of **63** with the iodo triarylamine **36** using PdCl$_2$(PPh$_3$)$_2$ and CuI as catalysts in DMF and diethylamine under microwave irradiation (2 x 30 min) gave **64** in 38%. The introduction of the aldehyde function could then be carried out starting from **64** with two different strategies: a Vilsmeier[58] formylation or by reaction with *n*-BuLi and DMF.[59]

At first we investigated the Vilsmayer formylation with POCl$_3$ in DMF at 80 °C (Scheme 4.29) in DMF, but only a complex mixture of products was obtained from which it was not possible to identify the desired compound
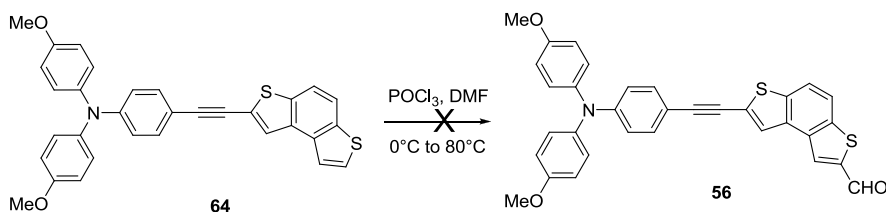


**Scheme 4.29**

The alternative strategy that is the formylation in the presence of *n*-BuLi, is currently under investigation.

# 4.5 PHOTOPHYSICS, ELECTROCHEMISTRY AND SOLAR CELLS ASSEMBLING

## 4.5.1 OPTICAL CHARACTERIZATION

**Dye 11**
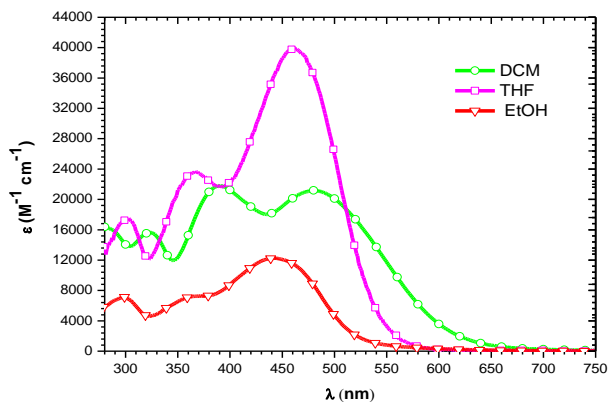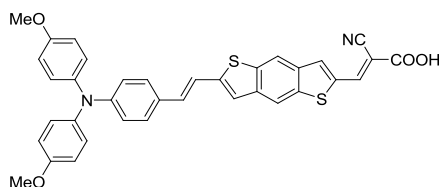




**(a)**
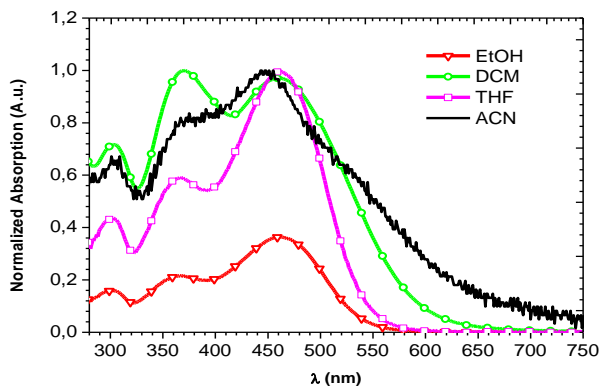


**(b)**

**Figure 4.16**

In Figure 4.16 (a) are reported the molar absorptivities of the dye in different solvents. Dye **11**, featuring the vinyl-**BDT$_1$** spacer, displays, between 300 and 750 nm, two main transitions; the first one, around 360-380nm, is characterized by small solvatochromic effects and is tentatively attributed to a π-π* transition of the conjugated D-π-bridge system. The second band, strongly solvatochromic (Figure 4.16 b), between 420-650 nm is attributed to the charge transfer transition originated from the electron-donating to acceptor moiety, which can be considered as an intra-molecular charge-transfer (ICT) band, as already described in the theoretical section.

Interestingly, **11** shows a significant change in molar absorptivities changing the solvent polarity (up to four fold increase in the CT band on going from EtOH to THF).

**Dye 14**
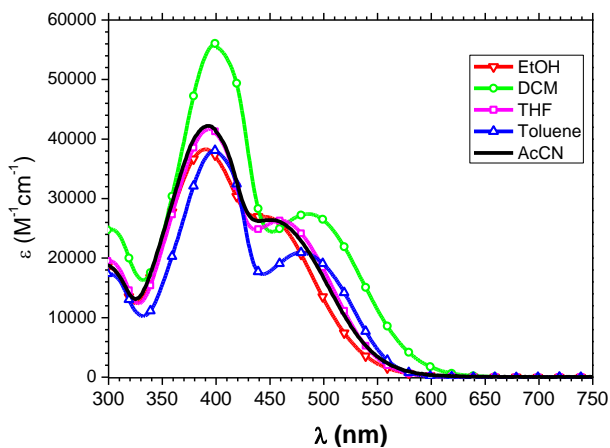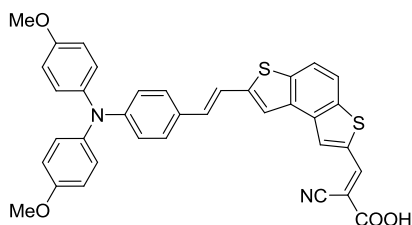




**(a)**
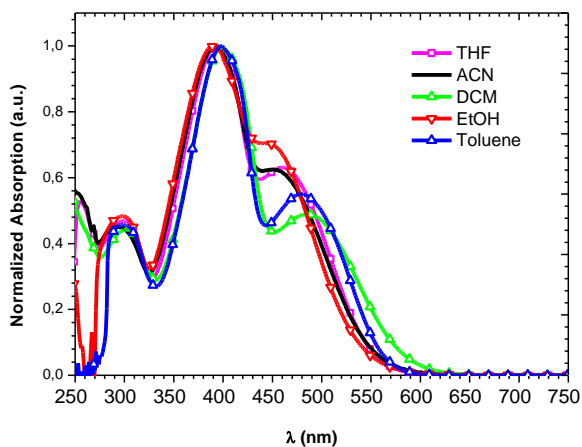
**(b)**
**Figure 4.17**

Dye **14**, featuring the isomeric vinyl-**BDT** spacer, (Figure 4.17 a and b), displays as well, between 300 and 750 nm, two main transitions; the most intense one, peaked around 400 nm and characterized by small solvatochromic effects, is tentatively attributed to a $\pi$-$\pi$* transition, similarly to **11**, of the conjugated D-$\pi$-bridge system. The second solvatochromic transition (clearly resolved from the first one only in DCM and toluene, green and blue line respectively), between 450-650 nm is attributed to the charge transfer transition. Differently from **11** in **14** the molar absorptivities remain almost constant in all the solvents apart from dichloromethane ($\varepsilon$= ~58000 $M^{-1}$ $cm^{-1}$). (Figure 4.17 a)

**Dye 18**
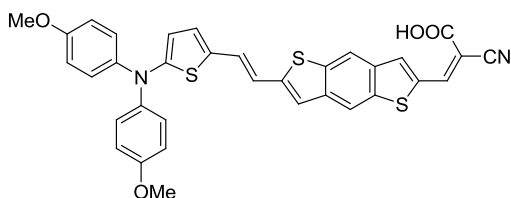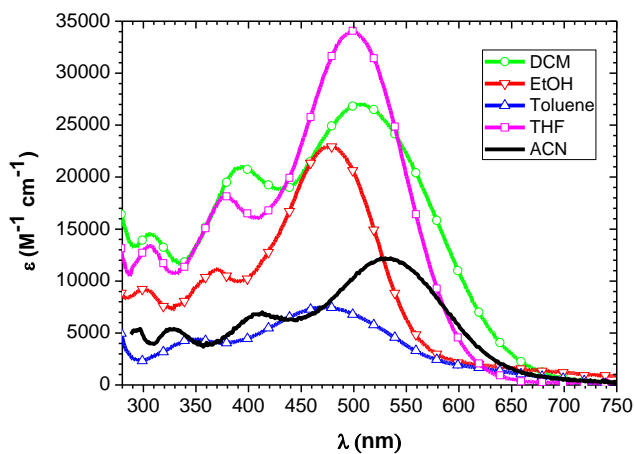
(a)
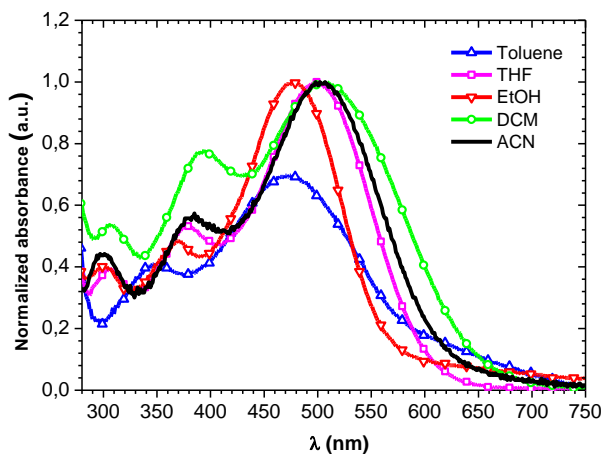


(b)

**Figure 4.18**

Dye **18**, containing the dimethoxyphenylthienylamine and the vinyl-**BDT**$_1$ spacer, shows two main transitions: the most intense one, peaked around 470-500 nm and characterized by a slightly solvatochromic effects is attributed to the charge transfer transition, the second one 350-380 nm is tentatively attributed to a $\pi$-$\pi$* transition of the conjugated D-$\pi$-bridge system. (Figure 4.18 a) Concerning the evaluation of the molar absorptivities, it has to be noted that the molecule has low solubility in acetonitrile and toluene and therefore these results have scarce significance. The

compound has the highest molar extinction coefficient in THF (33000 $M^{-1}cm^{-1}$) followed by EtOH and $CH_2Cl_2$ (23000 e 27000 $M^{-1}cm^{-1}$ respectively). (Figure 4.18 b)

**Dye 13**





(a)



(b)
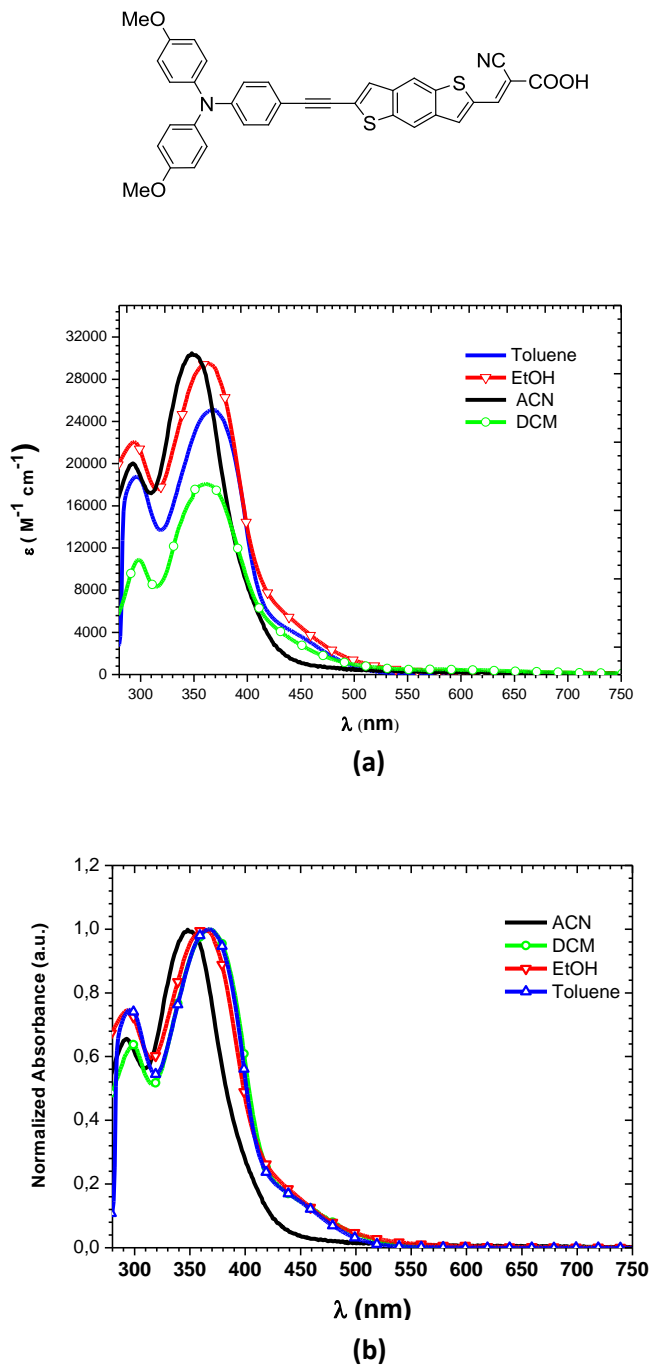
**Figure 4.19**

Dye **13** is characterized by the presence of an absorption band at 370 nm in dichloromethane, toluene and ethanol that shifts to 350 nm in acetonitrile. (Figure 4.19 b). The compound shows negative solvatochromism and hence its absorptions red-shift decreasing the solvent polarity; it has the highest molar extinction coefficient in acetonitrile (29000 $M^{-1}cm^{-1}$) followed by toluene, EtOH and $CH_2Cl_2$ (25000 $M^{-1}cm^{-1}$, 29500 $M^{-1}cm^{-1}$ e 18000 $M^{-1}cm^{-1}$ respectively). (Figure 4.19 b)

**Dye 17**
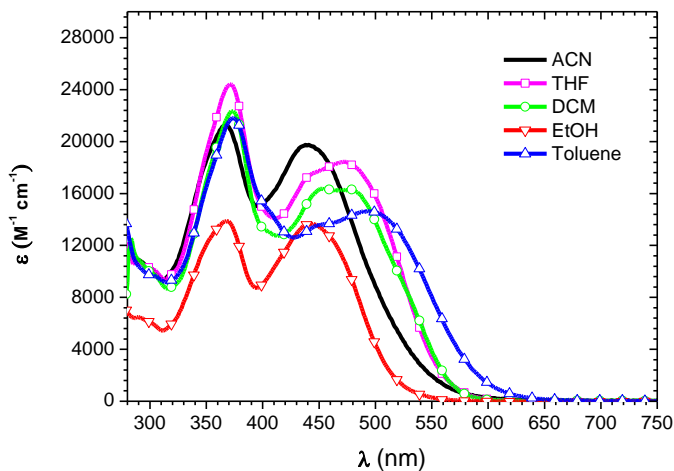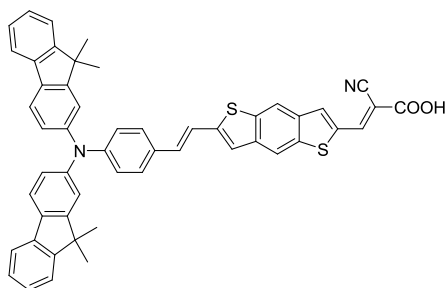




**(a)**
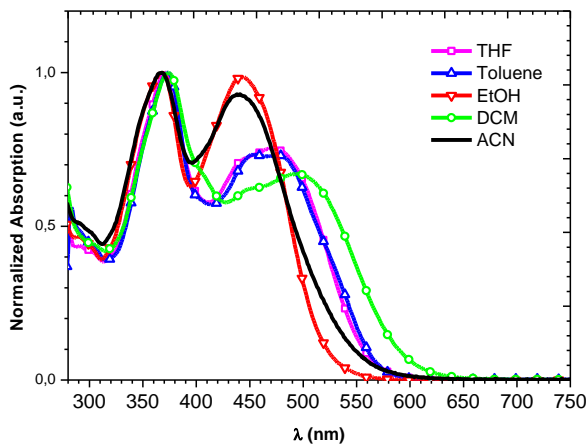
**(b)**

**Figure 4.20**

The chromophore bearing the difluorenyl moiety presents the first high energy most intense transition band at 370 nm without solvatochromic effect ($\varepsilon$ = 15000-25000 M$^{-1}$cm$^{-1}$, Figure 4.20 a), while the second one less intense at 480 nm, that changes of ± 20 nm varying the solvent. In particular, it shows a negative solvatochromic effect in ethanol and acetonitrile ($\lambda_{max}$ ~438 nm), in THF and toluene $\lambda_{max}$ ~505 while in DCM $\lambda_{max}$ ~520. (Figure 4.20 b)

**Dye 20**
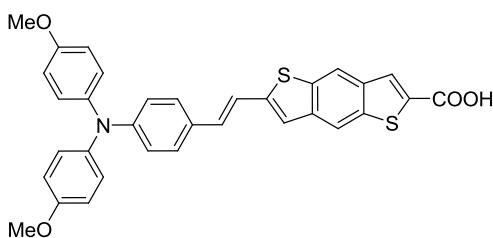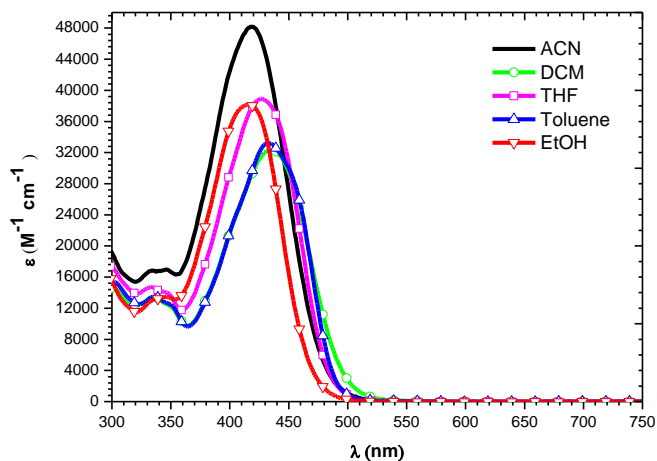
**(a)**
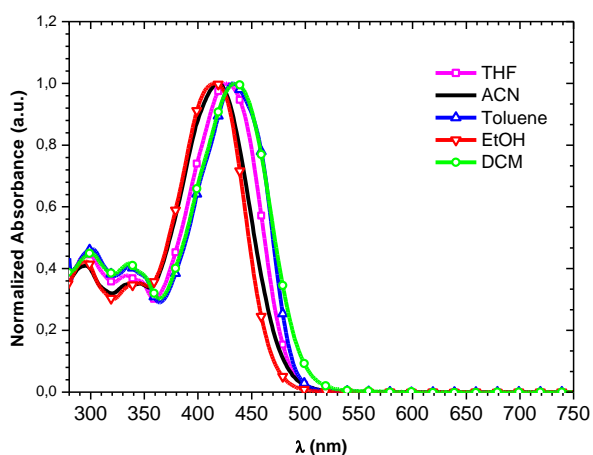


**(b)**

**Figure 4.21**

This dye, in which the anchoring group is a simple carboxylic acid, is characterized by an absorption band in the range of 380-480 nm with the highest extinction molar coefficient around 45000-50000 $M^{-1}cm^{-1}$ in acetonitrile. (Figure 4.21 a and b) The substitution of the cyanoacrylic moiety with the carboxylic group leads to a significant hypsochromic shift in the absorption spectra of dye **20** with respect to **11**, this might point to a reduced charge transfer character of the 420 nm band. This band can also be

ascribed to the superimposition of both π-π* and CT transitions. Theoretical calculation may better clarify the origin of such a transition.

## 4.5.2 ELECTROCHEMICAL CHARACTERIZATION

Dyes **11**, **13**, **14**, **18** and the corresponding parent molecules **BDT 8** and **BDT₁ 1** (Figure 4.1) plus the reference molecule bis(*p*-methoxyphenyl)phenylamine **38**, were characterized by cyclic voltammetry, CV, at potential scan rates typically ranging from 0.05 to 2 V s$^{-1}$, in a 4 cm$^3$ minicell, 0.5-0.75 mM solutions in $CH_2Cl_2$ (all chromophores) and ACN (**BDTs** and chromophores **13**, **18**) were used with 0.1 M TBAP or TBAPF$_6$ as the supporting electrolyte, deaerated by N$_2$ purging. The working electrode was a glassy carbon GC disk embedded in Teflon® (Amel, 0.071 cm$^2$) and platinum disk embedded in glass as counter electrode. The operating reference electrode was an aqueous saturated calomel one (SCE), but the experimental peak potentials have been normalized *vs* the Fc$^+$|Fc redox couple (the intersolvental redox potential reference currently recommended by IUPAC[60,61], having a redox potential of 0.39 V (in ACN) or of 0.495 V (in $CH_2Cl_2$) *vs* the operating SCE reference electrode. The ohmic potential drop was compensated by the positive feedback technique.[62]

Selected results are reported in Table 4.5 and Figures 4.22 and 4.23 . All data have been normalized to the ferrocene intersolvental reference redox couple.

In particular, **BDTs** required solvent ACN to allow observation of the first reduction peaks, located at very negative potentials. On the other hand, chromophores **11** and **14** were hardly soluble in ACN; however, in the chromophore case the cathodic potential window of $CH_2Cl_2$, granting good solubility, was sufficient, albeit narrower than the ACN one, on account of the much more positive reduction peak potentials. Therefore we have characterized the whole chromophores series in $CH_2Cl_2$, while only two of them in ACN; accordingly, in the following discussion when dealing with chromophores we will focus on the $CH_2Cl_2$ data.

| | $E_{Ic, ons}$ V(Fc$^+$\|Fc) | $E_{Ic, p}$ V(Fc$^+$\|Fc) | $E_{Ia, ons}$ V(Fc$^+$\|Fc) | $E_{Ia, p}$ V(Fc$^+$\|Fc) | $E_{IIa, p}$ V(Fc$^+$\|Fc) | $E_{L(ons)}$ eV | $E_{H(ons)}$ eV | $E_{g(ons-)}$ eV | $E_{L(max)}$ eV | $E_{H(max)}$ eV | $E_{g(max)}$ eV |
|---|---|---|---|---|---|---|---|---|---|---|---|
| $T_2$[i] | | -2.84 | | 0.88 | | | | ~3.6 | -1.96 | -5.68 | 3.72 |
| $BDT_1$[ii] | -2.75 | -2.93 | 0.87 | 1.01 | | -2.05 | -5.67 | 3.62 | -1.87 | -5.81 | 3.94 |
| BDT[ii] | -2.82 | -3.00 | 0.97 | 1.10 | | -1.98 | -5.77 | 3.79 | -1.80 | -5.90 | 4.10 |
| 14[iii] | -2.04 | -2.13 | 0.15 | 0.28 | 0.84 | -2.76 | -4.95 | 2.19 | -2.67 | -5.08 | 2.41 |
| 11[iii] | -1.86 / -2.14 | -1.96 / -2.21 | 0.14 | 0.26 | 0.85 | -2.94 / -2.66 | -4.94 | 2.00 / 2.28 | -2.84 / -2.59 | -5.06 | 2.22 / 2.47 |
| 11[ii] | -1.92 | -1.98 | 0.16 | 0.33 | | -2.88 | -4.96 | 2.08 | -2.82 | -5.13 | 2.31 |
| 13[iii] | -0.98 / -1.13 / -1.33 / -1.51 | *-1.07* / -1.22 / -1.40 / -1.63 | 0.15 | 0.30 | 1.41 | -3.82 / -3.67 / -3.47 / -3.29 | -4.95 | 1.13 / 1.28 / 1.48 / 1.66 | -3.73 / -3.58 / -3.40 / -3.17 | -5.1 | 1.22 / 1.37 / 1.55 / 1.78 |
| 13[ii] | -1.23 / -1.81 | -1.41 / -1.66 / -1.92 | 0.20 | 0.36 | 0.91 | -3.57 / -3.0 | -5.0 | 1.43 / 2.0 | -3.39 / -3.14 / -2.88 | -5.16 | 1.77 / 2.28 |
| 18[iii] | -1.56 | -1.74 | 0.04 | 0.06 | | -3.24 | -4.76 | 1.52 | -3.06 | -4.86 | 1.79 |
| 18[ii] | -1.41 | -1.61 | 0.08 | 0.15 | | -3.39 | -4.88 | 1.50 | -3.19 | -4.95 | 1,76 |
| MTPA[iii] | | | | 0.32 | 0.97 | | | | | | |
| MTPA[ii] | | | | 0.31 | 0.90 | | | | | | |

[i] $T_2$ = bithiophene compound, from Refs.[63] (anodic peak, in $CH_2Cl_2$ + 0.1 M TBAP) and [64] (cathodic peak, in dimethylacetamide + 0.1 M TBABr), here both referred to Fc$^+$\|Fc. [ii] in ACN + 0.1 M TBAP, at 0.2 V s$^{-1}$, referred to Fc$^+$\|Fc (this work). [iii] in $CH_2Cl_2$ + 0.1 M TBAPF$_6$, at 0.2 V s$^{-1}$, referred to Fc$^+$\|Fc (this work). Ons = ONSET.

**Table 4.5**

|  | $E_{\text{Ia, p}}$ V(Fc$^+$|Fc) | $E_{\text{IIa, p}}$ V(Fc$^+$|Fc) | $E_{\text{H(max)}}$ eV |
|---|---|---|---|
| Taras 1$^{\text{iv}}$ | 0.14 | 0.86 | -4.91 |
| Taras 3$^{\text{iv}}$ | 0.21 | n.d. | -4.98 |
| Taras 5$^{\text{iv}}$ | 0.28 | n.d. | -5.05 |
| Taras 2$^{\text{iv}}$ | 0.36 | n.d. | -5.12 |
| [iv] from Ref[65], 0.002 M in $CH_2Cl_2$ + 0.15 M TBAP on Pt electrode. Taras = Triarylamines | | | |

**Table 4.6**

From onset and peak potentials for first reduction and first oxidation LUMO and HOMO energies can be estimated from the following equations[60,61]

$E_{\text{LUMO}}$ (eV) = -1e × [ ($E_{\textbf{onset,I c}}$ /V(Fc$^+$|Fc)+ 4.8V(Fc$^+$|Fc vs zero)] *(onset criterion)*  eq. 4.1

$E_{\text{LUMO}}$ (eV) = -1e × [ ($E_{\textbf{p,I c}}$ /V(Fc$^+$|Fc)+ 4.8 V(Fc$^+$|Fc vs zero)] *(maxima criterion)*   eq. 4.2

$E_{\text{HOMO}}$ (eV) » -1e × [ ($E_{\textbf{p, I a}}$ /V(Fc$^+$|Fc)+ 4.8V(Fc$^+$|Fc vs zero)] *(maxima criterion)*   eq. 4.3

$E_{\text{HOMO}}$ (eV) » -1e × [ ($E_{\textbf{onset,I a}}$ /V(Fc$^+$|Fc)+ 4.8V(Fc$^+$|Fc vs zero)] *(onset criterion)*   eq. 4.4

ultimately based on the absolute value for the normal hydrogen electrode (NHE) critically assessed in a fundamental review paper.[62] The resulting values, together with the corresponding energy gaps $E_g$, are reported in Table 4.5, their counterparts obtained by electron absorption spectroscopy are reported in Table 4.7.

From the absorption spectra of the **BDTs** (dichloromethane, Figure 4.4) and of the cromophores (dichloromethane, acetonitrile, Figure 4.16-4.21 ) we also calculated the maximum (max) and onset (ons) HOMO-LUMO gaps, useful for comparison with electrochemical data. (Table 4.7)

|  | CH₃CN | | | | CH₂Cl₂ | | | |
|---|---|---|---|---|---|---|---|---|
|  | $\lambda_{max}$ (nm) | $\lambda_{ons}$ (nm) | $HL_{gap\,(ons)}$ [eV] | $HL_{gap\,(max)}$ [eV] | $\lambda_{max}$ (nm) | $\lambda_{ons}$ (nm) | $HL_{gap\,(ons)}$ [eV] | $HL_{gap\,(max)}$ [eV] |
| $T_2$[i] | 305 | 343 | 4,07 | 3,62 | - | - | - | - |
| BDT₁[ii] 1 | 336 | 348 | 3,70 | 3,57 | - | - | - | - |
| BDT[ii] 8 | 318 | 323 | 3,90 | 3,84 | - | - | - | - |
| 11 | - | - | - | - | 463 | 620 | 2.68 | 2,00 |
| 13 | 348 | 434 | 3,37 | 2,92 | 368 | 425 | 2,86 | 3,57 |
| 14 | 398 | 560 | 3,11 | 2,22 | 490 | 604 | 2.63 | 2,05 |
| 17 | 356 | 551 | 3,49 | 2,25 | 374 | 600 | 3,31 | 2,07 |
| 18 | 507 | 611 | 2,45 | 2,03 | 509 | 642 | 2,44 | 1,93 |
| 20 | 418 | 493 | 2,97 | 2,51 | 433 | 500 | 2,86 | 2,48 |

[i] in THF[63]
[ii] in CH₂Cl₂ (this work)
[iii] in ACN

**Table 4.7**

**BDT₁ 1** and **BDT 8** feature similar CV patterns, with chemically irreversible first oxidation and first reduction peaks (Figure 4.22), indicating that the corresponding radical cation and radical anion undergo following chemical reactions, albeit no conducting film deposition is observed, at least at our low operating concentrations. **BDT₁** has its first oxidation peak at a less positive potential and its first reduction peak at a less negative potential with respect to **BDT**; this shows that π conjugation is more effective in the former system than in the second one. In turn, the conjugation efficiency of **BDT₁** appears comparable to, or slightly lower than, the linear bithiophene one **T₂**[63] (Table 4.5) The electrochemical $E_g$ values show good consistency with the spectroscopic ones adopting the onset criterion, less if considering the maxima one; in particular, according to the latter, conjugation efficiency would appear slightly better in the **BDT** molecules than in the reference **T₂**. This could however simply be a consequence of the different solvents in which the spectra have been recorded. In any case, electrochemical and spectroscopic $E_g$ are often correlated but slightly different,[63] on account of the different processes to which they refer (electron transfer from/to the molecule vs electron

promotion between intramolecular energy levels, which can *e.g.* be differently affected by solvation and other parameters).
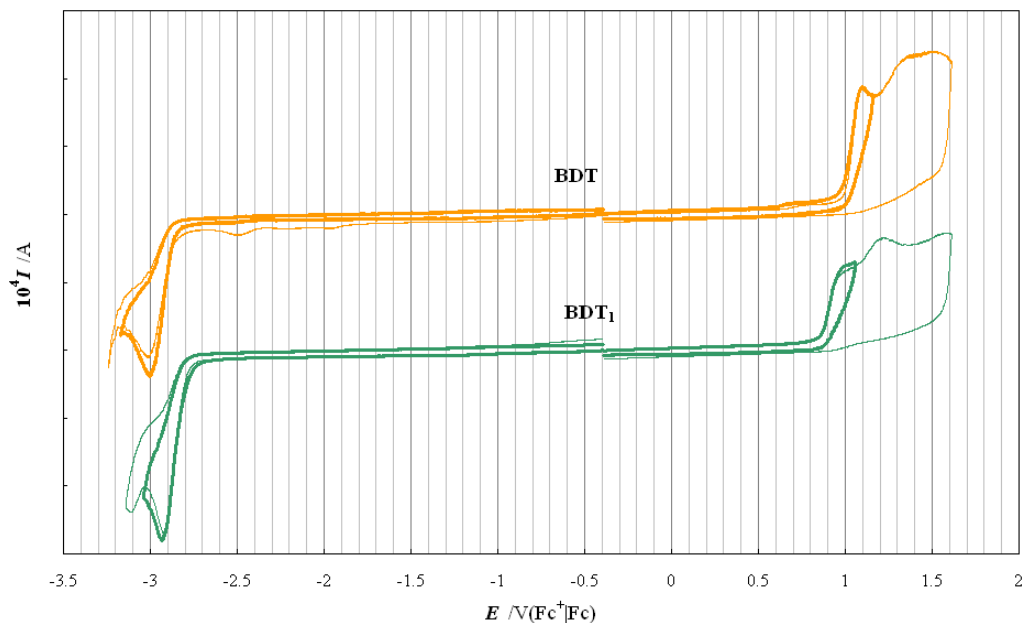


**Figure 4.22**

**11** and **14**, that differ for the presence of $BDT_1$ and **BDT** as intramolecular linker respectively, have similar CV patterns, which are quite different from the $BDT_1$ / **BDT** ones, since the addition of the push and pull moieties provide a couple of new electron rich and electron poor redox sites on which localized oxidation and reduction processes can take place at considerably lower energies. (Figure 4.23)
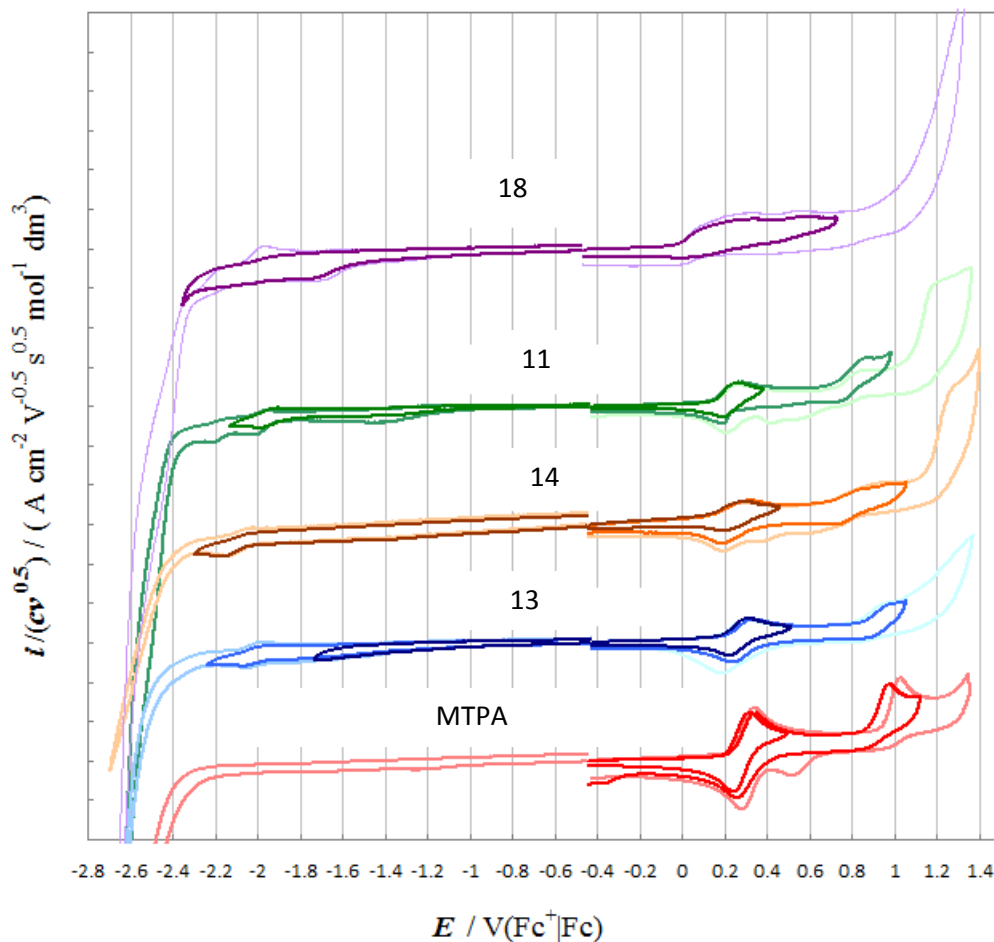
**Figure 4.23**

In particular, in Figure 4.23 for oxidations, two nearly merging two-peak systems, partially chemically reversible, or a single peak chemically reversible of associated charge comparable to the former system and significantly larger than 57 mV, followed by a complex multielectron irreversible shoulder on the background, can be observed. First oxidations, taking place at quite less positive potentials than in parent **BDT** molecules, must be localized on the electron rich triarylamino site, and in the case of *p*-alkoxyaryl substituents, possibly involve the C-O bonds besides the central nitrogen. The first oxidation potentials are slightly less negative than in reference molecule bis(paramethoxyphenyl)phenylamine **38** in the same experimental conditions; this is consistent with the trisarylamine building block being inserted in a more extended π

conjugated system, improving the delocalization of the incoming radical cation and henceforth lowering the oxidation potential. Considering the literature series of **Taras 1**, **3**, **5** and **2** triarylamines, having three *p*-methoxyphenyl, two *p*-methoxyphenyl and one *p*-tolyl, one *p*-methoxyphenyl and two *p*-tolyl, and three *p*-tolyl blades respectively,[65] our model amine appears somehow less oxidable than its most appropriate comparison, *i.e.* **Taras 3**; however, this observation could be associated to some difference in the operating conditions, like the working electrode material (Pt rather than GC) or the procedure for intersolvental standardization of the potential scales. The second oxidation peak or peak system of all our triarylamines, both the free one and the conjugated ones, are nearly coincident with the second oxidation peak of **Taras 1** (while **Taras 3** is reported not to display such a peak, without further details).[65]

The localized nature of the electron transfer together with the distance from the **BDT** or $BDT_1$ building block justifies the nearly equal oxidation potential in the chromophores **11** and **13**.

First reduction is accounted for by a monoelectronic, electrochemically reversible first reduction peak at a considerably less negative potential than in parent **BDT** molecules. Accordingly, it must correspond to localized reduction of the electron poor terminal double bond carrying a carboxylic and a cyano group. In this case the **BDT** linkers are immediately adjacent and their effect is clearly perceived, the reduction peak being located at significantly less negative potential in the linear **11** case. Moreover, the reduction peak appears electrochemically reversible (i.e. accounting for a fast electron transfer) in both cases, but chemically reversible only in the linear one.

Furthermore it is very interesting to notice that in **11** this first reduction peak is followed by a second monoelectronic reduction peak before the background; apparently each of these **11** two reduction peaks have an associated charge of about one half the **11** first oxidation peak system, which in turn, like the second one, appears the merging of two incipient oxidation peaks. On the other hand, in the above cited paper [65] the isolated Taras building block gave a neatly single first oxidation peak and a neatly single second oxidation peak. In this frame all the peculiarities observed in our case might be explained considering (a) for the first reduction peak the possible existence of two

isomers of the terminal electron-poor alkene system, which is nearer to the **BDTs** units and therefore more sensitive of their different nature (Figure 4.1-4.2), resulting in wide spacing between the two peaks; (b) for the first oxidation peak an isomer concerning the central double bond, having a much lower impact on the electron transfer localized on the MTPA building block and/or with one isomer prevailing on the other one.

In the angular **14** case, where conjugation is less efficient and therefore reduction takes place at more negative potentials, only a first reduction peak, with an associated charge about one half the first oxidation peak one, is neatly perceivable before a shoulder on the background, which might correspond to the second reduction peak of the former case

In the case of **13**, similar to **11** but having a triple bond rather than a double bond linker, first oxidation is at a similar (slightly more positive) potential, while first reduction takes place at significant less negative potentials. Interestingly, in this case the total charge of the first reduction step appears even more finely split with respect to the neat first oxidation peak than in the **11** case, resulting in a series of adjacent reduction peaks:
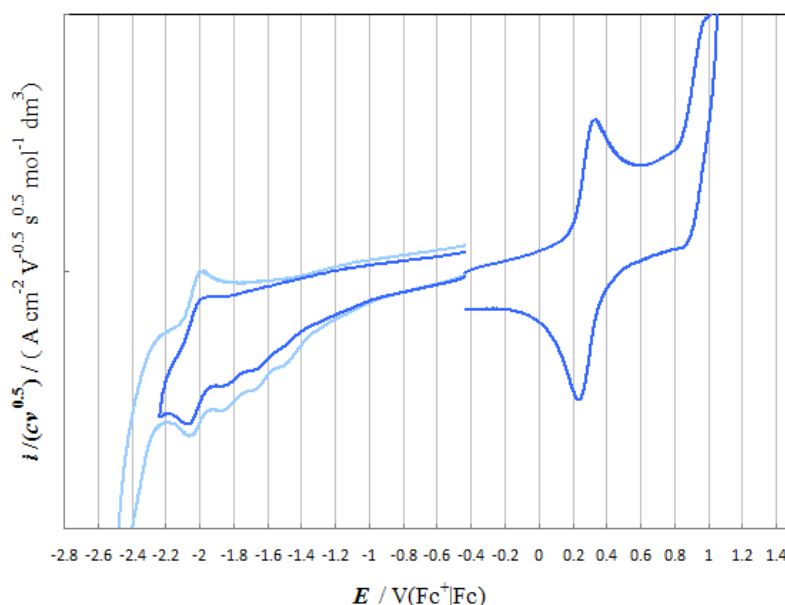


**Figure 4.24**

Actually theoretical computations point to the existence of four stable stereoisomers (two configurational and two conformational isomers, 13a-13d in figure 4.13) of this molecule, an isomerism stemming from the terminal double bond substituted with the COOH and the CN group, *i.e.* the first reduction site.

Explanations for the splitting of the first reduction peak in **11**, **13**, (and, possibly, **14**) alternative to stereoisomerism appear less probable; for instance:

- assuming the first reduction peak to account for one electron and the first oxidation one for two electrons appears less reasonable, because the first oxidation peak is electrochemically reversible (its potential remaining constant with scan rate) and therefore, considering its peak width, it must be monoelectronic; moreover, a concurrent, completely independent, oxidation of two blades at the same potential appears unlikely because of the necessary involvement of the central nitrogen atom in the incipient radical cation.

- assuming the signal splitting to account for acid-base equilibria involving the carboxyl group (either in combination with the amino one to give a zwitterionic form, or , according to some literature, alone) appears unlikely both because of the 50:50 splitting of the **11** reduction peak, and because protonation might well affect the oxidability of the nitrogen atom and therefore the first oxidation peak, but deprotonation of the carboxylic group should be less influential on the reduction of the electron poor terminal.

Substitution of the aryl linker with a thiophene one in the conjugated backbone (**18** vs **11**) results in significantly easier both first oxidation and first reduction processes (which might point to increased conjugation efficiency) and therefore in a much narrower gap; however, both signals appear much more complex and chemically irreversible with respect to the cases featuring an aryl linker.

In the cases where the study in the more polar ACN solvent was also possible (Figure 4.25), some differences with respect to the $CH_2Cl_2$ patterns remain even after intersolvental normalization, but appear not very remarkable (neither qualitatively nor quantitatively), pointing to a moderate solvent effect on the electron transfer process.
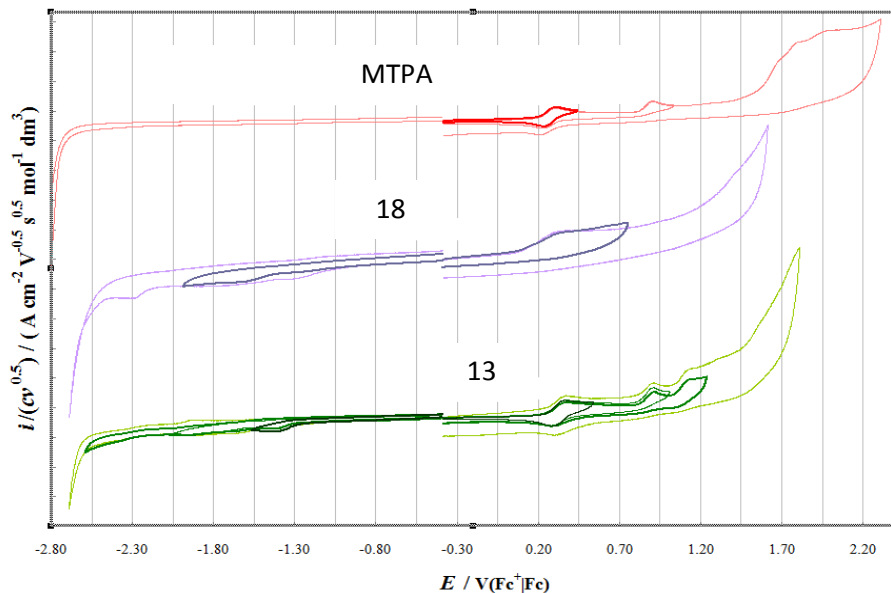
**Figure 4.25**

From point of view of the energy levels, all cromophores feature remarkably less extreme oxidation and reduction potentials with respect to the **BDTs** parent molecules, corresponding to a much higher HOMO level and a lower LUMO level (Table 4.5), which results in a much narrower HOMO-LUMO gap (by about 1.7 eV). The 0.15-0.20 eV difference between the more effectively conjugated linear (**BDT$_1$**) case and the less favourable angular one (**BDT**) is maintained also in the chromophores, mostly on account of the difference in the reduction peak potentials (i.e. in LUMO lowering), as we have pointed out before. This feature is in perfect agreement with the trend (not the absolute values) of the theoretical computations (Table 4.2). Instead is less evident in the spectroscopic approach, and even reversed adopting the maxima criterion, possibly as a consequence of the width and complexity of the first absorption band.

In a Grätzel cell, a driving force of at least 0.1-0.2 V is needed[66] for the electron transfer reactions; this implies that the dyes, to ensure the working of the cell, should have appropriate HOMO and LUMO levels. The LUMO have to be higher than the conduction band of the TiO$_2$ situated at -4.0 eV, while the HOMO have to be lower than the redox potential of the redox mediator (I$_3^-$/I$^-$) -4.80 eV. In particular, recently has been found that, in order to have an efficient regeneration of the oxidized dye the oxidation

121

potential of a sensitizer must be about 0.5 V more positive than the $I_3^-/I^-$ redox potential.[67]

From the data collected is clear that, excluding dye **18**, all the dyes synthesized are suitable for application in DSSCs since their HOMO- LUMO levels satisfy the in demand requisite. Dye **18** has the HOMO level really close (-4.86 eV) to that of the redox couple therefore is possible that the driving force will not be enough for the dye regeneration.

### 4.5.3 DEVICE FABRICATION AND PERFORMANCE

### 4.5.3.1 LIQUID STATE CELLS

DSSC photoanodes of 0.2 cm$^2$ were assembled from a single layer of TiO$_2$ paste (6-8 µm thick) on a FTO glass. CH$_3$CN solutions of the dyes (0.2 mM) containing 3mM CDCA were prepared. Sensitization was carried out for 6h. CDCA has mainly two functions, blocking the access of $I_3^-$ to the TiO$_2$ surface where not occupied by dye molecules and therefore restricting recombination of the injected electrons, and reducing the dye adsorption amount and therefore refraining dye aggregation. A commercial electrolyte solution (Iolitech ES-0004 HP), with 0.06M LiI added, was used. Moreover, an Ag conductive alloy has been deposed on the electrode to improve cell's performance. Photovoltaic features were recorded at 100 mW/cm$^2$ under AM 1.5 conditions both employing a black mask or exploiting the reflection phenomena.

For all of the devices fabricated, the characterization by IPCE is currently under progress.

**Dye 11**
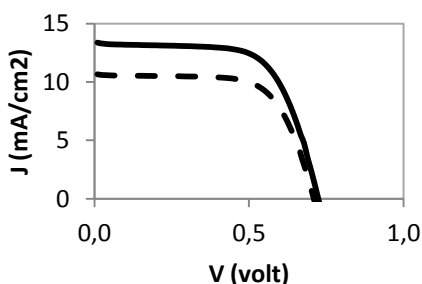


| | $J_{sc}$ (mA/cm$^2$) | $V_{oc}$ (V) | FF | η (%) |
|---|---|---|---|---|
| **A** | 10.65 | 0.710 | 0.675 | 5.11 |
| **B** | 13.3 | 0.725 | 0.658 | 6.38 |

**Table 4.8**

**Figure 4.26**

In Figure 4.26 are shown J/V curves for DSSCs with mask (dot line), without mask (solid line). While in Table 4.8 photovoltaic performance of the cell with mask (A) without mask (B) are reported.

**Dye 14**



| | $J_{sc}$ (mA/cm$^2$) | $V_{oc}$ (V) | FF | η (%) |
|---|---|---|---|---|
| **A** | 0.01 | 0.651 | 0.639 | 3.74 |
| **B** | 10.78 | 0.660 | 0.616 | 4.38 |
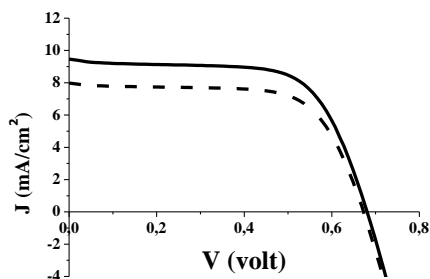
**Table 4.9**

**Figure 4.27**

In Figure 4.27 are shown J/V curves for DSSCs with mask(dot line), without mask (solid line). While in Table 4.9 photovoltaic performances of the cell with mask (A) without mask (B) are reported.

**Dye 13**

For this dye a dichloromethane solution (0.2 mM) containing 3mM CDCA were prepared. Sensitization was carried out for 18h.



| $J_{sc}$ (mA/cm$^2$) | $V_{oc}$ (V) | FF | η (%) |
|---|---|---|---|
| 4,88 | 0,72 | 0,705 | 2,64 |
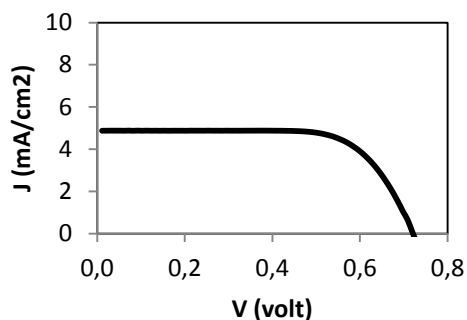
**Table 4.10**

**Figure 4.28**

In Figure 4.28 are shown J/V curves for DSSCs without mask. While in Table 4.10 photovoltaic performances of the cell are reported.

Due to the really poor performance, only measurements without mask have been done for this sensitizer.

**Dye 18**

| $J_{sc}$ (mA/cm$^2$) | $V_{oc}$ (V) | FF | $\eta$ (%) |
|---|---|---|---|
| 9.7 | 0,57 | 0,70 | 3.9 |

**Table 4.11**

In Table 4.11 very preliminary photovoltaic performances of the cell are reported.

Among the dyes tested, **11** gave the best results. In terms of photocurrent ($J_{SC}$) and photovoltage ($V_{OC}$) it's superior to **14** and **13**, while the fill factor (FF) values are very closed. In particular, in **18** $V_{oc}$ is quite low (0.57 instead of 0,70). This is probably due to the wrong position of its HOMO level. In fact, as it can be seen from the electrochemical data (Table 4.6) that the value of the HOMO (-4.86) it is too close to the redox potential of the couple I$^-$/I$_3^-$ (-4.80) to ensure dye regeneration. Interesting is the result obtained with **13**: it gave a very low efficiency, due to its blue-shifted absorption spectra and therefore a very low $J_{sc}$. However, the $V_{oc}$ is comparable to that of **11** and even more to that of **14**.

It is also worth of note that the efficiencies of **11**-based DSSC showed only a slight decrease of efficiency (10%) after 1 month, demonstrating a very good stability of the organic dye. This behavior is quite interesting in that, in general, the is generally a problem for this class of sensitizers.

An interesting comparison between cell parameters of our dyes and of similar chromophores **65a** and **65b** published in the literature (values shown in figure 4.29) is reported here below. Dyes **65a** and **65b** bear a thiophene instead of a benzodithiophene linked to the anchoring group with a double bond (**65a**)[38] or a triple bond (**65b**).[68]
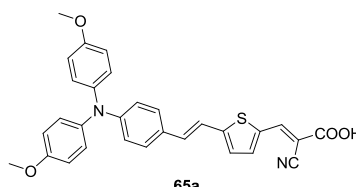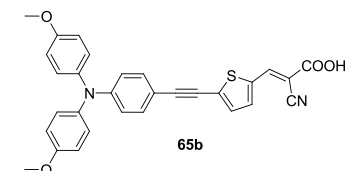
| $J_{sc}$ (mA/cm$^2$) | $V_{oc}$ (Volt) | FF | η (%) |
|---|---|---|---|
| 14 | 0,694 | 0,71 | ,90 |

Results obtained employing layer TiO$_2$ (7+5 μm)



| $J_{sc}$ (mA/cm$^2$) | $V_{oc}$ (Volt) | FF | η (%) |
|---|---|---|---|
| 8.04 | 0,684 | 0,70 | 3,86 |

**Figure 4.29**

**65a** and **11** have more or less the same absorption spectra (λ$_{max}$ ~ 460nm, ε = 33.000 M$^{-1}$cm$^{-1}$), and also similar FF and V$_{oc}$, the main difference is in J$_{sc}$, that is much more higher in the former: this could be perhaps explained with the different thickness of the TiO$_2$ layer.

Concerning **13,** the difference in cell efficiency is due to the great diversity in the absorption of the two dyes that lead to a J$_{sc}$ value of 8 in **65b** (CHCl$_3$ λ$_{max}$~480, ε = 33.000 M$^{-1}$cm$^{-1}$) and of 4 in **13** (CH$_2$Cl$_2$ λmax~380, ε = 18.000 M$^{-1}$cm$^{-1}$).

It has to be noted that **65b** is more red-shifted in respect to **65a** but the latter one has the best cell performance: this could be explained with an increasing of charge recombination phenomena due to higher planarity in the structure. [69]

For the evaluation of dye **18,** bearing a diphenylthienylamine, only one example of similar compound is reported in the literature (**66a**).[70] It contains two electron-rich spacers such as benzothiadiazole and thiophene, that could strongly influence the electronic of the structure. For this reason it's preferable to compare the trends observed between **66a-66b** - and **11 – 18** instead of the two dyes directly, (Figure 4.30)

| $J_{sc}$ (mA/cm$^2$) | $V_{oc}$ (Volt) | FF | η (%) |
|:---:|:---:|:---:|:---:|
| 10.4 | 0,54 | 0,66 | 3.77 |

**66b**



| $J_{sc}$ (mA/cm$^2$) | $V_{oc}$ (Volt) | FF | η (%) |
|:---:|:---:|:---:|:---:|
| 3.21 | 0,51 | 0,69 | 1.15 |

**66a**
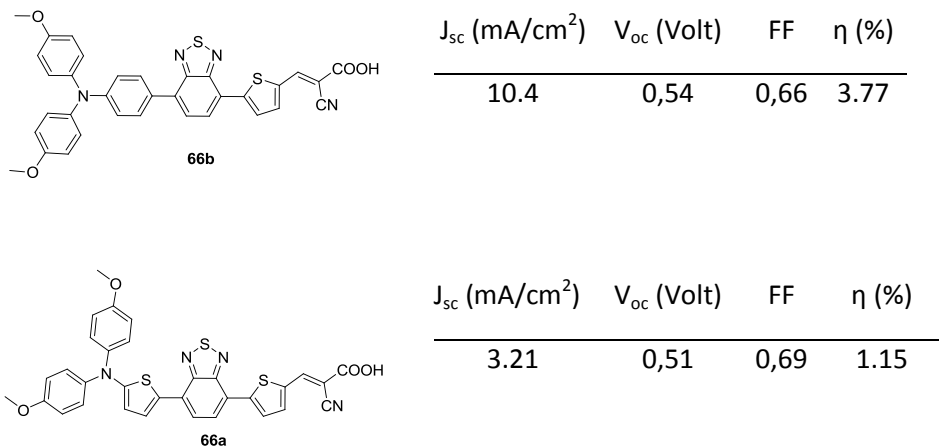
Figure 4.30

In **66a** and **18** the presence of the thienyl substituent greatly red-shifts the absorption spectra and lowers the energy gap; despite this, the efficiency of the cell is lower than the analogous compounds containing the classical triarylamine. In particular, it has to be noted that for **66a** there is a strong decrease in $J_{sc}$ while FF and $V_{oc}$ are very similar to that of **66b**, while in **18** not only $J_{sc}$ but also $V_{oc}$ are lowered. As mentioned before the reason for the low efficiency of **18**, in analogy to **66a**, could be attributed both to an increase planarity of the system, that favors the charge recombination and to an increase of the HOMO value that hamper efficient dye regeneration.

The results shown have been obtained in a preliminary test, a further study of optimization is under progress, involving use of different thickness of the TiO$_2$, lower concentration of CDCA, different electrolyte composition and also different solventfor the dye bath.

## 4.5.3.2    SOLID STATE DSSCS

Molecules **11** and **14** have been also tested in a solid state device where a molecular hole transporter, 2,20,7,70-tetrakis-(*N,N*-di-*p*-methoxyphenylamine)-9,90-spirobifluorene) (spiro-OMeTAD) is used instead of the liquid electrolyte. DSSC photoanodes of 0.2 cm$^2$ were assembled from a double layer of TiO$_2$ (compact, 100 nm + standard 1.8 μm thick) paste on a FTO glass. Acetonitrile: THF(10:1) solution 0.3 mM of the dyes were prepared containing (figure 4.30) or not containing (figure 4.31). 3mM

CDCA. Sensitization was carried out for 16 h. Spiro-OMeTAD as Hole Transporting Material (HTM) with addition of lithium bis(trifluoromethylsulfonyl)imide salt (Li-TFSI), 0.04M in acetonitrile was used. Moreover, an Ag conductive alloy has been deposed on the electrode to improve cell's performance.

For all the devices fabricated, the characterization by IPCE is currently under progress.

**Dye 14**

Cell fabricated in the absence of CDCA
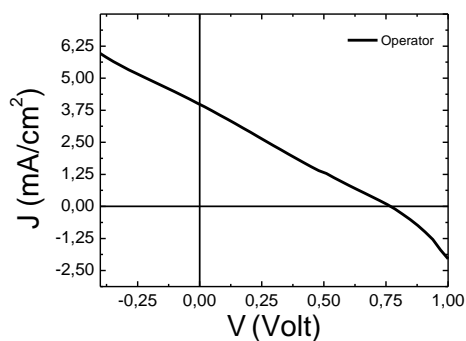


| $J_{sc}$ (mA/cm$^2$) | $V_{oc}$ (V) | FF | η (%) |
|---|---|---|---|
| 3.98 | 0.77 | 0.24 | 0.76 |

**Table 4.12**

**Figure 4.31**

In Figure 4.31 is shown the J/V curve for DSSC without mask, while in Table 4.12 photovoltaic performance of the cell are reported.

The performances obtained are not really promising, in particular we found a very low FF and $J_{sc}$.

**Dye 11**

Cell fabricated in the presence of CDCA.
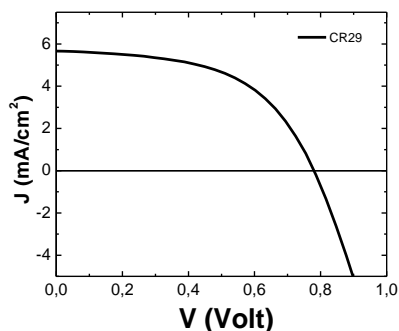
**Figure 4.32**

| $J_{sc}$ (mA/cm$^2$) | $V_{oc}$ (V) | FF | η (%) |
|---|---|---|---|
| 5.65 | 0.78 | 0.54 | 2.47 |

**Table 4.13**

In Figure 4.32 is shown the J/V curve for DSSCs without mask while in Table 4.13 photovoltaic performances of the cell are reported.

Cell fabricated in the absence of CDCA
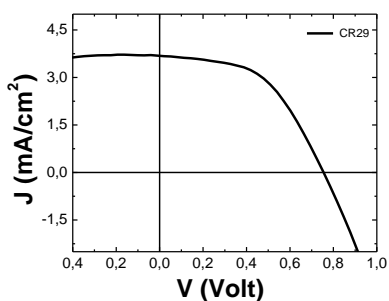


**Figure 4.33**

| $J_{sc}$ (mA/cm$^2$) | $V_{oc}$ (V) | FF | η (%) |
|---|---|---|---|
| 3.66 | 0.75 | 0.51 | 1.48 |

**Table 4.14**

In Figure 4.33 the curve J/V. for DSSC without mask is shown, while in Table 4.14 photovoltaic performances of the cell are reported.

From the data it's clear the benefic effect of the CDCA that greatly improves cell performances, in particular leads to an increase of $J_{sc}$ and therefore to a better efficiency.

The device is not fully optimized, however, it clearly shows the full potential of the metal free dye. Taking into account the value generally reported in the literature for DSSCs (4-

5%), it is straightforward the good photocurrent value driving the device performances, which is the result of an enhanced ability of the fully organic dye to harvest the sun light, together with good charge generation processes.

In this regard some preliminary studies have been carried out using Time-resolved Photoluminescence Spectroscopy in order to investigate the charge generation processes (i.e. electron transfer from the dye to the TiO$_2$ and hole transfer to the spiro OMeTAD).[70]



**(a)**



**(b)**
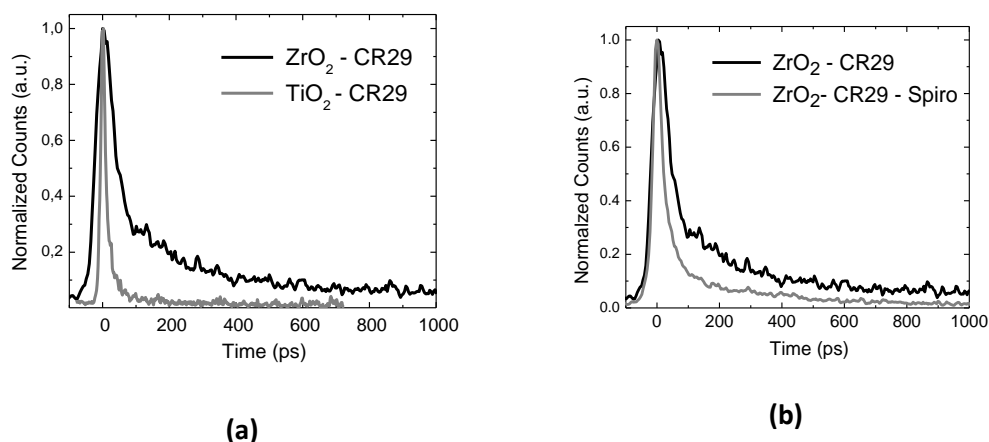
**Figure 4.34**

In figure 4.34 are reported time-resolved Photoluminescence (PL) spectra from a) **11** dye adsorbed on mesoporous films of ZrO$_2$ and TiO$_2$; b) **11** adsorbed on mesoporous films of ZrO$_2$ with and without spiro-OMeTAD infiltrated.

The decays have been fitted by a stretched exponential function in order to extract the average electron injection lifetime ($\tau_{inj} \sim$ 15ps) and the average exciton lifetime (($\tau_{obs} \sim$71ps) and finally calculate the electron injection efficiency ($\eta_{inj}$) according to the following expression[71]:

$$\eta_{inj} = \frac{1/\tau_{inj}}{1/\tau_{inj} + 1/\tau_{obs}}$$

Eq 4.5

It is worth noticing here that all samples present the same additives used in the device fabrication (Li-TFSI and 4-ter-butylpyridine) as it is known that they can strongly

influence the oxide and dye energetic and kinetics[71,72] In Figure 4.34 (b) the PL emission from the dye chemisorbed on a non-injecting substrate of $ZrO_2$ is shown with and without the spiro-OMeTAD. From these data we are able to estimate the hole transfer efficiency as described above. We calculate an electron injection efficiency of 76%, quite important for an organic dye, and a hole transfer efficiency of the order 53%. The latter can be underestimated as we estimate the charge transfer process starting from a neutral singlet exciton photogenerated on the dye, while, due to very efficient electron injection from the dye to the oxide, the hole transfer can happen from a more favorable energetic configuration.

# 4.6  RESULTS AND DISCUSSION

Analyzing the experimental data obtained in the context of the present investigation and making a comparison with theoretical calculations done, is possible to gain important information useful for the rational design of new dyes.

Starting from a comparison of the absorption spectra of the dyes in dichlomethane (Figure 4.35) it is clear how small changes in the dye structure affect the position and the amplitude of the absorption band.
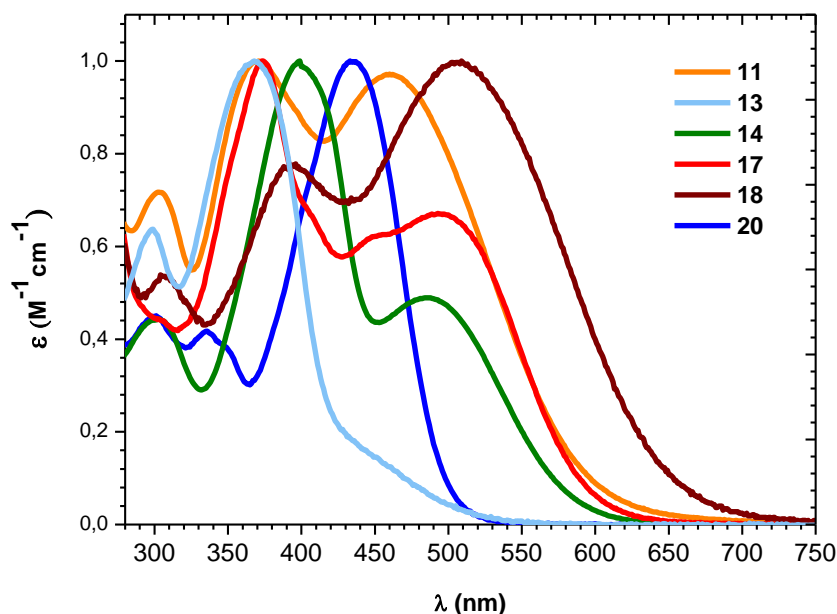


**Figure 4.35**

In particular, it can be noted that for dyes **11**, **14**, **17 and 18** two main bands are present: the first at higher energy that we assigned to a π-π* transition, while the second at lower energy relative to the charge transfer. On the contrary, in **13** and **20** only one band is shown, in the former it can be plausibly assigned to the π-π* transition, while it is not easy to interpret the latter.

The most red-shifted dye is, as expected, **18**, containing a thienyl substituent on the nitrogen in the donor part. It has $\lambda_{max}$ at 505 nm and an extended spectra till 700 nm; **11**

is blue-shifted in respect of **18** and has a quite broad spectrum with a maximum at 479 nm. TDDFT calculations (Figure 4.15) nicely reproduce the trends measured experimentally, as known in the literature the red-shifted of the predicted band is a common feature of organic optoelectronic materials and may be related to the solvent effect.[3]

 In dye **20**, that differs from **11** for the absence of a vinyl and CN group, is observable only one band strongly red-shifted, this could be due to the less electron-withdrawing power of the carboxylic group and therefore the less acceptor capability. In **14** the CT band is not only blue-shifted but also significantly decreased. This behavior, as also confirmed by theoretical calculation, is clearly related to the breakout of the conjugation across the donor-acceptor moieties resulting from the different spacer **BDT** instead of **BDT**$_1$ (dye **11**).

Dye **17** is characterized by the presence of dimethylfluorenylaniline as donor group, inserted instead of triarylamine with the aim to reduce the aggregation of dye on the $TiO_2$ surface,, as known in the literature.[73,56]

Dye **13**, that contains a triple bond between the **BDT**$_1$ and the donor unit instead of a double bond as in **11**, has the most blue-shifted absorption spectra with only one band at 350 nm and really low absorbance in the range 450-700 nm. The expected charge transfer band seems not to be present. This is an unpredictable and unexpected result, in opposite tendency to the results reported in literature for similar compounds and to TDDFT predictions. The calculation done, that demonstrated to be effective in reproducing the behavior of the other compounds, indeed predicted a spectrum very similar and comparable to that of **11** (Figura 4.15). As mentioned, the triple bond is useful in order to avoid energy losses due to photoisomerization and to increase planarity and therefore electronic coupling between acceptor (A) and donor (D), but also to red-shift the absorption spectrum. In literature are indeed reported two similar dyes, bearing a triple bond between a thiophene and a triarylamine moiety: in these cases, contrary to our molecule, and confirming the expectations, they are characterized by broad absorption band ending at ~550-600 nm with $\lambda_{max}$ around 460-480 nm.[68]

A possible explanation could be that, when is close to an electron donor moiety, a triple bond is more electronegative than a double bond. An electronegative property of triple bond will weaken electron-withdrawing ability of the electron acceptor because of the opposite dipole moments of triple bond and electron acceptor, in this way, absorption spectra of dyes with triple bond are expected to be blue-shifted in comparison with that of dyes with double bond. In our molecule, due to the extended π bridge, this effect could be more enhanced leading to the absorption spectrum observed.

However, the unexpected results obtained, prompted us to better investigate the photophysical properties of this dye., Even if this work is still under progress, the preliminary results on **13** are reported in the next **Chapter 5**.

Some other considerations could be drawn observing the data collected in Table 4.15.

| | | 11 | 13 | 14 | 17 | 18 | 20 |
|---|---|---|---|---|---|---|---|
| **λmax** nm | Teor | 516 | 481 | 367, 476(sh) | - | 547 | - |
| | Sper | 460[*] | 348 | 398, 470(sh)[*] | 356, 440(sh)[*] | 507[*] | 418[*] |
| | | 463 | 368 | 400, 490(sh) | 374, 480(sh) | 509 | 433 |
| **Egmax** eV | Teor | 3,19[*] | 3,35[*] | 3,29[*] | - | 3,12[*] | - |
| | Sp | 2,00 | 3,37 | 3,11 | 3,49 | 2,45 | 2,97 |
| | Ec | 2,22[a] | 1,77[a] | 2,41 | - | 1,76 | - |
| | | 2,31[*] | 1,22[*,a] | | | 1,79[*] | |
| **HOMO** eV | Teor[b] | -5,64 | -5,79 | -5,63 | - | -5,57 | - |
| | Ec | -5,06 | -5,17 | -5,08 | - | -4,86 | - |
| | | -5,13[*] | -5,16[*] | | | -4,95[*] | |
| **LUMO** eV | Teor[b] | -2,45 | -2,44 | -2,34 | - | -2,49 | - |
| | Ec | -2,84[a] | -3,73 | -2,67 | - | -3,06 | - |
| | | -2,82[*] | -3,79[*] | | | -3,19[*] | |
| **Efficiencies (liquid state)** | η % | 5,11 | 2,64 | 3,74 | - | 3,9 | - |
| **Efficiencies (solid state)** | η % | 2,47 | - | 0,76 | - | - | - |

Teor = from teorethical calculation, Sp = From spettroscopy, Ec = From electrochemistry. [*] Value in ACN. [a] First reduction peak. [b] Calcd. In vacuum.

**Table 4.15**

First, it can be noticed that the agreement between calculated and experimental spectra is quite good, confirming the adequacy of the employed level of theory. Indeed, the trend of calculated HOMO-LUMO gaps nicely compares with the spectroscopic data, showing that dyes are progressively red-shifted in the order **13**, **14, 11, 18** being **18** the most red-shifted one. Also, the electrochemical oxidation and reduction potential data are consistent with the trends in the calculated HOMOs and LUMOs energies for the dyes, showing an increase (decrease) of the HOMO (LUMO) energies in the same order from **13** to **18** which correlates with the small negative (positive) shifts measured for the oxidation (reduction) processes.

Is interesting also to observe that in dye **18** the energy gap measured electrochemically is lower than that found spectroscopically, This feature is quite uncommon and could be explained with the fact that the HOMO is mainly localization on the donor part of the molecule, while the LUMO is mainly localized on the acceptor part.

## 4.7 CONCLUSIONS

In this Ph. Thesis six new metal-free dyes shown in figure 4.34 have been synthesized. Among these dyes, **11**, **13**, **14** and **18** have been completely characterized and utilized as sensitizers in DSSCs for preliminary tests on their efficiency.

From our investigation we found that  triarylamine, with respect to difluorenylaniline and thienydiphenylamine, seems really to be the best donor group for this D-π-A systems, as confirmed by absorption spectra and cell efficiency.

However, it'll be interesting to study the performance of **17** in terms of $V_{oc}$ and $J_{sc}$ to evaluate the influence of the bulky fluorenyl unit on recombination and aggregation.

We also found that the cyanoacrylic moiety is the best candidate with elongated π system such as vinyl-**BDT**$_1$. Dye **20** indeed demonstrated that the carboxylic group itself is not enough electron-withdrawing to create a strong conjugated push-pull system, and therefore a strong blue-shift is observed in absorption spectra in comparison to the analogue dye **11**, bearing the cyanoacrylic group.

Dye **13**, which shows a low cell efficiency of 2.64% (without mask), due to the blue-shifted absorption band, has a very high $V_{oc}$, demonstrating that the recombination process of electrons from $TiO_2$ to oxidized dye and recombination of electrons from $TiO_2$ to $I^-/I^{3-}$ in the electrolyte are not responsible for the observed low efficiency .

Finally, dye **14**, bearing the **BDT**, shows how the different structure of the two **BDT** and **BDT**$_1$ isomeric spacers great influences the cell performance, due to the lower conjugation of the system. **BDT.** Dye **14** only gave 3.7% efficiency while the **11**, that incorporates **BDT**$_1$ as spacer, is the best candidate suitable for further investigation, it indeed has a good absorption spectra and lead to a very good cell efficiency of 5.11% in liquid state and a promising efficiency of 2.5% in solid state. Dye **18**, characterized from an important red-shift in the absorption spectra due to the presence of thiophenyl, let us think that with a judicious tailor of the structure in order to lower the HOMO level important improvements can be obtained.

In conclusion, we have demonstrate that **BDT**$_1$ is an interesting and well promising spacer for DSSCs application, in both liquid and solid state solar cell technology.

## 4.8    EXPERIMENTAL SECTION

All reagents and solvents were obtained from highest grade commercial sources and used without further purification unless otherwise stated. Column chromatography were carried out using silica gel 60 (70-230 mesh, Merck). $^1$H NMR spectra were acquired on a Bruker AVANCE DRX-400, Bruker AC300 and AMX at 300 MHz spectrometers; the chemical shifts ($\delta$) are reported in parts per million relative to the solvent residual peak (acetone-$d_6$, DMSO-$d_6$, CDCl$_3$). IR spectra were recorded on a Fourier Bruker Vector 22 FT, UV spectra were recorded by using a Jasco V-520 or Agilent 8453 UV/Vis spectrophotometer in a range of $\lambda$ from 190 nm to 800 nm at room temperature. HRMS spectra were recorded on Bruker Daltonics ICR-FTMS APEX II. Melting points were obtained with a Büchi B-540 melting point apparatus and are uncorrected. HPLC analyses were performed on an Agilent 1100 series equipped with a PDA detector and the reverse phase ZORBAX Eclipse XBD-C18, 4.6×150 mm, 5μm particle size; samples were analyzed with 1mL/min acetonitrile-water 80:20 with 0.1%

TFA. All the samples for cell fabrication were controlled via HPLC and the purity esteemed to be over 98%.

*Electrochemistry:*

Compounds were characterized by cyclic voltammetry, CV, at potential scan rates typically ranging from 0.05 to 2 V s$^{-1}$, in a 4 cm$^3$ minicell with 0.5-0.75 mM solutions in $CH_2Cl_2$ and ACN with 0.1 M TBAP as the supporting electrolyte, deaerated by $N_2$ purging. In particular, parent molecules required solvent ACN to allow observation of the first reduction peaks, located at very negative potentials. On the other hand, the chromophores were hardly soluble in ACN; however, in this case the cathodic potential window of $CH_2Cl_2$, granting good solubility, was sufficient, albeit narrower than the ACN one, on account of the much more positive reduction peak potentials.

The experiments were carried out using an AUTOLAB PGSTAT 12(8) potentiostat of EcoChemie (Utrecht, The Netherlands) run by a PC with the GPES 4.9 software of the same manufacturer.

The working electrode was a glassy carbon GC disk embedded in Teflon$^{®}$ (Amel, 0.071 cm$^2$). The optimized polishing procedure consisted in surface treatment with a synthetic diamond powder of 1 mm in diameter of Aldrich on a DP-Nap wet cloth of Struers.

The operating reference electrode was an aqueous saturated calomel one (SCE), but the experimental peak potentials have been normalized *vs* the Fc$^+$|Fc redox couple (the intersolvental redox potential reference currently recommended by IUPAC[74, 7576] having a redox potential of 0.39 V (in ACN) or of 0.495 V (in $CH_2Cl_2$) *vs* the operating SCE reference electrode. The counter electrode was a platinum disk embedded in glass. The ohmic potential drop was compensated by the positive feedback technique.[77]

*Computational methods:*

Calculations on the structure and simulated spectra were performed through Density Functional Theory, DFT, and its Time-Dependent formulation, TDDFT, as implemented in Gaussian program suite.[46] The ground state geometry for the protonated dyes were optimized in gas-phase within the B3LYP functional using a 6-31G* basis set. At the optimized ground state geometries we performed TDDFT (MPW1K/6-31G*)[20] excited state calculations in gas phase as well as in acetonitrile, adopting the non-equilibrium

Conductor-like Polarizable Continuum Model, CPCM.[21] This computational set-up has been previously shown to adequately describe the electronic and optical properties of similar push-pull dyes.[47, 48]

*Liquid electrolyte solar cell assembly:*

FTO glass (TEC-15/2.2 mm thickness, Solaronix) was used for transparent conducting electrodes. The substrate was first cleaned in a ultrasonic bath using a detergent solution, acetone and ethanol respectively (each step 15 min. long). The FTO glass plates were immersed into a 40mM aqueous $TiCl_4$ solution at 70 °C for 30 min and washed with water and ethanol. A commercial available $TiO_2$ paste (Dyesol 18NR-AO) was spread on the FTO glass plates by doctor blade technique. The $TiO_2$ coated electrodes (active area 0.2 $cm^2$) were gradually heated under air flow at 325 °C for 5 min, at 375 °C for 5 min, at 450 °C for 15 min, and 500 °C for 15 min. After the sintering process, the $TiO_2$ film was treated with 40mM $TiCl_4$ solution as described above, rinsed with water and ethanol.

$TiO_2$ electrodes were heated at 500 °C for 30 min and after cooling (80 °C) were immersed into sensitizing baths ($CH_3CN$ solutions of the dyes 0.2 mM, containing 3 mM 3a,7a-dihydroxy-5b-cholic acid (CDCA)) for 6h to complete the sensitizer uptake.

Counter electrodes were prepared by coating with a drop of $H_2PtCl_6$ solution (2 mg of Pt in 1 mL of ethanol) a FTO plate (TEC 15/2.2 mm thickness, Solaronix) and heating at 400 °C for 15 min. The $TiO_2$ sensitized photoanode and Pt counter electrode were assembled into a sealed sandwich-type cell by a hot-melt ionomer film (Surlyn, 25 $\mu$m thickness, Dyesol) as a spacer between the electrodes.

A commercial electrolyte solution (Iolitech ES-0004 HP, containing 1butyl-3methylimidiazolium iodide, iodine, guanidinium thiocyanate and *tert*-butylpyridine in a mixture of valeronitrile and acetonitrile), with 0.06M LiI, was used as electrolyte. Then, the hole was sealed by using additional Surlyn patch and a cover glass and finally a conductive Ag-based paint was deposed at the electrical contacts.

*Solid state solar cell assembly*

Fluorine doped tin oxide (FTO) coated glass sheets (15 Ω/sq Pilkington) were etched with zinc powder and HCl (2 Molar) to obtain the required electrode pattern. The sheets were then washed with soap (Hellmanex at 2% in water), de-ionized water, acetone,

methanol and finally treated under an oxygen plasma for 10 minutes to remove the last traces of organic residues. The FTO sheets were subsequently coated with a compact layer of $TiO_2$ (100 nm) by aerosol spray pyrolysis deposition at 450 ºC, using oxygen as the carrier gas.

The standard Dyesol $TiO_2$ paste was previously diluted down 1:3.5 in ethanol and stirred and ultrasonicated until complete mixing. The paste was then doctor-bladed by hand using scotch tape and a pipette on the $TiO_2$ compact layer coated FTO sheets to get a $TiO_2$ average thickness of 1.8 µm.

The sheets were then slowly heated to 550 ºC (ramped over 1 ½ hours) and baked at this temperature for 30 minutes in air. After cooling, slides were cut down to size and soaked in a 15 mM of $TiCl_4$ in water bath and oven-baked for 1 hour at 70 ºC. After rinsing with subsequently in water, ethanol and drying in air, they were subsequently baked once more at 550 ºC for 45 min in air, then cooled down to 70 ºC and finally introduced in a dye solution (0.3 mM in acetonitrile: THF (10:1)) for 16 hour. The Spiro-OMeTAD was dissolved in Chlorobenzene at a concentration of 90mg/mL; a solution of Lithium bis(trifluoromethylsulfonyl)imide salt (Li-TFSI) (0.04M in Acetonitrile) and 4-ter-butylpyridine was added to the Spiro-OMeTAD solution and spin-coated at 700 rpm for 60 s. The films were then placed in a thermal evaporator where 150 nm thick silver electrodes were deposited through a shadow mask under high vacuum ($10^{-6}$ mbar), to obtain pixel of an active area of ~ $0.08cm^2$.

*Photovoltaic Measurements*

Photovoltaic measurements were recorded by means of AM 1.5 solar simulator equipped with a Xenon lamp (LOT-ORIEL LS 0106). The power of incoming radiation, set at 100 mW/cm$^2$, was checked by a piranometer. J–V curves were obtained by applying an external bias to the cell and measuring the generated photocurrent with a Keithley model 2400 digital source-meter, under the control of dedicated LabTracer 2.0 software. A black shading mask was employed to avoid the overestimation of the measured parameters.

*Time-resolved Photoluminescence*

Time-resolved Photoluminescence spectra were taken using a Hamamatsu Picosecond Fluorescence Lifetime system based on a Strek camera with 2ps time response. Excitation (450nm) was provided by a 150fs ultrafast laser oscillator (Chamaleon, Coherent Inc.); emisson signals were detected at 700nm. All samples were measured at room temperature in a vacuum chamber ($10^{-4}$ mbar).

### 4.8.1   Synthesis of 3-bromothiophen-2-carbaldehyde[78,79]3
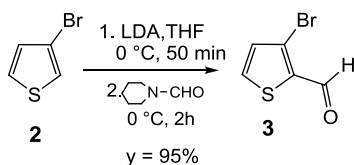


Under nitrogen, to a solution of DIPA (2,27 g; 22.5 mmol) in THF (50 mL) at 0°C, *n*-BuLi was added (14.4 mL; 22.5 mmol). The solution was left under stirring for 2.5 h at 0°C to generate LDA. Then a solution of 3-bromothiophene **2** (1.92 mL, 20.3 mmol) in THF was added dropwise and the mixture was left reacting 50 minutes. After this time *N*-formyl piperidine (3.4 mL, 30.6 mmol) was added and the solution was stirred for 2 h. The progress of reaction was monitored by TLC (hexane/AcOEt 9:1, $R_f$: 0.47). The mixture was then poured in $NH_4Cl_{s.s.}$ (65 mL) and the aqueous phase was then extracted with $Et_2O$ (3x20 mL). The organic phase was washed then with water, dried ($Na_2SO_4$), filtered and the solvent was evaporated under vacuum. The crude product was recovered without further affording **3** as a yellow oil, 3.68 g (95% yield). $^1$H-NMR (200 MHz, CDCl3): δ, ppm = 7.16 (d; *J* = 5 Hz, 2H); 7.72 (d; *J* = 5 Hz; 1H); 10 (s; 1H).

### 4.8.2   Synthesis of 3-bromo-α-(3-thienyl)-2-thiofenemethanol[80] 5
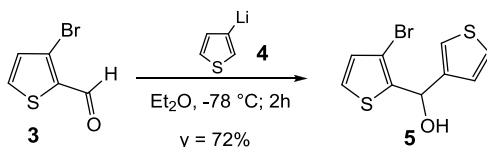


Under nitrogen, to a solution of *n*-BuLi (13.6 mL; 21.2 mmoli) in $Et_2O$ (20 mL) at -78°C, a solution of 3-bromo-thiophene **2** (2.0 mL; 21.1 mmol) in $Et_2O$ (8.5 mL) was added. The reaction was left under stirring 45 minutes. Then **3** (3.9 g; 20.2 mmol) dissolved in $Et_2O$
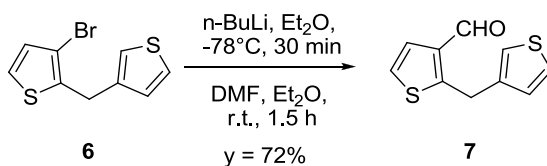
(8 mL) was added dropwise. The mixture was left reacting 2 h and the progress of reaction was monitored by TLC (hexane/AcOEt 9:1, $R_f$: 0.23). The mixture was then warmed to 0°C and poured in water (30 mL) and the aqueous phase was then extracted with $Et_2O$ (3x25 mL). The organic phase was washed then with water (3x10 mL) dried ($Na_2SO_4$), filtered and the solvent was evaporated under vacuum. The crude product was purified by column chromatography on silica gel (eluent: hexane) to afford **5** as an orange-yellow oil, 3.96 g (95% yield). ^{1}H-NMR (200 MHz, CDCl3): $\delta$, ppm = 2.52 (s b.; 1H; OH ); 6.26 (s; 1H); 6.98 (d; *J* = 5 Hz; 1H); 7.14 (d.; *J* = 5 Hz; 1H); 7.28 (d; *J* = 5 Hz; 1H); 7.32 (d.; *J* = 5 Hz; 1H); 7.35 (s; 1H).

### 4.8.3 Synthesis of 3-bromo-2,3'-dithienylmethane[81] 6



**5**          **6**
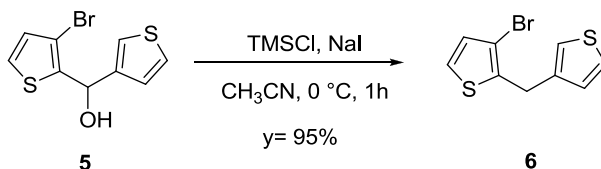
A solution of 3-bromo-2,3'-dithienylmethanol **5** (9.90 g, 35.95 mmol) in $CH_3CN$ (35 mL) was then dropped maintaining the temperature at 0°C. The resulting red solution was react for 2h and the progress of reaction was monitored by TLC (eluent: Hexane/AcOEt 9:1, $R_f$ 0.73 ). Afterwards the mixture was poured in water (30 mL), NaOH 5M was added until neutral pH. The mixture was then extracted with $CH_2Cl_2$ (4x30). The collected organic phase was then washed with $Na_2SO_3$ and water, dried ($Na_2SO_4$), filtered and the solvent was evaporated under vacuum. The crude product was purified by column chromatography on silica gel (eluent: hexane) to afford **6** as an orange oil, 8.50 g (81% yield). ^{1}H-NMR (200 MHz, CDCl3): $\delta$, ppm = 4.18 (s; 2H;); 7.00 (d; *J* = 5.32 Hz; 2H); 7.06 (d; *J* = 4.91 Hz; 1H); 7.10 (m; 1H); 7.17 (d; *J* = 5.32 Hz; 1H); 7.33 (d.; *J* = 4.91 Hz; 1H).

### 4.8.4 Synthesis of 2,3'-dithienylmethan-3-carboxaldehyde[32] 7



**6**          y = 72%          **7**

Under nitrogen, to a solution of *n*-BuLi (10.15 mL, 16.24mmol) in Et$_2$O (18 mL) at -78°C was added a solution of 3-bromo-2,3'-dithienylmethane **6** (3.51g, 13.53 mmol) in Et$_2$O (8 mL). The reaction was left under stirring 45 minutes. Then DMF (2.1 mL, 27.26 mmol) dissolved in Et$_2$O (4 mL) was added dropwise. The mixture was left reacting 90 minutes and the progress of reaction was monitored by TLC (hexane/AcOEt, 9:1, R$_f$: 0.29). The mixture was then poured in water (100 mL). After solvent evaporation the residue was washed with HCl 4 M to slightly acid pH. The aqueous phase was then extracted with CH$_2$Cl$_2$ (4x30 mL). The organic phase was dried (Na$_2$SO$_4$), filtered and the solvent was evaporated under vacuum. The crude product was purified by column chromatography on silica gel (eluent: hexane/AcOEt 9:1) to afford **7** as a orange solid, 2.04g (72.4% yield). ^{1}H-NMR (200 MHz, CDCl$_3$): δ, ppm = 4.52 (s; 2H;)6.94 (d; *J* = 4.94 Hz 1H;); 7.02 (s; 1H); 7.10 (d; *J* = 5.36 Hz; 1H); 7,27 (d.; *J* = 4.94; 1H); 7,40 (d; *J* = 5.4 Hz; 1H); 10,04 (s; 1H).

### 4.8.5   Synthesis of benzo[1,2-b:4,5-b']dithiophene [52,82] 1



**7**   **1**
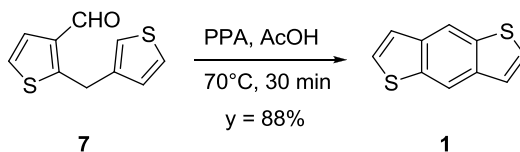
To 3.45 g of polyphosphoric acid, at 70 °C, a solution of **7** (2.04 g, 9.8 mmol) in AcOH (18 mL) was added. The mixture was left under stirring 30 min. The progress of the reaction was monitored by TLC. (eluent: Hexane/AcOEt 9:1, R$_f$ 0.80). The obtained gray suspension was then poured in H$_2$O (40 mL) causing the precipitation of the product **1**. The solid was then filtered and washed with water (20 mL), dried in oven at 70°C. The crude product was purified by column chromatography on silica gel (eluent: hexane) to give **7** as a white solid, 1.64 g, 8.6 mmol (88% yield). ^{1}H-NMR (300 MHz, CDCl$_3$): δ, ppm = 7.40 (d; *J* = 5.5 Hz; 2H); 7.50 (d.; *J* = 5.5 Hz; 2H); 8.36 (s; 2H).

### 4.8.6   Synthesis of 2-6-diformylbenzo [1,2-b:4,5-b']dithiophene[52] 22



**1**   **22**
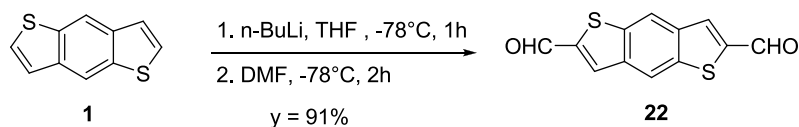
Synthesized according to the procedure reported in the literature.

### 4.8.7 Synthesis of {4-[bis(4-methoxyphenyl)amino]phenyl}carboxaldehyde[49,83] 26
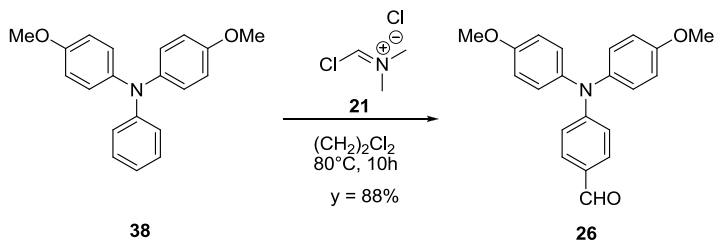


To a solution of MTPA **38** (400.0 mg, 1.31 mmol) in $(CH_2)_2Cl_2$ (20 mL) the Vilsmeier reactant (670.8 mg, 5.24 mmol) was added and the reaction mixture was heated at 80°C for 10 h and monitored by TLC ( eluent: hexane/AcOEt 7:3, $R_f$: 0.25). Then the solution was allowed to cool to ambient temperature, washed with a saturated solution of AcONa and extracted with $CH_2Cl_2$ (4x15mL). The organic phase was dried ($Na_2SO_4$), filtered and the solvent was evaporated under vacuum. The crude product was purified by chromatography on silica gel (eluent: hexane/AcOEt 9:1) to afford **26** as a yellow oil, 387 mg (88% yield). ^{1}H-NMR (300 MHz, CDCl$_3$): $\delta$, ppm = 3.80 (s; 6H); 6.84 (d; $J$ = 8.6 Hz; 2H); 6.88 (t; $J$ = 8.8 Hz; 4H); 7.13 (d; $J$ = 8.8 Hz; 4H); 7.62 (d; $J$ = 8.6 Hz; 2H); 9.74 (s; 1H).

### 4.8.8 Synthesis of {4-[bis(4-methoxyphenyl)amino]phenyl}methan-1-ol[49,84] 27
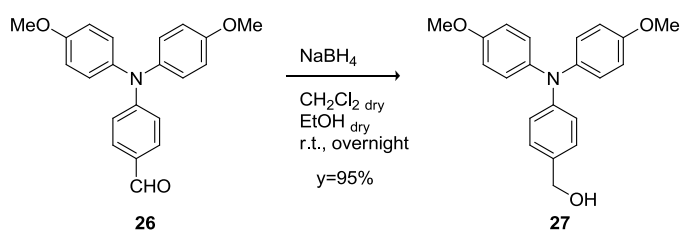


To a solution of $NaBH_4$ (21.4 mg, 0.57 mmol) in $CH_2Cl_2$/EtOH (2 mL:1.5 mL) 4-[bis(4-methoxyphenyl)amino]benzaldehyde **26** (125.5 mg, 0.38 mmol) was added rapidly and the resulting yellow solution was stirred at room temperature overnight. The progress of reaction was monitored by TLC (hexane/AcOEt 1:1, $R_f$: 0.45). The solution was poured into water (10 mL) with vigorously stirring and extracted with dichloromethane (3x10 mL).The organic phase was dried ($Na_2SO_4$), filtered and the solvent was evaporated

under vacuum. The crude product **27** was collected as a pale-yellow oil that not require further purification, 121.3 mg, (96% yield). ^{1}H NMR (300 MHz, CDCl$_3$): δ, ppm = 3.79 (s, 6H), 4.57 (s, 2H), 6.82 (d, 4H, *J*=8.9 Hz), 6.93 (d, 2H, *J*=8.4 Hz), 7.04 (d, 4H, *J*=8.9 Hz), 7.17 (d, 2H, *J*=8.4 Hz)

### 4.8.9 Synthesis of [[4-[Bis(4-methoxyphenyl)amino]phenyl]methyl] triphenylphosphonium bromide[84] **21**
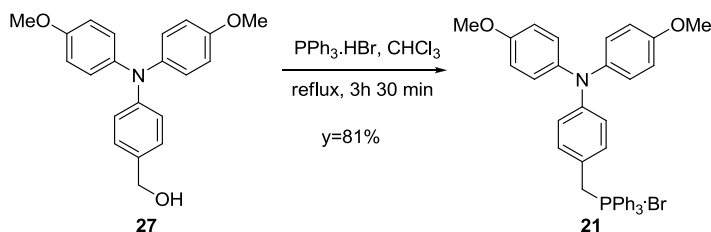


4-[bis(4-methoxyphenyl)amino]phenyl]methan-1-ol **27** (374.5 mg, 1.12 mmol) and PPh$_3$.HBr (421.5 mg, 1.23 mmol) was dissolved in CHCl$_3$ (6 mL) and refluxed under stirring for 3.5 h. The progress of reaction was monitored by TLC (esano/AcOEt 1:1, R$_f$: 0.0). After removing the solvent, the residue was solidified with ether (10 mL) and filtrated to obtain **21** as a white solid, 192.6 mg (81% yield). No further purification required.^{1}H NMR (300 MHz, Acetone-d$_6$): δ, ppm = 3.76 (s, 6H), 4.57 (s, 2H), 6.82 (d, 4H, *J*=8.9 Hz), 6.93 (d, 2H, *J*=8.4 Hz), 7.04 (d, 4H, *J*=8.9 Hz), 7.17 (d, 2H, *J*=8.4 Hz). [31]P (121 MHz, CDCl$_3$): δ, ppm = 23.09.

### 4.8.10 Synthesis of 6-[2-[4-[Bis-(4-methoxyphenyl)amino]phenyl]ethenyl]benzo[1,2-b:4,5-b']dithiophen-2-carboxy aldehyde [49,84] **23:**
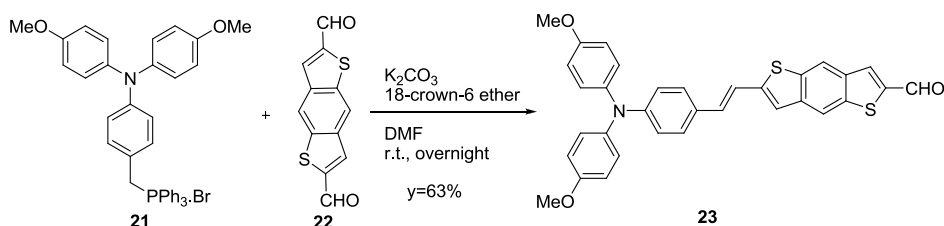


A solution of the phosphonium salt **21** (100 mg, 0.15 mmol) in DMF (4 mL) was slowly added, under stirring at room temperature, to a slurry of 2,6-benzo[1,2-b:4,5-b']dithiophenedicarboxyaldehyde**22**[52] (50 mg, 0.20 mmol), 18-crown-6 ether (3 mg) and

anhydrous $K_2CO_3$ (32 mg, 0.30 mmol) in DMF (4 mL). The resulting orange solution was stirred overnight at room temperature. The solution was then poured into water (10 mL) and extracted with dichloromethane (4×10 mL). The organic phase was washed with water (20 mL), dried over $Na_2SO_4$ and filtered. After evaporation of the solvent the crude dark orange product was purified by silica gel column chromatography (eluent: $CH_2Cl_2$/hexane 9:1) to afford **23** as a red solid, 51 mg (63% yield). M..p: 212-214 °C (dec).^{1}H NMR (300 MHz, DMSO-$d_6$): δ, ppm = 3.73 (s, 6H), 6.72 (d, 2H, J=8.6 Hz), 6.92 (d, 4H, J=8.9 Hz), 6.97 (d, 1H, J=16.4 Hz), 7.05 (d, 4H, J=8.9 Hz), 7.39 (d, 1H, J=16.4 Hz), 7.44 (d, 2H, J=8.6), 7.45 (s, 1H), 8.41 (s, 2H), 8.6 (s, 1H), 10.11 (s, 1H). ^{13}C NMR (75 MHz, CDCl_3): δ, ppm = 55.18; 114.96; 117.15; 118.16; 118.38; 119.06; 119.99; 121.68; 124.35; 126.95; 127.37; 127.58; 127.73; 127.86; 129.71; 132.53; 135.53; 139.60; 143.12; 148.35; 155.97; 185.95. IR (nujol, $cm^{-1}$): 1670 ($\nu_{CO}$). HRMS-EI *m/z*: calcd. for $C_{33}H_{25}NO_3S_2$: 547.127588, found: 547.126650. UV-Vis: $CH_3CN$, $\lambda_{max}$ = 298 nm ($1.8 \cdot 10^4$ $M^{-1}cm^{-1}$), 344 nm ($2.1 \cdot 10^4$ $M^{-1}cm^{-1}$), 451 nm ($3.6 \cdot 10^4$ $M^{-1}cm^{-1}$).

### 4.8.11 Synthesis of 2-cyano-3-{6-[2-[4-[bis(4-methoxyphenyl)amino] phenyl]ethenyl]benzo[1,2-b:4,5-b']dithiophen-2-yl} propenoic acid[49] 11
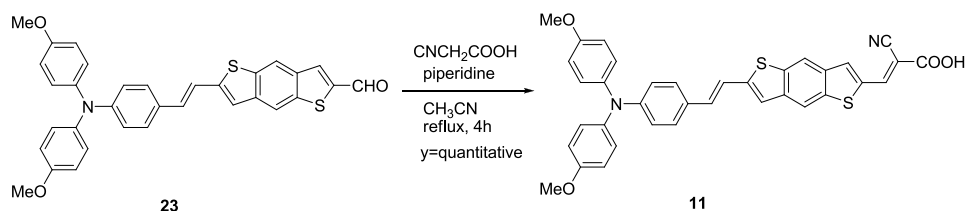


Cyanoacetic acid (20.0 mg, 0.24 mmol) and piperidine (5 mg, 0.05 mmol) were added to a suspension of **23** (70 mg, 0.13 mmol) in $CH_3CN$ (10 mL). The reaction mixture was stirred for 4 h at 80 °C. The solvent was then evaporated and the residue was taken up with a mixture HCl 0.1M (6 mL) and hexane (4 mL) and filtered affording 70 mg (95%) of **11** as a red solid. M.p.: 258-260 °C (dec). ^{1}H NMR (300 MHz, DMSO-d_6): δ, ppm = 3.76 (s, 6H), 6.74 (d, 2H, J=8.5 Hz), 6.95 (d, 4H, J=9 Hz), 6.97 (d, 1H, J=16.4 Hz), 7.08 (d, 4H, J=9 Hz), 7.42 (d, 1H, J=16.4 Hz), 7.47 (d, 2H, J=8.5), 7.45 (s, 1H), 8.35 (s, 2H), 8.47 (s, 1H), 8.58 (s, 1H), 8.64 (s,1H). ^{13}C NMR (75 MHz, CDCl_3): δ, ppm = 55.13, 101.17, 114.88, 115.84, 116.44, 118.26, 118.50, 119.02, 119.08, 121.51, 126.83, 126.95, 127.27, 127.55, 127.68, 127.81, 132.05, 135.06, 135.28, 135.35, 136.97, 139.06, 139.33, 140.89, 146.50,

147.12, 148.63, 155.98, 163.09. IR (nujol, cm$^{-1}$): 3402 ($v_{OH}$), 2360 ($v_{CN}$), 1569 ($v_{CO}$)..

HRMS-ESI *m/z* [M-H]$^-$ calcd. for $C_{36}H_{25}N_2O_4S_2$: 613.12557, found: 613.12579. UV-vis:

$CH_2Cl_2$ (6·10$^{-5}$ M), $\lambda_{max}$ = 370 nm (2.2 ·10$^4$ M$^{-1}$cm$^{-1}$), 460 nm (2.1·10$^4$ M$^{-1}$cm$^{-1}$); EtOH, (5·10$^{-5}$ M), $\lambda_{max}$ = 368 nm (7.2·10$^3$ M$^{-1}$cm$^{-1}$), 443 nm (1.2·10$^4$ M$^{-1}$cm$^{-1}$); THF (5·10$^{-5}$ M), $\lambda_{max}$ = 375 nm (2.9·10$^4$ M$^{-1}$cm$^{-1}$), 478 nm (3.7·10$^4$ M$^{-1}$cm$^{-1}$).

### 4.8.12 Synthesis of 2-6-diformylbenzo[1,2-b:4,3-b']dithiophene[53,84] 24



Synthesized according to the literature procedure.

### 4.8.13 Synthesis of 7-[2-[4-[bis-(4-methoxyphenyl)amino]phenyl]ethenyl] benzo[1,2-b:4,3-b']dithiophen-2-carboxy aldehyde 25
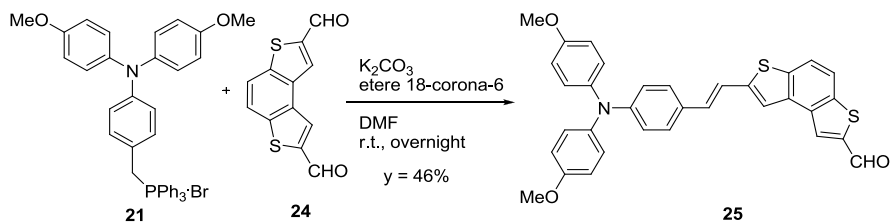


Following the same procedure used for the synthesis of **23**, the phosphonium salt **21** (0.30 mmol) was reacted with benzo[1,2-b:4,3-b']-2,7-dithiophenedicarboxyaldehyde **24**[53] (0.36 mmol) in DMF. A crude dark orange product was obtained which was purified by silica gel column chromatography (eluent: $CH_2Cl_2$/hexane 9:1) to afford 76 mg (46%) of **25** a as a red solid. M.p.: 160-162 °C. $^1$H NMR (300 MHz,CDCl$_3$): δ, ppm = 3.81 (s, 6H), 6.83-6.91 (m, 6H ), 7.01 (d, 1H, *J*=15.9 Hz), 7.03-7.09 (m, 4H), 7.13 (d, 1H, *J*=15.9 Hz), 7.32 (d, 2H, *J*=8.7 Hz), 7.5 (s, 1H,), 7.70 (d, 1H, *J*=8.7 Hz), 7.80 (d, 1H, *J*=8.7 Hz), 8.26 (s, 1H ), 10.12 (s, 1H). $^{13}$C NMR (75 MHz, CDCl$_3$): $^{13}$C NMR (75 MHz, CDCl$_3$): δ, ppm = 55.51; 114.83; 117.15; 118.81; 119.40; 119.9; 122.54; 126.97; 127.37; 127.52; 128.17; 131.64; 133.28; 135.74; 136.97; 140.57; 143.03; 146.10; 148.95; 156.34; 184.09. IR (nujol, cm$^{-1}$): 1646 ($v_{CO}$).. HRMS-EI *m/z*: calcd. for $C_{33}H_{25}NO_3S_2$: 547.12758, found: 547.127588. UV-vis:

CH$_3$CN (6.3·10$^{-5}$ M), λ$_{max}$= 299 nm (1.84·10$^4$ M$^{-1}$cm$^{-1}$), 354 nm (2.72·10$^4$ M$^{-1}$cm$^{-1}$), 439 nm (3.42·10$^4$ M$^{-1}$cm$^{-1}$).
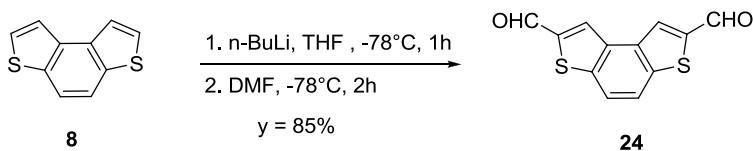
### 4.8.14  Synthesis of 2-cyano-3-{7-[2-[4-[bis(4-methoxyphenyl)amino]phenyl]ethenyl] benzo[1,2-b:4,3-b']dithiophen-2-yl} acrylic acid 14
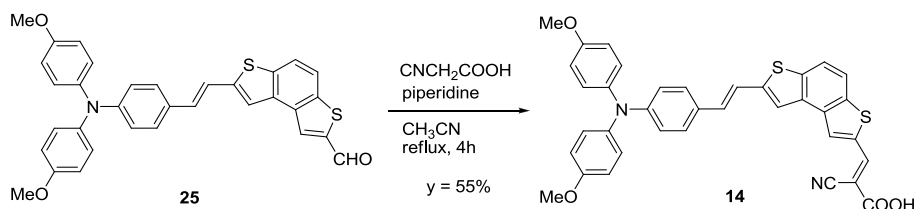


Synthesized following the same procedure of **11**, starting from 70 mg (0.13 mmol) of **25** to afford 46 mg (55%) of **14** as a red solid. M.p.: 198-200 °C. $^1$H NMR (300 MHz, DMF-$d_7$): δ, ppm = 3.80 (s, 6H), 6.74 (d, 2H, J=8.5 Hz), 6.95 (d, 4H, J=9 Hz), 6.97 (d, 1H, J=16.4 Hz), 7.08 (d, 4H, J=9 Hz), 7.42 (d, 1H, J=16.4 Hz), 7.47 (d, 2H, J=8.5 Hz), 7.45 (s, 1H), 8.35 (s, 2H), 8.47 (s, 1H), 8.58 (s, 1H), 8.64 (s,1H). $^{13}$C NMR (75 MHz, DMF-$d_7$): δ, ppm = 55.78, 115.67, 116.84, 119.57, 119.73, 121.23, 123.60, 127.97, 128.56, 128.76, 132.17, 133.59, 135.92, 136.50, 140.76, 146.84, 147.93, 149.85, 157.32, 164.13. IR (nujol, cm$^{-1}$): 3393 (ν$_{OH}$), 2342(ν$_{CN}$), 1560 (ν$_{CO}$)  MS-ESI (m/z): [M]- 614.3, 570.4 (-CO$_2$), 555.4 (-CH$_3$). UV-vis: EtOH (3.18·10$^{-5}$ M ), λ$_{max}$ = 391 nm (3.8·10$^4$ M$^{-1}$cm$^{-1}$); 441 nm (2.7·10$^4$ M$^{-1}$cm$^{-1}$); THF (3.21·10$^{-5}$ M), λ$_{max}$ = 394 nm (4.2·10$^4$ M$^{-1}$cm$^{-1}$), 460 nm (2.6·10$^4$ M$^{-1}$cm$^{-1}$); toluene (3.03·10$^{-5}$ M), λ$_{max}$ = 399 nm (3.8·10$^4$ M$^{-1}$cm$^{-1}$), 478 nm (2.1·10$^4$ M$^{-1}$cm$^{-1}$); CH$_3$CN (2.97·10$^{-5}$ M), λ$_{max}$ = 393 nm (4.2·10$^4$ M$^{-1}$cm$^{-1}$), 451 nm (2.6·10$^4$ M$^{-1}$cm$^{-1}$); CH$_2$Cl$_2$ (3.21·10$^{-5}$ M), λ$_{max}$ = 399 nm (5.6·10$^4$ M$^{-1}$cm$^{-1}$); 486 nm (2.74·10$^4$ M$^{-1}$cm$^{-1}$).

### 4.8.15  Synthesis of 5-[bis(4-methoxyphenyl) amino]thiophene[54] 30
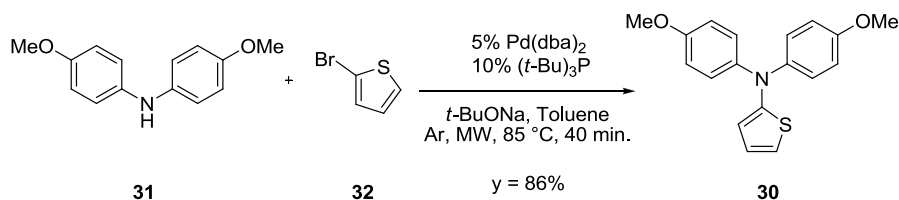
In anhydrous deoxygenated toluene (3 mL), $Pd_2dba_3$ (0.091 g, 0.10 mmol), the amine **31** (49.7 mg, 0.217 mmol), sodium *tert*butoxide (69.7mg, 0.725 mmol) 2-bromo thiophene **32** (84 mg, 0.515 mmol) and $P(t\text{-Bu})_3$ (5.8 mg, 0.029 mmol) were added under argon. The solution was stirred at room temperature under nitrogen for 5 minutes and then heated at 85°C for 40 minutes under MW irradiation. The reaction progress was monitored by TLC (eluent: hexane/AcOEt 8:2, $R_f$: 0.51 ). After removing the solvent, the crude product was purified by flash chromatography on silica gel (eluent: hexane/AcOEt 9:1) to give 120 mg of desired product **30** as a green oil (86% yield). ^{1}H-NMR (300 MHz, DMSO-d6): δ, ppm = 3.79 (s, 6H, OMe), 6.53 (dd, 1H), 6.84-6.80 (m, 6H, *J*=8.9 Hz), 7.08-7.05 (d, 4H, *J*=8.9 Hz).

### 4.8.16   Synthesis of 5-[bis(4-methoxyphenyl) amino]thiophenaldehyde[48] 33
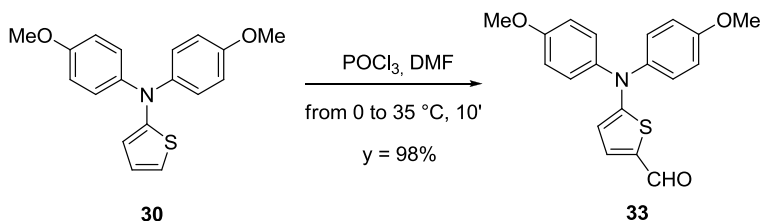


Under argon to a solution of thienyl-diarylamine **30** (80 mg, 0.26 mmol) in DMF (2 mL) at 0°C was slowly added $POCl_3$ (46 mg, 28 μl, 0.30 mmol). The reaction mixture was then heat at 35 °C for 10 minutes. The progress of the reaction was monitored by TLC (eluent: hexan/AcOEt 8:2, $R_f$: 0.26). The solution was then poured in $Na_2CO_3$ s.s. (10 mL) and extracted with AcOEt (3x10 mL). The organic phase, washed first $Na_2CO_3$ s.s. (2x10 mL) and then with water, was dried ($Na_2SO_4$), filtered and the solvent evaporated under vacuum affording 87 mg of the desired compound **33** as a bright yellow oil, 98% yield. ^{1}H-NMR (300 MHz, $CDCl_3$): δ, ppm = 3.82 (s, 6H, OMe), 6.17 (d, 1H, *J*=4.3 Hz), 6.92-6.88 (d, 4H, *J*=8.9 Hz), 7.25-7.22 (d, 4H, *J*=8.9 Hz), 7.40 (d, 1H, *J*=4.3 Hz), 9.55 (s, 1H, CHO). UV-vis: $CH_2Cl_2$ (8.0E-05 M), $\lambda_{max}$ = 243 nm ($1.29 \cdot 10^4$ $M^{-1}cm^{-1}$), 292 nm ($7.00 \cdot 10^4$ $M^{-1}cm^{-1}$), 384 nm ($2.10 \cdot 10^4$ $M^{-1}cm^{-1}$).

#### 4.8.17  Synthesis of {5-[bis(4-methoxyphenyl) amino]thiophenyl} methan-1-ol 34



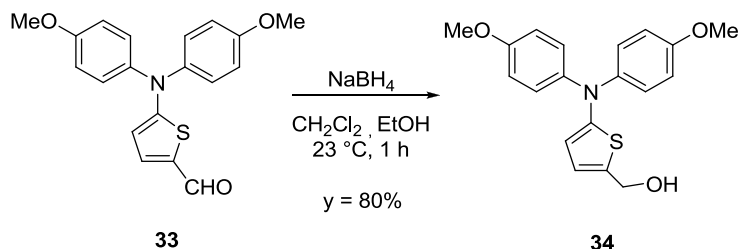**33**                                        **34**

Synthesized following the same procedure of **27**, starting from 271 mg (0.80 mmol) of **33** to afford in 1 h the desired product **34**. The crude product was washed with hexane to give 216 mg of **34** as a yellow oil in 80% yield. The reaction progress was monitored by TLC (eluent: hexane/AcOEt 8:2, $R_f$: 0.17). ^{1}H-NMR (200 MHz, CDCl$_3$): δ, ppm = 3.79 (s, 6H), 4.68 (s, 2H), 6.35 (d, 1H, J=3.7 Hz), 6.72 (d, 1H, J=3.7 Hz), 6.85-6.79 (d, 4H, J=8.1 Hz), 7.09-7.05 (d, 4H, J=8.1 Hz). ^{13}C-NMR (75 MHz, CDCl$_3$): δ, ppm = 55.51, 60.71, 114.52, 116.48,122.75, 124.41, 135.38, 141.58, 153.91, 155.76. MS-EI (m/z): [M]$^+$ 341, 324 (-OH), 214, 199, 129. HRMS-EI (m/z): [M]$^+$ calcd. for C$_{19}$H$_{19}$NO$_3$S$_1$: 341.108565, Found: 341.108180. IR (cm$^{-1}$): 3417 ($v_{OH}$).

#### 4.8.18  Synthesis of [[4-[Bis(4-methoxyphenyl)amino]thiophenyl]methyl] triphenylphosphonium bromide 28



**34**                                        **28**
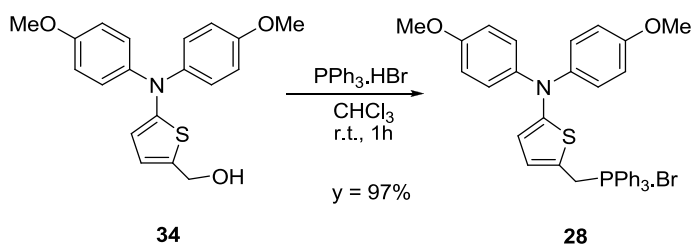
Synthesized following the same procedure of **21**, starting from 216 mg (0.63 mmol) of **5** to afford in 1 h 399 mg of **28** as a green oil (97% yield). No further purification was required. The reaction progress was monitored by TLC (eluent: hexane/AcOEt 6:4, $R_f$: 0.0). P.f.: 76.7-82.5 °C. ^{1}H-NMR (300 MHz, CDCl$_3$): δ, ppm = 3.73 (s, 2H) 3.75 (s, 6H), 5.50 (d, 1H), 6.73 (d, 5H), 6.90 (d, 4H), 7.78-7.63(m, 15H). [31]C-NMR (75 MHz, CDCl$_3$): δ, ppm =

27.40, 28.06, 55.57, 114.74, 117.30, 118.44, 124.34, 125.39, 130.34, 130.94, 134.24, 135.09, 141.05, 154.70, 155.95.

### 4.8.19 Synthesis of 7-[2-[5-[bis-(4-methoxyphenyl)amino]thiophenyl]ethenyl] benzo[1,2-b:4,3-b']dithiophen-2-carboxy aldehyde 37
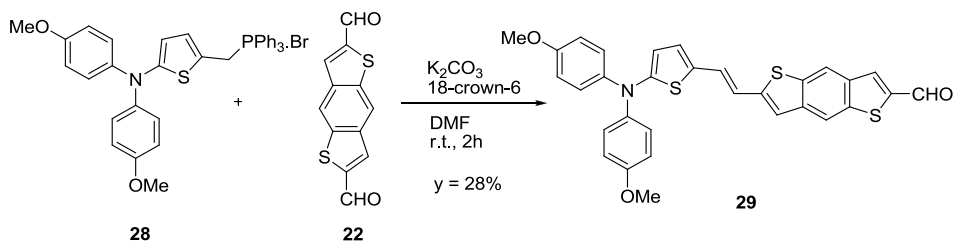


Following the same procedure used for the synthesis of **23**, the phosphonium salt **28** (337 mg, 0.52 mmol) was reacted with benzo[1,2-b:4,3-b']-2,7-dithiophenedicarboxyaldehyde **22** (129 mg, 0.52 mmol) in DMF for 2 h. The reaction was monitored by TLC (eluent: DCM). The crude product was obtained was purified by silica gel column chromatography (eluent: CH$_2$Cl$_2$/hexane 8:2, R$_f$ 0.63) to afford 80 mg (28%) of **29** as a dark red solid. ^{1}H-NMR (300 MHz, CDCl$_3$): δ, ppm = 3.81 (s, 6H, CH$_{3,MeO}$), 6.25 (d, 1H, J=3.9 Hz), 6.79-6.73 (d, 1H, J=15.5 Hz), 6.81 (m, 1H), 6.87-6.84 (d, 4H, J=8.9 Hz), 7.04-6.99 (d, 1H, J=15.5 Hz), 7.08 (s, 1H), 7.18-7.15 (d, 4H, J=8.9 Hz), 8.01 (s, 1H), 8.6 (s, 1H), 8.09 (s, 1H), 8.26 (s, 1H), 10.09 (s, 1H, CHO). ^{13}C-NMR (75 MHz, CDCl$_3$): δ, ppm = 29.72; 55.54; 113.42; 114.72; 116.56; 117.64; 119.30; 120.45; 125.25; 126.63; 128.35; 130.54; 133.62; 135.90; 136.90; 139.65; 140.59; 141.65; 143.09; 146.61; 155.31; 156.65; 184.45. IR (nujol, cm$^{-1}$): 1663 (v$_{CO}$). MS-EI (m/z): [M]$^+$ 553 (100%), 540 (10%, -CH$_3$), 517 (6%), 316(9%). HRMS-EI (m/z): [M]$^+$ calcd. for C$_{31}$H$_{23}$NO$_3$S$_3$: 553.084009, found: 553.090270. UV-vis CH$_2$Cl$_2$ (1.08·10$^{-5}$ M) λ$_{max}$ = 321 nm (1.84 ·10$^4$ M$^{-1}$cm$^{-1}$), 345 nm (1.78 ·10$^4$ M$^{-1}$cm$^{-1}$), 477 nm (3.92·10$^4$ M$^{-1}$cm$^{-1}$).

### 4.8.20 Synthesis of 2-cyano-3-{7-[2-[5-[bis(4-methoxyphenyl)amino]thiophenyl] ethenyl] benzo[1,2-b:4,3-b']dithiophen-2-yl} acrylic acid 18
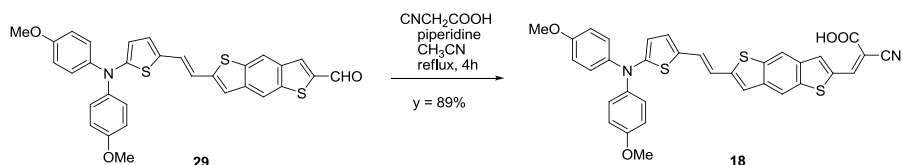


Synthesized following the same procedure of **11**, starting from 60 mg (0.11 mmol) of **29** to afford 62 mg (89%) of **18** as a red solid. ^{1}H-NMR (300 MHz, DMSO-d6): δ, ppm = 3.75 (s, 6H), 6.15 (d, 1H, J=3.9 Hz), 6.92-6.86 (d, 1H, J=17.2 Hz), 6.96 (d, 4H, J=8.9 Hz), 6.98 (d, 1H, J=3.9 Hz), 7.04 (s, 1H), 7.09 (m, 1H), 7.14 (d, 4H, **J**=8.9 Hz), 7.34 (s, 1H), 7.97 (s, 1H), 8.23 (s, 1H), 8.33 (s,1H), 8.35 (s, 1H). ^{13}C-NMR (300 MHz, CDCl₃): δ, ppm = 55.48, 113.34, 114.40, 114.68, 116.47, 117.56, 119.22, 120.39, 123.26, 123.77, 125.64, 126.56, 130.46, 134.05, 135.82, 136.82, 139.60, 140.57, 141.56, 143.00, 146.53, 155.27, 156.62, 184.26. IR (nujol, cm$^{-1}$): 3393 ($v_{OH}$), 1606 ($v_{CO}$), 1504 ($v_{CN}$). UV-vis: THF(1.3·10$^{-5}$ M), $\lambda_{max}$ = 381 nm (1.81 ·10$^4$ M$^{-1}$cm$^{-1}$); 499 nm (3.41 ·10$^4$ M$^{-1}$cm$^{-1}$) ;Toluene (2.3·10$^{-5}$ M): 393 (4.43 ·10$^3$ M$^{-1}$cm$^{-1}$); 519 (7.43 ·10$^3$ M$^{-1}$cm$^{-1}$) - CH₂Cl₂ (1.2·10$^{-5}$ M) $\lambda_{max}$ = 396 nm (2.11 ·10$^3$ M$^{-1}$cm$^{-1}$); 502 nm (2.70 ·10$^4$ M$^{-1}$cm$^{-1}$) - EtOH(1.4·10$^{-5}$ M) $\lambda_{max}$ =  303 nm (9.21 ·10$^3$ M$^{-1}$cm$^{-1}$); 370 nm (1.11 ·10$^3$ M$^{-1}$cm$^{-1}$); 480 nm (2.30 ·10$^3$ M$^{-1}$cm$^{-1}$) - CH₃CN (1.5·10$^{-5}$ M) $\lambda_{max}$ = 301 nm (5.40 ·10$^3$ M$^{-1}$cm$^{-1}$); 392 nm (6.73 ·10$^4$ M$^{-1}$cm$^{-1}$); 507 nm (1.22 ·10$^4$ M$^{-1}$cm$^{-1}$).

### 4.8.21 Synthesis of benzo[1,2-b:4,5-b']dithiophen-2-carboxaldehyde[53] 39
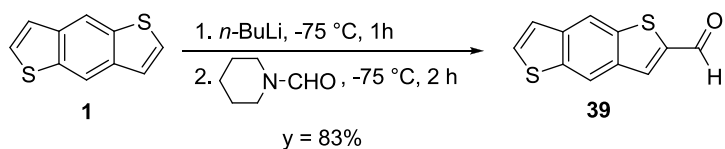


Under nitrogen, *n*-BuLi (1.6 M in hexane, 1.44 mL, 2.31 mmol) was added to a suspension of benzo[1,2-b:4,5-b']dithiophene **1** (400 mg, 2.10 mmol) at -75 °C in THF (7 mL). The mixture was stirred for 1 h and the color turn from white to yellow. Then *N*-formylpiperidine (0.47 mL, 4.20 mmol) was added dropwise. The resulting yellow solution was reacted for 2 h at -75 °C. The progress of reaction was monitored by TLC (hexane/EtOAc 9:1, R$_f$: 0.27). Afterwards the mixture was poured in a solution of NH₄Cl

(15 mL) and extracted with AcOEt (3x15 mL). After separation of the layers, the organic phase was washed with HCl 1M (2x10 mL) and $H_2O$ (10 mL), dried ($Na_2SO_4$), filtered and the solvent was evaporated under vacuum. The crude product was purified by column chromatography on silica gel (eluent: hexane/AcOEt 9:1) to afford **39** as a yellow solid, 380 mg (83% yield). P.f.: 187 °C. ^{1}H NMR (300 MHz, $CDCl_3$): δ, ppm = 7.43 (d; $CH_{tiof}$, $J$ = 5.5 Hz; 1H), 7.65 (d ; $CH_{tiof}$, $J$ = 5.5 Hz; 1H), 8.12 (s; $CH_{tiof}$, 1H); 8,37 (s, $CH_{ar}$, 1H); 8,50 (s, $CH_{ar}$, 1H); 10.17 (s; $CH_{ald}$, 1H). ^{13}C NMR (75 MHz, $CDCl_3$): δ, ppm = 117.59, 119.99, 123.03, 129.88, 134.02, 136.05, 137.95, 139.06, 140.55, 184.52. HRMS-EI (m/z): [M]$^+$ Calcd. for $C_{11}H_6O_1S_2$: 217.986008, found: 217.986420. MS-EI (m/z): [M]$^+$: 218, 189 ( − CHO), 145 ( − CHS$^+$). IR (nujol, cm$^{-1}$): 1681,62 cm$^{-1}$ ($v_{CO}$). UV-vis ($10^{-5}$ in $CH_2Cl_2$): $\lambda_{max}$ = 241 nm (9.4 $10^3$ $M^{-1}cm^{-1}$); 278 nm ($1.05\cdot10^4$ $M^{-1}cm^{-1}$); 330 nm ($9.6\cdot10^3$ $M^{-1}cm^{-1}$ $M^{-1}cm^{-1}$); 390 nm ($3.1 \cdot10^3$ $M^{-1}cm^{-1}$).

### 4.8.22  Synthesis of 6-bromo-benzo[1,2-b:4,5-b']dithiophen-2-carboxaldehyde[23] 40
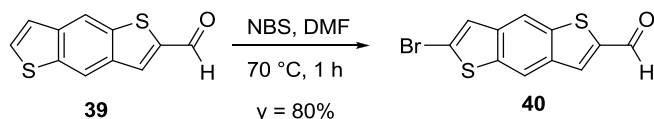


NBS (771 mg, 4.33 mmol) was added to a suspension of benzo[1,2-b:4,5-b']dithiophen-2-carboxaldehyde **39** (430 mg, 1.97 mmol) in DMF (28 mL). The mixture was stirred for 1 h at 70°C and the color turn from yellow to orange. The progress of reaction was monitored by TLC (hexane–EtOAc, 8:2, $R_f$: 0.32). Afterwards The DMF was distilled under vacuum at 60 °C, the residue was dissolved in $CH_2Cl_2$ (20 mL) and washed with water (3x15 mL). The organic phase was dried ($Na_2SO_4$), filtered and the solvent was evaporated under vacuum. The crude product was purified by flash chromatography on silica gel (eluent: hexane-AcOEt 8-2) to afford **40** as a yellow solid, 468 mg (80% yield). P.f.: 184-185 °C. ^{1}H NMR (200 MHz, $CDCl_3$): δ, ppm = 7.60 (s; 1H; $CH_{tiof}$); 8.10 (s; 1H; $CH_{tiof}$); 8.37 (s; 1H; $CH_{ar}$); 8.44 (s; 1H; $CH_{ar}$); 10.15 (s; 1H; $CH_{ald}$). ^{13}C NMR (50 MHz, $CDCl_3$): δ, ppm = 106.83, 117.51, 119.12, 126.74, 133.46, 136.38, 136.73, 138.20, 139.71,144.60, 184.49. HRMS-EI (m/z): [M]$^+$ Calcd. for $C_{11}H_5OS_2Br$: 295.896520, found: 295.896120. MS-EI (m/z): [M]$^+$: 298, 269 ( − CHO). IR (nujol, cm$^{-1}$): 1662 ($v_{CO}$). UV-vis ($10^{-4}$ in $CH_2Cl_2$): $\lambda_{max}$=

244 nm (5.4·10$^4$ M$^{-1}$cm$^{-1}$); 280 nm (7.0 ·10$^3$ M$^{-1}$cm$^{-1}$); 329 nm (5.6 ·10$^3$ M$^{-1}$cm$^{-1}$); 390 nm (1.9·10$^4$ M$^{-1}$cm$^{-1}$).

### 4.8.23  Synthesis 6-trimethylsilylethynylbenzo[1,2-b:4,5-b']dithiophen-2-carboxaldehyde[85] 41
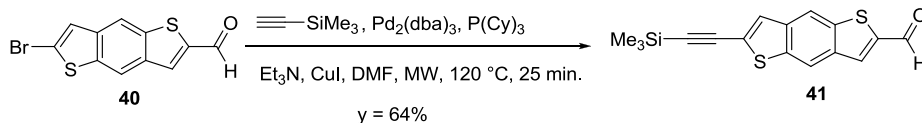


In a microwave reactor tube to a solution of 6-bromo-benzo[1,2-b:4,5-b']dithiophen-2-carboxaldehyde **40** (140 mg, 0.47 mmol) in DMF (4 mL) was added under nitrogen Pd$_2$(dba)$_3$ (25 mg, 2.83·10$^{-2}$ mmol), CuI (5.4 mg, 2.83·10$^{-2}$ mmol), P(Cy)$_3$ (26 mg, 9.42 ·10$^{-2}$ mmol), trimethylsilylacetylene (833 mg, 8.50 mmol) and Et$_3$N (1 mL, 714 mg, 7.06 mmol). The reaction mixture was heated in a microwave reactor at 120 °C for 25 minutes. The resulting orange suspension turned a black solution. The progress of reaction was monitored by TLC (hexane/CH$_2$Cl$_2$ 4:6, R$_f$: 0.34). The DMF was distilled under vacuum at 60°C, the residue was dissolved in CH$_2$Cl$_2$ (10 mL) and washed with water (3x10 mL). The organic phase was dried (Na$_2$SO$_4$), filtered and the solvent was evaporated under vacuum. The crude product was purified by column chromatography on silica gel (eluent: hexane/CH$_2$Cl$_2$ 4:6) to afford **41** as a yellow-orange solid, 95 mg (64% yield). P.f.: 141-142 °C (dec.) $^1$H NMR (300 MHz, C$_6$D$_6$): δ, ppm = 0.23 (s, 9H, CH$_{3TMS}$), 6.91 (s, 1H, CH$_{tiof}$), 7.21 (s, 1H, CH$_{tiof}$), 7.51(s, 1H, CH$_{ar}$),8.43 (s, 1H, CH$_{ar}$), 9.55 (s, 1H, CH$_{ald}$). $^{13}$C NMR (75 MHz, CDCl$_3$): δ, ppm = 0.05, 97.50, 117.15, 120.04, 133.48, 133.61, 136.75, 139.53, 139.81, 144.25, 184.29. HRMS-EI (m/z): [M]$^+$ Calcd. for C$_{16}$H$_{14}$OSiS$_2$: 314.025537, found: 314.025420. MS-EI (m/z): [M]$^+$: 314, 299( − CH$_3$). IR (nujol, cm$^{-1}$): 1668 (v$_{CO}$), 2149 (v $_{C≡C}$). UV-vis (10$^{-4}$ in CH$_2$Cl$_2$): λ$_{max}$ (M$^{-1}$cm$^{-1}$) = 230 nm (7.8·10$^3$ M$^{-1}$cm$^{-1}$ M$^{-1}$cm$^{-1}$), 239 nm (8.7 ·10$^3$ M$^{-1}$cm$^{-1}$), 280 nm (9.8 ·10$^3$ M$^{-1}$cm$^{-1}$), 293 nm (6.5 ·10$^3$ M$^{-1}$cm$^{-1}$), 330 nm (7.2 ·10$^3$ M$^{-1}$cm$^{-1}$), 392 (2.8·10$^3$ M$^{-1}$cm$^{-1}$).

**4.8.24 Synthesis of 2-ethynylbenzo[1,2-b:4,5-b']dithiophene-6-carboxaldehyde[86] 35**
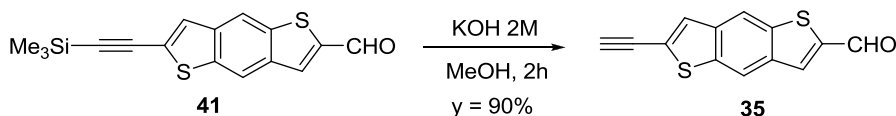


KOH 2M (1.8 mL**,** 3.60 mmol) was added to a suspension of 2-trimethylsilylethynylbenzo[1,2-b:4,5-b']dithiophene **41** (315 mg, 0.42 mmol) in MeOH (6 mL). The mixture was stirred for 2 h at room temperature and the color turn from orange to red. The progress of reaction was monitored by TLC (hexane/AcOEt, 9:1, $R_f$: 0.33). Afterwards the solvent was removed the residue was dissolved in $CH_2Cl_2$ (8 mL) and washed with water (3x8 mL). The organic phase was dried ($Na_2SO_4$), filtered and the solvent was evaporated under vacuum. The crude product **35** was collected as an orange solid that not require further purification, 103 mg (90% yield). P.f.: 125-126 °C. $^1$H NMR (300 MHz, CDCl₃): δ, ppm = 3.38 (s, 1H, $CH_{C≡C}$), 7.84 (s, 1H, $CH_{tiof}$), 8.09 (s, 1H, $CH_{tiof}$), 8.43 (s, 1H, $CH_{ar}$), 8.48 (s, 1H, $CH_{ar}$), 10.14 (s, 1H, $CH_{ald}$). $^{13}$C NMR (75 MHz, CDCl₃): δ, ppm = 80.67, 117.34, 120.17, 133.59, 134.42, 139.89, 144.40, 184.56. HRMS-EI (m/z): $[M]^+$ Calcd. per $C_{13}H_6OS_2$: 241.986008, found: 241.986530. MS-EI (m/z): $[M]^+$: 242, 213 ( − CHO). IR (nujol, cm$^{-1}$): 1659($v_{CO}$), 3259 ($v_{C≡H}$). UV-vis ($10^{-4}$ in $CH_2Cl_2$): $λ_{max}$ = 230 nm ($6.6·10^3$ M$^{-1}$cm$^{-1}$); 237 nm ($6.5·10^3$ M$^{-1}$cm$^{-1}$); 278 nm ($8.0 ·10^3$ M$^{-1}$cm$^{-1}$); 329 nm ($6.2 ·10^3$ M$^{-1}$cm$^{-1}$); 376 nm ($1.9 ·10^3$ M$^{-1}$cm$^{-1}$); 390 nm ($2.1 ·10^3$ M$^{-1}$cm$^{-1}$).

**4.8.25 Synthesis of *N,N*-bis(4-methoxyphenyl)-phenylamine[39] 38**
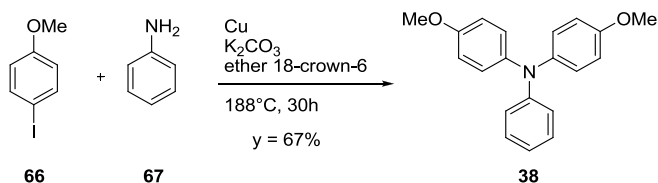


A mixture of aniline **67** (1.0 g, 10.7 mmol), copper powder (4.8 g, 75.1 mmol), $K_2CO_3$ (19.5 g, 139.6 mmol), 18-crown-6 (100 mg), and iodoanisol **66** (17.6 g, 75.1 mmol) was heated to reflux at 188 °C under nitrogen atmosphere with stirring for 30 h. The reaction was monitored by TLC (eluent: hexane/AcOEt 8:2). The mixture was allowed to cool to ambient temperature, dissolved in $CH_2Cl_2$ and filtered on celite. The filtrate was then

washed with water, and the organic phase was dried with $Na_2SO_4$ and concentrated by evaporation. The crude product was purified by column chromatography on silica gel (eluent: hexane/AcOEt 9:1) to afford **38** as a white solid, 2.2 g (67% yield). $^1$H-NMR (300 MHz, CDCl$_3$): $\delta$, ppm = 3.79 (s; 6H); 6.81 (d; *J* = 8.9 Hz; 4H); 6.88 (t; *J* = 6.8 Hz; 1H); 6.93 (d; *J* = 7.9 Hz; 2H); 7.04 (d; *J* = 8.8 Hz; 4H); 7.13-7.19 (m; 2H). MS-EI (m/z): [M$^+$] 305, 290 (-CH$_3$).

### 4.8.26  Synthesis of *N,N*-bis(4-methoxyphenyl)-4'-iodophenylamine[23] **36**
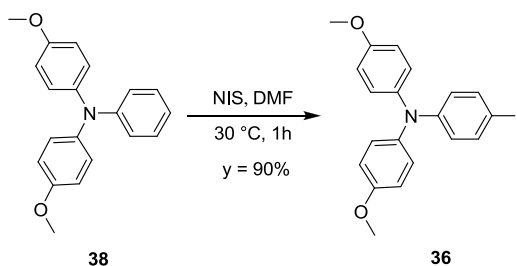


NIS (324 mg, 1.44 mmol) was added to a solution of *N,N*-di(4-methoxyphenyl)phenylamine **38** (400 mg, 1.31 mmol) in DMF (10.4 mL) The reaction mixture was stirred for 1 h at 30 °C. The resulting orange solution became brown. The progress of reaction was monitored by TLC (CH$_2$Cl$_2$, R$_f$: 0.73). The DMF was distilled under vacuum at 60°C, the residue was dissolved in CH$_2$Cl$_2$ (8 mL) and washed with water (3x8 mL). The organic phase was dried (Na$_2$SO$_4$), filtered and the solvent was evaporated under vacuum. The crude product **36** was collected as an orange-pink oil that not require further purification, 510 mg (90% yield). $^1$H NMR (300 MHz, CDCl$_3$): $\delta$, ppm = 3.80 (s, 6H, CH$_{3\,OMe}$), 6.71 (d, *J* = 8.8 Hz, 2H, CH$_{ar}$), 6.85 (d, *J* = 6.7, 4H, CH$_{ar}$), 7.06 (d, *J* = 6.7, 4H, CH$_{ar}$), 7.43 (d, *J* = 8.8, 2H, CH$_{ar}$).

**4.8.27 Synthesis of 6-[2-[4-[Bis-(4-methoxyphenylamino)phenyl]ethynyl] benzo[1,2-b:4,5-b']dithiophen-2-carboxaldehyde[56] 37**
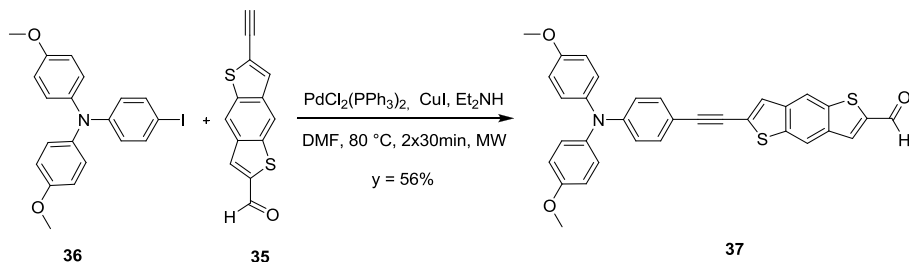


In a microwave reactor tube to a solution of 2-ethynyl-benzo[1,2-b:4,5-b']dithiophene-6-carboxaldehyde **35** (90 mg, 0.37 mmol) in DMF (10.4 mL) was added under nitrogen *N,N*-di(4-methoxyphenyl)-4'-iodophenylamine **36** (320 mg, 0.73 mmol), PdCl$_2$(PPh$_3$)$_2$ (19 mg, 2.71·10$^{-2}$ mmol), CuI (2 mg, 1.11·10$^{-2}$ mmol) and Et$_3$N (0.6 mL, 407 mg, 5.56 mmol). The reaction mixture was heated in a microwave reactor at 80 °C two times for 25 minutes. The resulting orange suspension turned a black solution. The progress of reaction was monitored by TLC (hexane/AcOEt 8:2, R$_f$: 0.17). The DMF was distilled under vacuum at 60°C, the residue was dissolved in CH$_2$Cl$_2$ (10 mL) and washed with water (3x10 mL). The organic phase was dried (Na$_2$SO$_4$), filtered and the solvent was evaporated under vacuum. The crude product was purified by flash chromatography on silica gel (eluent: hexane/AcOEt 8:2) to afford **37** as a yellow-orange solid, 112 mg (56% yield). $^1$H NMR (300 MHz, CDCl$_3$): δ, ppm = 3.81 (s, 6H, CH$_{3\,OMe}$), 6.87 (m, 4H, CH$_{ar}$), 7.10 (d, *J* = 8.64, 2H, CH$_{ar}$), 7.41 (d, *J* = 8.6, 2H, CH$_{ar}$), 7.74 (s, 1H, CH$_{tiofBDT1}$), 8.09 (s, 1H, CH$_{tiofBDT1}$), 8.42 (s, 1H, CH$_{arBDT1}$), 8.50 (s, 1H, CH$_{arBDT1}$), 10.13 (s, 1H, CH$_{ald}$). $^{13}$C NMR (75 MHz, CDCl$_3$): δ, ppm = 55.47, 80.83, 93.39, 113.00, 114.83, 117.41, 118.19, 119.03, 120.14, 127.17, 131.72, 132.56, 133.84, 136.54, 136.91, 139.47, 140.02, 144.14, 149.17, 156.41, 184.56. HRMS-EI (m/z): [M]$^+$ Calcd. for C$_{33}$H$_{23}$NO$_3$S$_2$: 545.111937, found: 545.111760. MS-EI (m/z): [M]$^+$: 545, 530 ( − CH$_3$). IR (nujol, cm$^{-1}$): 1670(v$_{CO}$). UV-vis (10$^{-5}$ in CH$_2$Cl$_2$): λ$_{max}$ = 288 nm (9.7·10$^3$ M$^{-1}$cm$^{-1}$), 330 nm (1.2 ·10$^4$ M$^{-1}$cm$^{-1}$), 332 nm (1.2·10$^4$ M$^{-1}$cm$^{-1}$).

## 4.8.28 Synthesis of 2-cyano-3-{6-[2-[4-(bis(4-metoxyphenylamino)phenyl]ethynyl] benzo[1,2-b:4,5-b']dithiophen-2-yl} acrylic acid[39] 13
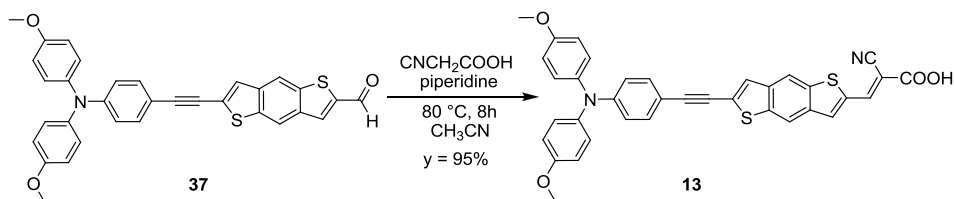


To a suspension of 6-[2-(4-bis(4'-methoxyphenylamino) phenyl]ethynyl)benzo[1,2-b:4,5-b']dithiophen-2-carboxaldehyde **37** (100 mg, 0.18 mmol) in $CH_3CN$ (7 mL) was added under nitrogen flow cyanoacetic acid (31 mg, 0.37 mmol) and piperidine (0,7 μl, 6 mg, 7,32 $10^{-2}$ mmol) The reaction mixture was stirred for 8 h at 80 °C. The progress of reaction was monitored by TLC (esano-AcOEt-AcOH, 6-2-2, $R_f$: 0.44). Afterwards the solvent was removed under vacuum. The residue was precipitated with HCl 0.1M (6 mL) and hexane (4 mL) and filtered affording product **13** a red solid 510 mg (95% yield). ^{1}H NMR (300 MHz, DMSO): δ, ppm = 3.73 (s, 6H, $CH_3$, OMe), 6.70 (d, *J* = 7.66, 2H, $CH_{ar}$), 6.93 (d, *J* = 7,80, 4H, $CH_{ar}$), 7.08 (d, *J* = 7.840, 4H, $CH_{ar}$), 7.47 (d, *J* = 7.66, 2H, $CH_{ar}$), 8.18 (s, 1H, $CH_{tiofBDT1}$), 8.34 (s, 1H, $CH_{tiofBDT1}$), 8.59 (s, 1H, $CH_{c=c}$), 8.69 (s, 2H, $CH_{arBDT1}$). ^{13}C NMR (75 MHz, DMSO): δ, ppm = 55.20, 81.02, 93.16, 111.82, 115.06, 115.97, 116.55, 116.84, 117.45, 120.13, 132.54, 133.28, 135.86, 136.31, 136.45, 136.59, 139.06, 139.15, 146.79, 148.91, 156.37, 162.99. HRMS-ESI (m/z): [M]- Calcd. for $C_{36}H_{23}N_2O_4S_2$ (-1): 611.11047, found: 611.10944. MS-ESI (m/z): [M]-: 567.11876 ( − $CO_2$). IR (nujol, $cm^{-1}$): 3447 ($v_{OH}$), 2213 ($v_{CN}$),1716 ($v_{CO}$). UV-vis ($10^{-5}$ in $CH_2Cl_2$): $\lambda_{max}$ = 299 nm (1.1·$10^4$ $M^{-1}cm^{-1}$), 368 nm (1.8·$10^4$ $M^{-1}cm^{-1}$).

## 4.8.29 Synthesis of 9,9-dimethyl-2-iodofluorene[87] 46
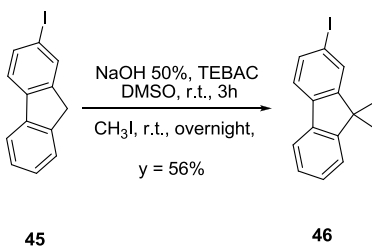
To a solution of 2-iodofluorene **45** (500.0 mg, 1.71 mmol) in DMSO (5 mL), TEBAC (27.3mg, 0.12mmol) was added. Then a NaOH$_{50\%}$ solution (0.54 mL) was added dropwise and the obtained dark red solution was reacted at room temperature for 3h. The methyl-iodide (728.84mg, 5.13mmol) was then slowly dropped into the solution keeping the temperature constant and the reaction mixture was left stirring overnight at room temperature. The progress of the reaction was monitored by TLC (eluent Hexane/AcOEt 98:2, R$_f$:0.70). The solution was poured in water (20mL), HCl was added until neutral pH and then extracted with AcOEt (3x15 mL). The organic phase was dried (Na$_2$SO$_4$), filtered and the solvent removed under vacuum affording, without further purification, 19 mg of the desired product **46** (yellow solid, 95%). $^1$H NMR (300 MHz, CDCl$_3$): δ, ppm = 1.52 (s, 6H), 7.37-7.48 (m, 3H), 7.51 (d,1H, *J*=7.95Hz), 7.72 (dd, 1H, *J*=7.95Hz, *J*=1.42Hz), 7.74 (d, 1H, *J*=8.7Hz), 7.85 (d, 1H, $^4$*J*=1.42Hz). MS-EI (m/z): [M]$^+$: 320, 305 (-CH$_3$), 193 (-I), 178 (-CH$_3$)

### 4.8.30  Synthesis of *N,N*-bis(9,9-dimethylfluoren-2-yl)aniline 47
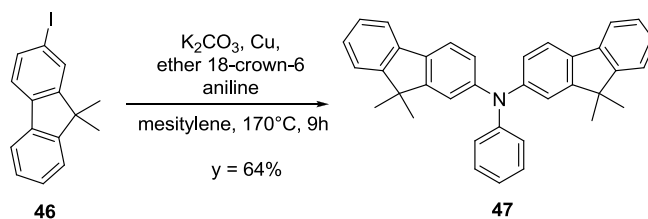


A mixture of 9,9-dimethyl-2-iodofluorene **46** (306.4 mg, 0.96 mmol), aniline (33.7 mg, 0.36 mmol), copper powder (121.6 mg, 1.9 mmol), K$_2$CO$_3$ (215.6 mg, 1.56 mmol) and ether 18-crown-6 (8.7 mg, 0.03mmol) in mesitylene (7 mL) was reacted under stirring at reflux (170°C) for 9h. The solvent is then removed under vacuum at room temperature and the obtain crude product purified by means of silica gel column chromatography (eluent: hexane) to afford 110 mg of **47** as an oil (64% yield). $^1$H NMR (200 MHz, CDCl$_3$): δ, ppm = 1.43 (s, 12H), 7.04-7.67 (m, 19H). MS-EI (m/z): [M]$^+$: 477, 403 (-C$_6$H$_4$$^{+\cdot}$), 328 (-C$_6$H$_4$$^{+\cdot}$ ), 285 (-C$_3$H$_7$).

### 4.8.31 Synthesis of 4-[*N,N*-bis(9,9-dimethylfluoren-2-yl)amino]-benzaldehyde[49] 48
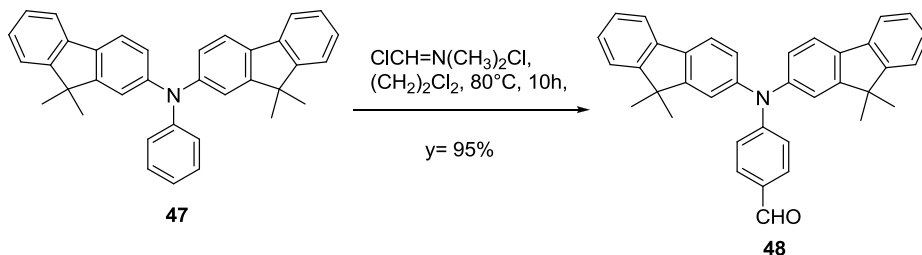


Synthesized following the same procedure of **26**, starting from 110 mg (0.23 mmol) of **47** to afford 116 mg (95%) of **48**. No further purification required. The reaction progress was monitored by TLC (eluent: hexane/AcOEt 1:1, $R_f$: 0.87).

$^1$H NMR (200 MHz, CDCl$_3$): δ, ppm = 1.43 (s, 12H), 7.16-7.75 (m, 18H), 9.84 (s, 1H).

### 4.8.32 Synthesis of 4-[*N,N*-bis(9,9-dimethylfluoren-2-yl)phenyl-amino] methan-1-ol[49] 49
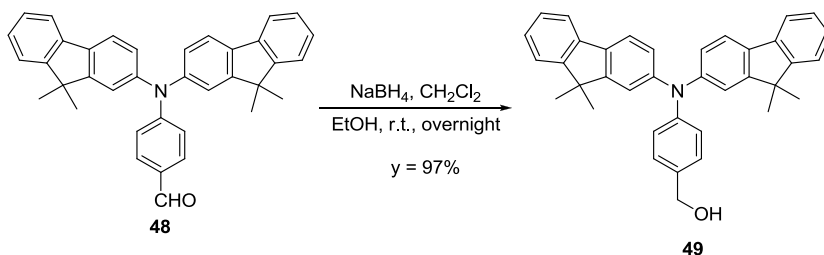


Synthesized following the same procedure of **27**, starting from 116.0 mg (0.23 mmol) of **48** to afford 113mg (97%) of **49** as a yellow oil. No further purification required. The reaction progress was monitored by TLC (eluent: hexane/AcOEt 1:1, $R_f$: 0.64). $^1$H NMR (300 MHz, CDCl$_3$): δ, ppm = 1.44 (s, 12H), 4.69 (s, 2H), 7.01-7.72 (m, 18H). $^{13}$C NMR (50 MHz, CDCl$_3$): δ, ppm = 27.04, 29.69, 46.80, 65.05, 118.46, 119.37, 120.58, 122.46, 123.02, 124.10, 126.45, 126.98, 127.46, 128.29, 130.03, 131.59, 134.07, 135.07, 138.96, 147.39, 147.55, 153.49, 155.04. MS-EI (m/z): [M]$^+$: 507, 491 (-CH$_3$ ), 477(-CH$_3$ ).

**4.8.33 Synthesis of {4-[(*N,N*-bis(9,9-dimethylfluoren-2-yl) amino)phenyl] triphenylphosphonium bromide) 44**
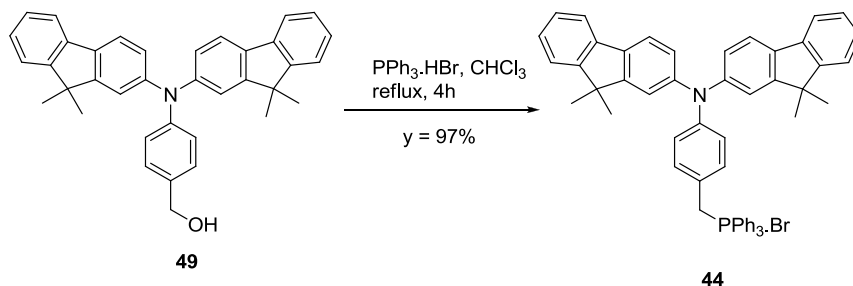


Synthesized following the same procedure of **21**, starting from 110 mg (0.21 mmol) of **49** to afford 180.5 mg (97%) of **44**. No further purification required. The reaction progress was monitored by TLC (eluent: hexane/AcOEt 1:1, $R_f$: 0.0). $^1$H NMR (300 MHz, CDCl$_3$): δ, ppm = 1.35 (s, 12H), 2.02 (s, 2H), 7.11-7.73 (m, 18H). $^{31}$P-NMR (121 MHz, CDCl$_3$): δ, ppm = 23.43. $^{13}$C-NMR (75 MHz, CDCl$_3$): δ, ppm = 27.05, 29.66, 46.80, 117.34, 118.48, 118.84, 119.50, 120.66, 122.49, 123.26, 127.04, 128.68, 129.57, 130.17, 132.27, 134.09, 134.34, 135.11, 138.73, 146.72, 148.27, 153.44, 155.13. IR (film, cm$^{-1}$): 2090 ($v_{PPh3.Br}$). MS-EI (m/z): [M]$^+$: 491 (-PPh$_3$·Br), 477(-CH$_3$ ).

**4.8.34 Synthesis of 6-[2-[4-[Bis-(9,9-dimethylfluorenyl)amino]phenyl]ethenyl] benzo[1,2-b:4,5-b']dithiophen-2-carboxy aldehyde 43**
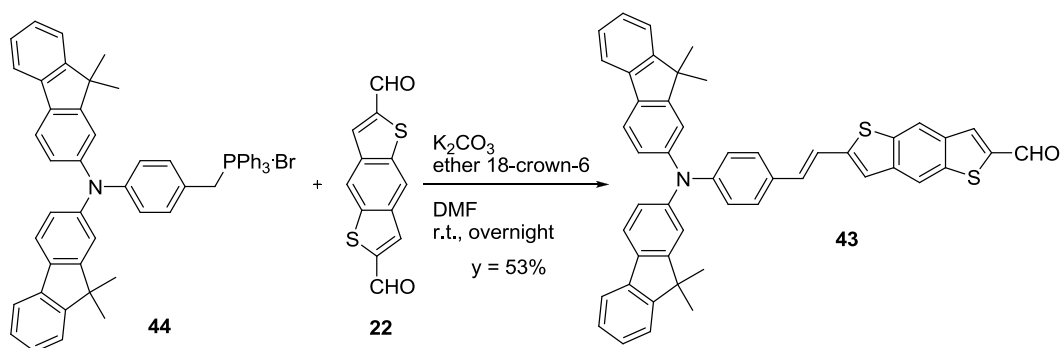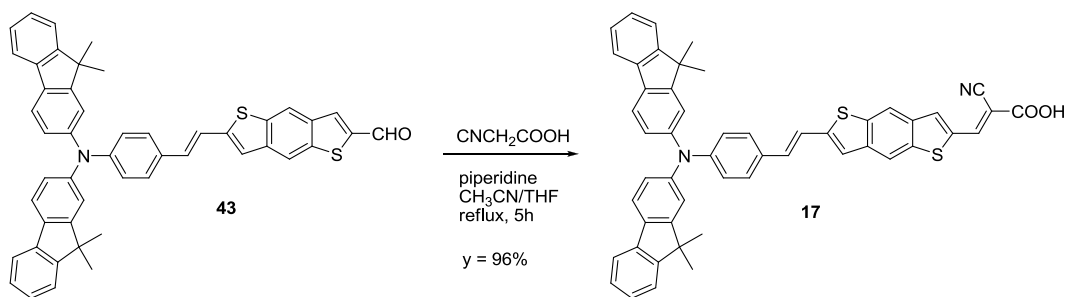


Synthesized following the same procedure of **23**, starting from 64 mg (0.26 mmol) of **44** to afford 82.4 mg (53%) of **43** as an orange solid. No further purification required. The reaction progress was monitored by TLC (eluent: hexane/AcOEt 1:1, $R_f$: 0.60). $^1$H-NMR

(300 MHz, CDCl$_3$): δ, ppm = 1.43 (s, 12H), 6.99-7.44 (m, 17H), 7.61-7.67 (m, 4H), 8.02 (s, 1H), 8.14 (s, 1H), 8.30 (s, 1H), 10.10 (s, 1H). $^{13}$C-NMR (75 MHz, CDCl$_3$): δ, ppm = 27.05, 29.71, 46.88, 116.89, 119.10, 119.52, 120.05, 120.70, 121.43, 122.53, 123.16, 123.62, 126.68, 127.05, 127.80, 130.00, 134.00, 134.74, 136.14, 137.04, 138.87, 141.50, 146.85, 148.43, 153.59, 155.21, 184.42. IR (nujol, cm$^{-1}$): 1674 (ν$_{CO}$). MS-EI (m/z): [M]$^+$: 719, 691(-CHO). UV-vis: CH$_2$Cl$_2$ (4.3 ·10$^{-5}$M), λ$_{max}$ = 361 nm (4.3 ·10$^4$ M$^{-1}$cm$^{-1}$), 454 nm (4.3·10$^4$ M$^{-1}$cm$^{-1}$

## 4.8.35 Synthesis of 2-cyano-3-{6-[2-[4-[bis(dimethylfluorenyl)amino]phenyl]ethenyl] benzo[1,2-b:4,5-b']dithiophen-2-yl} propenoic acid[49] **17**



Synthesized following the same procedure of **11**, except for the use of a mixture of solvent:CH$_3$CN/THF (2:1). Starting from 34.00 mg (0.047 mmol) of **43**, 35 mg of the desired product was obtained **17** (96% yield) as an orange solid. No further purification required. The reaction progress was monitored by TLC (eluent: hexane/AcOEt/AcOH 6:2:2, R$_f$: 0.45). $^1$H-NMR (300 MHz, DMSO-d6): δ, ppm = 1.31 (s, 12H), 7.01-7.7 (m, 21H), 8.29 (s, 1H), 8.41 (s, 1H), 8.50 (s, 1H), 8.60 (s, 1H). $^{13}$C-NMR (75 MHz, DMSO-d6): δ, ppm = 27.18, 29.48, 46.94, 101.79, 109.60, 116.48, 117.28, 119.22, 119.82, 119.95, 120.10, 121.03, 121.65, 122.79, 123.14, 123.82, 127.25, 127.56, 128.40, 128.63, 130.45, 132.28, 134.69, 135.80, 136.04, 137.00, 137.72, 138.66, 139.69, 141.44, 146.78, 147.84, 148.12, 153.66, 155.32, 163.72. IR (nujol, cm$^{-1}$): 3403 (ν$_{OH}$), 1713 (ν$_{CO}$). MS-EI (m/z): [M]$^+$ 742 (-CO$_2$), 705 (-C$_3$H$^+$). UV-vis, EtOH(2.9·10$^{-5}$ M), λ$_{max}$ = 368(1.4 ·10$^4$); 442 nm (1.4·10$^4$ M$^{-1}$cm$^{-1}$) - THF(3.3 ·10$^{-5}$ M): 371 nm (2.4 10$^4$ M$^{-1}$cm$^{-1}$); 473(1.8·10$^4$ M$^{-1}$cm$^{-1}$) - Toluene (3.3·10$^{-5}$ M): 374 nm (2.2·10$^4$ M$^{-1}$cm$^{-1}$); 451 nm (1.6·10$^4$ M$^{-1}$cm$^{-1}$); 457 nm (1.6·10$^4$ M$^{-1}$cm$^{-1}$) - CH$_3$CN

(3.2·10$^{-5}$ M): 368 nm (2.1·10$^4$ M$^{-1}$cm$^{-1}$); 438 nm (1.9·10$^4$ M$^{-1}$cm$^{-1}$) - CH$_2$Cl$_2$ (4.0·10$^{-5}$ M): 373 nm (2.2·10$^4$ M$^{-1}$cm$^{-1}$); 493 nm (1.5·10$^4$ M$^{-1}$cm$^{-1}$).

### 4.8.36   Synthesis of 2-(benzo[1,2-b:4,5-b']dithiophen-2-yl)-1,3-dioxolane[88] 54
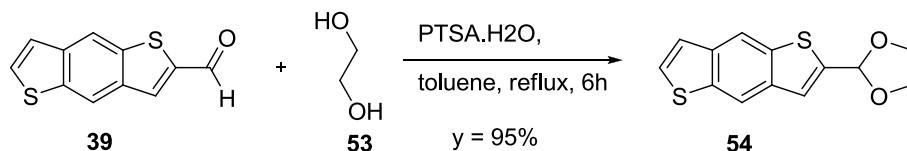


To a solution of 2-formyl-benzo[1,2-b:4,5-b']dithiophene **39** (100.0mg, 0.46mmol) in toluen (5 mL), ethylene gliycol (184.8 mg, 2.98 mmol) and p-toluen-solfonici acido monohydrate (4.35 mg, 0.023 mmol) were added. The reaction mixture was refluxed under water separation for 6 h. The progress of reaction was monitored by TLC (eluent: hexane/AcOEt 9:1, R$_f$: 0.27). The solution was then washed with NaHCO$_3$ (2x5 mL) and H$_2$O (2x5 mL) and extracted with CH$_2$Cl$_2$ (3x 4 mL). The organic phase was dried (Na$_2$SO$_4$), filtered and the solvent was evaporated under vacuum affording, without further purification, **54**, 126.5 mg (95% yield). $^1$H-NMR (300 MHz, CDCl$_3$): δ, ppm = 4.07 (m, 1H), 4.18 (m, 1H), 6.22 (s, 1H), 7.35 (d, 1H, *J*=5.5Hz), 7.42 (s, 1H), 7.47 (d, 1H, *J*=5.5Hz), 8.25 (s, 1H), 8.26 (s, 1H).

### 4.8.37   Synthesis of 2-formyl-(benzo[1,2-b:4,5-b']dithiophen-6-ethoxycarbonyl[89] 52
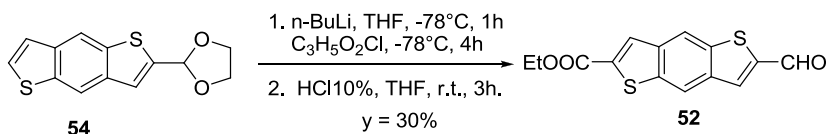


To a suspension of 2-(benzo[1,2-b:4,5-b']dithiophen-2-yl)-1,3-dioxolane **54** (110.18 mg, 0.42mmol) in THF (3 mL) at -78°C, *n*-BuLi (0.42 mL, 0.63 mmol) was added and the reaction mixture was stirred for 1h. Then ethyl chloroformate (91.15mg, 0.074 mL, 0.0.84mmol) was added and the solution reacted for 4h. The progress of reaction was monitored by TLC (esano/AcOEt 8:2, R$_f$: 0.67). The mixture was then poured in a solution of NH$_4$Cl (5mL) and extracted with CH$_2$Cl$_2$ (3x5 mL) The organic phase was dried (Na$_2$SO$_4$), filtered and the solvent was evaporated under vacuum. Without further

purification of the intermediate product the deprotection of the aldehyde was carried out.

To a solution of the crude product (45 mg) in THF (1 mL) a solution of $HCl_{10\%}$ (1 mL) was added and the mixture was left under stirring for 3 h. The solvent was then evaporated. The residue was dissolved in $CH_2Cl_2$ and washed with a saturated solution with NaCl. The organic phase was dried ($Na_2SO_4$), filtered and the solvent removed under vacuum. After evaporation of the solvent the crude dark orange product was purified by silica gel column chromatography (eluent: $CH_2Cl_2$/hexane 7:3) to afford **52** as a yellow solid, 35.1 mg (30% yield). $^1$H-NMR (200 MHz, CDCl$_3$): δ, ppm =1.42 (t, 3H, *J*=7.1Hz), 4.43 (q, 2H, *J*=7.1Hz), 8.05 (s, 1H), 8.07 (s, 1H), 8.37 (s, 1H), 8.41 (s, 1H). $^{13}$C-NMR (50 MHz, CDCl$_3$): δ, ppm = 14.28, 61.93, 119.59, 119.83, 120.20, 129.20, 133.49, 136.90, 137.89, 139.19, 144.92, 162.80, 184.52. IR (nujol, cm$^{-1}$): 1721 ($v_{CO}$), 1659 ($v_{CO}$). MS-EI (m/z): [M]$^+$: 274, 254, 241. HRMS-EI (m/z): [M]$^+$ calcd. for $C_{14}H_{10}O_3S_2$: 290.003766, found: 290.002620. UV-vis: $CH_2Cl_2$ (8.1·10$^{-5}$M), $\lambda_{max}$ = 276 nm (2.3·10$^4$ M$^{-1}$cm$^{-1}$), 324 nm (2.0·10$^4$ M$^{-1}$cm$^{-1}$), 338 nm (2.7·10$^4$ M$^{-1}$cm$^{-1}$), 387 nm (5.5·10$^4$ M$^{-1}$cm$^{-1}$), 404 nm (6.1·10$^3$ M$^{-1}$cm$^{-1}$).

### 4.8.38 Synthesis of 6-[2-[4-[Bis-(4-methoxyphenyl)amino]phenyl]ethenyl]benzo[1,2-b:4,5-b']dithiophen-2-ethoxycarbonyl[49] 51
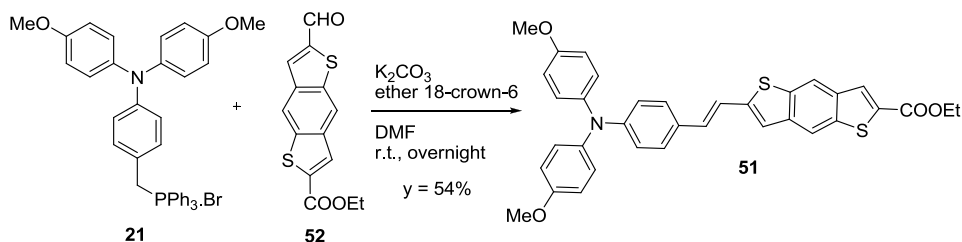


Following the same procedure used for the synthesis of **23**, the phosphonium salt **21** (54.6 mg, 0.083 mmol) was reacted with 2-formyl-(benzo[1,2-b:4,5-b']dithiophen-6-carboxyethyl **52**[49] (20.1 mg, 0.07 mmol) in DMF (2 mL). The crude product was purified by silica gel column chromatography (eluent: $CH_2Cl_2$/hexane 1:1) to afford 22.5 mg (54%) of **51** a as a yellow solid. $^1$H-NMR (300 MHz, C$_6$D$_6$): δ, ppm = 1.03 (t, 3H, *J*=6.9Hz), 3.31 (s, 6H), 4.13 (q, 2H, *J*=6.9Hz), 6.70 (d, 1H, *J*=17.3Hz), 6.75 (d, 4H, *J*=8.9Hz), 7.08 (d, 2H, *J*=9.0Hz), 7.09 (d, 4H, *J*=8.9Hz), 7.10 (d, 1H,

*J*=17.3Hz), 7.24 (d, 2H, *J*=9.0Hz), 7.25 (s, 1H), 7.55 (s, 1H), 7.61 (s, 1H), 7.97 (s, 1H). ^{13}C-NMR (75 MHz, $C_6D_6$): δ, ppm = 14.65, 30.5, 55.40, 61.81, 115.62, 117.10, 119.31, 120.31, 120.83, 122.15, 127.60, 127.69, 128.56, 129.29, 130.51, 132.76, 141.29, 146.44, 149.94, 157.26. IR (nujol, cm$^{-1}$): 1714 ($v_{CO}$). MS-EI (m/z): [M]$^+$: 591, 576(-CH$_3$ ) UV-vis: $CH_2Cl_2$ (7.2·10$^{-5}$M), $\lambda_{max}$ = 301 nm (1.1·10$^4$ M$^{-1}$cm$^{-1}$), 336 nm (9.99·10$^3$ M$^{-1}$cm$^{-1}$), 431 nm (2.5·10$^4$ M$^{-1}$cm$^{-1}$).

## 4.8.39 Synthesis of 6-[2-[4-[Bis-(4-methoxyphenyl)amino]phenyl]ethenyl] benzo[1,2-b:4,5-b']dithiophen-2-carboxylic acid[49] 20
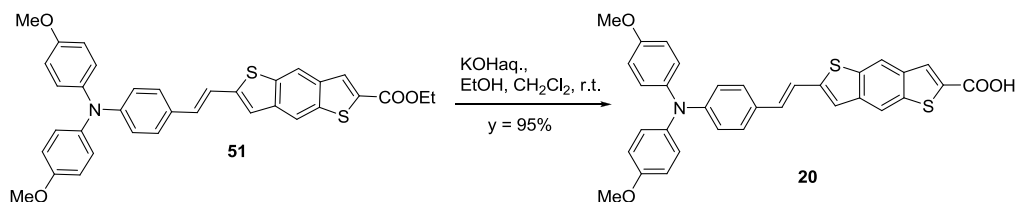


To a solution of **51** (20.1mg, 0.034mmol) in $CH_2Cl_2$ (3mL) aand EtOH (4mL), an aqueous solution of KOH (2M, 0.15mL) was added. The mixture was left stirring at room temperature overnight. The progress of the reaction was monitored by TLC (toluene-dioxane-AcOH, 45:10:5, R$_f$: 0.34). The solvent was then removed under vacuum. The residue was dissolved in $CH_2Cl_2$ and acidic water and extracted with con $CH_2Cl_2$ (5x10 mL). The organic phase was dried (Na$_2$SO$_4$), filtered and the solvent removed under vacuum affording, without further purification, 19 mg of the desired product **20** (yellow solid, 95%). ^{1}H-NMR (300 MHz, DMSO): δ, ppm = 3.75 (s, 6H), 6.71 (d, 2H, *J*=7.9Hz), 6.90 (d, 4H, *J*=8.8Hz), 6.92 (d, 1H, *J*=18.5Hz), 7.03 (d, 4H, *J*=8.8Hz), 7.90 (d, 1H, *J*=18.5Hz), 7.42 (d, 2H, *J*=7.9Hz), 8.07 (s, 1H), 8.34 (s, 1H), 8.46 (s, 1H), 13.06 (broad, 1H). ^{13}C-NMR (300 MHz, DMSO): δ, ppm = 55.74, 115.51, 117.23, 118.98, 119.43, 119.74, 122.13, 127.58, 128.01, 128.35, 130.11, 132.16, 135.12, 136.26, 136.82, 139.02, 140.02, 140.49, 145.83, 149.16, 156.59, 163.93. IR (nujol, cm$^{-1}$): 3407 ($v_{OH}$), 1679.69 ($v_{CO}$). MS-EI (m/z): [M]$^+$: 563, 519(-CO$_2$), 504 (-CH$_3$). HRMS-EI (m/z): [M]$^+$ calcd. for $C_{33}H_{25}NO_4S_2$: calcd. :563.122502 found: 563.123050. UV-vis,: EtOH(3.8·10$^{-5}$M), $\lambda_{max}$ = 416 nm (3.8 ·10$^4$ M$^{-1}$cm$^{-1}$) - THF(4.1·10$^{-5}$M), $\lambda_{max}$ = 426 (3.9·10$^4$ M$^{-1}$cm$^{-1}$) - Toluene (4.3·10$^{-5}$M), $\lambda_{max}$ = 432 nm (3.3·10$^4$

$M^{-1}cm^{-1}$)- $CH_3CN$ (2.8·$10^{-5}$M) $\lambda_{max}$ = 418 nm (4.8·$10^4$ $M^{-1}cm^{-1}$) - $CH_2Cl_2$ (2.9·$10^{-5}$M), $\lambda_{max}$ = 433 nm (3.2·$10^4$ $M^{-1}cm^{-1}$).

### 4.8.40 Synthesis of 2 iodo-benzo[1,2-b:4,3-b']dithiophene[90] 61
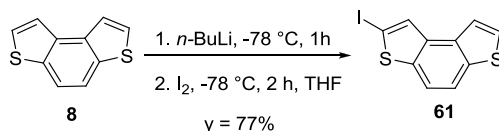


Synthesized following the procedure reported in Ph.D. Thesis A. Bossi, 2004.

### 4.8.41 Synthesis of Benzo[1,2-b:4,3-b']dithiophen-2-yl-acetylene 62[91]
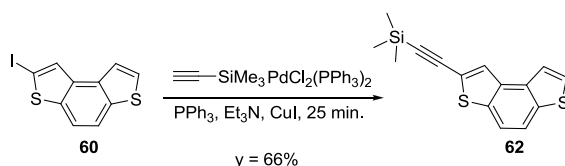


Synthesized following the procedure reported in Ph.D. Thesis A. Bossi, 2004.

### 4.8.42 Synthesis of benzo[1,2-b:4,3-b']dithiophen-2-yl-(trimethylsilyl)-acetylene[92] 63
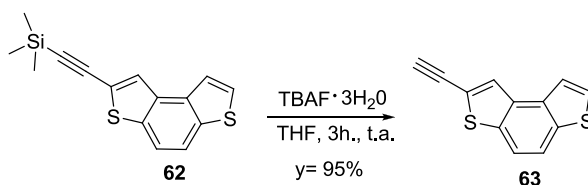


Synthesized following the procedure reported in Ph.D. Thesis A. Bossi, 2004.

### 4.8.43 Synthesis of 2-[4-[bis(4-methoxyphenyl)amino]phenyl]ethynyl]benzo[1,2-b:4,3-b']dithiophene 64
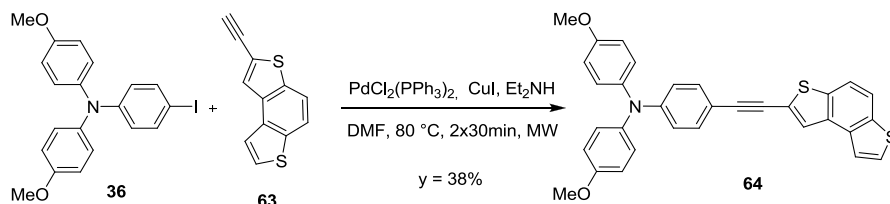


In a microwave reactor tube to a solution of 2-ethynyl-benzo[1,2-b:4,3-b']dithiophene **63** (60 mg, 0.28 mmol) in DMF (5 mL) was added under nitrogen *N,N*-di(4-methoxyphenyl)-4'-iodophenylamine **36** (181.3 mg, 0.42 mmol), PdCl$_2$(PPh$_3$)$_2$ (10 mg, 1.40·$10^{-2}$ mmol), CuI (2 mg, 1.11·$10^{-2}$ mmol) and Et$_3$N (0.44 mL, 307 mg, 4.2 mmol). The

164

reaction mixture was heated in a microwave reactor at 80 °C two times for 25 minutes. The resulting orange suspension turned a black solution. The progress of reaction was monitored by TLC (hexane/ AcOEt 9:1, $R_f$: 0.28). The DMF was distilled under vacuum at 60°C, the residue was dissolved in $CH_2Cl_2$ (5 mL) and washed with water (3x6 mL). The organic phase was dried ($Na_2SO_4$), filtered and the solvent was evaporated under vacuum. The crude product was purified by flash chromatography on silica gel (eluent: hexane/AcOEt 9:1) to afford **64** as a pale yellow solid, 55 mg (38% yield). ^{1}H NMR (300 MHz, $CDCl_3$): δ, ppm = 3.81 (s, 6H, $CH_{3\ OMe}$), 6.86 (d, *J* = 8.52, 4H, $CH_{ar}$), 7.09 (d, *J* = 8.52, 2H, $CH_{ar}$), 7.34 (d, *J* = 8.40, 2H, $CH_{ar}$), 7.56 (d, *J* = 5.31, 1H, $CH_{thBDT1}$), 7.66 (d, *J* = 5.31, 1H, $CH_{tiofBDT1}$), 7.71 (s, 1H, $CH_{thBDT1}$), 7.84 (s, 1H, $CH_{arBDT1}$). ^{13}C NMR (75 MHz, $CDCl_3$): δ, ppm = 55.50, 81.80, 96.11, 113.03, 114.92, 118.15, 118.94, 119.61, 121.91, 124.33, 125.81, 126.67, 127.08, 127.27, 132.45, 134.35, 136.02, 140.06, 149.29, 156.56.

## REFERENCES

[1] W. Zeng, Y. Cao, Y. Bai, Y. Wang, Y. Shi, M. Zhang, F. Wang, C. Pan, P. Wang, *Chem. Mater.*, **2010**, *22*, 1915.

[2] H. Choi, I. Raabe, D. Kim, F. Teocoli, C. Kim, K. Song, J. H. Yum, J. Ko, M. K. Nazeeruddin , M. Grätzel, *Chem.–Eur. J.*, **2010**, *16*, 1193.

[3] G. Zhang, Y. Bai, R. Li, D. Shi, S. Wenger, S. M. Zakeeruddin, M. Grätzel and P. Wang, *Energy Environ. Sci.,* **2009**, *2*, 92.

[4] L.-Y. Lin, C.-H. Tsai, K.-T. Wong, T.-W. Huang, C.-C. Wu, S.-H. Chou, F. Lin, S.-H. Chenc, A.-I Tsai, *J. Mater. Chem.*, **2011**, *21*, 5950.

[5] Refs. 3, 10-12,14,17,20-23,26-29, 33-43 **Chapter 3** of this thesis.

[6] Lin, J. T.; Chen, P.-C.; Yen, Y.-S.; Hsu, Y.-C.; Chou, H.-H.; Yeh, M.-C. P. *Org. Lett.* **2009**, *11*, 97.

[7] R. Li, X. Lv, D. Shi, D. Zhou, Y. Cheng, G. Zhang, P. Wang, *J. Phys. Chem. C*, **2009**, 113, 7469.

[8] Y.-S. Yen, Y.-C. Hsu, J. T. Lin, C.-W. Chang, C.-P. Hsu, D.-J. Yin, *J. Phys. Chem. C*, **2008**, *112*, 12557.

[9] D.-Y. Chen, Y.-Y. Hsu, H.-C. Hsu, B.-S. Chen, Y.-T. Lee, H. Fu, M.-W. Chung, S.-H. Liu, H.-C. Chen, Y. Chi, P.-T. Chou, *Chem. Commun.* **2010**, *46,* 5256.

[10] G. Zhang, H. Bala, Y. Cheng, D. Shi, X. Lv, Q. Yu, P. Wang, *Chem. Commun.,* **2009**, 2198.

[11] M. P. Boone, Y. Dienes, T. Baumgartner, *Arkivoc*, **2009**,90.

[12] I. Akimoto, S. Tsuzuki, H. Uzawa, M. Hinatsu, Y. Nishide, H. Osuga, H. Sakamoto, *Phys. Status Solidi C.*, **2011**, *8,* 124.

[13] K. Marcel, K. Silke, M. Klaus, G. Peng, B. Dirk, F. Xinliang, : WO2009EP57985 20090625.

[14] L. Huo, S. Zhang, X. Guo, F. Xu, Y. Li, J. Hou, *Angew. Chem. Int. Ed.*, **2011**, *50*, 9697.

[15] Y. Liang, L. YU, *Accounts of Chemical Research*, **2010**, *43*, 9, 1227.

[16] B. Wex, B. R. Kaafarani, R. Schroeder, L. A. Majewski, P. Burckel, M. Grell, D. C. Neckers, *J. Mater. Chem.,***2006**, *16*, 1121.

[17] Y. Nishide, H. Osuga, M. Saito, T. Aiba, Y. Inagaki,Y. Doge, K. Tanaka., *.J. Org. Chem.*, **2007***, 72*(24), 9144.

[18] B. Wex, B. R. Kaafarani, E. O. Danilov, D. C. Neckers, *J. Phys. Chem. A*, **2006**, *110*, 13754.

[19] K. Takimiya, Y. Konda, H. Ebata, N. Niihara, T. Otsubo, *J. Org. Chem.*, **2005**, *70*, 10569.

[20] Y. Zhang, S. K. Hau, H.-L. Yip, Y. Sun, O. Acton, A. K.-Y Jen, *Chem Mater* **2010**, *22*(9), 2696.

[21] Y. He, Y. Zhou, G. Zhao, J. Min, X.Guo, B. Zhang, M. Zhang, J. Zhang, Y. Li, F. Zhang, O. Inganaes, *J. Pol. Sci. Part A: Polymer Chem*., **2010**, *48*(8), 1822.

[22] T. T. M. Dang, S-J. Park, J-W. Park, D-S. Chung, C. E. Park, Y-H Kim and S-K. Kwon *J. Pol. Sci. Part A: Polymer Chem*., **2007**, *45*, 5277.

[23] K. Takimiya, Y. Konada, H. Ebata, N. Niihara, T. Otsubo, *J. Org. Chem.*, **2005**, *70*, 10569.

[24] M. H. Garcia, P. Florindo, M. F. M. Piedade, M. T. Duarte, M. P. Robalo, J. Heck, C. Wittenburg, J. Holtmann, E. Licandro, *Journal of Organometallic Chemistry*, **2008**, *693*(18), 2987.

[25] Tierney, Steven; Blouin, Nicolas; Mitchell, William; Wang, Changsheng; Carrasco-Orozco, Miguel; Meyer, Frank Egon From *PCT Int. Appl.*, **2011**,WO2011131280, A120111027.

[26] Tatsuo, T.; Katsura, H.; Chiyoko, T.; Hiroshi, K.; *Jpn. Kokai Tokkyo Koho* , **2005**, JP 2005206750 A 20050804.

[27] F. B. Mallory, C. W. Mallory, *Organic Reactions* , **1984**, 30.

[28] X. Hao, M. Liang, X. Cheng, X. Pian, Z. Sun, S. Xue, *Org. Lett*., **2011**, 13(20), 5425.

[29] J.Hou, M.-H. Park, S. Zhang, Y. Yao, L.-M. Chen, J.-H. Li, Y. Yang, *Macromol.*, **2008**, *41*, 6012.

[30] S.C. Price, A.C. Stuart, W. You, *Macromolecules,* **2010**, *43*, 4609.

[31] P. Beimling, G. Ko mehl, *Chem Ber.*, **1986**, *119*, 3198.

[32] V. G. Nenajdenko, I. L. Baraznenok, E.S. Balenkova, *J. Org. Chem* , **1998**, *63*, 6132.

[33] P.E. Gordon, *Arkivoc,* **2005,** *VI*, 393.

[34] N. Aggarwal, D. W. H. MacDowell, *Org. Prepar. Proc. Int.*, **1979**, *11(5)*, 247.

[35] R. M. Kellogg, M. B. Groen, H.J. *Wynberg, Org. Chem*. **1967**, *32*, 3093.

[36] J. Nakayama, T. Fujimori, *Heterocycles,* **1991**, *32*, 991.

[37] D. H. Lee, M. J. Lee, H. M. Song, B. J. Song, K. D. Seo a, M. Pastore,C. Anselmi, S. Fantacci ,F. De Angelis, M. K. Nazeeruddin,M. Grätzel, H. K. Kim, *Dyes and Pigments*, **2011,** *91,* 192e198.

[38] D. P. Hagberg, J. H. Yum, H. Lee, F. De Angelis, T. Marinado, K. M. Karlsson, R. Humphry-Baker, L. C. Sun, A. Hagfeldt, M. Grätzel, M. K. Nazeeruddin, *J. Am. Chem. Soc.,* **2008**, *130*, 6259.

[39] A. Mishra, M. K. R. Fischer, P. Bäuerle, *Angew. Chem. Int. Ed,.* **2009**, *48*, 2474.

[40] S. Kim, H. Choi, D. Kim, K. Song, S. O. Kang, J. Ko, *Tetrahedron,* **2007**, *63*, 9206.

[41] S. Kim, H. Choi, C. Baik, K. Song, S. O. Kang, J. Ko,*Tetrahedron,* **2007**, *63*, 11436.

[42] M. Velusamy, K. R. J. Thomas, J. T. Lin, Y. C. Hsu, K. C. Ho, *Org. Lett.,* **2005**, *7*, 1899.

[43] Gaussian 09, Revision **A.1**; M. J. Frisch, Gaussian, Inc.: Wallingford CT, 2009.

[44] D. P. Hagberg, J.-H. Yum, H. Lee, F. De Angelis,T. Marinado, K. M. Karlsson, R. Humphry-Baker, L. Sun, A. Hagfeldt, M. Grätzel, M. K. Nazeeruddin, *J. Am. Chem. Soc.,* **2008**, *130*, 6259.

[45] S. Kim, J. K. Lee, S. O. Kang, J. Ko, J.-H. Yum, S. Fantacci, F. De Angelis, D. Di Censo, M. K. Nazeeruddin, M. Grätzel*, J. Am. Chem. Soc,.* **2006**, *128*, 16701.

[46] V. A. Rassolov, J. A. Pople, M. A. Ratner, T. L. Windus, *J. Chem. Phys,.* **1998**, *109*, 1223.

[47] B. J. Lynch, P. L. Fast, M.Harris, D. G. Truhlar, *J. Phys. Chem. A,* **2000**, *104*, 4811.

[48] T.Haining, Y. Xichuan, C. Ruikui, Z. Rong, H. Anders, S. Licheng, *J. Phys. Chem.C*, **2008**, 11023.

[49] G. Kossmehl, P. Beimling, G. Manecke, *Makromolek Chem.* **1983**, *184*(3), 627.

[50] D. Shi, Y. Cao, N. Pootrakulchote, Z Yi, M Xu, S M. Zakeeruddin, M. Grätzel, P. Wang, *J. Phys Chem* C **2008**, *112*, 17478.

[51] P. Beimling, G. Koβmehl, *Chem. Ber,***1986***.* 119, 3198.

[52] S. Maiorana, A. Papagni, E. Licandro, R. Annunziata, P. Paravidino, D. Perdicchia, C. Giannini, M. Bencini, K. Clays, A. Persoons, *Tetrahedron*, **2003**, *59*, 6481.

[53] S. Odom, K. Lancaster, L. Baverina: *Chem. Eur. J,.* **2007***, 13,* 9637.

[54] T. T. M. Dang, S.-J. Park, D.-S. Chung, C. E. Park, Y.-H. Kim, S.-K. Kwon, *J. of Polymer Science: Part A: Polymer Chemistry*, **2007**, *45*, 5277.

[55] C. Lambert, G. Nöll, E.Schmälzlin, K. Meerholz, C.Bräuchle, *Chem. Eur. J.*, **1998**, *4*, 2129.

[56] J.-H. Lin, A. Elangovan, T.-I. Ho, *J. Org. Chem.,* **2005**, *70*, 7397.

[57] A.-S. Castanet, F.Colobert, P.-E. Broutin, *Tetrahedron Letters*, **2002**, 43, 5047.

[58] G.Zhang, H.Bala, Y. Cheng, D. Shi, X. Lv, Q. Yu, P. Wang, *Chem. Comm.*, **2009**, 2198.

[59] C.-H. Chen, Y.-C. Hsu, H.-H. Chou, K. R. Justin Thomas, J. T. Lin, C.-P. Hsu, *Chem. Eur. J,.* **2010**, *16*, 3184.

[60] W.-Y. Wong, X.-Z. Wang, Z. He, A. B. Djurisic, C.-T. Yip, K.-Y. Cheung, H. Wang, C. S. K. Mak, W.-K. Chan, Nature Materials, **2007,** *6,* 521.

[61] R. S. Ashraf, M. Shahid, E. Klemm, M.Al-Ibrahim, S. Sensfuss, Macromol. Rapid Commun. 27 (2006), 1454.

[62] S. Trasatti, Pure Appl. Chem. **1986**, *58*, 955.

[63] C. Ma, E. Mena-Osteriz, T. Debaerdemaeker, M.M. Wienk, R.A.J. Janssen, P. Bauerle, *Angew.Chem. Int. Ed.* **2007**, *46*, 1679.

[64] K. Meerholz, J. Heinze, *Electrochimica Acta* **1996**, *41*, 1839.

[65] S. Amthor, B. Noller, C. Lambert, *Chem. Phys*. **2005**, 316, 141

[66] A. Hagfeldt, M. Grätzel, *Chemical Reviews*, **1995**, *95(1)*, 51.

[67] A. Hagfeldt, G. Boschloo, L. Sun, L. Kloo, H. Pettersson, *Chemical Reviews*, **2010**, *110*(11), 6595.

[68] J.-L. Song, P. Amaladass, S.-H. Wen, K. K. Pasunooti, A. Li, Y.-L. Yu, X. Wang, W.-Q. Deng, X.-W. Liu, *New J. Chem.,* **2011**, *35*, 127.

[69] M. Velusamy, K. R. J. Thomas, J. T. Lin, Y. C. Hsu, K. C. Ho, *Org. Lett.* **2005**, *7*, 1899.

[70] A. Listorti, C. Creager, P. Sommeling, J. Kroon, E. Palomares, A. Fornelli, B. Breen, P. R. F. Barnes, J. R. Durrant, C. Law, B. O'Regan, *Energy Environ. Sci.*, **2011**, 4, 3494.

[71] Yu Q et al, ACS Nano, 4, 10, 2010.

[72] A. Abrusci, R. S. S. Kumar, M. Al-Hashimi, M. Heeney, A. Petrozza, H. J. Snaith, *Adv Func. Mat*, **2011**, 21, 2571-2579

[73] S. Kim et al.; *Tetrahedron,* **2007***, 63*, 11436.

[74] J. Larsen, K. Bechgaard, *Acta Chem. Scand.*, **1996**, 50, 71.

[75] W.-Y. Wong, X.-Z. Wang, Z. He, A. B. Djurisic, C.-T. Yip, K.-Y. Cheung, H. Wang, C. S. K. Mak, W.-K. Chan, Nature Materials, **2007,** *6,* 521.

[76] R. S. Ashraf, M. Shahid, E. Klemm, M.Al-Ibrahim, S. Sensfuss, *Macromol. Rapid Commun*., **2006**, *27*, 1454.

[77] S. Trasatti, Pure Appl. Chem. **1986**, *58*, 955.

[78] Sahu, B. et al. *Eur. J. Org. Chem.*, **2007**, 2477.

[79] L. S. Fuller, et al. *J. Chem. Soc. Perkin Trans.*, **1997**, *1*, 3465.

[80] MacDowell, D. W. H.; Wisowaty, J. C. *J. Org. Chem.*, **1971**, *36 (26)*, 3999.

[81] Nanajdenko, V. G. et al.; *J. Org. Chem.*, **1998**, *63 (18)*, 6132

[82] Aggarwal, N.; MacDowell, D. W. H. *Org. Prepar. Proc. Int.*, **1979**, *11 (5)*, 247

[83] L. R. Dalton, A. K.-Y. Jen, T. Londergan, W. B. Carlson, G. Phelan, D. Huang, D. Casmier, T. Ewy, N. Buker, WO/2002/008215, PCT/US2001/023339, 2002.

[84] H.W. Gschwend, , H. R. Rodriguez, Organic Reactions **1979** (Hoboken, NJ, United States), *26*.

[85] Erdélyi, M.; Gogoll; A. *J. Org. Chem.*, **2001**, *66*, 4165-4169

[86] T.-G. Zhang, Y Zhao, K. Song, I. Asselberghs, A. Persoons, K. Clays, M. J. Therien, *Inorganic Chemistry*, **2006**, *45*(24), 9703.

[87] S. H. Lee, T. Nakamura, T. Tsutsui , *Org. Lett.,* **2001***, 3*(13), 2005.

[88] A. Bossi, Ph.D. Thesis, "New functionalised heterohelicenes: synthesis and applications", **2004**, pg. 281.

[89] C. Rigamonti, M.T. Ticozzelli, A. Bossi, E. Licandro, C. Giannini, S. Maiorana, *Heterocycles*, **2008**, *76*(2), 1439.

[90] A. Bossi, Ph.D. Thesis, "New functionalised heterohelicenes: synthesis and applications", **2004**, pg. 299.

[91] A. Bossi, Ph.D. Thesis, **2004**, "New functionalised heterohelicenes: synthesis and applications", pg. 301.

[92] A. Bossi, Ph.D. Thesis, **2004**, "New functionalised heterohelicenes: synthesis and applications",pg. 303.

# CHAPTER 5

# PHOTOPHYSICAL CHARACTERIZATION OF TRIPLE BOND CONTAINING DYE 13

## 5.1   INTRODUCTION

Work done in collaboration with Prof. Luisa De Cola at Müenster University.

The experimental data collected and discussed in the previous chapter highlight some discrepancies between theoretical calculation and experimental optical properties.

In particular, dye **13**, Figure 5.1 (a), which carries a *N,N*-bis(p-methoxyphenyl)aniline as the donor group, a cyanoacrylic acid as the acceptor/anchoring group and the ethynyl-**BDT₁** spacer, leads to a poor absorption in the visible region. The most striking difference between **13** and **11** (Figure 5.1 (b)) is the absence, in the UV spectrum of **13**, of the broad and featureless CT absorption band around 470 nm for the vinyl-**BDT₁** system.



**(a)**                    **(b)**
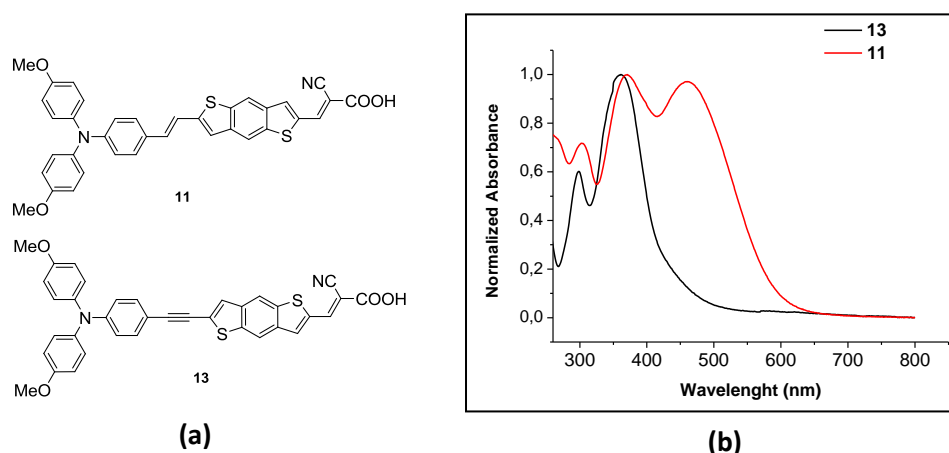
**Figure 5.1**

The DSSC sensitized with **13**, displays an overall efficiency of 2.64%, significantly lower than that of the cell sensitized with **11**. Cell parameters (Table 5.1) show that the value mainly responsible for the poor cell performance is the photocurrent density ($J_{sc}$), which correlates to the light harvesting ability of the dye. (Figure 5.2 a and b)
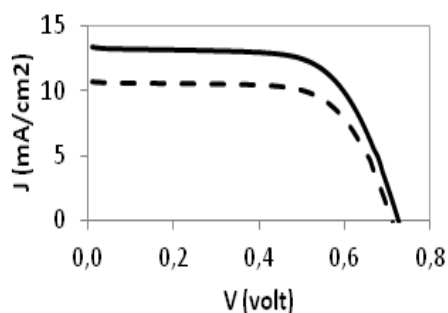
Figure 5.2a: DYE 11*
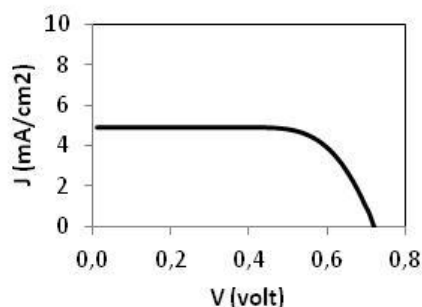


Figure 5.2b: DYE13*

**\*Solid line: without mask; dot line: with mask.**

| Dye | Mask | $J_{sc}$ (mA/cm$^2$) | $V_{oc}$ (V) | FF | η (%) |
|---|---|---|---|---|---|
| 11 | With | 10.65 | 0.710 | 0.675 | 5.11 |
| 11 | Without | 13.3 | 0.725 | 0.658 | 6.38 |
| 13 | Without | 4,88 | 0,721 | 0,705 | 2,64 |

**Table 5.1**

As shown in Figure 5.1 (b) **13** has an absorption spectra characterized by a blue-shifted band centered at 350-370 nm characterized by molar absorptivity of the order of $1.7 \cdot 10^4 M^{-1} cm^{-1}$, whereas, in the visible region below 400 nm, absorbance are characterized by molar absorptivities in the range of $5 \cdot 10^3 M^{-1} cm^{-1}$. Accordingly to the quantum mechanical interpretation of a given optical transition, the molar absorptivity, the integrated area underneath a transition, correlates to the transition oscillator strength (f) through:

$$f = 1.44 \times 10^{-19} \int \varepsilon\,(\nu)d\nu \qquad \text{eq. 5.2}$$

Where $\nu$ is the frequency, and $\varepsilon(\nu)$ is the molar absorbtivity at each frequency in units of L mol$^{-1}$cm$^{-1}$. The integral cover the entire absorption band corresponding to the

transition. Thus, the oscillator strength can be determined from the area under the quantitative absorption spectrum of a given transition.

In this perspective, the CT band in chromophore **13** has a very low probability.

This experimental result contrasts with both the theoretical calculations which foresee a transition of the CT type in the 460 nm region with large oscillator strength (Figure 5.3), and with similar compounds reported in the literature.[1] Push pull metal free dyes bearing one or two thiophene units instead of **BDT$_1$** show a quite broad absorption spectra with maxima at 480 and 520 nm respectively and cell efficiencies around 4-5%.
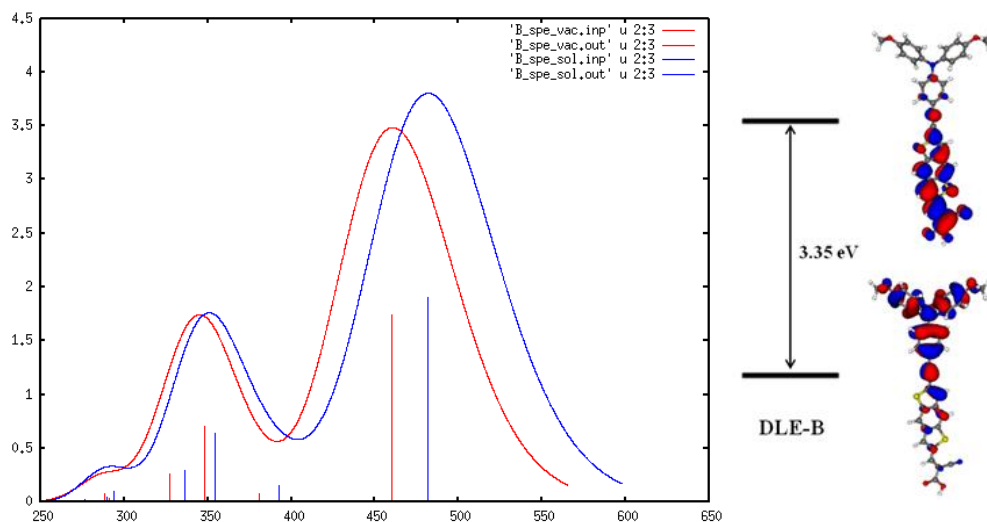


**Figure 5.3**

In order to investigate this unexpected results a photophysical study of dye **13** has been carried out in collaboration with Prof. De Cola's group. Even if this work is still under progress, the preliminary results on **13** are reported.

## 5.2   ROOM TEMPERATURE MEASUREMENT

### 5.2.1  ELECTRONIC ABSORPTION

The absorption spectra of dye **13** in dichloromethane, acetonitrile and ethanol are shown in figure 5.4. The bands at 350 nm can be assigned to π-π* transitions, molar extinction values for the peak maximum are ~ 27000 $M^{-1}$ $cm^{-1}$ in $CH_3CN$ ($\lambda_{max}$= 350nm), ~ 18000 $M^{-1}$ $cm^{-1}$ in $CH_2Cl_2$ ($\lambda_{max}$= 362nm), ), ~ 30100 $M^{-1}$ $cm^{-1}$ in EtOH ($\lambda_{max}$= 353nm).
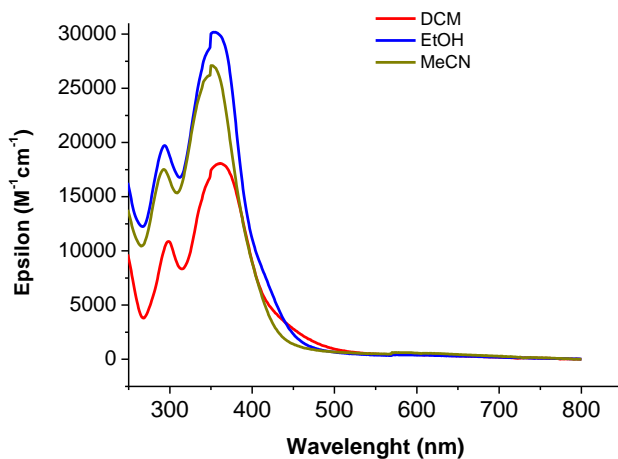
**Figure 5.4**

The dye shows negative solvatochromism, (Figure 5.4) and hence its absorptions are red-shifted by decreasing the solvent polarity; negative solvatochromism is typical of ground state dipolar molecule (like the metal free dyes) characterized by a significantly less polar excited state (implying a different stabilization of the two states promoted by the solvent).[2]

An alternative explanation for the blue shift observed for the dye in the polar aprotic solvent acetonitrile could be ascribed to the partial deprotonation of the carboxylic acid in the ground state.[2] Such a deprotonation equilibrium would reduce the electron-accepting strength of the acceptor moiety, and therefore reduce the polarization of the chromophore itself. This phenomenon would blue shift the absorptions as well.

This hypothesis has been supported by the fact that addition of a base such as triethylamine to the acetonitrile solution of the dye slightly blue shift the absorption peak while addition of trifluoroacetic acid to the solution of the dye led to a red shift of the absorption maximum (Figure 5.5). These observations suggest the presence of a protonation-deprotonation equilibrium for the dye in solution. To confirm this observation the experiment will be repeated in an apolar solvent, such as toluene, where the dye is expected to be predominantly in protonated form. In this solvent both addition of the base and of the acid should have a strong influence on dye's absorption spectrum.

Since is known in the literature that the p*K*a of the conjugate acid of triphenylamine is --5.0, while that of trifluoroacetic acid is 0.5, it's clear that the trifluoroacetic acid is a weaker acid than the protonated triphenylamine. Therefore, it is unlikely that the amine unit will be protonated in the presence of trifluoroacetic acid and therefore the effect of the acid is presumably the protonation of the -COO$^-$, partially generated in acetonitrile, to restore the –COOH group responsible for the observed red-shift. (Figura 5.5)
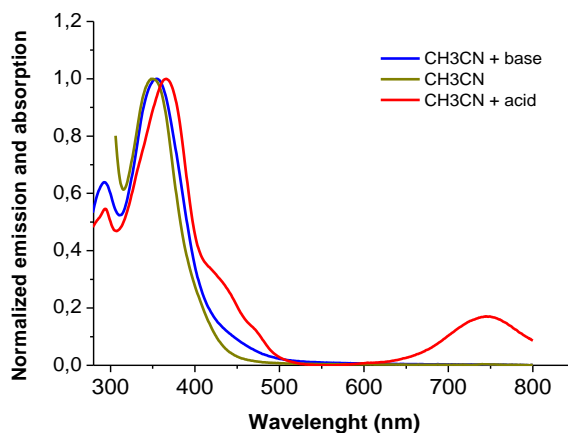


**Figure 5.5**

Therefore, observing the spectra recorded upon addition of the acid it can be noted a red-shift of 16 nm, from350 nm to 366 nm, the increase of the of the transition around 450 nm and the appearance of a new band at 750nm; investigation on the nature of these bands is currently ongoing. However repeating the measurement after 4 days, no evidence of the band at 750 nm has been found, and this could be attributed to the formation of a radical cation on the amine moiety as a consequence of a partial oxidation by some impurities .[3]

## 5.2.2 EMISSION SPECTROSCOPY

When a fluorophore absorbs a photon, an energetically excited state is formed. The fate of this species depends upon the nature of the fluorophore and its surrounding environment. The excited states can undergo radiation or radiationless deactivation to the ground state or undergo internal conversion between states before relaxing to the ground state. The main deactivation processes which occur are fluorescence (loss of

energy by emission of a photon), internal conversion and vibrational relaxation (non-radiative loss of energy as heat to the surroundings), and intersystem crossing to the triplet manifold and subsequent radiative (phosphorescence) or non-radiative deactivation.

The fluorescent spectra of the dye **13** in acetonitrile ($\lambda_{max}$= 512nm), dichloromethane ($\lambda_{max}$= 492nm) and ethanol ($\lambda_{max}$= 488nm) are shown in Figure 5.6. Contrarily to the absorption, dye **13** emission undergoes red-shift in more polar solvent. As a result of such positive solvatochromism, points to stronger stabilization of the excited state in polar solvents. This is ascribed to the intermolecular charge transfer (ICT) nature of the emissive state.
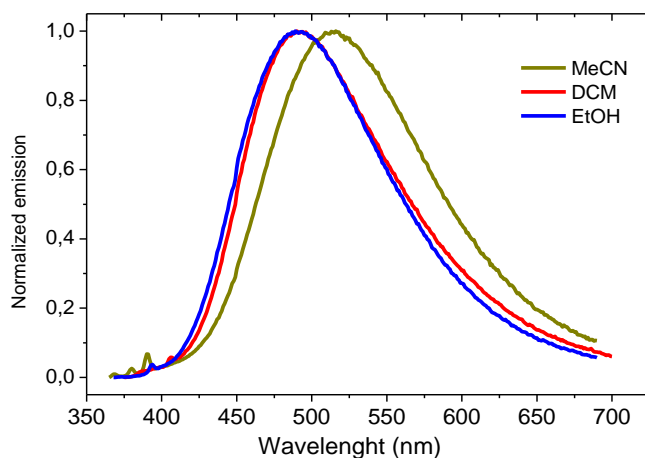


**Figure 5.6**

The blue shifted CT emission in ethanol solvent, compared to that in aprotic solvent of similar polarity, could be explained with the formation of hydrogen bonds between the hydroxyl group of the alcohol and the nitrogen of the amine. This partially reduce the donor ability of the amino group and therefore lead to a high energy CT bandwith and a large blue-shift of the emission band.[4]

In Figure 5.6 are combined emission (dash line) and absorption (solid line) spectra of the dye **13** in $CH_3CN$, EtOH and $CH_2Cl_2$. The dye shows a Stokes shift of 164 nm, 130 nm and 130 nm in acetonitrile, ethanol and dichloromethane respectively.
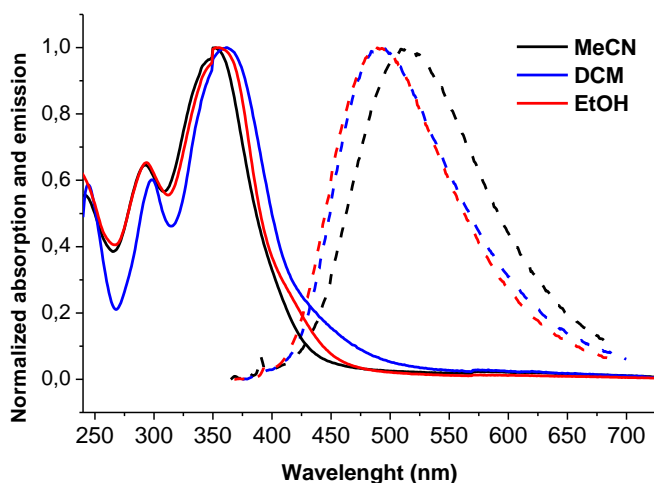
**Figure 5.7**

## 5.2.3 QUANTUM YIELD

The fluorescence quantum yield ($\Phi_F$) is the ratio of photons absorbed to photons emitted through fluorescence. In other words the quantum yield gives the probability of the excited state being deactivated by fluorescence rather than by other non-radiative mechanism.

There are two approaches to measure $\Phi_F$ : an absolute method and a comparative one. The absolute method take advantage of an "integrating sphere" setup. The inner surface of the integrating sphere is highly reflective such that all light entering the sphere has only two possible fates: absorption by the sample or collection by the fluorimeter detection optics. So, the integrated area under the corrected fluorescence spectrum of the sample represents the *total* number of photons emitted (per unit time) by the sample. This experiment is quick and easy, often providing reasonable efficiency values carrying 5-10% uncertainties. .

However, weakly emissive samples, often require comparison of data collected with the integrating sphere and other methods to achieve the same value. The complementary approach and method to measure $\Phi_F$ is the comparative method of Williams *et al.*,[5] which involves the use of well characterized standard samples with known $\Phi_F$ values. Essentially, a solution of the standard and test samples with identical absorbance at the same excitation wavelength are assumed to absorb the same number of photons. The

reference must emit in the same region of the sample. Hence, a simple ratio of the integrated fluorescence intensities of the two solutions (recorded under identical conditions) will yield the ratio of the quantum yield values. Since $\Phi_F$ for the standard sample is known, it is trivial to calculate the $\Phi_F$ for the test sample.

In practice several are the factors that have to be taken in account, such as the presence of concentration effects, *e.g.* self-quenching, the use of different solvents due to different solubility for standard and test samples, the validity in using the standard sample and its $\Phi_F$ value.

Therefore to obtain a reliable value is necessary to work within a carefully chosen concentration range and include the solvent refractive indices within the ratio calculation.

Table 5.2 summarizes the quantum efficiencies of dye **13** in different solvents and compares the absolute and relative measured $\Phi_F$.

The quinine sulfate 0.5M in $H_2SO_4$, was employed as the standard: it has an absorption spectrum around 350 nm and an emission around 450 nm. (Table 5.2) The $\Phi_F$ has been calculated with the formula:

$$\Phi_x = \Phi_r \left[ \frac{A_r(\lambda_r)}{A_x(\lambda_x)} \right] \left[ \frac{I_r(\lambda_r)}{I_x(\lambda_x)} \right] \left[ \frac{n_x^2}{n_r^2} \right] \left[ \frac{D_x}{D_r} \right] \qquad \text{eq 5.2}$$

where *A* is the absorbance at the excitation wavelength ($\lambda$), *I* is the intensity of the excitation light at the excitation wavelength ($\lambda$), *n* is the refractive index of the solvent, *D* is the integrated intensity of the luminescence and $\Phi$ is the quantum yield. The subscripts *r* and *x* refer to the reference and the sample, respectively.

|  | Integration sphere Φ% | Relative method Φ% |
|---|---|---|
| MeCN | 0.4 | 0.47 |
| EtOH | 0.5 | 0.46 |
| $CH_2Cl_2$ | 0.9 | 0.63 |

**Table 5.2**

### 5.2.4 LIFETIME MEASUREMENT

Fluorescence lifetimes of **13** in different solvents were determined by Time Correlated Single Photon Counting methods (TCSPC) employing a laser source at 378 nm and the data are summarized in Table 5.3. The fluorescence decays are well fitted by biexponential functions in ethanol and acetonitrile and by triexponential in dichloromethane.

| Solvent | λ abs | λ em | Φ% | $\tau_1$ (ns) | $\tau_2$ (ns) |
|---------|-------|------|------|-------------|-------------|
| MeCN | 350 | 514 | 0.47 | 2.93 (69%) | 4.34 (23%) |
| EtOH | 353 | 491 | 0.46 | 2.21 (76%) | 4.24 (7%) |
| $CH_2Cl_2$ | 362 | 492 | 0.63 | 2.60 (76%) | 4.56 (21%) |

**Table 5.3**

In all the solvents two different lifetimes component are observed. With the largest contribution estimated for the shortest component of about 2ns.

Due to short living nature of the excited state the presence or absence of the oxygen does not change the excited state lifetimes or the emission quantum yield.

## 5.3 SOLID MATRIX MEASUREMENT

### 5.3.1 77K MEASUREMENT

Measurement in solid matrix have been performed in a mixture $CH_2Cl_2$/MeOH 1:1 upon cooling to 77 K. Figure 5.8 shows the emission spectrum which is compared with the room temperature emission.
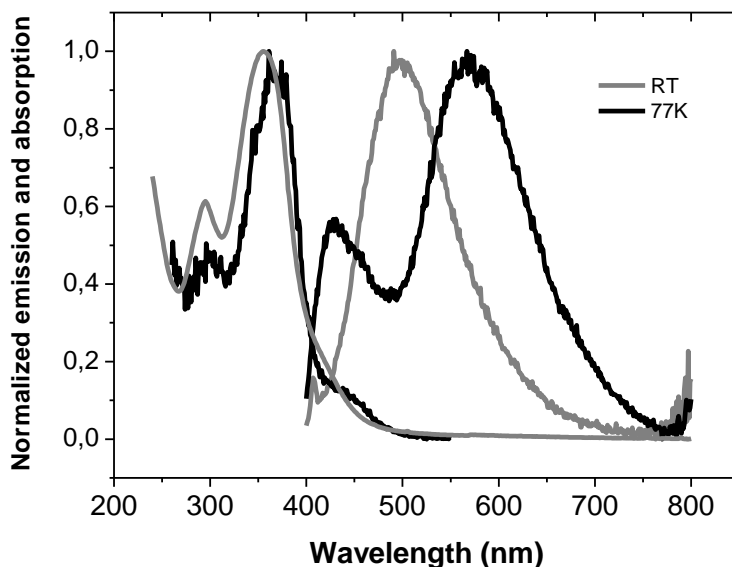
**Figure 5.8**

As can be observed in the spectra shown above (Figure 5.8), at 77K the emission band is strongly red-shifted from 491 nm to 567 nm. The first low band at around 400 nm has been attributed to the solvent matrix.

| CH$_2$Cl$_2$/MeOH 1:1 | λ ex. (nm) | λ abs (nm) | λ em (nm) | τ$_1$ (ns) | τ$_2$ (ns) |
|---|---|---|---|---|---|
| r.t. | 362 | 360 | 491 | 1.91 (49%) | 5.96 (12%) |
| 77 K | 362 | 375 | 567 | 2.51 (58%) | 7.24 (24%) |

**Table 5.4**

The fluorescence decays are well fitted by biexponential functions at room temperature and the same trend is observed at 77k. As seen before lifetimes with the largest contribution are in the order of 2ns.

## 5.3.2 MEASUREMENT IN PMMA SOLID MATRIX

To study the behavior of the dye in solid state, we prepared a series of PMMA doped samples with different amount of chromophore **13** (Table 5.5 ). The procedure involves the preparation of the solution in the desired concentration (in weight) of both the dye and PMMA in an appropriate solvent, in our case dichloromethane. The solutions are

spincoated on quartz substrate. The concentration of the dye in PMMA ranges from 5 to 75%.
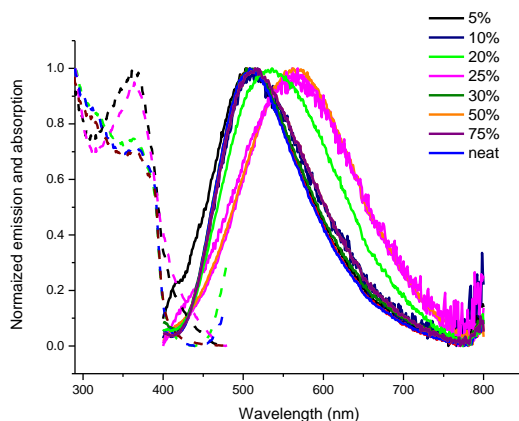


**Figure 5.9**

In Figure 5.9 excitation (dash line) and emission (solid line) of the sample are reported.

It can be observed that all the samples gave the same excitation spectra with $\lambda_{max}$ around 345 nm, while the emission spectra shift from 511 nm (5%, 10%, 50%, 75%, neat) to 525 nm (20%, 25%, 30%) and also 563 nm for 25% (Table 5.5). The different values for the same sample measurement come from the fact that we tried to investigate the surface in several different point, observing that only certain concentration shown different emission spectra varying the irradiation point. To confirm these uncommon results the preparation of the sample has been repeated several times, also varying some parameters such as the rpm speed and the time, finding always the same behavior. Is also interesting to note that absorption maxima found for 25% concentrated dye is the same at 77 K. (Figure 5.8)

| % DLE195 | % PMMA | λ Ex | λ em |
|----------|--------|------|------|
| 5 | 95 | 345 | 509 |
| 10 | 90 | 345 | 511 |
| 20 | 80 | 345 | 523 |
| 25 | 75 | 345 | 508,525,563 |
| 30 | 70 | 345 | 510, 527 |
| 50 | 50 | 345 | 508 |
| 75 | 25 | 345 | 510 |
| Neat | - | 345 | 511 |

**Table 5.5**

With the aim to understand the meaning of this behavior further experiments will be performed, such as the study of the influence of the solvent in the spincoating process.

In Table 5.6 the lifetime measurements are reported. Observing the data collected, i is not possible to identify a trends of lifetime increasing the concentration of dye in PMMA. Quantum yields are also reported: the really low values are not trustable because in the error range of the integration sphere.

| % DLE195 | % PMMA | $\tau_1$ (ns) | $\tau_2$ (ns) | Φ% |
|---|---|---|---|---|
| 5 | 95 | 0.66 (17%) | 2.84 (6%) | 0.33 |
| 10 | 90 | 2.21 (76%) | 4.24 (7%) | 0.20 |
| 20 | 80 | 4.56 (21%) | - | 0.30 |
| 25 | 75 | 1.62 (30%) | 5.28 (11%) | 0.33 |
| 30 | 70 | 1.38 (24%) | 4.61 (7%) | 0.15 |
| 50 | 50 | 0.96 (23%) | 4.13 (7%) | 0.17 |
| 75 | 25 | 0.85 (8%) | 3.60 | 0.10 |
| Neat | - | 0.66 (17%) | 2.85 (6%) | 0.23 |

**Table 5.6**

### 5.3.3  UPS MEASUREMENT

In addition to the HOMO-LUMO calculation using the data from the electrochemical experiments,(see **chapter 4**) UPS measurement have been carried out. A value of -5.22 e V has been extimated for the HOMO.

## 5.4   CONCLUSION

Among the synthesized metal free dyes, the system **13** revealed some noteworthy peculiarities such as the absence of a strong CT absorption band in the visible region In the absorption spectrum. With the aim to understand the behavior of dye **13** which only absorbs in the UV and near UV region, the chromophore has been photophysically characterized in terms of room temperature and low temperature emission properties, quantum efficiencies and emission lifetime both in solution and solid (film) samples.

We found that the broad and featureless emission band is clearly a CT band. This is also confermed by the positive solvatocromism observed and the poor quantum yield (also linked to the low epsilon value of the correspondent absorption band). This phenomena entirely explain that dye **13** is anyhow suitable for DSC application since the lowest excited state is localized in the acceptor moiety. entirely explain that dye **13** is anyhow suitable for DSC application since the lowest excited state is localized in the acceptor moiety.

From the first result obtained it's clear that the system in study hasn't a straightforward behavior and is not trivial to explain, indeed being a push-pull system composed of three different parts, a donor unit D, an acceptor unit A and a spacer, several are the processes that can occur. For this reason the study of each single part of the D-π-A system will be undertaken.

As already mentioned, this work is currently ongoing, in particular for comparative investigation, we are synthesizing compound **67** (Figure 5.10) lacking of the anchoring group. This new molecule, that is no more a push-pull system, should be a simpler system to study as starting point for the comprehension of dye **13**'s behavior.



**Figure 5.10**

## 5.5   EXPERIMENTAL SECTION

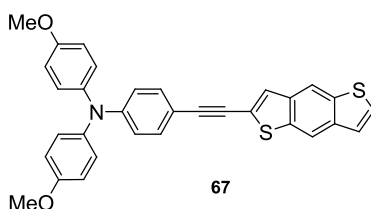Photophysics. Absorption spectra were measured on a Varian Cary 5000 double-beam UV-vis-NIR spectrometer and baseline corrected. Steady-state emission spectra were recorded on an Edinburgh FS920 spectrometer equipped with a 450W xenon-arc lamp, excitation and emission monochromators (1.8 nm/mm dispersion, 1800 grooves/mm blazed at 500 nm), and a Hamamatsu R928 photomultiplier tube. Emission and

excitation spectra were corrected for source intensity (lamp and grating) by standard correction curves.

Time-resolved measurements were performed using the Single Photon Counting (TCSPC) option on an Edinburgh LifeSpec II with MCP-PMT. A picosecond laser diode (378 nm; pulse width <8 ps; fwhm >70 mW) was used. Steady-state emission spectra of solid matrix experiments were performed with a Spex FluoroLog-3 spectrofluorometer (Horiba-Jobin-Yvon Inc.) equipped with a TBX detector and double excitation and emission monochromators. The emission spectra were corrected for monochromator and detector efficiency and for the source intensity (450W xenon lamp). The thin films having polymethylmetacrylate (PMMA) and different amounts of Pt(II) complex were spin-coated on the top of the quartz using chloroform as the solvent.

Emission quantum yields were determined with a Hamamatsu Photonics absolute PL quantum yield integration sphere system (C9920-02) equipped with a L9799-01 CW Xenon light source (150 W), monochromator, and C7473 photonic multichannel analyzer and employing U6039-05 PLQY measurement software (Hamamatsu Photonics, Ltd., Shizuoka, Japan).

All solvents were spectrometric grade. Deaerated samples were prepared by the freeze-pump-thaw technique.

UV Photoelectron Spectroscopy (UPS). UPS was measured on a Riken Keiki AC-2 system using the low-energy electron counter method with a deuterium lamp as the light source and a grating type monochromator as the spectrometer.

**REFERENCES**

[1] J.-L. Song, P. Amaladass, S.-H. Wen, K. K. Pasunooti, A. Li, Y.-L. Yu, X. Wang, W.-Q. Deng and X.-W. Liu, *New J. Chem*., **2011**, *35*, 127.

[2] A. Baheti, P. Tyagi, K. R. J.Thomas, Y.-C. Hsu,. J. T. Lin, *J. Phys. Chem. C*, 2009, *113*, No. 20, 8541.

[3] G. Zhou, N.Pschirer, J. C. Schöneboom, F. Eickemeyer, M. Baumgarten, K. Müllen, *Chem. Mater.* **2008,** *20,* 1808.

[4] L.-H. Ma, Z.-B. Chen, Y.-B. Jiang , *Chemical Physics Letters,* **2003**, 372104.

[5] A. T. R. Williams, S. A. Winfield and J. N. Miller, *Analyst*, 1983, **108**, 1067.

# CHAPTER 6

# METAL-BASED DYES
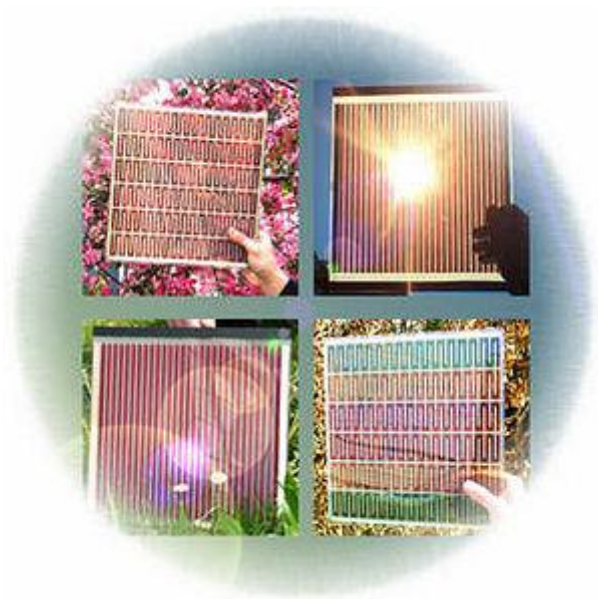
# 6.1  METAL COMPLEXES

Metal complexes have been intensively investigated for DSC application because of their broad absorption spectra and favourable photovoltaic properties. In fact a ruthenium bipyridine complex was used in the first efficient DSSC cell example reported in the breaktrough article by M. Grätzel and O'Regan in 1991.[1] Generally a metal complex consists of a central metal ion with ancillary ligands bearing at least one anchoring group. In these structure light absorption in the visible part of the solar spectrum is due to a metal to ligand charge transfer (MLCT) process. The central metal ion is therefore a crucial part of the complex in which ancillary ligands, typically bipyridines or terpyridines, can be tuned by different substituents (alkyl, aryl, heterocycle, etc.) to change the photophysical and electrochemical properties and thus improve the photovoltaic performance. Anchoring groups are employed to link the dye with the semiconductor and facilitate the injection of the excited electron into the CB of the semiconductor. Any part of the complex can be modified to tune the energy levels of the MLCT states and to optimize electron injection and dye regeneration kinetics.

In particular, the MLCT excited states of $d\pi^6$ coordination complexes have emerged as the most efficient for solar harvesting and sensitization of wide-bandgap semiconductor materials. As the name MLCT implies, light absorption promotes an electron from the metal d orbitals to ligand empty $\pi^*$ orbitals ($d(\pi) \rightarrow \pi^*$, Figure 6.1).[2,3,4] The classical example of a complex with such transition is $Ru(bpy)_3^{2+}$, which is arguably the most studied coordination compounds.
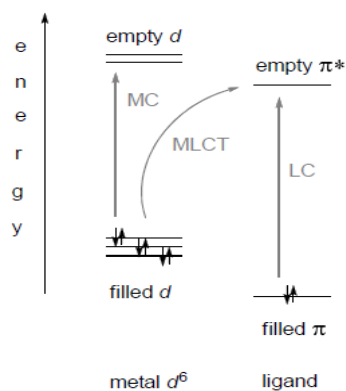


**Figura 6.1**

## 6.1.1 RUTHENIUM COMPLEXES

Among the metal complexes, Ru complexes[5,6,7] have shown the best photovoltaic properties: a broad absorption spectrum, suitable excited and ground state energy levels, relatively long excited-state lifetime, and good (electro)chemical stability. Up to now several Ru complexes, usually bearing variedly functionalized polypyridine ligands, used in DSCs have reached more than 10% solar cell efficiency under standard measurement conditions.

For these sensitizers, the metal-to-ligand charge transfer (MLCT) excited state is populated after light absorption (1). (Figure 6.2) According to the Franck- Condon principle, the initially formed excited state has the same structural symmetry as the ground state. This $^1$MLCT is followed by the formation of a



**Figura 6.2**

$^3$MLCT manifold (2) that can also inject electron (3b, ).[8]

In particular an electron is promoted from a molecular orbital (MO) that is largely Ru (II) based (filled $t_{2g}$ level) to a MO that is largely ligand base (empty $\pi^*$ orbital). Thus the smaller energy gap the more red-shifted is the related MLCT transition.



**Figure 6.3**

The MLCT transition energy and therefore the absorption spectrum of these compounds can be tune, tuning the metal based MO ($t_{2g}$) or tuning the ligand based MO ($\pi^*$). In figure 6.3 is shown a schematic representation of $t_{2g}$ tuning of polypyridine complexes.
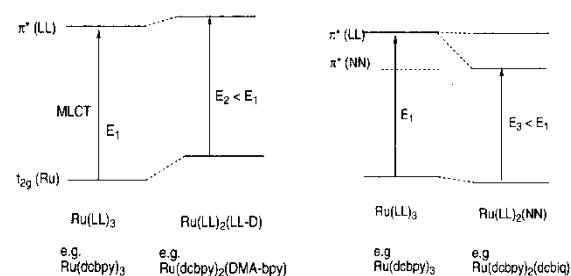
On the left $t_{2g}$ is tuned by replacement of an acceptor by a donor group in one of the bipyridine ligand, on the right $\pi^*$is tuned changing the nature of one of the ligands. The energy level of $t_{2g}$ is determinated largely by the electron density at the metal center, therefore electron-donating substituents (such as -NMe$_2$ or -OMe) on the ligand raise
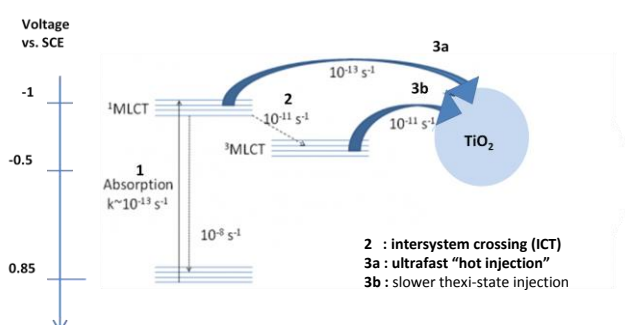
this level, decreasing the energy associated with MLCT transition. On the contrary, electron withdrawing groups (as –COO-) lower the level. [9,] Moreover addition of substituents with low lying $\pi$ orbitals, such as aromatics or esters, can enhance MLCT extinction coefficients, relative to unsubstituted structure. [1011]These changes will also affect the redox potential of the dye and therefore have to be monitored in detail to avoid mismatching with the $TiO_2$ conduction band and the redox potential of $I^-/I_3^-$ .

In these years many efforts have been made to optimize the Ruthenium photosensitizers and improve their efficiency in DSCs, looking for ligands that could also extend the spectral response region to the near-IR region.

The first high performance ruthenium, the complex cis-(SCN)2bis(2,2'-bipyridyl-4,4'-dicarboxylate)ruthenium(II), known as **N3** (Figure 6.4), was reported by Nazeeruddin *et al*. in 1993.[12] It was found to exhibit outstanding properties, such as broad visible light absorption spectrum and a incident photon-to-current conversion efficiency (IPCE) spectrum extending to 800 nm and achieving 90% at 600 nm, sufficiently long excited state lifetime (~ 20 ns), and strong adsorption on the semiconductor surface due to binding with up to four carboxyl groups. As a result, a solar-to-electric energy conversion efficiency of 10% was obtained.

Investigations on the effect exerted by the proton content of the **N3** dye on the performance of DSCs,[13] revealed that the doubly protonated form, (Bu4N)2[Ru(dcbpyH)2(NCS)2], named **N719** (Figure 6.4), has improved power conversion efficiency. **N3** and **N719** dyes are considered as reference dyes for DSC and are used as bases for designing other Ru photosensitizers, by changing ancillary ligands.

Dye **N749**, [14] also called the "black dye", (Figure 6.4) have been published from the same group. Differently from the previous two, in this dye, Ru center has three thiocyanato ligands, that enhance the absorption of visible light, and one terpyridine ligand substituted with three carboxyl groups wich allow   ligation to the surface via the formation of bidendate ester linkages. It is characterized by a red shift in the MLCT band aand a smaller gap $t_{2g}$- $\pi^*$, due to the decrease in the $\pi^*$ level of the terpyridine ligand and an increase in the energy of the $t_{2g}$ metal orbital. Based on this dye, an IPCE

spectrum was obtained over the whole visible range extending into the near-IR region up to 920 nm and a 10.4% conversion efficiency.[15]
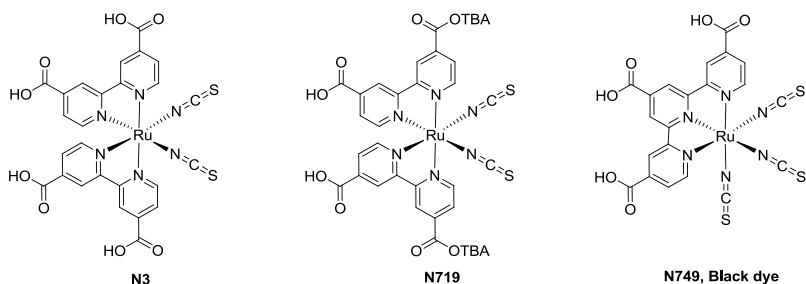


**Figure 6.4**

Grätzel and co-workers also investigated the substitution of the ancillary 2,2'-bipyridyl ligand with different

groups (alkyl, alkoxyl, phenylene, etc.) to increase the molar extinction coefficient, suppress dye aggregation on the semiconductor, and optimize the redox potential of the photosensitizer.

Among the large numbers of dye synthesized the most promising resulted the so called **Z907** and **Z910**. (Figure 6.5)



**Figure 6.5**

The amphiphilic heteroleptic ruthenium sensitizer, **Z907**, demonstrated prominent thermal stability due to the introduction of two hydrophobic alkyl chains on the bipyridyl ligand[16,17,18] In combination with hexadecyl phosphonic acid as a coadsorber, it maintained 7% power conversion efficiency under a long-term thermal stress

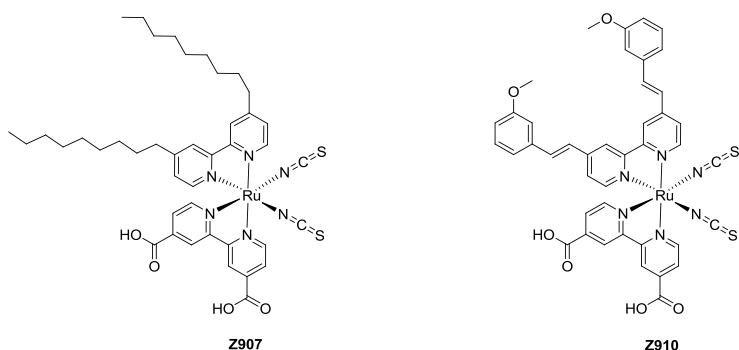measurement.[17]Dye **Z910**, bearing 3-methoxystyryl on the ancillary ligand, was designed with the aim of further extend the $\pi$-conjugated system of the bipyridine and enhance the harvesting of solar light. The dye exhibited prominent efficiency (10.2%) and impressive stability.[19]

Thelakkat, Durrant, and co-workers developed Ru dyes with **MTA** triarylamine-based electron donor groups at the bipyridyl ligands and studied charge recombination kinetics and solar cell performance.[20, 21] When the triarylamine moiety is connected with a conjugated link, a substantial increase of the extinction coefficient is found (about 2-fold). Upon excitation of the dye and electron injection, rapid intramolecular hole transfer from the Ru center to the donor was found and a long-lived charge separation between photoinjected electrons and the oxidized donor group was observed.With the Ru complex **MTA** an overall efficiency of 10.3 % was achieved. [22] Figure 6.6
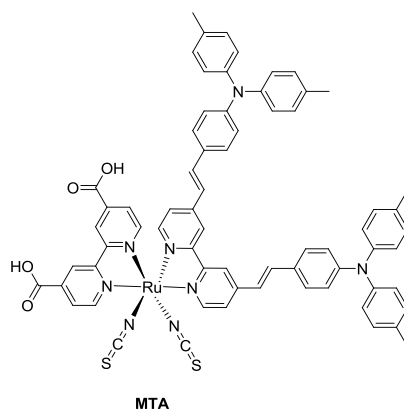


**MTA**

**Figure 6.6**

Wu and co-workers developed a series of Ru complexes where one of the bipyridyl ligands is substituted with alkyl thiophene,[23] ethylene-dioxythienyl (EDOT),[24] or carbazole.[25] The energy levels of the metal center and the LUMO of the ligands can be raised with incorporation of thiophene ligands, and as a consequence, the MLCT band will be red-shifted.

They also functionalized the thiophene-derived Ru complexes with a hole-transport moiety, alkyl-substituted carbazole, and obtained efficient sensitizers. The efficiency of a DSC based on sensitizer **CYC-B6S** was 9.7% (N3, 8.5%). Figure 6.7
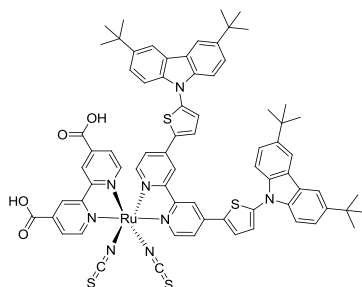


**CYC-B6S**

**Figure 6.7**

In the last years a lot of optimization work have been done on the cell leading the efficiency of the first Ruthenium dyes reach value above 11%, in particular 11.03% for N3, 11.18% for N719, 11.1% for N749,[26] however recently a new dye has been published by Wang and coworker[27] achieving a higher efficiency of 11.4%.

The dye **C106** synthesized   (Figure 6.8)feature a hexylthiothiopheneconjugated bipyridine ligand that remarkably enhance the optical absorptivity of mesoporous titania film. The merit of introducing sulfur between hexyl and thiophene together with extending the π-conjugated system of ancillary ligands in heteroleptic ruthenium complexes is ensuring a good light-harvesting efficiency and efficient conversion of light energy to electricity even with thin nanocrystalline $TiO_2$ layer.
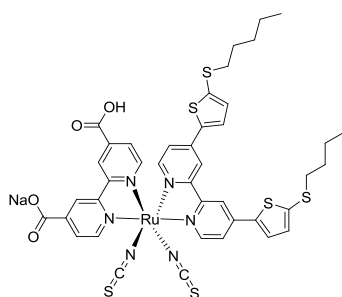


**C106**

**Figure 6.8**

It can be noticed that, the most efficient Ru dyes used since 1993, bear thiocyanate (SCN) ligands as the electron-donating groups in .Neverthless the SCN group has been shown to be the weakest part of Ru complex from a chemical stability point of view. Many efforts to replace it have been made using for instance cyclometalated ruthenium complexes, [Ru(C^N^N)-(N^N^N)] type. Recently, a thiocyanate-free cyclometalated ruthenium sensitizer, bis(4,4'-dicarboxy-2,2'-bipyridine) 2-(2,4-difluorophenyl)pyridine ruthenium(II), **F1** (Figure 6.9) was reported by Bessho and co-workers, which exhibited an IPCE value of 83% and prominent conversion efficiency, 10.1% at AM 1.5 G. This opens up possibilities to design the next generation of ruthenium sensitizers.[28]



**F1**
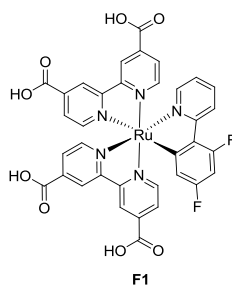
**Figure 6.9**

## 6.1.2 OTHER METAL COMPLEXES

As described before ruthenium complexes have provided highest efficiencies and have been therefore widely studied. However there are still many problems to be addressed in terms of their not very high molar extinction coefficient, ruthenium metal and high synthetic cost, therefore other metal complexes have also been investigated.

Many attempts have also been made to construct sensitizers with other metal ions, such as Os (II), Fe (II), Pt (II), and Cu (I). Iron, ruthenium and osmium are in the same triad of the periodic table. As a first row transition metal, iron has the weakest ligand field and osmium, a third row metal, has the strongest one ($t_{2g}$-$e_g$* splitting). Assuming a regular octahedral structure with $O_h$ symmetry, for osmium and ruthenium the $e_g$* metal orbitals



**Figura 6.10**

are substantially higher than the π* molecular orbital from the polypyridine ligand, whereas for iron, the $e_g$* metal orbitals are lower in energy and comprise the lowest excited state orbitals (see Figure 6.10). As a consequence, not only are the MLCT lifetimes of the iron complexes shortened, but also the 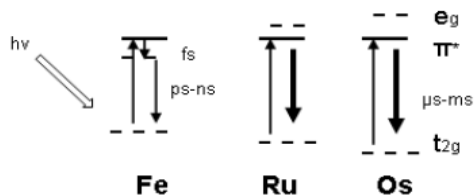population of the $e_g$* metal orbitals spatially removes the excited electron from the bipyridyl ligand  and can render the complex unstable.

Ferrere and co-workers engineered Fe(II) complexes for DSC application [FeII(2,2'-bipyridine)$_2$(CN)$_2$],[29] which showed a low efficiency with IPCE values only around 10-11% in DSCs. Figure 6.11



[FeII(2,2'-bipyridine)$_2$(CN)$_2$]
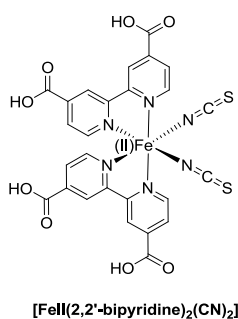
**Figure 6.11**

Osmium (Os(II)) complexes were found to be promising photosensitizers for DSCs due to the prominent MLCT absorption band in comparison with the Ru complex. In osmium polypyridyl complexes indeed, there is an additional absorption band at longer wavelengths, because direct excitation of the triplet state $^3$MLCT is less forbidden. Figure 6.12



**Figura 6.12**

Lewis and co-workers focused on developing this kind of sensitizer and reported a class of Os polypyridines.[30,31,32] Dyes **Os(H$_2$L')$_2$(CN)$_2$** and **Os(H$_2$L')$_2$(SCN)$_2$**, (Figure 6.13) obtained by replacing the Ru metal ion with Os, extended the light response region without sacrifying the good photovoltaic performance in DSCs. Bignozzi and co-workers also optimized Os complexes and obtained broad photoaction

spectra. Dye **OsH2dcbpyCl** showed an extended IPCE spectrum up to 1100 nm.[33] Bignozzi and co-workers demonstrated that the lower photocurrent efficiency of Os complexes was due to slower electron transfer from the iodide electrolyte to the osmium dye cation.[34]



Os(H₂L')₂(CN)₂                    Os(H₂L')₂(SCN)₂                    OsH2dcbpyCl
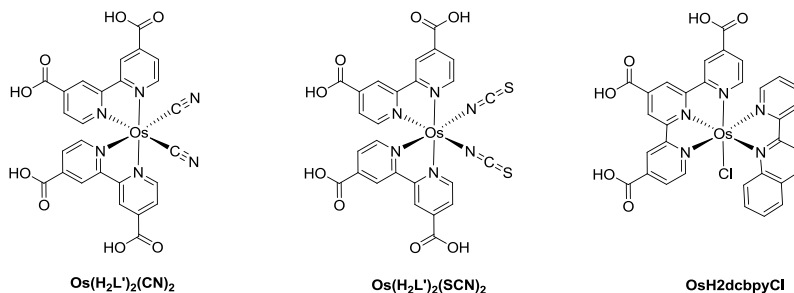
**Figure 6.13**

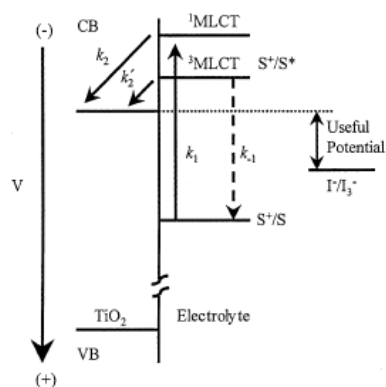Platinum and copper have been also tested but with poor results. Islam *et al*. synthesized square planar platinum(II) diimine dithiolate complexes that can also efficiently sensitize nanocrystalline $TiO_2$.[35,36] They reached efficiencies up to 3%. However, recombination and aggregation problems typical of these platinum (II) complexes seem to stop these sensitizers from being more efficient.

Cu(I) complexes were introduced into DSCs by Sauvage and co-workers because of their similar photophysical properties to Ru complexes.[37] Up to now the best efficiencies of 2.3% have been reached by Constable and co-workers.

## 6.2 PORPHYRINS AND PHTHALOCYANINES

Ruthenium bipyridyl complexes, in addition to the problems aforementioned, are characterized by limited absorption in the near-infrared region of the solar spectrum. On the contrary porphyrin and phthalocyanines exhibit intense spectral response bands in the near-IR region and possess good chemical, photo-, and thermal stability, providing rather good potential candidates for photovoltaic applications.

## 6.2.1 PHTHALOCYANINES

Phthalocyanines possess intense absorption in the Q-band (around 700 nm), as well as promising electrochemical, photochemical, and thermal properties, for these reasons are of interest as NIR photosensitizers for DSCs. They have also some drawbacks such as poor solubility and strong tendency to aggregate on the semiconductor surface, thus in order to facilitate the dye-sensitization process, a structural optimization is needed.

To date, a large number of phthalocyanine dyes have been synthesized for applications in DSCs,[38, 39, 40] herein are reports some of the most efficient.

Grätzel and-co-workers, in a pioneering work, employed a Ru phthalocyanine photosensitizer **PT1** (Figure 6.14)to fabricate a DSCs and obtained a IPCE value exceeding 60%.[41] The most important result was the establishment of a new pathway for grafting phthalocyanines to semiconductor surfaces, through axially attached pyridine ligands, opening up a new way to improve the near-IR response of DSCs.

They also developed an efficient Zn phthalocyanine **PT2** dye which showed a IPCE of 45% in the NIR but a corresponding efficiency of 1%.[42]
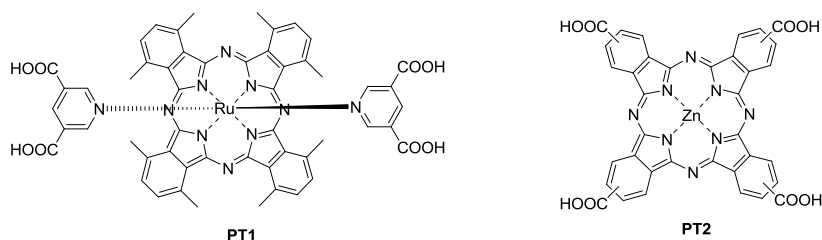


**Figure 6.14**

In following work, Durrant and co-workers investigated several metal phthalocyanines containing axial ligands with a carboxyl group,[43, 44, 45] such as **PT3** and **PT4.** (Figure 6.15)
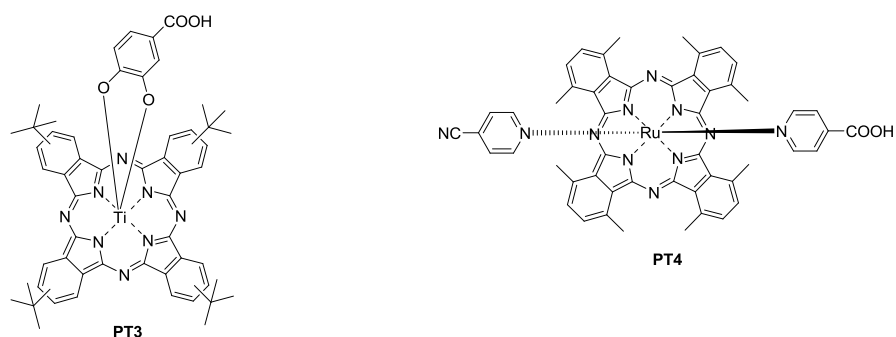
**Figure 6.15**

Their study revealed that this kind of structures can suppress dye aggregation, and they point out that a key factor in achieving further improvements in phthalocyanine-based DSCs is optimization of the electron injection yield from singlet and triplet state and the suppression of recombination pathways with the electrolyte.

To date the best phtalocynine based dye has been reported by Nazeeruddin and co-workers in developed the unsymmetrical zinc phthalocyanines[46] **PT5** yielded a maximum IPCE value of 75% and a conversion efficiency of 3.0%. Figure 6.16
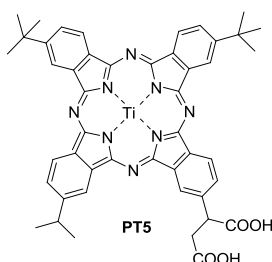


**Figure 6.16**

## 6.2.2 PORPHYRINS

The introduction of porphyrins as DSC photosensitizers is of particular interest given their primary role in photosynthesis; plants and bacteria capture solar energy using porphyrin-based chromophores for converting it into chemical energy.

Porphyrines have several intrinsic advantages, such as good photostability, rigid molecular structures with very strong absorption of the Soret band in the 400-450 nm region, as well as the Q-band in the 500-700 nm region. They also possess appropriate LUMO and HOMO energy levels and many sites for possible functionalization, thus

allowing feasible tuning of their optical, physical, and electrochemical properties to make them suited as panchromatic photosensitizers Furthermore several studies have demonstrated that they show efficient photoinduced electron injection into the conduction band of semiconductors.[47,48,49]

For these reasons in these years a lot of efforts have been spent to design novel efficient porphyrins to replace Ruthenium complexes in DSSCs.[50,51,]

Kay and Grätzel reported the first study on sensitization of $TiO_2$ with chlorophyll derivatives and related natural porphyrins, using **Cu-2-α-oxymesoisochlorin *e4*** high IPCE values over 80% but an efficiency value of 2.6% were obtained.[52]



**Cu-2-α-oxymesoisochlorin *e₄***
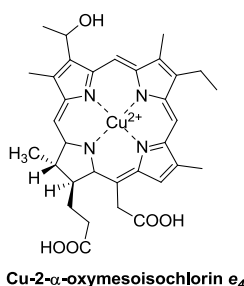
**Figure 6.17**

They found that the reason of such a low efficiencies with respect to ruthenium complexes was due to the presence of recombination process and problems in dye's regeneration. While electron injection into the semiconductor only changes the oxidation state of the ruthenium center, chlorophyll like molecules are oxidized to a cation radical which is susceptible to side reactions before being reduced. They also discover to the importance of using coadsorbers to prevent unfavorable aggregation of this dye.

Some years later Wamser and Cherian obtained IPCE values of 55% at the Soret peak and 25-45% at the Q-band, achieving an overall energy conversion efficiency of about 3.5% using a tetra(4-carboxyphenyl)porphyrin (TCPP)[47,53,54] (without any metal ions) that is the most common porphyrin photosensitizer for DSCs.

The reasons of such low efficiencies were not clear therefore trying to understand the behavior of this dyes, Durrant and co-workers studied the different electron injection and charge recombination properties of **N3**, **TCPP**, and **Zn-TCPP** (Figure 6.18) on $TiO_2$.[47]

They found that in porphyrin dyes the cation state is delocalized over the conjugated macrocycle while in **N3** is located on the ruthenium and NCS moieties of the dye, thereby keeping this state away from the TiO$_2$ surface and favoring a slow charge recombination. However, the similar electron recombination kinetics between these dyes indicated that the location of the cation within the sensitizer has only a minor influence. It is possible then that the lower efficiency of porphyrin-sensitized DSCs is due to dye aggregation on the TiO$_2$ surface or difficult dye regeneration, as already observed with Osmium complexes.[34]
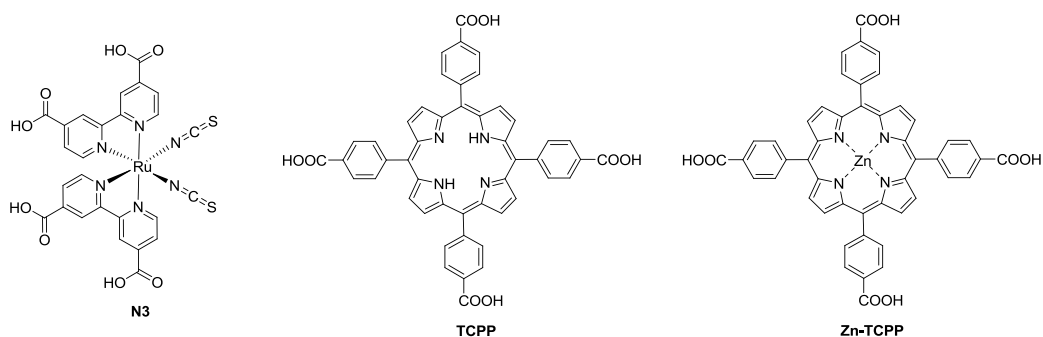


**Figure 6.18**

Studying dyes **P1** and **P5** (Figure 6.19) Bignozzi et al.[55] found that in porphyrins, after excited state generation the radiative process competes with the electron injection, thus decreasing the branching ratio between these two deactivation channels and leading to low IPCE. They also observed that the electronic coupling with TiO$_2$ of this type of dyes is an important factor, certainly one of the key parameters for the design of efficient sensitizers. The importance of electronic coupling to the efficiency of electron injection is convincingly demonstrated by the IPCE variations between porphyrins **P1** (9%) and **P5** (21%). It seems to be remarkably sensitive to the substitution position of the anchoring group (phosphonate). This can be interpreted as due to differences in the orientation and distance of the dye with respect to the TiO$_2$ surface imposed by the directionality of the anchoring groups. Porphyrin **P5** may lie closer to that with para substituents (dye **P1**). Consequently, these variations may bring about significant differences in the magnitude of the electronic coupling.
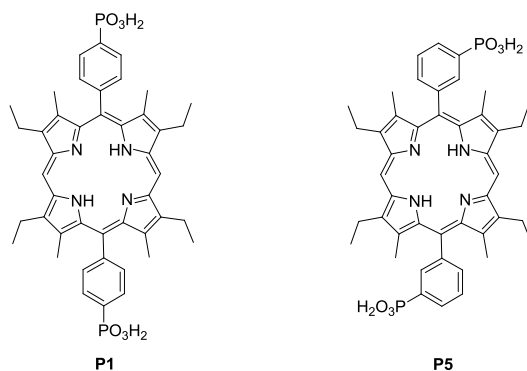
**Figure 6.19**

Nazeeruddin and co-workers developed a family of porphyrin dyes with different central metal ions: Cu(II) or Zn(II) and different anchoring groups (-COOH or -PO$_3$H$_2$).[56] They concluded that for porphyrins bearing carboxylic binding groups, the diamagnetic Zn-porphyrins exhibites superior efficiences in comparison to that of the paramagnetic Cu-porphyrins. They also demonstrated that porphyrins with a phosphonate anchoring group showed lower efficiencies than those with a carboxylate. In particular they established that carboxylate group are bound to the TiO$_2$ surface via a bridging bidentate mode and that, despite the fact that the anchoring group does not participate in the $\pi$-$\pi$* excitation responsible for the visible bands, electronic coupling of the excited state to the Ti (3d) conduction band is strong enough that charge injection is very efficient. Among these dyes, dye **ZnCTPP2** achieved a higher IPCE value of 75% and overall efficiency of 4.8%. Figure 6.20
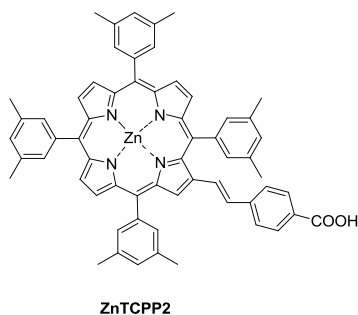


**Figure 6.20**

Officer and co-workers synthesized a series of porphyrin photosensitizer bearing differentially substituted aryl groups as electron donors and the malonic acid binding

group as an accept or (e.g. **ZnTCPP3**, **ZnTCPP4**, Figure 6.21 ). As mentioned before, the interaction between the porphyrin $\pi$-system and an olefin-linked electron acceptor present on the *β*-pyrrolic position is strong enough to permit electron injection, in addition the malonic acid group facilitates stronger binding to the semiconductor surface with a consequent improvement in the electronic coupling of the dye.[57, 58]

They also studied the effect of the substitution of the aryl group in *meso* position, founding that a cell based on dye **ZnTCPP3** that bear simple aryl group yielded up to 75% IPCE with a corresponding overall efficiency of 5.1%.[59, 60] Dye **ZnTCPP4**, in which the aryl group is a 4-methylphenyl, exhibited again an IPCE value of up to 75% but an impressive efficiency of 7.1%.



ZnTCPP3                          ZnTCPP4
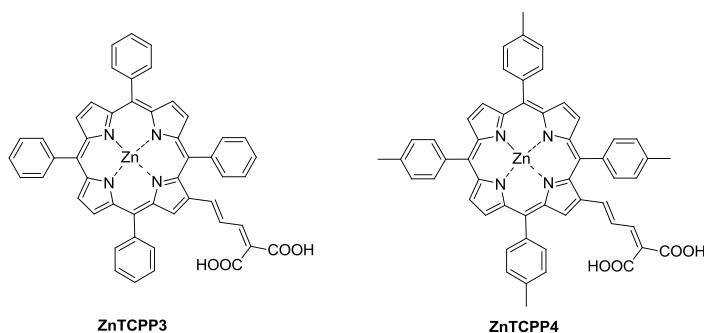
**Figure 6.21**

Following the same strategy, Imahori and co-workers also optimized the porphyrin dyes by substituting the *meso*-position of porphyrin with different $\pi$ systems, such as thienyl and furyl, bearing a carboxylic group as anchoring group to guarantee the single anchorage of the porphyrin molecule on the $TiO_2$. As shown for dye Zn5S (Figure 6.22), Three methyl groups are introduced into 2,4,6-positions of the *meso*-phenyl groups of the porphyrin. The resulting large steric hindrance around the porphyrin is expected to reduce the aggregation of the porphyrin molecules on the $TiO_2$, leading to the suppression of undesirable quenching of the porphyrin excited singlet state and eventually efficient photocurrent generation. The different $\pi$-bridges showed different effect on DSC performance due to variation of adsorption behavior and saturated coverage on the TiO2 surface. Dye **Zn5S** showed an IPCE value of ca. 65% and an efficiency of 3.1%.[61]

Zn5S
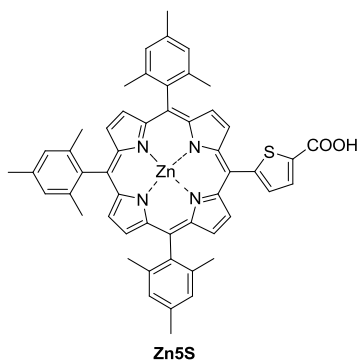
**Figure 6.22**

The role of para-alkyl substituents on *meso*-phenylporphyrin sensitized DSCs was also studied by Ballester and coworkers, who discovered that in **FbP2** (Figure 6.23) the presence of hydrophobic alkyl chains on the molecular structures of porphyrins could decrease the recombination between the injected electrons and the electrolyte without influencing the electron recombination between the injected electrons and the oxidized dye and dye regeneration.[62]



FbP2
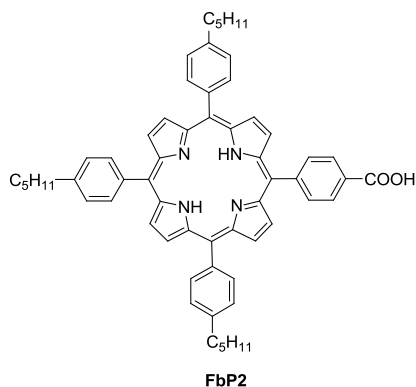
**Figure 6.23**

Kim and co-workers, also investigated electronic and photovoltaic properties of functionalized porphyrins such as **Zn-2b-bdta** (Figure 6.24) bearing at *meso* and *β*-positions with different carboxylic acid groups in DSCs and claimed that the effective electronic coupling through the bridge played an important role in the charge injection process.[63] If the coupling is strong enough and result in broadening and red shifting of the absorption bands, the longer is the distance between the dyes and the $TiO_2$ surface the better performance are shown, due to a slow charge recombination rate.

206
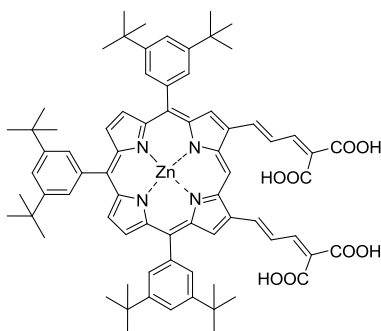
**Zn-2b-bdta**

**Figure 6.24**

Yeh and co-workers also designed and synthesized many *meso-* and *β*-derivatized porphyrins with a π-bridge linked carboxyl group for DSCs.[64]

Absorption spectra of porphyrins such as **YD1** (Figure 6.25) with a phenylethynyl bridge show that both Soret and Q bands are red-shifted with respect to those of porphyrin with only a phenyl bridge. This phenomenon is more pronounced for porphyrins which have a π-conjugated electron-donating group at the *meso* position opposite the anchoring group, indeed red shifts and broadening of the absorption band increase systematically with increasing π conjugation.[65] They found also that substitution of carboxyphenyl at the β-position causes no significant red shift of either Soret or Q bands because of an orthogonal orientation between the carboxyphenyl and porphyrin rings. In addition porphyrin of these series bear 3,5-di-tert-butylphenyl groups at the *meso* positions introduced with the aim to reduce the formation of dye aggregates on the semiconductor surface.[66]

Dye **YD1** as one of these dyes, showed the best photovoltaic properties with 6.0% efficiency.

YD1
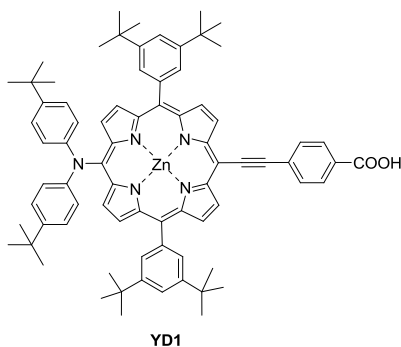
**Figure 6.25**

Lin and co-workers synthesized and studied a family of zinc porphyrins with one to four $\pi$-conjugated phenylethylnyl (PE) units as a linker of controlled length with the aim to investigate the interfacial electron transfer.[67] When these porphyrin photosensitizers were tested into DSCs, the efficiency of these devices decreased systematically with increasing length of the linker, although the rates of electron injection between these dyes and TiO$_2$ were equal. DFT calculations also indicated that the electron densities of the HOMO and LUMO are localized in the porphyrin ring and extended only to the first unit of the PE link. The best efficiency, 2.7%, was obtained by dye **PE1**. Figure 6.26



PE1
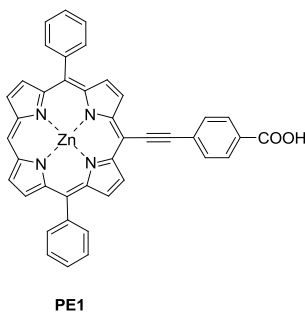
**Figure 6.26**

Recently, Tan and co-workers reported several new porphyrin dyes with a D-$\pi$-A structure (**PZn-T**, **PZn-HT**, Figure 6.27): the porphyrin acted as a donor and cyanoacrylic acid acted as an acceptor/anchoring group; different thiophene derivatives acted as a $\pi$ bridge to broaden the absorption of the dyes.[68] Their results clearly show that the thiophene $\pi$-conjugation unit can improve the light harvesting capability of porphyrin dyes and therefore extend the spectral response region of porphyrin dyes, and the alkyl

chain on this unit can influence the electron transport efficiency improving the photovoltaic performance of DSCs.

Dye **PZnT** without a hexyl group showed an efficiency of 4.3%. However, dye **PZnHT** containing the hexyl chain achieved higher efficiency of 5.1% and a maximum IPCE value of 72%.
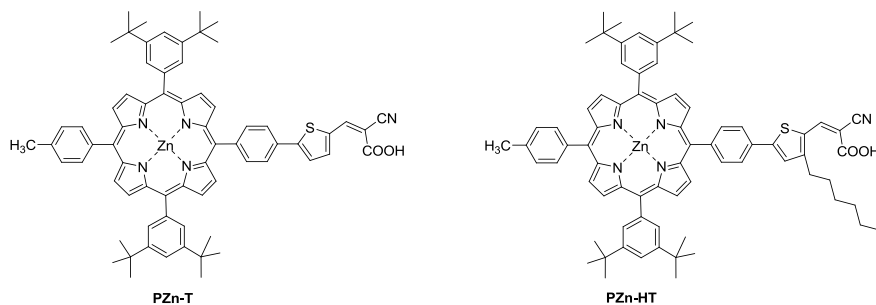


**Figure 6.27**

Diau et al. synthesized a series of dark-green porphyrin sensitizers containing diarylamino and/or triphenylamino moieties in various *meso*-positions and with phenylethylnyl-carboxyl acceptor–anchors group. Porphyrin chromophore itself constitutes the π-bridge in this particular D–π–A structure.[69, 70] The best dye **YD2** (Figure 6.28) reach an efficiencies of 5.6% with a 2.4 μm thick TiO$_2$ film and 8.8% with an increase TiO$_2$ thickness of 11.2 μm. They found that there is effective electronic coupling between the diarylamino group and the porphyrin core that makes the IPCE spectra broader and red-shifted compared to a porphyrin ring bearing only an aryl substituent. In addition, the diarylamino group attached at the *meso* position of the porphyrin core not only extends the absorption spectrally to a region of greater wavelength but also pushes the excited electrons spatially toward the TiO$_2$ film for an improved charge separation. Also diminished recombination between I$_3^-$ and conduction-band electrons was observed, because I$_3^-$ might attach to the positively charged diarylamino moiety far from the TiO$_2$ surface.

YD2
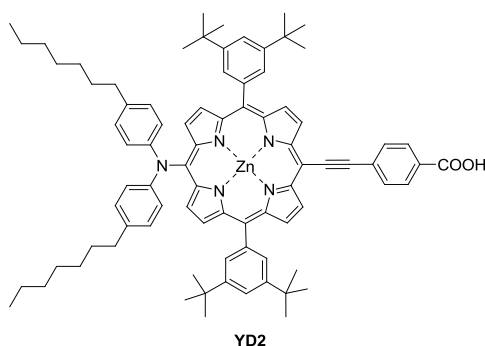
**Figure 6.28**

The best efficiency for a porphyrinic system have been reached newly by Yella et al. with the structure **YD2Oc8** (Figure 6.29), which incorporates two octyloxy groups in the orto positions of each *meso*-phenyl ring that producing a striking amelioration of the photo-induced charge separation in DSCs using Co(II/III)tris(bipyridyl)–based redox electrolyte. High PCE values reaching 11.9% have been achieved with this molecular photovoltaic system, which produces a $V_{oc}$ of 965 mV, a $J_{sc}$ of 17.3 mA/cm$_2$, and a fill factor (FF) of 0.71 under standard AM 1.5 sunlight at 995 W/m$_2$ intensity.



YD2Oc8
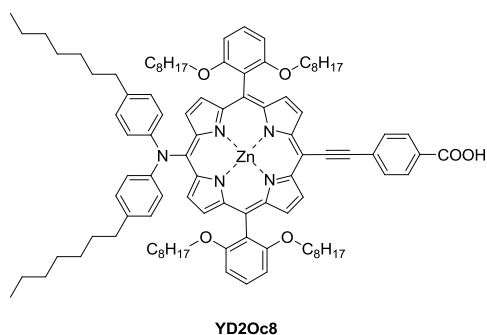
**Figure 6.29**

## 6.3   CONCLUSION

Summarizing the state of the art of metal-based complex, it's clear that Ru complexes, still remain among the best performant dye, but their efficiency have been reached and recently also overcame by porphyrinic dye. In these years for both a great research work have been done to optimize the structures and improve the efficiency of the dye.

In particular for Ruthenium complexes emerged that 4,4'-dicarboxylate-bipyridine ligand provides good anchoring to $TiO_2$ as well as good electronic coupling of the dye excited states with $TiO_2$ conduction band states. A second bipyridyl ligand can be modified with electron donor moieties to broaden the absorption spectra and to increase the molar extinction coefficient. The remaining ligands are usually isothiocyanate ligands (-NCS), which raise the HOMO energy of the complex, leading to a red-shifted absorption. For stability reasons, these monodentate ligands may need replacement. Some promising results have been obtained in this respect with cyclometalated ligands.

Concerning porphyrin, Zn-porphyrin result the most promising candidate, the better result have been reached substituting one of the *meso* position with the anchoring group, preferably linked to an aromatic or heteroaromatic system to elongate the conjugation and therefore red-shift the absorption spectra, and the others with bulky donor group to create an electron-enriched system, again to red-shift and widen the absorption band. It can be seen that terbutyl-phenyl group are commonly used to avoid dye aggregation, arylamine as strong donor group while to get more elettronrich and conjugate system thiophene rings are often used.

The very good result recently obtain with **Y2DOc8** is encouraging to continue the research of new judiciously tailored system and cell condition in order to achieve always increase efficiency.

## REFERENCES

[1] B. O'Regan, M. Grätzel, *Nature,* **1991**, *353*, 737.

[2] J. P. Paris, W. W. Brandt, *J. Am. Chem. Soc*., **1959**, *81*, 5001.

[3] F. E. Lytle, D. M. Hercules, *J. Am. Chem. Soc*., **1969**, 91, 253.

[4] F. Felix, J. Ferguson, H. U. Guedel, A. Ludi, *J. Am. Chem. Soc*., **1980**, *102*, 4096.

[5] D. B. Kuang, C. Klein, S. Ito, J. E. Moser, R. Humphry-Baker, N. Evans, F. Duriaux, C. Grätzel, S. M. Zakeeruddin, M. Grätzel, *Ad*V*. Mater.* **2007**, *19*, 1133.

[6] D. Kuang, S. Ito, B. Wenger, C. Klein, J.-E. Moser, R. Humphry-Baker, S. M. Zakeeruddin, M. Grätzel, *J. Am. Chem. Soc.* **2006**,*128*, 4146.

[7] A. Hagfeldt, G. Boschloo, L. Sun, L. Kloo, H. Pettersson, *Chem. Rev.* **2010,** *110,* 6595.

[8] M. D. Archer, A. J. Nozik, *Nanostructured and photoelectrochemical systems for solar photon conversion,* **2003**.

[9] K. Kalyanasundaram, M. Grätzel, *Coord. Chem.,* **1998**, *77,* 347.

[10] H. J. Snaith, C. S. Karthikeyan, A. Petrozza, J. Teuscher, J. E. Moser, M. K. Nazeeruddin, M. Thelakkat, M. Grätzel, *J. Phys. Chem. C* **2008**, *112*, 7562.

[11] S. Ardo, G. J. Meyer, *Chem. Soc.*, **2009**, *38*, 115.

[12] M. K. Nazeeruddin, A. Kay, I. Rodicio, R. Humphry-Baker, E. Mueller, P. Liska, N. Vlachopoulos, M. Grätzel, *J. Am. Chem. Soc.*, **1993**, *115*, 6382.

[13] M. K. Nazeeruddin, S. M. Zakeeruddin, R. Humphry-Baker, M. Jirousek, P. Liska, N. Vlachopoulos, V. Shklover, C. H. Fischer, M. Grätzel, *Inorg. Chem.* **1999**, *38*, 6298.

[14] M. K. Nazeeruddin, P. Pechy, M. Grätzel, *Chem. Commun.* **1997**, *18,* 1705.

[15] M. K. Nazeeruddin, P. Pechy, T. Renouard, S. M. Zakeeruddin, R. Humphry-Baker, P. Comte, P. Liska, L. Cevey, E. Costa, V. Shklover, L. Spiccia, G. B. Deacon, C. A. Bignozzi, M. Grätzel, *J. Am. Chem. Soc.,* **2001**, *123*, 1613.

[16] P. Wang, S. M. Zakeeruddin, I. Exnar, M. Grätzel, *Chem. Commun* **2002**, 2972.

[17] P. Wang, S. M. Zakeeruddin, R. Humphry-baker, J. E. Moser, M.Grätzel, *Ad*V*. Mater. (Weinheim, Ger.),* **2003**, *15*, 2101.

[18] P. Wang, S. M. Zakeeruddin, J. E. Moser, M. K. Nazeeruddin, T. Sekiguchi, M. Grätzel, *Nat. Mater.,* **2003**, *2*, 498.

[19] P. Wang, S. M. Zakeeruddin, J. E. Moser, R. Humphry-Baker, P. Comte, V. Aranyos, A. Hagfeldt, M. K. Nazeeruddin, M. Grätzel, *Ad*V*. Mater.,* **2004**, *16*, 1806.

[20] S. A. Haque, S. Handa, K. Peter, E. Palomares, M. Thelakkat, J. R. Durrant, *Angew. Chem. Int. Ed.* **2005**, *44*, 5740.

[21] S. Handa, H. Wietasch, M. Thelakkat, J. R. Durrant, S. A. Haque, *Chem. Commun.* **2007**, 17, 1725.

[22] J. H. Yum, I. Jung, C. Baik, J. Ko, M. K. Nazeeruddin, M. Grätzel, *Energy En*V*iron. Sci.,* **2009**, *2*, 100.

[23] C.-Y. Chen, S.-J. W., C.-G. Wu, J.-G. Chen, K.-C. Ho, *Angew. Chem, Int. Ed.* **2006**, *45*, 5822.

[24] C.-Y. Chen, S.-J. Wu, J.-Y. Li, C.-G. Wu, J.-G. Chen, K.-C. Ho, *Ad*V*. Mater. (Weinheim, Ger.)* **2007**, *19*, 3888.

[25] C.-Y. Chen, J.-G. Chen, S.-J. Wu, J.-Y. Li, C.-G. Wu, K.-C. Ho, *Angew. Chem., Int. Ed.* **2008**, *47*, 7342.

[26] J.-K. Lee, M. Yang, *Materials Science and Engineering B,* **2011***,17,6 1142.*

[27] Y.M. Cao, Y. Bai, Q.J. Yu, Y.M. Cheng, S. Liu, D. Shi, F.F. Gao, P. Wang, J. *Phys. Chem. C,* **2009**, *11,3* 6290.

[28] T. Bessho, E. Yoneda, J. H. Yum, M. Guglielmi, I. Tavernelli, H. Imai, U. Rothlisberger, M. K. Nazeeruddin, M. Grätzel, *J. Am.Chem. Soc.,* **2009**, *131*, 5930.

[29] S. Ferrere, B. A. Gregg, *J. Am. Chem. Soc.*, **1998**, *120*, 843.

[30] D. Kuciauskas, J. E. Monat, R. Villahermosa, H. B. Gray, N. S. Lewis, J. K. McCusker, *J. Phys. Chem. B,* **2002**, *106*, 9347.

[31] G. Sauve, M. E. Cass, G. Coia, S. J. Doig, I. Lauermann, K. E. Pomykal, N. S. Lewis, *J. Phys. Chem. B,* **2000**, *104*, 6821.

[32] G. Sauve, M. E. Cass, S. J. Doig, I. Lauermann, K. Pomykal, N. S. Lewis, *J. Phys. Chem. B,* **2000**, *104*, 3488.

[33] S. Altobello, R. Argazzi, S. Caramori, C. Contado, S. Da Fre, P. Rubino, C. Chone, G. Larramona, C. A. Bignozzi, *J. Am. Chem.Soc.,* **2005**, *127*, 15342.

[34] M. Alebbi, C. A. Bignozzi, T. A. Heimer, G. M. Hasselmann, G. J Meyer*,. J. Phys. Chem. B,* **1998**, *102*, 7577.

[35] A. Islam, H. Sugihara, K. Hara, L. Pratap Singh, R. Katoh, M. Yanagida, Y. Takahashi, S. Murata, H. Arakawa, *New J. Chem.*, **2000**, *24*, 343.

[36] A. Islam, H. Sugihara, K. Hara, L. P. Singh, R. Katoh, M. Yanagida, Y. Takahashi, S. Murata, H. Arakawa, G. Fujihashi, *Inorg. Chem.*, **2001**, 40, 5371.

[37] N. Alonso-Vante, J.-F. Nierengarten, J.-P. Sauvage, *J. Chem. Soc.,Dalton Trans.* **1994**, *11*, 1649.

[38] B. C. O'Regan, I. Lopez-Duarte, M M. V.artinez-Diaz, A. Forneli, J. Albero, A. Morandeira, E. Palomares, T. Torres, J. R. Durrant, *J. Am. Chem. Soc.* **2008**, *130*, 2906.

[39] X. Li, H. Wang and H. Wu, in Structure and Bonding: Functional Phthalocyanine Molecular Materials, ed. J. Jiang, Springer, Heidelberg, **2010**, vol. 135, pp. 229.

[40] M. V. Martínez-Díaz , M. Ince Monatsh Chem **2011**, *142*, 699.

[41] M. K. Nazeeruddin, R. Humphry-Baker, M. Grätzel, B. A. Murrer, *Chem. Commun.* **1998**, *6*, 719.

[42] M. K. Nazeeruddin, R. Humphry-Baker, M. Grätzel, D. Wohrle, G. Schnurpfeil, G. Schneider, A. Hirth, N. Trombach, *J. Porphyrins Phthalocyanines* **1999**, *3*, 230.

[43] B. C. O'Regan, I. Lopez-Duarte, M. V. Martinez-Diaz, A. Forneli, J. Albero, A. Morandeira, E. Palomares, T. Torres, J. R. Durrant, *J. Am. Chem. Soc.,* **2008**, *130*, 2906.

[44] E. Palomares, M. V. Martinez-Diaz, S. A. Haque, T. J. R. Torres,Durrant, *Chem. Commun.,* **2004**, *18*, 2112.

[45] A. Morandeira, I. Lopez-Duarte, M. V. Martinez-Diaz, B. 'Regan, C. Shuttle, N. A. Haji-Zainulabidin, T. Torres, E. Palomares, J. R. Durrant, *J. Am. Chem. Soc.,* **2007**, *129*, 9250.

[46] P. Y. Reddy, L. Giribabu, C. Lyness, H. J. Snaith, C. Vijaykumar, M. Chandrasekharam, M. Lakshmikantam, J. H. Yum, K. Kalyanasundaram, M. Grätzel, M. K. Nazeeruddin, *Angew. Chem.Int. Ed.,* **2007**, *46*, 373.

[47] S. Cherian, C. C. Wamser, *J. Phys. Chem. B,* **2000**, *104*, 3624.

[48] Y. Tachibana, S. A. Haque, I. P. Mercer, J. R. Durrant, D. R. Klug, *J. Phys. Chem. B,* **2000**, *104*, 1198.

[49] F. Fungo, L. A. Otero, L. Sereno, J. J. Silber, E. N. Durantini, *J. Mater. Chem.,* **2000**, *10*, 645.

[50] A. Hagfeldt, G. Boschloo, L. Sun, L. Kloo, H. Pettersson, *Chem. Rev*. **2010**, *110*, 6595.

[51] W. M. Campbell, K. W. Jolley, P. Wagner, K. Wagner, P. J. Walsh, K. C. Gordon, L. Schmidt-Mende, M. K. Nazeeruddin, Q. Wang, M. Grätzel, D.L. Officer, *J.Phys. Chem. C Letters,* **2007**, *111*, 11760.

[52] A. Kay, M. Grätzel, *J. Phys. Chem.,* **1993**, *97*, 6272.

[53] T. L. Ma, K. Inoue, H. Noma, K. Yao, E. Abe, *J. Photochem. Photobiol. A,* **2002**, *152*, 207.

[54] T. Ma, K. Inoue, K. Yao, H. Noma, T. Shuji, E. Abe, J. Yu, X. Wang, B. Zhang, *J. Electroanal. Chem.,* **2002**, *537*, 31.

[55] F. Odobel, E. Blart, M. Lagree, M. Villieras, H. Boujtita, N. El Murr, S. Caramori, C. A. Bignozzi, *J. Mater. Chem.,* **2003**, *13*, 502.

[56] M. K. Nazeeruddin, R. Humphry-Baker, D. L. Officer, W. M. Campbell, A. K. Burrell, M. Grätzel, *Langmuir,* **2004**, *20*, 6514.

[57] Q. Wang, M. Campbell Wayne, E. Bonfantani Edia, W. Jolley Kenneth, L. Officer David, J. Walsh Penny, K. Gordon, R. Humphry-Baker, M. K.Nazeeruddin, M. Grätzel, *J Phys Chem B,* **2005**, *109*, 15397.

[58] W. M. Campbell, K. W. Jolley, P. Wagner, K. Wagner, P. J. Walsh, K. C. Gordon, L. Schmidt-Mende, M. K. Nazeeruddin, Q. Wang, M. Grätzel, D. L. Officer, *J. Phys. Chem. C* **2007**, *111*, 11760.

[59] W. M. Campbell, A. K. Burrell, D. L. Officer, K. W. Jolley *Coordination Chemistry Reviews,* **2004**, *248, 1363.*

[60] L. Schmidt-Mende, W. M. Campbell, Q. Wang, K. W. Jolley, D. L. Officer, M. K. Nazeeruddin, M. Grätzel, *ChemPhysChem,* **2005**, *6*, 1253.

[61] S. Eu, S. Hayashi, T. Umeyama, A. Oguro, M. Kawasaki, N. Kadota, Y. Matano, H. Imahori, *J. Phys. Chem. C,* **2007**, *111*, 3528.

[62] A. Forneli, M. Planells, M. A. Sarmentero, E. Martinez-Ferrero, B. C. O'Regan, P. Ballester, E. Palomares, *J. Mater. Chem.,* **2008**,*18*, 1652.

[63] J. K. Park, H. R. Lee, J. P. Chen, H. Shinokubo, A. Osuka, D. Kim, *J. Phys. Chem. C,* **2008**, *112*, 16691.

[64] C.-W. Lee, H.-P .Lu, C.-M. Lan, Y.-L. Huang, Y.-R. Liang, W.-N. Yen, Y.-C. Liu, Y.-S. Lin, R. W. Diau, -G. C.-Y. Yeh, *Chem.sEur. J.,* **2009**, *15*, 1403.

[65] J.-C. Chang, C.-J. Ma, G.-H. Lee, S.-M. Peng, C.-Y. Yeh, Dalton. Trans., **2005**, *18*, 1504.

[66] S. Kim, J. K. Lee, S. O. Kang, J. Ko, J.-H. Yum, S. Fantacci, F. D. Angelis, D. D. Censo, M. K. Nazeeruddin, M. Grätzel, *J. Am. Chem. Soc*., **2006**, *128*, 16701.

[67] C.-Y. Lin, C.-F. Lo, L. Luo, H.-P. Lu, C.-S. Hung, E. W.-G. Diau, *J. Phys. Chem. C,* **2009**, *113*, 755.

[68] Y. J. Liu, N. Xiang, X. M. Feng, P. Shen, W. P. Zhou, C. Weng, B. Zhao, S. T. Tan, *Chem. Commun.,* **2009**, *18*, 2499.

[69] S.-L. Wu, H.-P. Lu, H.-T. Yu, S.-H. Chuang, C.-L. Chiu, C.-W. Lee, E. W.-G. Diau, C.-Y. Yeh, *Energy Environ. Sci.,* **2010**, *3*, 949.

[70] T.Bessho, S.M. Zakeeruddin, C.-Y .Yeh, E. W.-G. Diau, M. Grätzel, Angewandte Chemie International Edition*,* **2010**, *49(37)*, 6646.
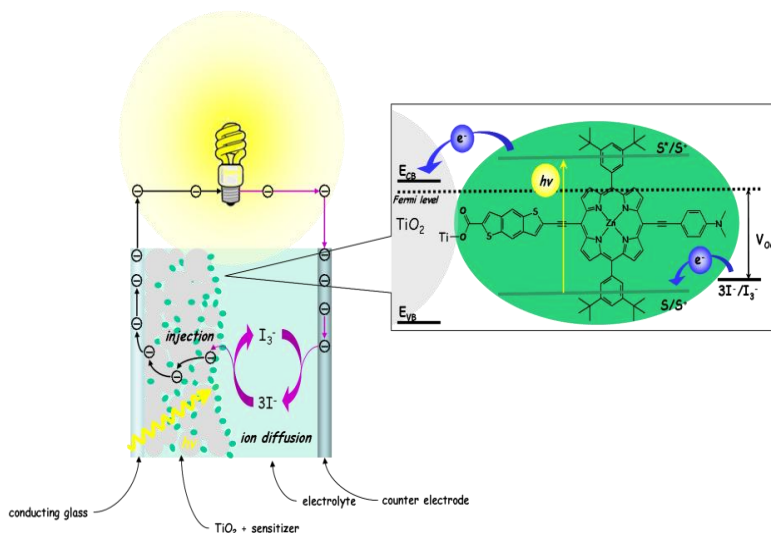
# NOVEL BDTs-BASED PORPHYRIN COMPLEXES



*Image by courtesy of Alessio Orbelli Biroli*

## 7.1  INTRODUCTION

As reviewed before, the intrinsic advantages of porphyrin-based dyes are their rigid, highly conjugate molecular structures characterized by large absorption coefficients in the visible region and many reaction sites available for functionalization, four *meso* and eight β positions. Moreover, these systems possess charge-transfer kinetics indistinguishable from those of ruthenium polypyridyl complexes and undergoes facile reduction and oxidation processes. In addition, their optical, photophysical, and electrochemical properties can be systematically tailored by the peripheral substitutions and/or inner metal complexations.

Porphyrins, however, still have limited light absorption, poor matching to solar light distribution, and consequently possess a non ideal value of short circuit current.

At present with the aim to achieve higher η, the strategy used have been: elongate the π-system and lower the symmetry of the macro-cycle, in order to achieve a significantly broadened Soret-band and a red-shifted Q-band absorptions.

Aiming to lower the symmetry of the system, the incorporation of ''push-pull'' porphyrin (D–π–A, D = donor, π = bridge, A = acceptor) derivatives in DSSCs has led to remarkable progress in this family of sensitizers.[1,2]

Porphyrin based push–pull dyes, indeed, show large conjugation and strong electronic interaction between D and A chromophores as previously reported,[3, 4] easy directioning of electron injection, reduced aggregation on a $TiO_2$ surface, tuning of the excited state level and increased electron coupling between the sensitizers and the semiconductor.

As seen in **chapter 3**, in the field of metal free dyes, the panorama of acceptors, donors and π-bridges investigated is really vast, and numerous are the combinations employed. On the contrary, not very much has been tried in the development of new push-pull porphyrinic systems and the field is quite open.

Within this context, the present Ph. D. research project has focused on the synthesis of new phoprhyrinic dyes characterized by a Donor-Spacer-Acceptor (D-π-A) structure, in which the novelty is represented by the presence of benzo-condensed thiophene units

(benzo[1,2-*b*:4,5-*b'*]dithiophene, **BDT₁**, and benzo[1,2-*b*:4,3-*b'*]dithiophene, **BDT**) as π

spacer. In **chapter 4** properties and synthesis of these systems are discussed, here we

exploited these systems to extend the conjugation of a tailored porphyrin with the aim

to improve its photophysical properties and investigate its efficiency in a DSSCs.

The work has been carried out in collaboration with the research group of Prof. Pizzotti.

## 7.2 AIM OF THE WORK

Encouraged by the results obtained in this field in recent literature, we designed a series

of unsymmetrical D–π–A porphyrin based dyes with the general structure shown in

Figure 7.1 to be used for dye sensitized solar cells (DSSCs).

These porphyrin derivatives are differently functionalized in 5,15 and 10,20 *meso*

positions.

In positions 5 and 15 aromatic rings bearing bulky groups are present, to avoid

aggregation on the semiconductor surface,[5] which could drastically reduce the dye light-

harvesting by a filtering effect.[6] In 10,20 *meso* positions the structure presents two π-

delocalized aromatic systems with opposite electronic properties, one electron-

withdrawing (A), the other electron-donating (D).



Ar = BDT₁, BDT, Ph

A = COOH

D = -CH=N-NR₂, NMe₂

M = Zn⁺⁺
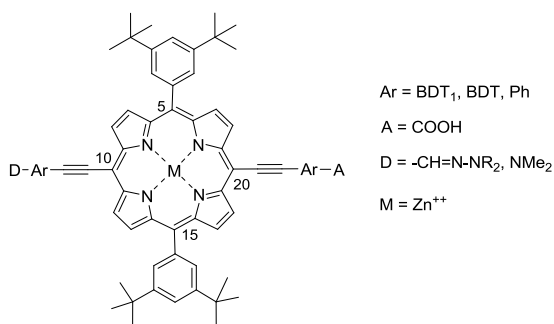
**Figure 7.1**

It has been clarified that the position and nature of the bridge (π), connecting the

porphyrin ring to the acceptor and donor groups has significant influences on the

spectral, electrochemical, and photovoltaic properties of these sensitizers. In almost all

the porphyrinic structures applied in DSSCs, the substituents at the meso-positions are

phenyl units, but in recent years, interest is growing in the smaller five-membered 2-

thienyl rings.[7] It offers reduced steric hindrance compared with the larger six-membered 4-phenyl ring and in addition the 2-thienyl group lacks one *o*-phenyl-H to β-pyrrole-H interaction which allows for greater easy rotation of the thien-2-yl porphyrins, favoring a coplanar arrangement.[8] Moreover, it is known that the use of thiophenyl units with varied substituents as π-bridges for linking the donors (D) and the anchoring-acceptor groups (A), usually can induce a bathochromic shift, an intensification of the light absorptivity and an increased lifetime of the excited-state.[8] However, recently, in research on porphyrin-based push–pull chromophores for DSSCs applications, bridges of the ethyne type have attracted great interest.[9,10,11] Indeed they allow efficient conjugation and strong electronic interaction between the porphyrinc core and the linked unit, provide a well-defined and rigid structural arrangement[12] (as the acetylene is linear, it cannot twist out of conjugation with the porphyrin).[13] This might facilitate electron transfer from the excited dye to the $TiO_2$ surface, and therefore lead to an improved efficiency of energy conversion.

In this context, our approach to the enhancement of porphyrin dyes' absorption in the visible region is to expand the π-conjugation system, using ethynyl functionalized benzo-condensed thiophene as π-bridge (or spacer) to link the donor or the acceptor part, with the intention of obtaining a red shift and a broadening of both Soret and Q bands.


## 7.2.1 DYE DESIGN

After an extensive study of the literature and assisted by preliminary time dependent density functional theory (TD-DFT) calculations, done in collaboration with the Angelis' group, we designed the synthesis of several novel benzodithiophene-based dye sensitizers. (Figure 7.2)
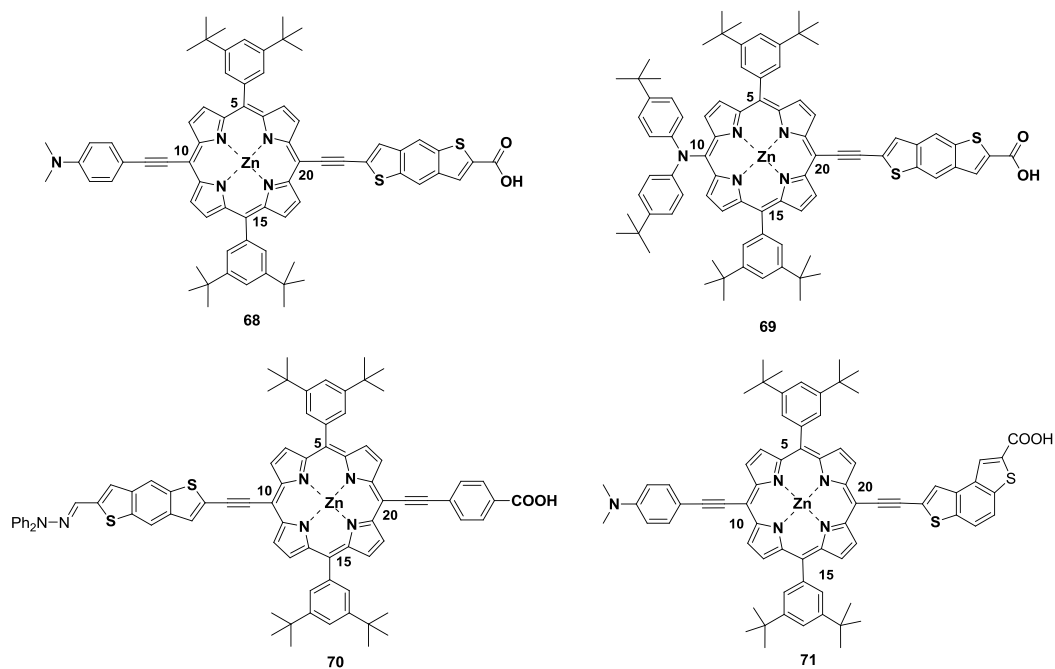
**Figura 7.2**

All of the structures bear in positions 5 and 15 3,5-di-*tert*-butylphenyl groups but different acceptor and donor groups. The main novelty introduced in this new porphyrins is the use of the two benzodithiophene isomers (**BDT** and **BDT₁**) as heteroaromatic π-bridge for the linkage of A or D.

In particular, dye **68** and **69** present the carboxylic acid function as the acceptor-anchoring group, linked to the porphyrin core in position 20 through an ethynyl-benzo[1,2-b:4,5-b']dithiophene conducting bridge. In addition, to increase the electron-donating ability of the porphyrin ring, a *N,N*-dimethylamino-phenylethynyl or a bis(4-*tert*-butylphenyl)amine are inserted in position 10. Dye **70,** following the same building concept, bears a 4-carboxy phenylethynyl as acceptor-anchoring group and the new **BDT₁** derivative 6-ethynylbenzo[1,2-b:4,5-b']dithiophen-2-*N,N*-diphenylhydrazone as donor. Finally, dye **71** is an analogue of **68** in which the benzodithiophene isomer **BDT** (benzo[1,2-b:4,3-b']dithiophene) is employed.

These compounds have been judiciously designed to evaluate the potentiality of **BDT** and **BDT₁** as conjugate spacer in the donor and acceptor part of the push-pull system.

## 7.2.1.1 THEORETICAL INVESTIGATIONS

Before dye synthesis, to gain insight into the molecular and electronic structures of the ground and excited states of these newly designed dyes, theoretical calculations have been performed through Density Functional Theory, DFT, and its extension to the Time-Dependent formulation, TDDFT, as implemented in Gaussian program suite.[14] DFT ground state geometries were optimized by using the B3LYP exchange-correlation functional,[15] along with a 6-311G* basis set. For sake of simplicity, the *tert*-butyl groups linked to the phenyl groups have been replaced by hydrogen atoms and a $C_s$ symmetry was used for geometry optimizations. All the calculations have been performed by the Gaussian 03 program package.[16] The non-equilibrium C-PCM solvation model[17,18] was employed for TDDFT calculations in solution.

Between the series of sensitizers designed we started to investigate **68** and **71**. The optimized molecular structures of the dyes are reported in Figure 7.3.
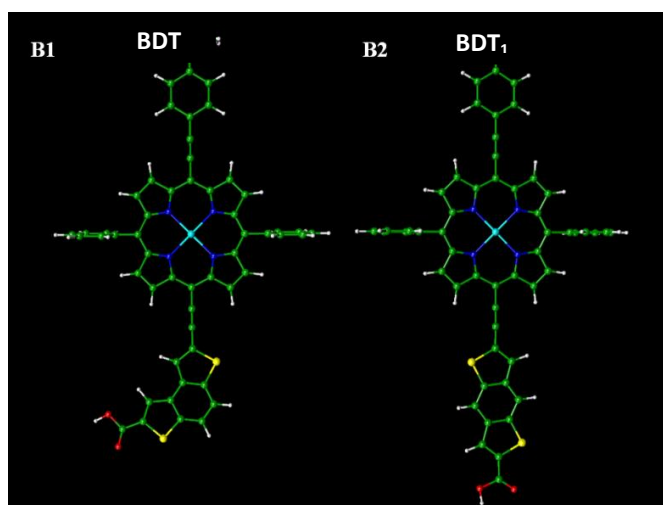


**Figure 7.3**

The geometries of the different sensitizers are similar and characterized by a planar donor-acceptor arrangement. The main results, in terms of molecular orbitals diagram, are reported in Figures 7.4a and b for **BDT** and **BDT$_1$**, respectively.
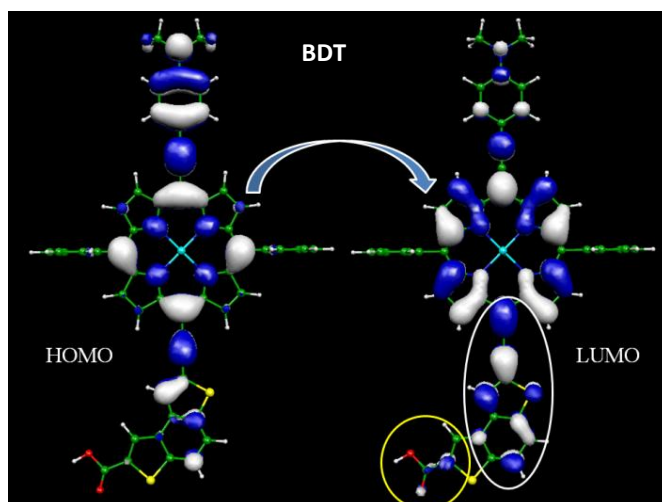
**Figure 7.4a**
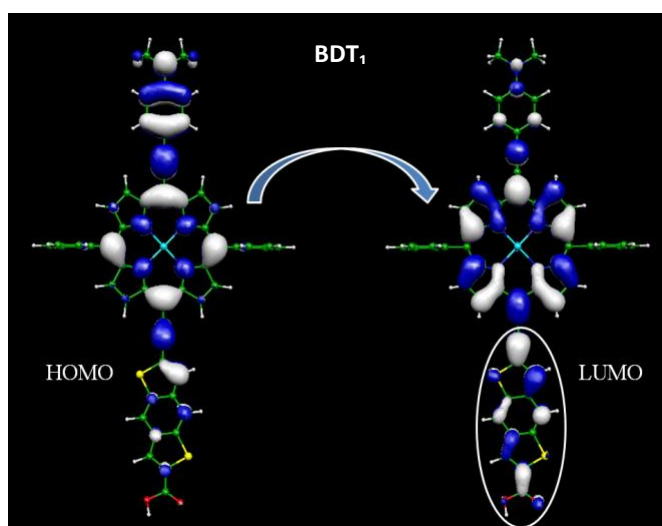


**Figure 7.4b**

It can be noticed that the HOMOs and LUMOs have a similar character in **BDT** and **BDT$_1$**. The HOMO is in all cases localized on the donor moiety of the push-pull system and partly on the porphyrin macrocycle, while the LUMO extends from the porphyrin macrocycle to the acceptor moiety bearing the carboxylic acid anchoring group. The main difference is that while in **BDT$_1$**, the LUMO, which represents the final states in the lowest and more relevant excited state, results delocalized across the benzodithiophene

moiety with sizable contribution on the anchoring COOH group, in **BDT** such a conjugation is suppressed. However in both the directional and strong electron transfer along the push-pull system from the donor -NMe2 is confirmed. In addition for **BDT$_1$** we calculate the lowest excited state at 669 nm with an oscillator strength of 1.38 a.u. This makes **BDT$_1$** the most interesting candidate for application in DSSCs. We finally notice that both **BDT** and **BDT$_1$** show a similar alignment of the energy levels with the TiO$_2$ and I$^-$/I$_3^-$ electrolyte system.

We mention, however, that our data do not take into account the possible effect of the interaction of the dye with the TiO$_2$ surface and in particular of the deprotonation due to the anchoring, obviously controlled by the strength of the carboxylic group. Such effects could lead to slightly different values for the excited state energies when absorbed on TiO$_2$.

By combining the ground and excited state energies calculated for dyes, an estimate of the excited state oxidation potential for the dyes can be obtained according to a procedure developed by some of us.[19] The excited state oxidation potentials calculated for dyes **68** and **71** can thus be compared to the energy levels of the TiO$_2$ conduction band edge calculated for a TiO$_2$ cluster of nanometric dimensions (Figure 7.5a).[20]

The calculated energy level of HOMO and LUMO of BDT$_1$ dye are reported in figure 7.5a together with the energy level of the TiO$_2$ conduction band. For a direct comparison are also reported the HOMO and LUMO levels of a similar Zn$^{II}$-porphyrin **P** (Figure 7.5b), bearing a simple phenyl as spacer between the porpyrinic core and the –COOH acceptor group, recently published by us.[21] The dyes have an excited state oxidation potential substantially higher than the TiO$_2$ conduction band, implying thus favorable energetics for electron injection.
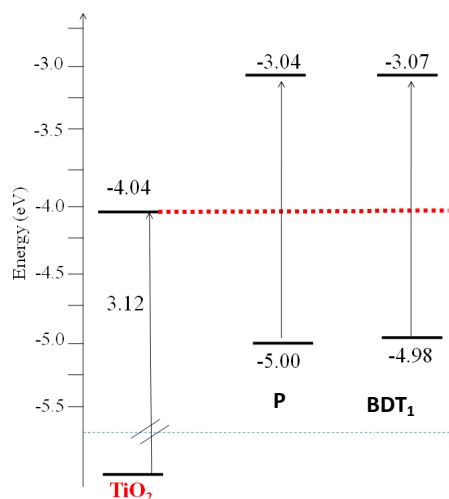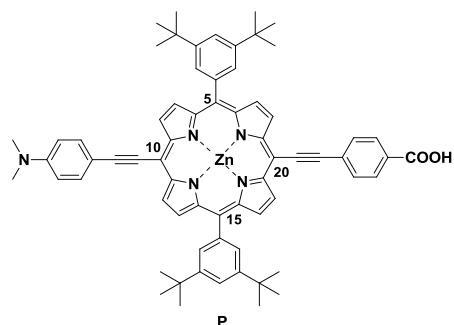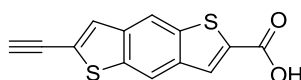
Figure 7.5a



Figure 7.5b

In spite of the discouraging prediction for system **BDT,** we decided to synthesize also the structure **71** to verify the reliability of the calculation method for this kind of structure.

## 7.3 SYNTHESIS AND CHARACTERIZATION

In order to synthesize the asymmetrical push-pull Zn(II) porphyrinates **68**, **69**, **70** and **71** reported in Figure 7.2, the strategy envisaged is a statistical two step approach. Starting from the symmetrical [5,15-diiodo-10,20-bis(3,5-di-*tert*-butylphenyl)porphyrinate]Zn(II) (**72**)[22] it is possible to selectively introduce, by the Sonogashira reaction,[23] first the donor moiety and then the acceptor moiety.

We began our investigation from dye **68**, that bears 4-ethynyl-*N,N*-dimethylaniline as donor and 6-ethynyl-benzo[1,2-b:4,5-b']dithiophen-2-carboxylic acid **72** as acceptor. (Figure 7.6) The former has been synthesized according to the literature[24] while the **BDT₁** derivative is new and its synthesis it has been object of an intensive study in our laboratories.



**73**

**Figure 7.6**

It has to be underlined indeed, that only few examples of mono-substituted or symmetrically di-substituted **BDT$_1$** systems have been reported in literature, while almost nothing is known about the introduction of two different substituents in 2 and 6 positions. This is a very important goal in view of inserting the **BDT$_1$** systems into porphyrin skeleton.

## 7.3.1    SYNTHESIS    OF    6-ETHYNYLBENZO[1,2-B:4,5-B']DITHIOPHEN-2-CARBOXYLIC ACID

In principle the synthesis of the target derivative **73** (Figure 7.6) can be run following two different strategies. The first involves the preparation of the 2,6-dibromo or diodo derivative of **BDT$_1$** (**74-75**), then the selective substitution of one halogen atom by a carboxylic group, a Sonogashira reaction for the introduction of the TMS protected triple bond and finally the concomitant hydrolysis of the ester group and TMS deprotection (Scheme 7.1)
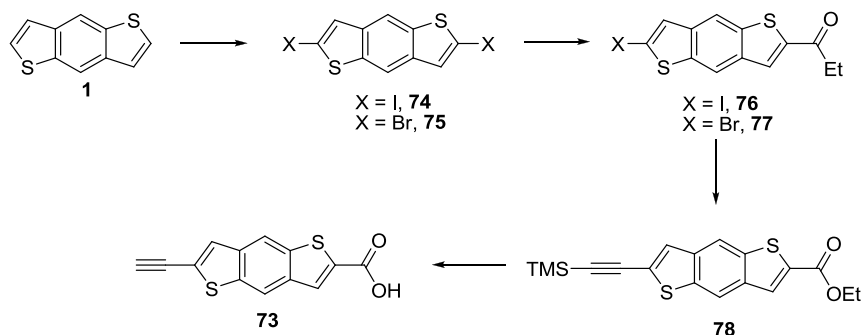


**Scheme 7.1**

In the second strategy, indeed, the first step is the functionalization of **BDT$_1$** in position 2 with the carboxylic group, then an halogen atom is introduced in position 6 for the subsequent Sonogashira reaction. (Scheme 7.2)

225
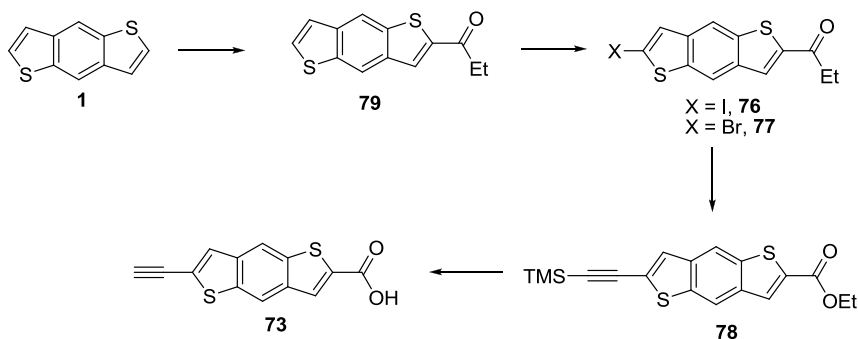
**Scheme 7.2**

We started to investigate the first strategy.

The two dihalogenated derivative of **BDT₁** are known in the literature, the dibromo **75** is prepared reacting **BDT₁** with NBS,[25] while the diiodo derivative **74** is prepared starting from the 2,6-bistrimethylsilyl benzodithiophene.

For simplicity, we decided to prepare first the 2,6-dibromo benzo[1,2-b:4,5-b']dithiophene **75**, performing the reaction according to the literature procedure: using NBS in DMF at 80° C the compound was obtained in 80% yield. Scheme 7.3
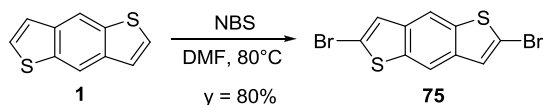


**Scheme 7.3**

Then the halogen substitution with the ethyl-cloroformate in the presence of *n*-BuLi was performed but without recovering the desired product.
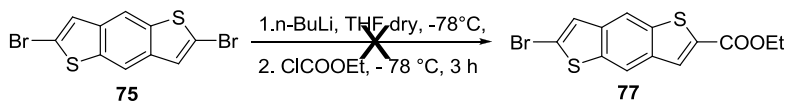


**Scheme 7.4**

We investigated also the possibilities of using the NIS for preparing the 2,6-diiodo benzo[1,2-b:4,5-b']dithiophene **74** following the same procedure used for **75** but the reaction didn't work. We therefore decided to begin the study of the second synthetic route proposed that was revealed to be the winner one.
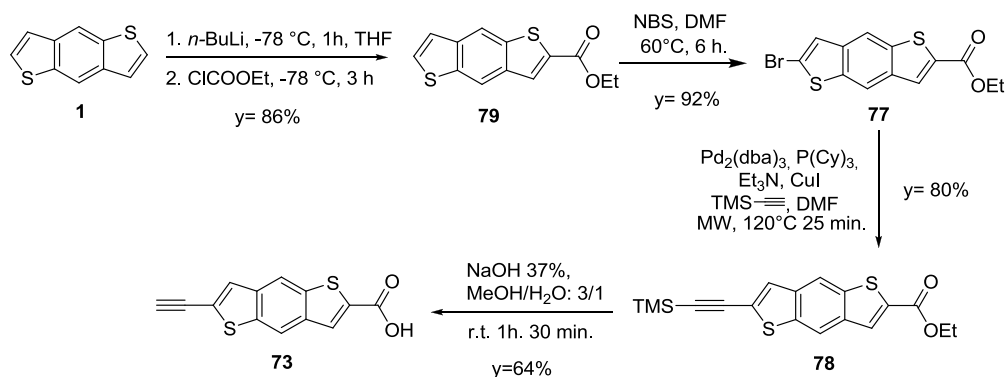
**Scheme 7.5**

The procedure involves at first the alkylation of **BDT₁ 1** with ethyl-chlorofomate in THF, in presence of *n*-BuLi, affording **79** in 86% yield. This derivative was then transformed in 6-bromo-benzo[1,2-b:4,5-b']dithiophen-2-ethoxycarbonyl **77** in 80% yield using NBS as brominating agent in DMF at 60 °C.

The insertion of the triple bond on compound **77** by a Sonogashira coupling with trimethylsilylacetilene was accomplished using Pd₂(dba)₃ as the catalyst, CuI as co-catalyst, diethylamine as a base, under microwave irradiation obtaining **78** (64% yield).

The last step was the hydrolysis of ethyl ester and TMS elimination; the treatment of **73** with 37% NaOH in MeOH/H₂O: 3/1 at room temperature for 1 h 30 min allowed both the reactions and gave the desired product **73** as yellow solid in 64% yield.

Is it known in the literature that in Sonogashira couplings the iodo derivatives are more reactive than the bromo ones. However, several reaction conditions were tried without success with the aim to obtain the 6-iodo-benzo[1,2-b:4,5-b']dithiophen-2-ethoxycarbonyl **76**. (Scheme 7.6)
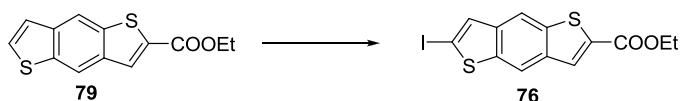


**Scheme 7.6**

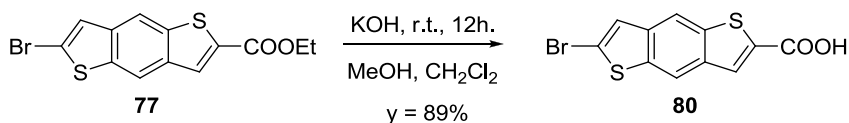| Attempt | Reaction condition | Results |
|---------|--------------------|---------|
| 1 | 1.*t*-BuLi, THF dry, -78°C, 2.I$_2$, - 78 °C, 3 h | Product in a complex mixture with starting material and other by-products |
| 2 | NIS, 0°C, DMF, then r.t, 3 h | No reaction |
| 3 | NIS, DMF, Δ | No reaction |
| 4 | NIS, DMF, 40°C, CF$_3$COOH (cat.) | Complex mixture of products |
| 5 | Ph(COOCF$_3$)$_2$, I$_2$, CCl$_4$, r.t. 3h | Complex mixture of products |

**Table 7.1**

In Table 7.1 are reported the conditions we tried. In particular, the reaction in the presence of NIS didn't give any product while with *t*-BuLi-I$_2$ and the more reactive mixture Ph(COOCF$_3$)$_2$/I$_2$, a complex mixture of products was recovered. It is interesting to note the completely different behavior of NIS with respect to NBS. Also heating for a long time, NIS is unreactive. As it can be seen, only the addition of a catalytic amount of trifluoroacetic acid that brings to the formation of the more electrophilic species CF$_3$COO$^-$ I$^{+26}$ lead to the obtainment of the desired compound in a complex mixture with by-products which was not possible to purify.

The insertion of the triple bond was also attempted in different conditions. We started investigating this reaction on the 6-bromo-benzo[1,2-b:4,5-b']dithiophen-2-carboxylic acid **80**, prepared by hydrolysis of compound **77** with KOH in MeOH and CH$_2$Cl$_2$ as the solvent at room temperature, affording the product in 89% yield. (Scheme 7.7)



**Scheme 7.7**

The Sonogashira reaction (scheme 7.8) was then performed on **80** using the reaction conditions reported in Table 7.2 without any positive result.
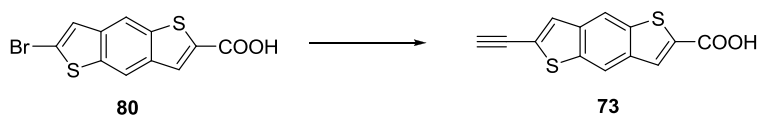
**Scheme 7.8**

| Attempt | Reaction Condition | Results |
|---------|--------------------|---------|
| 1 | Pd(OAc)$_2$, P(Cy)$_3$, Et$_3$N, CuI, C$_2$H$_2$, THF/CH$_3$CN, 45°C, 16h | No reaction |
| 2 | Pd(PPh$_3$)$_2$, P(Cy)$_3$, Et$_3$N, CuI, C$_2$H$_2$, THF/CH$_3$CN, 45°C, 16h | No reaction |

**Table 7.2**

Because of the failure of the above described reaction, we decided to investigate the use of microwave to carry out the coupling reaction, also increasing the temperature of the reaction and setting up the synthesis of **73** as shown in scheme 7.5. We worked on the ethyl ester moiety **77** for stability reason, due to the employment of more drastic reaction conditions.

So, it was not a trivial goal to set up the Sonogashira reaction on these substrates. However, eventually, by running the reaction under microwave irradiation with the catalytic system shown in Scheme 7.5 it was possible to isolate the desired product.

## 7.3.2  SYNTHESIS OF PORPHYRINE DERIVATIVE 68

The properly functionalized **BDT$_1$ 73** obtained was then reacted with the porphyrin derivative **81** prepared starting from the porphyrin **82** as depicted in Scheme 7.9. This part of the work has been done by Pizzotti's research group.
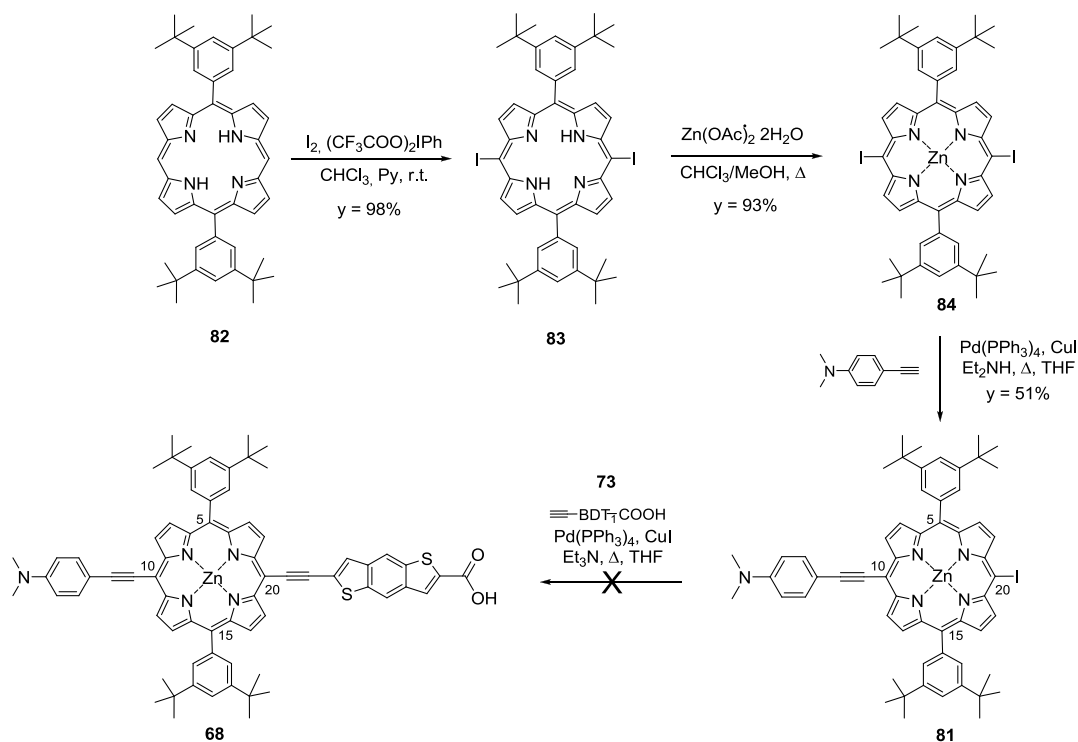
**Scheme 7.9**

The first step was the iodination of the porphyrin **82** with $I_2$ in presence of bistrifluoroacetoxy iodobenzene and pyridine in chloroform at room temperature affording compound **83** in 98%, then the Zn complexation was carried out using $Zn(OAc)_2$ at reflux in a mixture dichloromethane/methanol, giving **84** in 93% yield. The following step was the Sonogashira coupling with the donor moiety, performed using $Pd(PPh_3)_4$, CuI and diethylamine as catalytic system, heating at reflux in THF and obtaining **81** in 51%. The introduction of 6-ethynyl-benzo[1,2-b:4,5-b']dithiophen-2-carboxylic acid **73** was then tried in the same condition just described but using triethylamine instead of diethylamine. This reaction, due to the presence of free carboxylic function, didn't give good results, therefore we decided to prepare the 6-ethynyl-benzo[1,2-b:4,5-b']dithiophen-2-ethoxycarbonyl **85** starting from compound **78** and changing the deprotection condition. (Scheme 7.10)
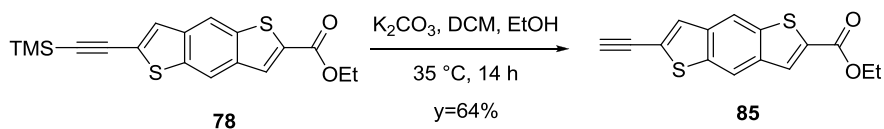
**Scheme 7.10**

The final step was then accomplished in presence of $K_2CO_3$ in DCM/MeOH to give the desired product **85** in 64% yield.

Finally this compound was coupled with the iodo-porphyrin **81**, synthesized as shown before, to give **86** in the conditions reported in Scheme 7.11.
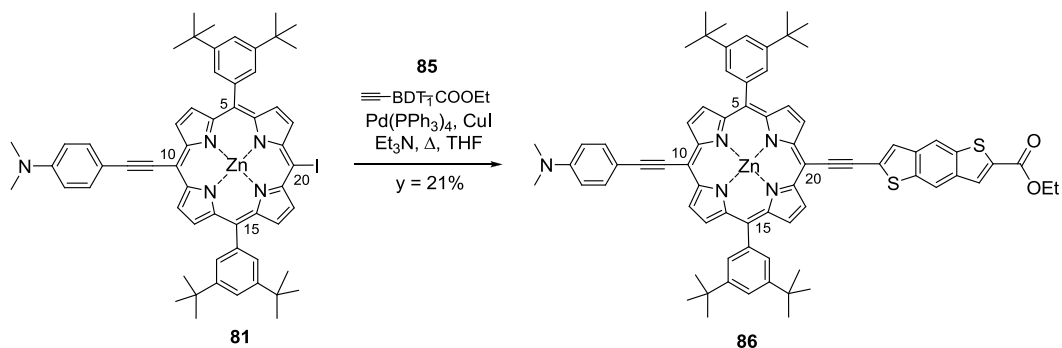


**Scheme 7.11**

The final step was the hydrolysis of the ethyl ester carried out with NaOH in presence of THF, EtOH and water under heating. The desired product is isolated in 69% yield. (Scheme 7.12)
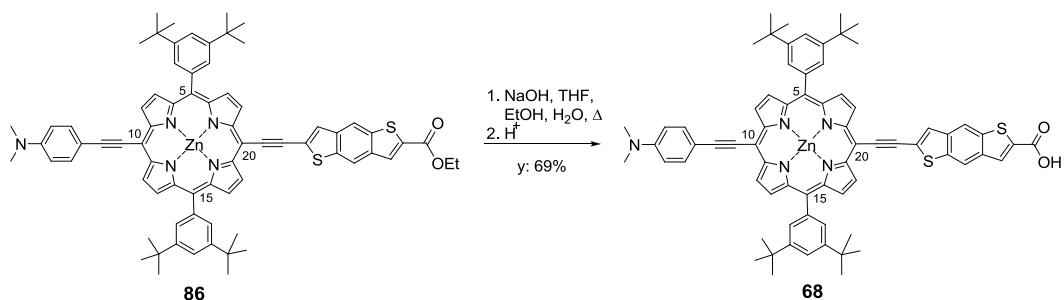


**Scheme 7.12**

The molecular structure of the dyes was confirmed by NMR, and MS characterizations. Reverse phase high performance liquid chromatography (HPLC) was employed to

establish the purity of the samples submitted to DSSC fabrication being, in all cases, higher than 98%.

## 7.4   WORK IN PROGRESS

At present the work is prosecuting with the synthesis of the porphyrin structure **3** that bears the **BDT$_1$** derivative **87** as donor substituent (D). (Figure 7.13)
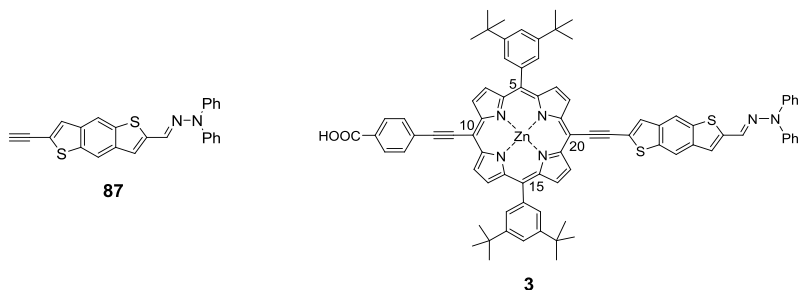


**Figure 7.7**

For the synthesis of **87** (Scheme 7.13) at first, benzodithiophene **1** was formylated with *N*-formylpiperidine in the presence of *n*-BuLi to give benzo[1,2-b:4,5-b']dithiophen-2-carboxyaldehyde **39** in 83% yield. This aldehyde derivative was then transformed in 6-bromo-benzo[1,2-b:4,5-b']dithiophen-2-carboxaldehyde **40** in 80% yield using NBS as brominating agent. To insert the triple bond a Sonogashira coupling on compound **40** with trimethylsilylacetilene was accomplished using Pd$_2$(dba)$_3$ as the catalyst, under microwave irradiation obtaining **41** (64% yield). Then, the formation of  hydrazone derivative was carried out reacting **41** at reflux with diphenyl-hydrazine in a EtOH-THF mixture, affording **88** in 38% yield. The final step was then the deprotection of the triple bond in presence of KOH and MeOH (**87**, 85% yield).
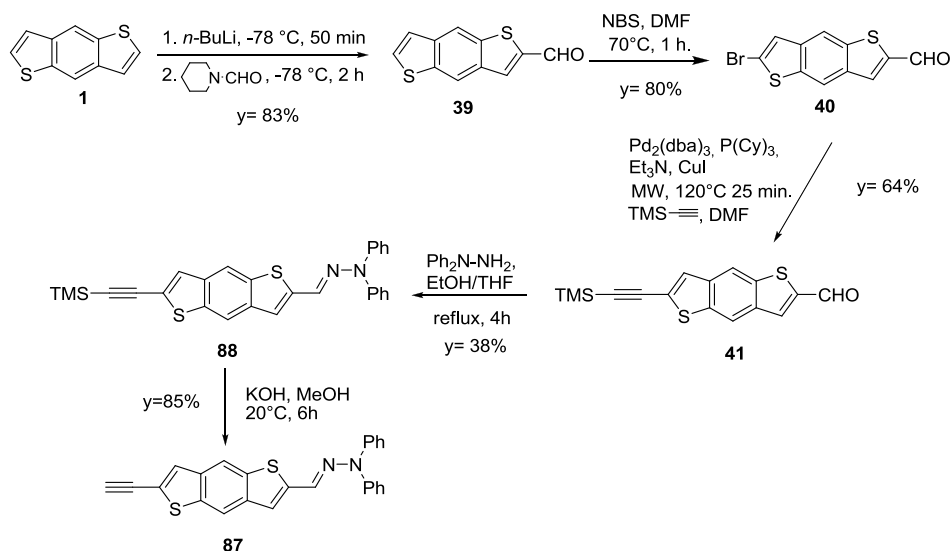
**Scheme 7.11**

The linkage of derivative **87** to the porphyrin core is currently under progress in Prof. Pizzotti's research group.

## 7.5 PHOTOPHYSICS, ELECTROCHEMISTRY AND SOLAR CELLS ASSEMBLING

### 7.5.1 OPTICAL PROPERTIES

In figure 7.8 are reported UV-vis spectra in THF of **68** (**a**) and, for comparison, of **P** (**b**) and of a meso diphenylporphyrin (**ZnBPP**, **c**). Porphyrin **68** and **P** show two absorption bands: the B band (or Soret band) at higher energy (460 nm) and a quite intense Q band at 699 nm, (Table 1) due to the HOMO-LUMO transition. Is notable the red-shift of **68** in respect of **P** in both the absorption band and that in comparison to **ZnBPP** (**c**), both the absorption bands of our push-pull systems are strongly red-shifted, moreover the Q band is greatly increased.

a



b



c
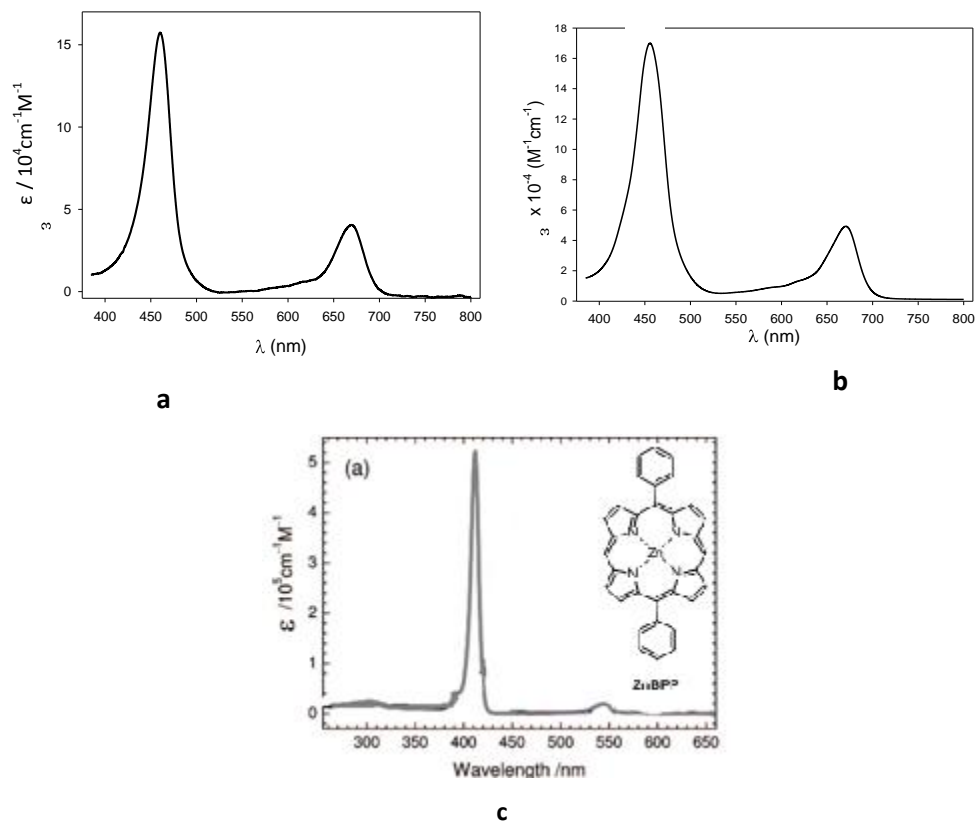
**Figure 7.8**

| porphyrin | $l_B$ (nm) | Log ($\varepsilon$) | $l_Q$ (nm) | Log ($\varepsilon$) |
|-----------|-----------|---------|-----------|---------|
| **68** | 460 | 5.20 | 699 | 4.6 |
| **P** | 456 | 5.23 | 671 | 4.69 |
| **ZnBPP** | 412 | 5.72 | 543 | 4.27 |

**Table 7.3**

## 7.5.2  ELECTROCHEMICAL PROPERTIES

Cyclic voltammetry (CV) on dye **68** has been performed at potential scan rate of 100 mV· s$^{-1}$ in deareated THF solution with 0.1 M tetrabutylammonium hexafluorophosphate TBA(PF$_6$) as supporting electrolyte. The voltammogram (Figure 7.9) shows three reversible process, the first oxidation process is related to the oxidation of the −NMe$_2$ group,[27] the other ones are correlated to the oxidation/reduction of the porphyrinic

234

core. The energy of the HOMO-LUMO gap and that of HOMO and LUMO levels are currently under investigation.
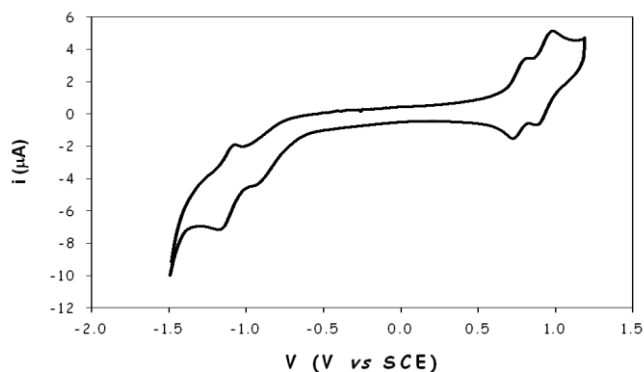


**Figure 7.9**

In a Grätzel cell for the electron transfer reactions at least 0.1-0.2 V is needed as driving force,[28] this implies that the dyes to ensure the working of the cell should have appropriate HOMO and LUMO levels. The LUMO have to be higher than the conduction band of the TiO$_2$ situated at -4.0 eV, while the HOMO have to be lower than the redox potential of the redox mediator (I$_3^-$/I$^-$) -4,80 eV. In particular, recently has been found that because an efficient regeneration occur the oxidation potential of a sensitizer must be about 0.5 V more positive than the I$_3^-$/I$^-$ redox potential.[29] Electrochemistry is therefore useful for preliminary screening of structures.

## 7.5.3 DEVICE FABRICATION AND CHARACTERIZATION

DSSC photoanodes were assembled from a single layer of TiO$_2$ paste ( about 6μm thick) on a FTO glass. Sensitization were carried out in the dark from a containing 8mM chenodeoxycholic acid solution of the dye in EtOH/THF 9:1. CDCA has mainly two function, blocking the access of I$_3^-$ to the TiO$_2$ surface where not occupied by dye molecules and therefore restricting recombination of the injected electrons, and reducing the dye adsorption amount and therefore refraining dye aggregation. The electrolyte solution used id PMII 0.6 M/LiI 0.1M/I$_2$ 0.02 M in methoxypropionitrile.

Before device fabrication further studies on dye supported on $TiO_2$ have been carried out. Herein are reported the UV-vis spectra of porphyrin **68** (Figure 7.10 a and b) and **P** (Figure 7.10c) absorbed on transparent $TiO_2$, performed in order to evaluate the light harvesting efficiency (LHE) that is calculable according to the formula LHE (l) = 1-T = 1- $10^{-Abs}$.
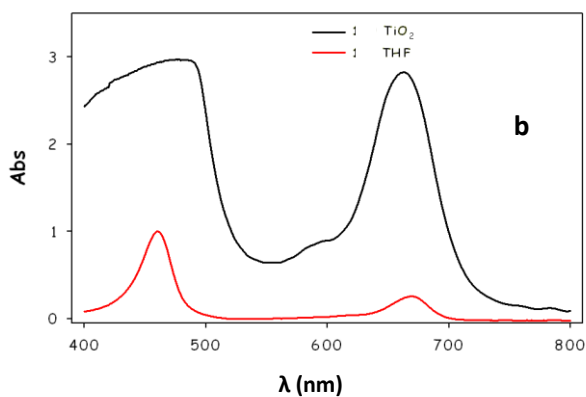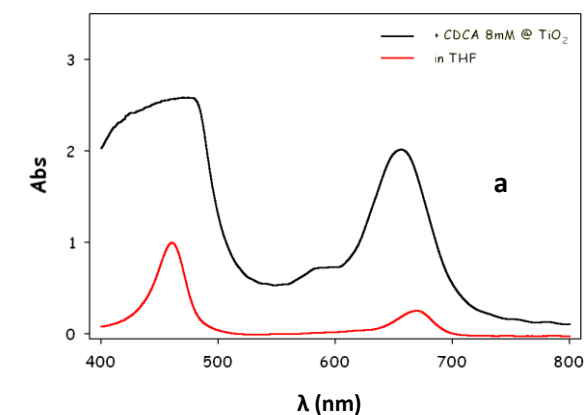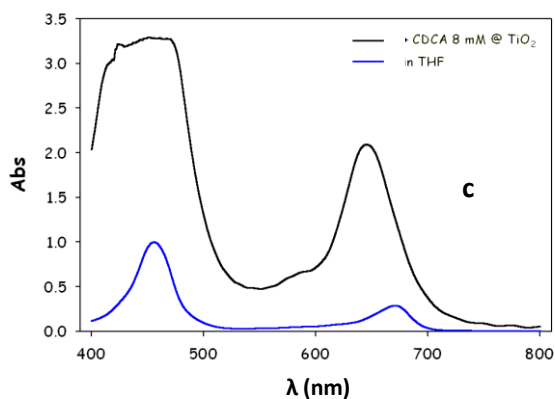
**Figure 7.10**

Observing the spectra (Figure 7.10) it can be noticed that **68** (a), in respect of **P** (c), is characterized by an enhanced absorption of the band at 650 nm, especially when adsorbed without added chenodeoxycholic acid (b). Since the absorption Q band is originated (as previously shown for analogous push-pull systems[30] and confirmed by the reported DFT and TDDFT calculations) from the HOMO-LUMO directional charge transfer, towards the carboxylic group along the push-pull system, the red shift of the Q band of **68**, if compared to that of **P**, and its stronger intensity, make **68** a promising dye for application in a DSSC solar cell.

The photoaction spectra of dyes **68** and **P** absorbed on opaque $TiO_2$, obtained with a liquid electrolyte consisting of 0.6 M PMII/0.1 M LiI/0.02 M $I_2$ in methoxypropionitrile (MPN) are shown below. (Figure 7.11) Dye **68** (Figure 7.10a) presents two maxima of IPCE (incident photon-to-current conversion efficiency) of ~20% in correspondence of the B Soret band (about 450 nm) and of the Q band (about 650 nm), while **P** has a maxima of ~35% at 450 nm (B band) and another one less intense (~35%) at 650 nm (Q band). Figure 7.11
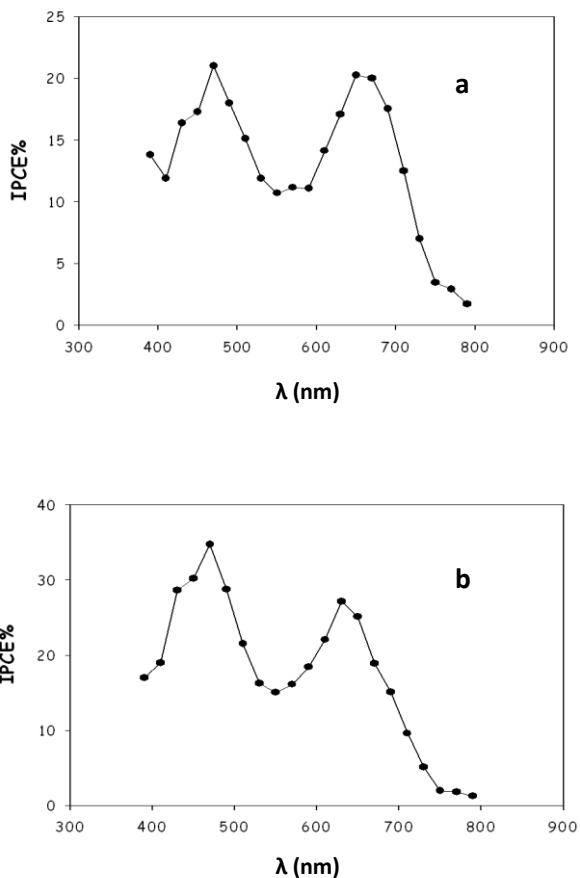
**Figure 7.11**

IPCE spectra are not in agreement with the reflectance spectra of the absorbed dyes, seems indeed that, in opposite tendency to the UV-Vis spectra of dyes anchored on $TiO_2$, (Figure 7.10) porphyrin system **P**, showing a slightly higher IPCE, could lead to better performance in cell.

The J-V curves (Figure 7.12) under AM1.5 G (100 mW/cm$^2$) illumination follow the trend qualitatively expected on the basis of the photoaction spectra. The calculated photovoltaic parameters of the DSSC cells based on **68** and **P** absorbed on opaque $TiO_2$, operating with a 0.6 M PMII/ 0.1 M LiI/ 0.02 M $I_2$ electrolyte and PEDOT as counter electrode are reported in the Table 7.4..
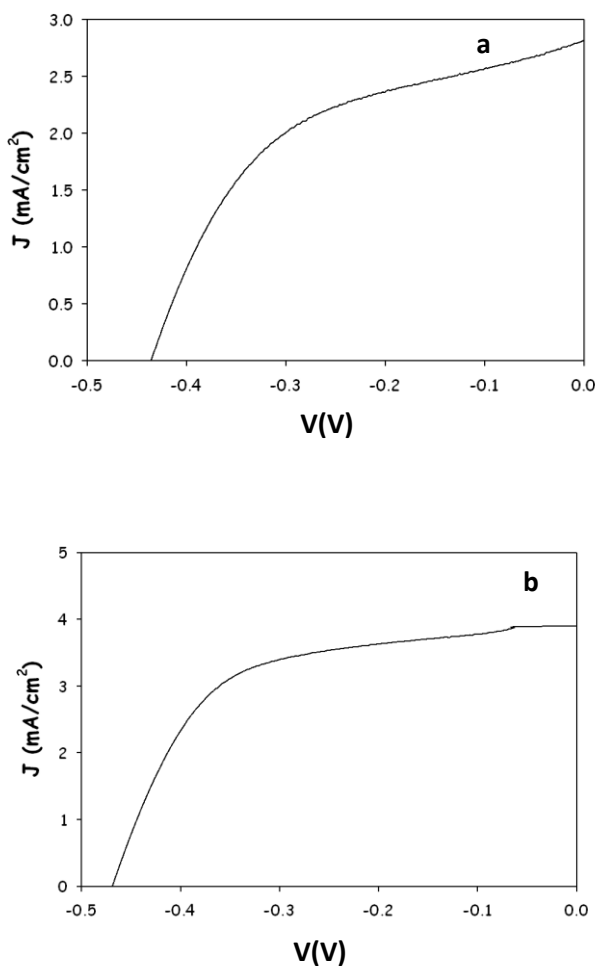
**Figure 7.12**

| DYE | $J_{sc}$ (mA/cm$^2$) | $V_{oc}$ (V) | FF | $\eta$ (%) |
|-----|-----|-----|-----|-----|
| **68** | 2.7 | 0.47 | 0.51 | 0.60 |
| **P** | 3.9 | 0.47 | 0.59 | 1.08 |

**Table 7.4**

Preliminary studies conducted on the application of these dyes in DSSCs show that both gave very low efficiency and in particular, according the IPCE spectrum, porphyrin **68** shows a lower value of 0.60% (Figure 7.12a, Table 7.4) with respect to 1.08% of **P**. (Figure 7.12b, Table 7.4). Looking to cells parameters the limiting factor for **68** seems to

be the $J_{sc}$, (Table 7.4) that is around 2.7 mA/cm$^2$ (3.9 mA/cm$^2$ for **P**, Table 7.4). The fill factor is instead nearly constant (about 0.5) suggesting that the series resistance of the cell is essentially the same. It must be pointed out that the optimization of the efficiency of the DSSC cells has not been considered, since this investigation has been done only with the aim of getting a comparative analysis of the photoelectrochemical properties of push-pull porphyrins **68** and **P,** acting as dyes in a DSSC cell. In fact, all of the photovoltaic parameters reported in Table 7.4 and consequently the efficiency of our DSSC solar cells based on the dyes **P**, are lower than those reported for DSSC solar cells based on the same dye **P** reported by C.-Y. Lin and coworkers, and reported in our previous work[31] However, quite different characteristics of the fabrication of the DSSC solar cells and slightly different experimental conditions were in both cases used.[32]

From spectroscopic data we expected a better (or at least comparable) performance of **68** with respect to **P**, therefore to understand the results gained additional experiments of photophysics on solid semiconductor films have been carried out. Indeed, comparative steady state emission studies on porphyrins **68** and **P** loaded on transparent ZrO$_2$ electrodes, an electrochemically inactive substrate, and TiO$_2$ have been done. As shown in Figure 7.13 with both dyes complete quenching going from ZrO$_2$ to TiO$_2$ is observed meaning that the injection process occurs effectively.
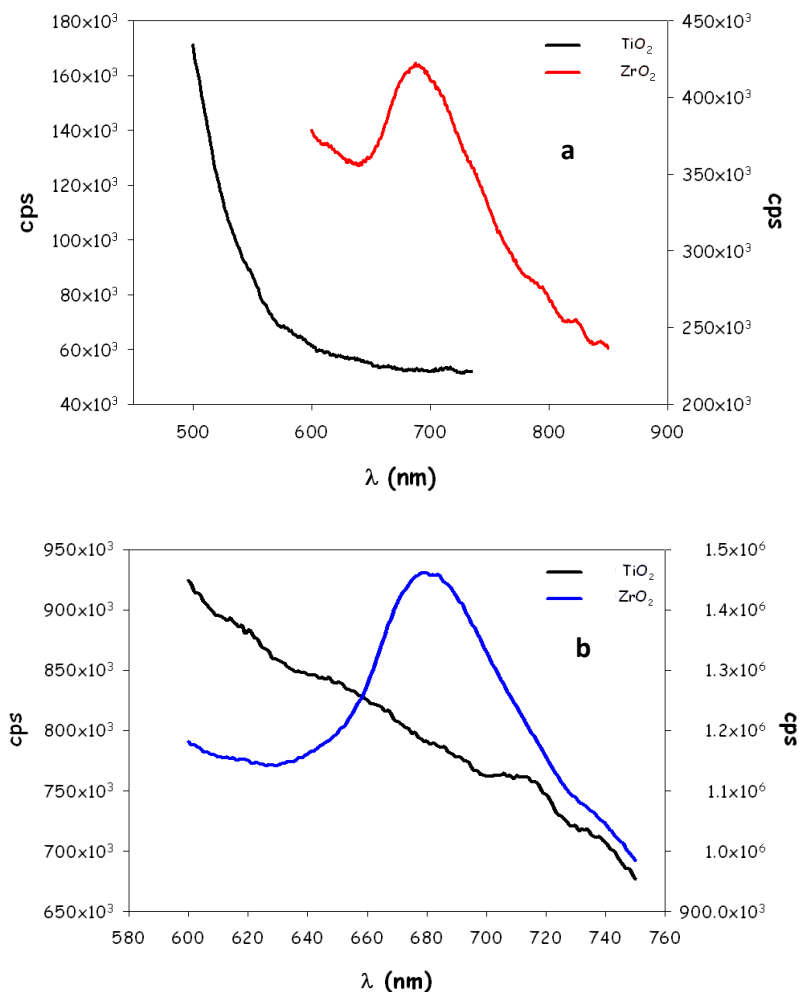
**Figure 7.13**

Moreover experiments of dye regeneration kinetics have been performed measuring the cation lifetime first in presence of only $LiClO_4$ ($\tau_{2/3}$ ($Li^+$), Table 7.5) and then after addition of the electrolyte solution ($\tau_{2/3}$ ($I^-$), Table 7.5). From the ratio of the lifetime measured ($\tau_{2/3}$ ($Li^+$)/$\tau_{2/3}$ ($I^-$)) is possible to establish the shortening of the cation lifetime and therefore the dye regeneration capability.
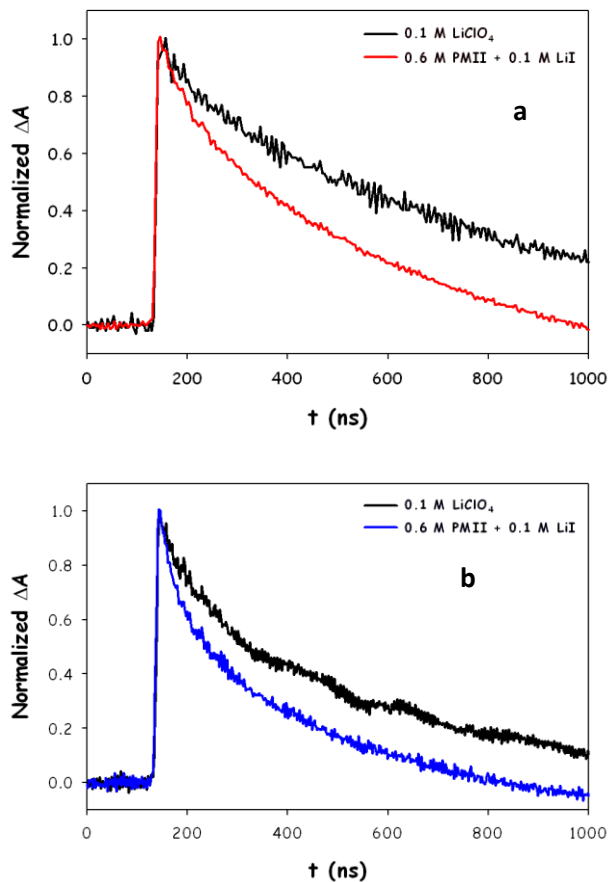
**Figure 7.14**

In figure 7.14a and 7.14b are reported the lifetime of **68** and **P** respectively. In particular, the measurements indicate that both dyes are able to establish a favorable interaction with the electron mediator (PMII/LiI), showing a double fold shortening of the cation lifetime in the presence of I⁻. We found similar results in terms of dye cation lifetime (slightly better in the case of **2**). (Table 7.5) This is most probably related to the successful hole transfer to the amino group which, being able to establish a good coupling with the electron donor, promotes the subsequent electron transfer event.

|  | $\tau_{2/3}$ (Li$^+$) | $\tau_{2/3}$ (I$^-$) | Ratio |
|---|---|---|---|
| **68** | 624 ns | 326 ns | 1.9 |
| **P** | 374 ns | 184 ns | 2 |

**Table 7.5**

In summary, it appears that a facile electron transfer along the push-pull system occurs in these new push-pull system as well as efficient charge injection into the TiO$_2$ semiconductor.

## 7.6 CONCLUSION

The synthesis of a new push-pull Zn(II) porphyrin dye **68** has been carried out inserting the benzo[1,2-*b*:4,5-*b'*]dithiophene, **BDT$_1$** as novel policonjugate spacer linking the anchoring group. In addition, a comparative study with a similar structure **P** recently published by us has been undertaken with the aim of identifying how structural and electronic properties are controlling the efficiency of photon to electron conversion in DSSC solar cells. In particular, we found that dye **68**, that shows an improved absorption spectra in solution and also once adsorbed on TiO$_2$, with respect to **P**, presents a worse IPCE and cell efficiency. We gain an efficiency of 0.60% and 1.08% for **68** and **P** respectively. The main difference between the two dyes is the slightly higher IPCE of **P**. Preliminary studies on injection efficiencies and dye regeneration capability didn't give an explanation to such behavior, but other investigations are currently ongoing.

At present an optimization work on cell fabrication is also under progress. First results showed an increased efficiency from 2.41% to 2.54% by changing the electrolyte composition (Iolitech ES-0004-HP) and using a Platinum counter electrode, and also increasing LiI concentration from 0.1 M to 0.3 M, improving in this way the charge injection.[33]

In addition, we are prosecuting the work synthesizing the other compounds **68-71** to study the effect of insertion of **BDT**s in this kind of structures for DSSCs application.

**BDT**s are indeed important frameworks largely employed in functional organic materials for optoelectronic devices and therefore very promising also in the field of Grätzel cells.

## 7.7 EXPERIMENTAL SECTION

All reagents and solvents were obtained from highest grade commercial sources and used without further purification unless otherwise stated. Column chromatography were carried out using silica gel 60 (70-230 mesh, Merck). $^1$H NMR spectra were acquired on a Bruker AVANCE DRX-400, Bruker AC300 and AMX at 300 MHz spectrometers; the chemical shifts ($\delta$) are reported in parts per million relative to the solvent residual peak (acetone-$d_6$, DMSO-$d_6$, CDCl$_3$). IR spectra were recorded on a Fourier Bruker Vector 22 FT, UV spectra were recorded by using a Jasco V-520 or Agilent 8453 UV/Vis spectrophotometer in a range of $\lambda$ from 190 nm to 800 nm at room temperature. HRMS spectra were recorded on Bruker Daltonics ICR-FTMS APEX II. Melting points were obtained with a Büchi B-540 melting point apparatus and are uncorrected. HPLC analyses were performed on an Agilent 1100 series equipped with a PDA detector and the reverse phase ZORBAX Eclipse XBD-C18, 4.6×150 mm, 5μm particle size; samples were analyzed with 1mL/min acetonitrile-water 80:20 with 0.1% TFA. All the samples for cell fabrication were controlled via HPLC and the purity esteemed to be over 98%.

*Photophysical measurement:* Electronic absorption spectra in solution were recorded on a Jasco V-530 spectrophotometer. Diffuse reflectance spectra on solid TiO$_2$ thin films were recorded on a Jasco V570 UV-Vis-NIR spectrophotometer equipped with a ISN 470 integrating sphere. Emission spectra were obtained with a Jobin Yvon Spex spectrofluorimeter equipped with a R 3896 phototube, by using a band pass of 2 nm, an integration time of 0.5 s and an excitation wavelength of 450 nm. Emission spectra on optically diluted (Q band absorption < 0.3) sensitized transparent thin films (either TiO$_2$ or ZrO$_2$) were recorded by using a thin film holder which allowed a fixed excitation angle of 33°. An excitation wavelength of 450 nm, a spectral bandwidth of 10 nm. and an integration time of 1 s were employed. The resulting emission spectra were

background subtracted, integrated and divided by the film Light Harvesting Efficiency (LHE = 1-10$^{-A450}$) were A450 was the film absorbance at 450 nm. In all cases the LHE factors were very close to unity. The quenching ratio was defined by

where $I_{TiO_2}$ and $I_{ZrO_2}$ are the integrated emission intensities calculated as specified above. Transient Absorption Spectroscopy by using the 355 nm excitation generated by a pulsed Q-switched Nd :YAG laser Continuum Surelite II (FWHM = 7 ns, 8 Hz) laser. The probe beam, orthogonal to the excitation pulse, generated by a pulsed Xe lamp was focused on an Acton Spectra Pro 2300i triple grating monochromator and detected with an Hamamatsu R 3896 photomultiplier.

*Electrochemical measurements:* Cyclic voltammetry was performed in THF with an EcoChemie PGSTAT 30/2 electrochemical workstation without dynamic ohmic drop compensation at 20 mV/s by using a glassy carbon working electrode, a Pt wire counter electrode. Potentials were referred to SCE (Saturated Calomel Electrode). The supporting electrolyte was (TBA)PF$_6$ 0.1 M . Prior to each measurement the working electrode was accurately cleaned by brushing the carbon surface on an alumina (0.5 μm) pad followed by sonication and rinsing with acetone.

*Photoelectrochemical measurements:* Photon to current action spectra were collected by focusing the monochromatic light generated by an Applied Photophysics monochromator (spectral bandwidth = 10 nm) onto the photoanode of sandwich type photoelectrochemical cell. The illuminated area was 0.25 cm$^2$. Short circuit photocurrents were measured with an Agilent 34401A multimeter. IPCE was calculated according to the equation (IPCE % = 1.24 ×10$^3$ (V nm)                                        ) where J is the monochromatic photocurrent density, P is the radiant power density and λ is the wavelength of the incident light. J-V curves were obtained under simulated solar illumination AM 1.5 G generated by an ABET sun simulator by using an EcoChemie PGSTAT 30/2 electrochemical workstation controlled by the Ecochemie GPES 4.9 software. The linear potential sweep rate was 10 mV/s . Incident white light irradiance was measured with a Molectron Powermax 5200 Power-meter.

*Cell preparation:* TiO$_2$ or ZrO$_2$ gels were cast onto well cleaned FTO substrates by doctor blading. The resulting film was gently dried in warm air and fired at 450 °C for 45 minutes. The TiO$_2$ layer so obtained (about 6 ⬚m thick)was then treated with TiCl$_4$ according to literature[3] and annealed at 450 C° before being immersed, still hot, in the dye solution. DSSC photoanodes were assembled from a single layer of TiO$_2$ paste (about 6μm thick) on a FTO glass. Sensitization were carried out in the dark from a containing 8mM chenodeoxycholic acid solution of the dye in EtOH/THF 9:1. PEDOT counter electrodes were obtained from 10$^{-2}$ EDOT (ethylenedioxythiophene) solution in 0.1 M LiClO$_4$ by potentiostatic deposition on well cleaned FTO substrates at 1.6 V vs SCE for 30 s. The resulting deep blue coated electrodes were rinsed with acetonitrile and ethanol, dried and stored in the dark. Parafilm® sealed DSSC cells were built by pressing the TiO$_2$sensitized photoanode against a PEDOT counter electrode equipped with a Parafilm® frame used to confine the liquid electrolyte (PMII 0.6 M/LiI 0.1M/I$_2$ 0.02 M in methoxypropionitrile) inside the cell. The thickness of the liquid layer corresponded roughly to the thickness of the frame borders (about 120 μm).

*Theoretical DFT and TDDFT calculations*: DFT ground state geometries of dyes **1-3** were optimized by using the B3LYP exchange-correlation functional,[28] along with a 6-311G* basis set. For sake of simplicity, the *tert*-butyl groups linked to the phenyl groups have been replaced by hydrogen atoms and a $C_s$ symmetry was used for geometry optimizations. TDDFT excited state calculations were performed on the DFT optimized geometries at the same B3LYP/6-311G* level of theory, both *in vacuo* and in solution. The lowest 15 excitation energies were calculated, spanning approximately 3.5 eV. All the calculations have been performed by the Gaussian 03 program package.[29] The non-equilibrium C-PCM solvation model[30] was employed for TDDFT calculations in solution.
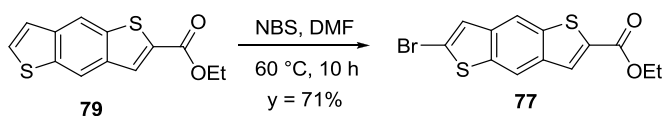
## 7.7.1    Synthesis of benzo[1,2-b:4,5-b']dithiophen-2-ethoxycarbonyl[34] 79
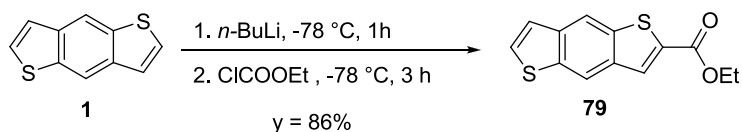
Under nitrogen, *n*-BuLi (1.5 M in hexane, 1.93 mL, 2.89 mmol) was added to a suspension of benzo[1,2-b:4,5-b']dithiophene **1** (500 mg, 2.63 mmol) in THF (30 mL) at -78 °C. The mixture was stirred for 1 h and the color turn from white to yellow. Then ethylchloroformate (0.75 mL, 7.89 mmol) was added dropwise. The resulting yellow solution was reacted for 3 h at -78 °C. The progress of reaction was monitored by TLC (hexane/AcOEt 9:1, $R_f$: 0.44). Afterwards the mixture was poured in a solution of NH$_4$Cl (25 mL) and extracted with CH$_2$Cl$_2$ (3x25 mL). The organic phase was dried (Na$_2$SO$_4$), filtered and the solvent was evaporated under vacuum.

The crude product was purified by column chromatography on silica gel (eluent: hexane/AcOEt 9:1) to afford **79** as a yellow solid, 600 mg (86% yield). P.f.: 122-123 °C. $^1$H NMR (200 MHz, CDCl$_3$): δ, ppm = 1.43 (t, 3H, CH$_3$, *J* = 7.1 Hz), 4.42 (q, 2 H, CH$_2$, *J* = 7.1 Hz), 7.38 (d, 2H, CH$_{tiof}$, *J* = 5.6 Hz), 7.55 (d, 2H, CH$_{tiof}$, *J* = 5.6 Hz), 8.10 (s, 1H, CH$_{tiof}$), 8.29 (s, 1H, CH$_{ar}$), 8.38 (s, 1H, CH$_{ar}$). $^{13}$C NMR (75 MHz, CDCl$_3$): δ, ppm = 14.34, 61.62, 117.04, 119.05, 122.94, 128.84, 129.65, 134.24, 136.38, 137.65, 138.95, 139.54, 162.5. HRMS-EI (m/z): [M]$^+$ Calcd. for C$_{13}$H$_{10}$O$_2$S$_2$: 262.012223, found: 262.012880. MS-EI (m/z): [M]$^+$: 262, 234 ( − C$_2$H$_4$), 217 ( − OH), 190 ( − CO), 145 ( − CHS$^+$). IR (nujol, cm$^{-1}$): 1697 ($\nu_{CO}$). UV-vis (10$^{-5}$ in CH$_2$Cl$_2$): $\lambda_{max}$ = 240 nm (1.9·10$^4$ M$^{-1}$cm$^{-1}$), 273 (3.4·10$^4$ M$^{-1}$cm$^{-1}$), 307 (1.3·10$^4$ M$^{-1}$cm$^{-1}$), 319 (2.2·10$^4$ M$^{-1}$cm$^{-1}$), 357 (6.5·10$^3$ M$^{-1}$cm$^{-1}$), 368 (8.3·10$^3$ M$^{-1}$cm$^{-1}$).

## 7.7.2 Synthesis of 6-bromo-benzo[1,2-b:4,5-b']dithiophen-2-ethoxycarbonyl[25] 77



NBS (910 mg, 5.11 mmol) was added to a suspension of benzo[1,2-b:4,5-b']dithiophen-2-ethoxycarbonyl **79** (650 mg, 2.48 mmol) in DMF (18 mL). The mixture was stirred for 10 h at 60°C and the color turn from yellow-orange to brown. The progress of reaction was monitored by TLC (hexane/CH$_2$Cl$_2$ 4:6, $R_f$: 0.30). The DMF was then distilled under vacuum at 60 °C, the residue was dissolved in CH$_2$Cl$_2$ (35 mL) and washed with water (3x20 mL). The organic phase was dried (Na$_2$SO$_4$), filtered and the solvent was

evaporated under vacuum. The crude product was purified by flash chromatography on silica gel (eluent: hexane/$CH_2Cl_2$ 4:6) to afford **77** as a pale green solid, 600 mg (71% yield). P.f.: 148 °C (subl.). ^{1}H NMR (200 MHz, $CDCl_3$): δ, ppm = 1.44 (t, 3H, $CH_3$, $J$ = 7.1 Hz), 4.44 (q, 2 H, $CH_2$, $J$ = 7.1 Hz), 7.54 (s, 1H, $CH_{tiof}$), 8.10 (s, 1H, $CH_{tiof}$), 8.31 (s, 1H, $CH_{ar}$), 8.34 (s, 1H, $CH_{ar}$). ^{13}C NMR (75 MHz, $CDCl_3$): δ, ppm = 14.34, 61.78, 106.75, 117.03, 119.26, 122.96, 125.80, 129.31, 136.01, 137.09, 137.50, 139.95, 162.50. HRMS-EI (m/z): $[M]^+$ Calcd. for $C_{13}H_9O_2S_2Br$: 339.922734, found: 339.92212. MS-EI (m/z): $[M]^+$: 340, 312 ( – $C_2H_4$), 295 ( – OH), 267 ( – CO), 261 ($M^+$– Br), 233 ($M^+$– $C_2H_4$).188 (267– Br), 145 ( 188– $CHS^+$). IR (nujol, $cm^{-1}$): 1714 ($v_{CO}$), 1071 ($v_{C-Br}$). UV ($10^{-6}$ in $CH_2Cl_2$): $\lambda_{max}$ = 241 nm ($2.9 \cdot 10^4$ $M^{-1}cm^{-1}$), 274 nm ($7.6 \cdot 10^4$ $M^{-1}cm^{-1}$), 307 nm ($1.8 \cdot 10^4$ $M^{-1}cm^{-1}$), 319 nm ($3.8 \cdot 10^4$ $M^{-1}cm^{-1}$), 356 nm ($1.1 \cdot 10^4$ $M^{-1}cm^{-1}$), 370 nm ($1.6 \cdot 10^4$ $M^{-1}cm^{-1}$).

### 7.7.3 Synthesis of 6-trimethylsilyl-ethynylbenzo[1,2-b:4,5-b']dithiophen-2-ethoxycarbonyl[35] 78
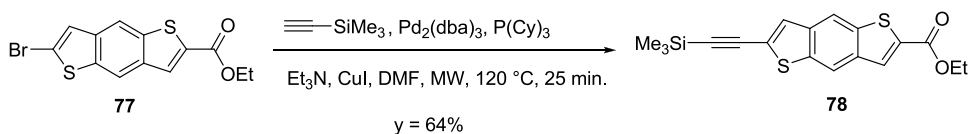


In a microwave reactor tube to a solution of 6-bromo-benzo[1,2-b:4,5-b']dithiophen-2-ethoxycarbonyl **77** (100 mg, 0.29 mmol) in DMF (3.5 mL) was added under nitrogen $Pd_2(dba)_3$ (16 mg, $1.71 \cdot 10^{-2}$ mmol), CuI (3 mg, $1.74 \cdot 10^{-2}$ mmol), $P(Cy)_3$ (16 mg, $5.8 \cdot 10^{-2}$ mmol), trimethylsilylacetylene (510 mg, 5.22 mmol) and $Et_3N$ (0.61 mL, 440 mg, 4.35 mmol). The reaction mixture was heated in a microwave reactor at 120 °C for 25 minutes. The resulting yellow suspension turned a black solution. The progress of reaction was monitored by TLC (hexane/$CH_2Cl_2$ 6:4, $R_f$: 0.22). The DMF was distilled under vacuum at 60°C, the residue was dissolved in $CH_2Cl_2$ (10 mL) and washed with water (3x10 mL). The organic phase was dried ($Na_2SO_4$), filtered and the solvent was evaporated under vacuum. The crude product was purified by column chromatography on silica gel (eluent: hexane/ $CH_2Cl_2$ 4:6) to afford **78** as an orange solid, 66 mg (64% yield). P.f.: 141-142 °C (dec.). ^{1}H NMR (300 MHz, $CDCl_3$): δ, ppm = 0.34 (s, 9H, $CH_3$), 1.44

(t, 3H, CH$_3$, *J* = 7.1 Hz), 4.44 (q, 2 H, CH$_2$, *J* = 7.1 Hz), 7.74 (s, 1H, CH$_{tiof}$), 8.10 (s, 1H, CH$_{tiof}$), 8.33 (s, 1H, CH$_{ar}$), 8.38 (s, 1H, CH$_{ar}$). $^{13}$C NMR (75 MHz, CDCl$_3$): δ, ppm = 0.07, 14.34, 61.70, 97.81, 116.86, 117.69, 119.19, 129.48, 133.00, 134.96, 136.49, 136.95, 138.90, 139.47, 163.00. HRMS-EI (m/z): [M]$^+$ Calcd. for C$_{18}$H$_{18}$O$_2$SiS$_2$: 358.051752, found.: 358.051570. MS-EI (m/z): [M]$^+$: 358, 343( − CH$_3$), 315 ( − C$_2$H$_4$), 271 ( − CO$_2$), 285 ( M$^+$− CO$_2$C$_2$H$_5$) IR (nujol, cm$^{-1}$): 1250 (v$_{C-Si}$), 1699-1719 (v$_{CO}$), 2148 (v$_{C≡C}$). UV-vis (10$^{-5}$ in CH$_2$Cl$_2$): λ$_{max}$ = 236 nm (2.0·10$^4$ M $^{-1}$cm$^{-1}$), 275 nm (2.5·10$^4$ M $^{-1}$cm$^{-1}$), 308 nm (9.5·10$^3$ M $^{-1}$cm$^{-1}$), 320 nm (1.3·10$^4$ M $^{-1}$cm$^{-1}$), 336 nm (3.9·10$^3$ M $^{-1}$cm$^{-1}$), 359 nm (5.3·10$^3$ M $^{-1}$cm$^{-1}$), 372 nm (6.3·10$^3$ M $^{-1}$cm$^{-1}$).

### 7.7.4 Synthesis of 2-ethynylbenzo[1,2-b:4,5-b']dithiophene-6-ethoxycarbonyl[35] 85
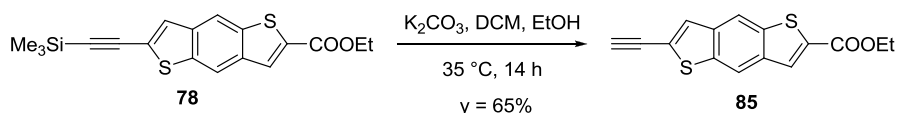


To a solution of 6-trimethylsilyl-ethynylbenzo[1,2-b:4,5-b']dithiophen-2-ethoxycarbonyl **78** 230 mg (0.64 mmol) in CH$_2$Cl$_2$ (1.5 mL) and EtOH (5 mL), K$_2$CO$_3$ (28 mg, 0.21 mmol) was added. The mixture was warmed at 35°C and left under stirring for 14 h. The progress of reaction was monitored by TLC (eluent: hexane/AcOEt 9:1, R$_f$: 0.69). Afterwards the suspension was filtered and the filtrate was evaporated under vacuum. The crude product **85** was purified by column chromatography on silica gel to afford **6** as an yellow solid, 178 mg (65% yield). P.f.: 125-126 °C. $^1$H NMR (300 MHz, CDCl$_3$): δ, ppm = 1.43 (t, 3H, CH$_3$, *J* = 6.9 Hz), 3.36 (s, 1H, CH$_{C≡C}$), 4.43 (q, 2 H, CH$_2$, *J* = 6.9 Hz), 7.61 (s, 1H, CH$_{tiof}$), 8.09 (s, 1H, CH$_{tiof}$), 8.32 (s, 1H, CH$_{ar}$), 8.41 (s, 1H, CH$_{ar}$). $^{13}$C NMR (75 MHz, CDCl$_3$): δ, ppm = 14.32, 61.70, 80.36, 86.33, 116.47, 116.72, 119.16, 129.40, 135.05, 136.43, 136.97, 138.86, 139.54, 162.59. HRMS-EI (m/z): [M]$^+$ Calcd. for C$_{15}$H$_{10}$O$_2$S$_2$: 286.012223, found: 286.011900. MS-EI (m/z): [M]$^+$: 286, 258 ( − C$_2$H$_4$), 241 ( − OH), 213 ( − CO) IR (nujol, cm$^{-1}$): 1697-1715 (v$_{CO}$), 3281 (v$_{C≡H}$). UV-vis (10$^{-5}$ in CH$_2$Cl$_2$): λ$_{max}$ = 235 nm (6.9·10$^4$ M$^{-1}$cm$^{-1}$), 274 nm (1.3·10$^4$ M$^{-1}$cm$^{-1}$), 307 nm (4.3 ·10$^3$ M$^{-1}$cm$^{-1}$), 318 nm (7.1·10$^3$M$^{-1}$cm$^{-1}$), 357 (2.8·10$^3$ M$^{-1}$cm$^{-1}$), 371 nm (3.5·10$^3$ M$^{-1}$cm$^{-1}$).

### 7.7.5  Synthesis of 2-ethynylbenzo[1,2-b:4,5-b']dithiophene-6-carboxylic acid[35] 73
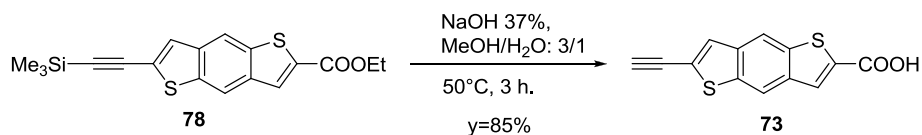


To a suspension of **78** (40 mg, 0.15 mmol) in MeOH/water (3/1mL) NaOH 32% (0.88 mL) was added. The mixture was heated at 50°C for 3h obtaining an orange solution. The progress of reaction was monitored by TLC (eluent: hexane/CH$_2$Cl$_2$/AcOH 5.5:4:0.1, R$_f$: 0.52). The solvent was then evaporated under vacuum and the residue dissolved in CH$_2$Cl$_2$ (8 mL) and acidic water and extracted with CH$_2$Cl$_2$ (3x10mL). The organic phase was then dried (Na$_2$SO$_4$), filtered and the solvent was evaporated under vacuum. The product **73** obtained as a pale yellow solid didn't require further purification, 38 mg (98% yield). P.f.: 286 °C (dec.). $^1$H NMR (300 MHz, Acetone-d$_6$): δ, ppm = 4.01 (s, 1H, CH$_{C≡C}$), 8.11 (s, 1H, CH$_{tiof}$), 8.22 (s, 1H, CH$_{tiof}$), 8.54 (s, 1H, CH$_{ar}$), 8.67 (s, 1H, CH$_{ar}$). $^{13}$C NMR (75 MHz, Acetone-d$_6$): δ, ppm = 77.55, 81.90, 117.17, 120.09, 130.0, 134.48, 137.33, 138.26, 139.67. HRMS-EI (m/z): [M]$^+$ Calcd. for C$_{13}$H$_6$O$_2$S$_2$: 257.980680, found: 257.980923. MS-EI (m/z): [M]$^+$: 258, 241 ( − OH), 241 ( − OH), 213 ( − CO) IR (nujol, cm$^{-1}$): 1670 (v$_{CO}$), 3281 (v$_{C≡H}$), 3404 (v$_{OH}$). UV-vis (10$^{-5}$ in CH$_2$Cl$_2$): λ$_{max}$ = 231 nm (2.1·10$^4$ M$^{-1}$cm$^{-1}$), 274 (2.8·10$^4$ M$^{-1}$cm$^{-1}$), 308 nm (1.1·10$^4$ M$^{-1}$cm$^{-1}$), 320 (1.6·10$^4$ M$^{-1}$cm$^{-1}$), 376 (7.2·10$^3$ M$^{-1}$cm$^{-1}$).
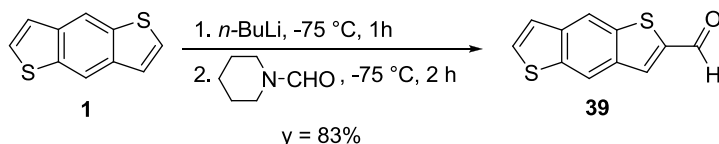
### 7.7.6  Synthesis of 2-bromobenzo[1,2-b:4,5-b']dithiophene-6-carboxylic acid[35]  80
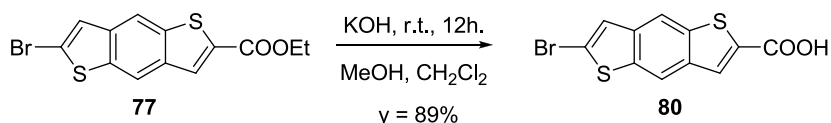


To a suspension of **77** (150 mg, 0.44 mmol) in MeOH/CH$_2$Cl$_2$ (15/5mL) KOH (850, 14 mmol) was added. The mixture was left at 25°C for 12h. The progress of reaction was monitored by TLC (eluent: hexane/AcOH 9:1, R$_f$: 0.12). The solvent was then evaporated under vacuum and the solid recovered with water, filtered and washed with CH$_2$Cl$_2$. The

crude product **80** obtained as pale yellow solid 123 mg (89% yield), was employed in the successive reaction without further purification. $^1$H NMR (300 MHz, DMF-d$_6$): δ, ppm = 3.52 (s, 1H, CH$_{C≡C}$), 7.69 (s, 1H, CH$_{tiof}$), 7.98 (s, 1H, CH$_{tiof}$), 8.28 (s, 1H, CH$_{ar}$), 8.50 (s, 1H, CH$_{ar}$). $^{13}$C NMR (75 MHz, DMF-d$_6$): δ, ppm = 105.78, 116.05, 118.51, 123.41, 125.59, 149.95, 165.63. MS-EI (m/z): [M]$^+$: 268 ( − COOH), 190( − Br) IR (nujol, cm$^{-1}$): 3405 (ν$_{OH}$), 1670 (ν$_{CO}$), 3281 (ν$_{C≡H}$).

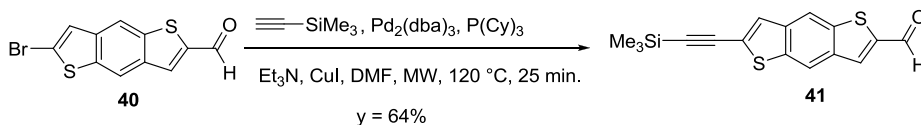### 7.7.7 Synthesis of benzo[1,2-b:4,5-b']dithiophen-2-carboxaldehyde 39



Synthesized as reported in **Chapter 4**, page 150.

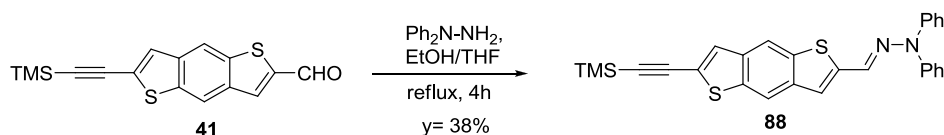### 7.7.8 Synthesis of 6-bromo-benzo[1,2-b:4,5-b']dithiophen-2-carboxaldehyde[25] 40
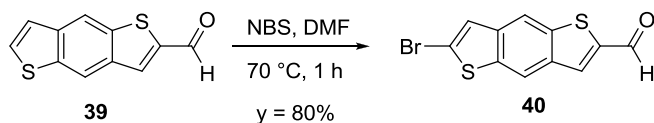


Synthesized as reported in **Chapter 4**, page 151.

### 7.7.9 Synthesis of 6-trimethylsilylethynylbenzo[1,2-b:4,5-b']dithiophen-2-carboxaldehyde[35] 41



Synthesized as reported in **Chapter 4,** page 152.

**7.7.10 Synthesis of 6-trimethylsilylethynylbenzo[1,2-b:4,5-b']dithiophen-2-diphenylhydrazone[36] 88**



To a solution of **41** (122 mg, 0.39 mmol) in EtOH diphenylhydrazine was added and the resulting reaction mixture heated at 40°C. The progress of reaction was monitored by TLC (eluent: hexane/AcOEt 8:2, $R_f$: 0.12). The solvent was then evaporated under vacuum and the crude product purified by column chromatography on silica gel (eluent: hexane/CH$_2$Cl$_2$ 9:1) to afford **88** as a pale yellow solid, 71 mg (38% yield). P.f.: 122-124 °C (dec). $^1$H NMR (300 MHz, Acetone-d$_6$): δ, ppm = 0.35 (s, 3H, CH$_3$ TMS), 7.13 (s, 1H, CH), 7.24 (m, 6H, CH$_{Ph}$), 7.37 (s, 1H, CH), 7.46 (m, 4H, CH$_{Ph}$), 7.63 (s, 4H, CH$_{ar}$), 8.05(s, 1H, CH). 8.29(s, 1H, CH).

**7.7.11 Synthesis of 6-ethynylbenzo[1,2-b:4,5-b']dithiophen-2-diphenylhydrazone[37] 87**
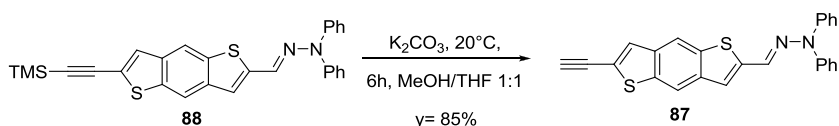


To a solution of **88** (70 mg, 0.121 mmol) in MeOH/THF (1:1) was added K$_2$CO$_3$ (12 mg, 0.08 mmol) and the mixture reacted overnight at room temperature. The progress of reaction was monitored by TLC (eluent: hexane/ CH$_2$Cl$_2$ 7:3). The solvent was then evaporated under vacuum. The residue was then dissolved in CH$_2$Cl$_2$ (5 mL) and washed with water. The organic phase was then dried (Na$_2$SO$_4$), filtered and the solvent was evaporated under vacuum. The obtained oil is then washed with hexane affording the compound **87** as an orange solid 40 mg (85%). P.f.: 158-160 °C (dec). $^1$H NMR (300 MHz, Acetone-d$_6$): δ, ppm = 3.35 (s, 1H, CH$_3$ C≡C), 7.13 (s, 1H, CH), 7.24 (m, 6H, CH$_{Ph}$), 7.37 (s, 1H, CH), 7.46 (m, 4H, CH$_{Ph}$), 7.68 (s, 4H, CH$_{ar}$), 8.07(s, 1H, CH). 8.35(s, 1H, CH).

# REFERENCES

[1] C.-W. Lee, H.-P. Lu, C.-M. Lan, Y.-L. Huang, Y.-R. Liang, W.-N. Yen, Y.-C. Liu, Y.-S. Lin, R. W.-G. Diau, C.-Y. Yeh, *Chem.sEur. J.* **2009**, *15*, 1403.

[2] A. Forneli, M. Planells, M. A. Sarmentero, E. Martinez-Ferrero, B. C. O'Regan, P. Ballester, E. Palomares, *J. Mater. Chem.* **2008**,*18*, 1652.

[3] S.-L. Wu, H.-P. Lu, H.-T. Yu, S.-H. Chuang, C.-L. Chiu, C.-W. Lee, E. W.-G. Diau, C.-Y. Yeh, *Energy Environ. Sci.*, **2010**, *3*, 949.

[4] T. Bessho, S. M. Zakeeruddin, C.-Y. Yeh, E. W.-G. Diau, M. Grätzel, *Angew. Chem. Int. Ed.*, *47*, **2010**, 6646.

[5] C.-W. Lee, H.-P. Lu, C.-M. Lan, Y.-L. Huang, Y.-R. Liang, W.-N. Yen, Y.-C. Liu, You-S. Lin, E. W.-G. Diau, C.-Y. Yeh, *Chem. Eur. J,.* **2009**, *15*, 1403.

[6] S. Kim, J. K. Lee, S. O. Kang, J. Ko, J.-H. Yum, S. Fantacci, F. D. Angelis, D. D. Censo, M. K. Nazeeruddin, M. Grätzel,*J. Am. Chem. Soc.,* **2006**, *128*, 16701.

[7] Y. J. Liu, N. Xiang, X. M. Feng, P. Shen, W. P. Zhou, C. Weng, B. Zhao, S. T. Tan, *Chem. Commun.* **2009**, *18*, 2499.

[8] N.M. Boylea, J. Rochfordb, M.T. Prycea., *Thienyl-appended porphyrins: synthesis, photophysical and electrochemical properties and their applications. Coordination Chemistry Reviews* , **2010**, *254*, 77.

[9] S. Kim, J. K. Lee, S. O. Kang, J. Ko, J.-H. Yum, S. Fantacci, F. D. Angelis, D. D. Censo, M. K. Nazeeruddin, M. Grätzel, *J. Am. Chem. Soc.*, **2006**, *128*, 16701.

[10] C.-Y. Lin, C.-F. Lo, L. Luo, H.-P Lu, C.-S. Hung, E. W.-G Diau, *J. Phys. Chem. C* **2009**, *113*, 755.

[11] S.-L. Wu, H.-P. Lu, H.-T. Yu, S.-H. Chuang, C.-L. Chiu, C.-W. Lee, E. W.-G. Diau, C.-Y. Yeh, *Energy Environ. Sci.*, **2010**, *3*, 949.

[12] C.-W. Lee, H.-P. Lu, C.-M. Lan, Y.-L. Huang, Y.-R. Liang, W-N. Yen, Y.-C. Liu, Y.-S. Lin, E. W.-G. Diau, C.-Y. Yeh, *Chem. Eur. J.*, **2009**, *15*, 1403.

[13] P. N. Taylor, J. Huuskonen, G. Rumbles, R. T. Aplin, E. Williams, H. L. Anderson, *Chem. Commun*. **1998**,*8*, 909.

[14] Gaussian 09, Revision **A.1**; Frisch, M. J. *et al*. Gaussian, Inc.: Wallingford CT, 2009.

[15] A. D. Becke, *J. Chem. Phys*. **1993**, *98*, 5648.

[16] Gaussian 03, Revision B.05, Frisch, M. J. *et al.* Gaussian, Inc., Pittsburgh PA, 2003.

[17] M. Cossi, V. Barone, *J. Chem. Phys.,* **2001**, *115*, 4708.

[18] M. Cossi, N. Rega, G. Scalmani, V. Barone, *J. Comp. Chem.,* **2003**, *24*, 669.

[19] F. Angelis, S. Fantacci, A. Selloni, *Nanotech.,* **2008**, *19*, 424002.

[20] F. De Angelis, A. Tilocca, A. Selloni, *J. Am. Chem. Soc.,* **2004**, *126*, 15024.

[21] A. Orbelli Biroli, F. Tessore, M. Pizzotti, C. Biaggi, R. Ugo, S. Caramori, C. Bignozzi, F. De Angelis, G. Giorgi, E. Licandro, E. Longhi, *manuscript submitted to J. Phys. Chem. C.*, **2011**, *115 (46)*, 23170.

[22] S. M. LeCours, H.-W.Guan, S. G. DiMagno, C. H. Wang, M. J. Therien, *J. Am. Chem. Soc.,* **1996**, *118*, 1497.

[23] K. Sonogashira, *J. Organomet. Chem.* **2002**, *653*, 46.

[24] A.Elangovan, Y.-H. Wang, T.-I. Ho, *Org. Lett.* **2003**, *5*, 1841.

[25] T T. M. Dang, S.-J. Park, J.-W. Park, D.-S. Chung, C. E. Park, Y.-H. Kim, S.-K. Kwon, *Journal of polymer science. Part A, Polymer chemistry*, **2007**, *45 (22),* 5277.

[26] A.-S. Castanet, F. Colobert, P.-E. Broutin, *Tetrahedron Letters* , **2002**, *43*, 5047.

[27] T. Morotti, M. Pizzotti, R. Ugo,; S. Quici, M. Bruschi, P. Mussini, S.Righetto, *Eur. J. Inorg. Chem*., **2006**, *9*, 1743.

[28] A. Hagfeldtt, M. Grätzel, *Chemical Reviews*, **1995**, *95 (1)*, 49.

[29] A. Hagfeldt, G. Boschloo, L. Sun, L. Kloo, H. Pettersson, *Chemical Reviews*, **2010**, *110(11)*, 6595.

[30] F. De Angelis, S. Fantacci, A. Sgamellotti, M. Pizzotti, F. Tessore, A. Orbelli Biroli, *Chem. Phys. Lett.,* **2007**, *447*, 10.

[31] A. Orbelli Biroli, F. Tessore, M. Pizzotti, C. Biaggi, R. Ugo, S. Caramori, A. Aliprandi, C. A. Bignozzi, F. De Angelis, G. Giorgi, E. Licandro, E. Longhi, *J. Phys. Chem. C*, **2011**, *115 (46)*, 23170.

[32] C.-F. Lo, S.-J. Hsu, C.-L. Wang, Y.-H. Cheng,. H.-P. Lu, E. W.-G. Diau, C.-Y. Lin *J. Phys. Chem*. *C,* **2010**, *114*, 12018.

[33] M. Pizzotti, R. Ugo, F. Tessore, S. Maiorana, E. Licandro, E. Longhi, C. Baldoli, A. Orbelli Biroli, F. De Angelis, *Patent Appl.*, **2011**, MI2011A000181.

[34] C. Rigamonti, M. T. Ticozzelli, A. Bossi, E. Licandro, C. Giannini, S. Maiorana, *Heterocycles,* **2008**, *76* (2), 1439.

[35] M. Erdélyi, A. Gogoll, *J. Org. Chem.*, **2001**, *66*, 4165.

[36] J. Ostrauskaite, V. Voska, J. V. Grazulevicius, *Monatshefte fur chemie*, **2002**, *133*, 599.

[37] N. Zhou, Y. Zhao, *J. Org. Chem.*, **2010**, *75*, 1498.

CHAPTER **8**

# CONCLUSIONS

## 8.1 CONCLUSIONS

In this Ph.D. thesis a systematic study concerning the use of novel push-pull systems of type "donor-π-spacer-acceptor" (D-π-A) to be utilized as sensitizers in photovoltaic DSSC cells, is reported.

In particular, both metal-based and metal-free dyes, all characterized by the presence of a **BDT** or **BDT$_1$** moiety as innovative part of the π-spacer, have been synthesized.

The potential of the new **BDT** and **BDT$_1$** π -spacers inserted in the D-π-A structure of chromophores was previously validated by theoretical calculations, done in collaboration with Dr. Filippo De Angelis of CNR-ISTM of Perugia, that allowed to gain insight into the molecular, ground and excited state electronic structure of the new chromophores. These calculations and spectra simulation were performed through Density Functional Theory, DFT, and its extension to the Time-Dependent formulation, TDDFT.

As a consequence of this study, a small library of chromophores containing the **BDT** and **BDT$_1$** moieties as part of the D-π-spacer, has been designed and synthesized; in some cases, a careful and deep optimization of the reaction conditions has been carried out to find the most efficient synthetic strategy. Indeed, the reactivity of these two systems have not been deeply investigated in the literature, therefore the set up of the appropriate methodology for the synthesis of the target molecules has not been trivial. Moreover **BDT** and **BDT$_1$** show completely different reactivity, and only in few cases it has been possible to apply the same synthetic procedure known for the preparation of analogous compounds.

Almost all the dyes synthesized have also been characterized from a photophysical as well as electrochemical point of view, with the aim of identifying, among them, the most interesting and promising compounds for application in solar cells and try to clarify the relationship between the chemical structure and photovoltaic performances. The main information inferred from these studies was that the π conjugation is more effective in **BDT$_1$** than in **BDT**, and therefore that the former is able to act as a better π-spacer in a

D-π-A structure, leading to a better electronic communication between the D and A part of the push-pull system.

The last part of the work of this Ph.D. thesis has been devoted to the fabrication of solar cells using, as sensitizers, some of the prepared dyes. The results obtained in this more applicative part of the thesis are also interesting, in that sufficiently high efficiency values for the assembled solar cells were observed, and could be correlated to the photophysical and electrochemical behavior of dyes.

The collected information and rationalization of all these data have make it possible the identification, among all the dyes prepared, of a lead molecule, that is **11**, which showed the quite high efficiency of 5.11% in liquid electrolyte and of 2.64% in solid state solar cells, besides a high chemical stability. Even if in this field a direct comparison among solar cell efficiencies based on different typologies of dyes has no particular significance, the cell efficiency found for **11**, which is however still under optimization, allows us to say that this dye ranks among the promising dyes to date reported in literature. In addition, it must be pointed out that dye **11** seems to possess most of the essential chromophore characteristics required for obtaining high-performance DSSCs.

The systematic study developed during the present Ph.D. thesis will be very useful for future improvement of the structures synthesized, and for the development of successful strategies aiming to future improvement of photovoltaic performances in DSSCs.

This thesis is the result of an interdisciplinary work were theoretical calculations, synthesis, photophysical and electrochemical studies, in addition to the evaluation of dyes in a laboratory device, have been strongly coordinated in order to address all efforts to the main scientific objects. I'm convinced that nowadays, the concept of multidisciplinary collaboration is essential to be successful in all of the field of science.

**APPENDIX**

List of Abbreviation

| | |
|---|---|
| **ACN** | acetonitrile |
| **AcOH** | acetic acid |
| **BDT** | benzodithiophene |
| **CDCA** | chenodeoxycholic acid |
| **DCM** | dichloromethane |
| **DMF** | dimethylformamide |
| **DMSO** | dimethylsulfoxide |
| **EtOH** | ethanol |
| **LDA** | lithium disopropylamide |
| **MeOH** | methanol |
| **NBS** | *N*-bromosuccinimide |
| **NIS** | *N*-iodosuccinimide |
| **PMMA** | polymethylmetacrylate |
| **PPA** | polyphosphoric acids |
| **TBAF·H$_2$O** | Tetra-*n*-butylammonium fluoride |
| **TMSCl** | Trimethylsilylchloride |
| **TEA** | triethylamine |
| **TFA** | trifluoroacetic acid |
| **EI** | electron impact mass |
| **ESI** | electronspray ionization mass |
| **ET** | electron transfer |
| **CT** | charge transfer |
| **FT-IR** | Fourier transformate infrared |

| | |
|---|---|
| **NMR** | nuclear magnetic resonance |
| **UPS** | ultraviolet photoemission spectroscopy |
| **TMS** | tetramethyl silane |
| **UV-VIS** | ultraviolet visible |

# ACKNOWLEDGEMENTS